Analysis and interpretation of ambient data for CO_2, CH_4 and CO recorded in Southwest London during 2000 to 2012

Iván Yassmany Hernández Paniagua

Royal Holloway, University of London

A thesis submitted for the degree of Doctor of Philosophy

August 2014

Declaration of Authorship

I, Iván Yassmany Hernández Paniagua, hereby declare that this thesis

Analysis and interpretation of ambient data for CO_2, CH_4 and CO recorded in Southwest London during 2000 to 2012

and the work presented in it is entirely my own. Where I have consulted the work of others, this is fully cited and referenced, and/or with the appropriate acknowledgment given.

Signature:

Date: 28 July 2014

Name of Student: Mr. Iván Yassmany Hernández Paniagua

Name of supervisors: Dr Kevin C. Clemitshaw
Dr David Lowry
Professor Euan G. Nisbet

ABSTRACT

CO_2 and CH_4 current levels are the highest recorded during the Anthropocene epoch due, mostly, to emissions from anthropogenic activities. These emissions have modified the biochemical cycle of C and earth's thermal equilibrium. In contrast, CO emissions have decreased since 2000 following the strict controls on vehicle emissions. Atmospheric observations can be used to detect trends and changes in CO_2, CH_4 and CO concentrations, and also, to locate and characterize natural and anthropogenic sources. In situ measurements of atmospheric CO_2, CH_4 and CO have been performed at Royal Holloway University of London since 2000 to 2012 and standardised using NOAA calibration gases.

CO_2, CH_4 and CO varied on time scales ranging from minutes to inter-annual and annual cycles. Diurnal cycles were observed and varied with the length daylight which influences the net soil uptake of CO_2, the concentration of OH radicals and, the degree of vertical mixing. There is a greater influence of CO_2 and CO anthropogenic emissions during weekdays when fossil fuel use and combustion processes are higher than at weekends not observed for CH_4. CO_2 showed an increasing trend of 2.45 ppm yr^{-1} data for the whole dataset; a higher rate of increase than the observed global trend due to higher regional combustion emissions such as airplanes, houses and cars on highly loaded motorways. By contrast, CO showed a progressive decline not linear, but if linearized the decline rate was 15.3 ppb CO yr^{-1}, while CH_4 concentration remained steady.

The data set was split into 8 categories (45°) using wind sector analysis. This shows that the greatest concentrations for the three carbon gas are recorded from the NE, E and SE sectors. The lowest concentrations were observed for air from the S and SW sectors. Back trajectory and meteorological analysis of the data confirmed that the dominant sources of CO_2, CH_4 and CO are anthropogenic emissions from Greater London area and the dense local road network to the East of the measurement site.

Nowadays, compared with Mace Head (West Ireland) data, the CO_2 measured at Egham is slightly higher than at Mace Head while CO and CH_4 is not far above Atlantic background levels during large periods of the year when prevailing S-SW winds reach the site. The Egham record implies that controls on CO emissions subsequent to legislation have been extremely successful the UK.

DISSEMINATION OF RESEARCH

Publications

I.Y. Hernández-Paniagua, D. Lowry, R.E. Fisher, J.L. France, M. Lanoiselle, M. Ramonet, K.C. Clemitshaw, E.G. Nisbet. Diurnal, seasonal, and annual trends in atmospheric CO_2 at southwest London during 2000-2012: Wind sector analysis and comparison with Mace Head, Ireland. *Submitted to Atmospheric Environment (2014a).*

I.Y. Hernández-Paniagua, D. Lowry, R.E. Fisher, J.L. France, M. Lanoiselle, K.C. Clemitshaw, E.G. Nisbet. Analysis and interpretation of CO observations at southwest London during 2000-2012. *In preparation for Atmospheric Environment (2014b).*

I.Y. Hernández-Paniagua, D. Lowry, R.E. Fisher, J.L. France, M. Lanoiselle, K.C. Clemitshaw, E.G. Nisbet. Diurnal, seasonal and annual trends in atmospheric CH_4 at the EGH site in SE England during 2000-2012. *In preparation for Atmospheric Environment (2014c).*

D. Lowry, M. Lanoisellé, R.E. Fisher, M. Martin, C.M.R. Fowler, J. France, **I.Y. Hernández-Paniagua,** S. Sriskantharajah, P. O'Brien, N. Rata, C. Holmes, Z. Fleming, G. Zazzeri, M. Pommier, C.A. McLinden, K.C. Clemitshaw, E.G. Nisbet. Marked long-term decline in ambient CO mixing ratio in SE England, 1997-2012: evidence of policy success in improving air quality. *In preparation for Atmospheric Chemistry and Physics.*

Verbal presentations

I.Y. Hernández-Paniagua, D. Lowry, E.G. Nisbet and K.C. Clemitshaw. CO_2 observations in SE England: Seasonal and interannual variations. Presented at the European Union General Assembly 2013. Vienna Austria, April 2013.

I.Y. Hernández-Paniagua, D. Lowry, E.G. Nisbet and K.C. Clemitshaw. CO_2 observations in SE England: Seasonal and interannual variations 13-years of measurements. Presented to the MSc in Environmental Diagnosis and Management, Royal Holloway, University of London, UK. February 2013.

I.Y. Hernández-Paniagua, D. Lowry, E.G. Nisbet and K.C. Clemitshaw. CO_2 observations in SE England: Seasonal and interannual variations “Importance of the C cycle”. Presented at the XI Mexican symposium of students and studies. University of Sheffield. 12 July 2013.

I.Y. Hernández-Paniagua, D. Lowry, E.G. Nisbet and K.C. Clemitshaw. Interpretation of 13-years of measurements of CO_2, CO and CH_4 observations in SE England. Presented to the Bioprocesses Research Group, Centre for Research and Advanced Studies, National Polytechnic Institute. Mexico, D. F. 4 December 2013.

I.Y. Hernández-Paniagua, D. Lowry, E.G. Nisbet and K.C. Clemitshaw. CO_2, CO and CH_4 observations in SE England: analysis and interpretation of 13-years of measurements. Presented to the MSc in Environmental Diagnosis and Management, Royal Holloway, University of London, UK, February 2014.

Poster presentations

Iván Y. Hernández-Paniagua, Dave Lowry, Euan Nisbet and Kevin C. Clemitshaw. Long-term decline of the CO mixing ratio in SW London from 2000 to 2012: An example of policy success in improving air quality. Presented at the 2013 American Geophysical Union Fall Meeting. San Francisco, California, USA.

Iván Y. Hernández-Paniagua, Dave Lowry, Kevin C. Clemitshaw and Euan G. Nisbet. Anthropogenic influences on atmospheric boundary layer CO_2 and CH_4 in SW London. Presented at the 2014 Goldschmidt Conference. Sacramento, California, USA.

ACKNOWLEDGMENTS

I would like to express the deepest appreciation to Dr Kevin C. Clemitshaw for his guidance and accurate comments in every aspect of this project and also for the invaluable talks over the last three years. Without his guidance and persistent help this thesis would not have been possible.

I would like to thank too to Dr David Lowry for his helpful discussion and comments during my PhD. I am extremely grateful and indebted to him for expert, sincere and valuable guidance and encouragement extended to me.

I also thank Professor Euan G. Nisbet for his great interest and assistance in the pursuit of these studies and in the preparation of this thesis.

I would like to thank Dr Rebecca E. Fisher and Dr James France for helping with the analyses and interpretation of the dataset.

I consider myself very fortunate for having a chance to share the last three years with friends and colleagues at the Earth Sciences Department of Royal Holloway University of London. Working with them was a great learning experience for me. I really value the knowledge and insight they have, and their willingness to share it with me.

Most importantly, none of this would have been possible without the love and patience of my family. My family, to whom this dissertation is dedicated to, has been a constant source of love, concern, support and strength all these years. I would like to express my heart-felt gratitude to my father, to my mother and to my brother.

The research presented in this thesis was funded by The National Council on Science and Technology (CONACYT) and by The Mexican Secretariat of Public Education (SEP).

I would like to extend my gratitude to the Department of Earth Sciences Research Committee at Royal Holloway University of London for funding allocated to attend conferences.

CONTENTS

List of Figures

List of Tables

1. INTRODUCTION

1.1. Background

In recent decades, anthropogenic activities have emitted to the atmosphere large quantities of air pollutants (IPCC, 2013). Air pollutants can be divided into those that can have adverse impacts on human health, and those that have effects on climate, Greenhouse Gases (GHGs) (Figure 1.1). Large concentrations in the environment of air pollutants such as carbon monoxide (CO) and sulphur dioxide (SO_2) can increase the number deaths or worse cardiovascular and respiratory diseases including asthma (Schwela, 2000; Anderson et al., 2001). The World Health Organization (WHO) estimates that outdoor air pollution causes 1.3 million deaths per year worldwide (WHO, 2014).

Exposure to air pollutants is beyond individual control to some extent; therefore the action of authorities to control the air pollutants levels at international, national and regional levels is required. Since 1955, many countries have issued Air Quality (AQ) policies to control the levels in the environment and the emissions of air pollutants and GHGs such as the UK Air Quality Strategy (Defra, 2007).

Increasing concentrations of GHGs such as carbon dioxide (CO_2), methane (CH_4) and nitrous oxide (N_2O) may alter the thermal equilibrium of the Earth. Large emissions of GHGs since the beginning of the Industrial Era have modified the Earth's climate balance, which is thought has led the planet to global warming. Decades ago, the climate problem was thought only related to the increasing CO_2 atmospheric levels; however nowadays it is widely recognized that the atmospheric increase of GHGs during the last 250 years has had important effects in terms of greenhouse forcing (IPCC, 2013). As result of this, unprecedented efforts from non- and governmental-organisations have been carried out to mitigate and to abate their emissions.

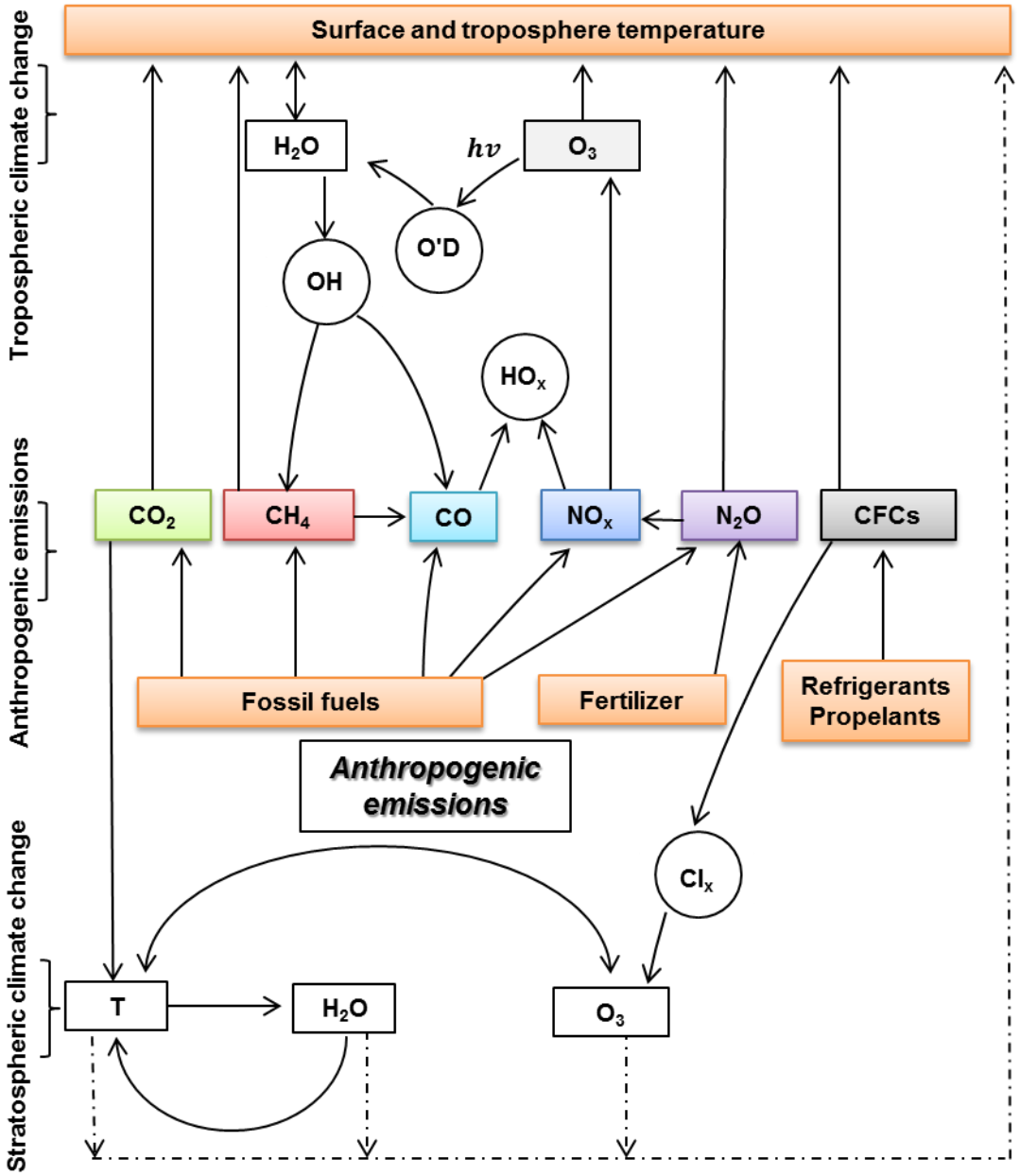

Figure 1.1. Schematic diagram of chemistry-climate interactions and sources of air pollutants. *Source: Ramanathan and Feng, 2009.*

This thesis presents a detailed study of records of CO_2, CH_4 and CO from 2000 to 2012 at the semi-rural monitoring station of Royal Holloway University of London in Egham, UK (EGH). Detailed insights can provide vital clues to understand and to predict long- and short-term trends, seasonal and interannual variations of CO_2, CH_4 and CO in response to measures to control their emissions.

1.2. The atmosphere

The atmosphere is a thin and fragile envelope of air surrounding the Earth, which plays a crucial role as it affects the environment in which organisms live. It is held around the Earth by gravitational attraction (Brasseur et al., 1999). The atmosphere can be considered as two regions: the lower and upper atmosphere. Figure 1.2 shows the vertical structure and temperature profile of the atmosphere. The lower atmosphere extends from the surface to the top of the stratosphere at an altitude about 48-50 km. The upper atmosphere goes from the top of the stratosphere to the top of the thermosphere at an altitude of 120 km.

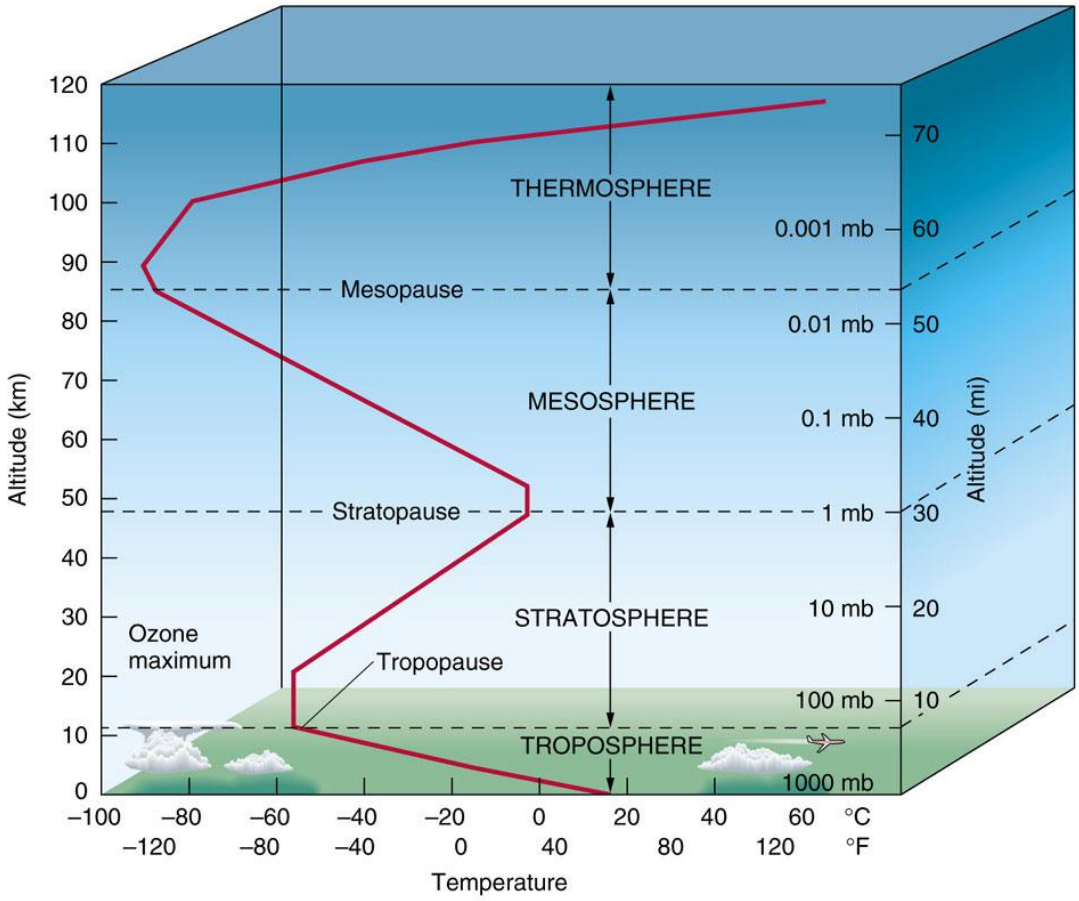

Figure 1.2. Vertical profile of the temperature between the surface and 120 km of altitude as defined in the U.S. Standard Atmosphere (1976) and related atmospheric Layers. *Source: Available at* http://www.srh.noaa.gov/jetstream/atmos/*atmprofile.htm*

1.2.1. The vertical structure of the atmosphere

1.2.1.1. The troposphere

The research in this thesis is focused only on processes that occur in the troposphere. The troposphere extends from the surface to the tropopause at an

altitude about 18 km in the tropics, 12 km at mid-latitudes, and 6 to 8 km near the Poles. The temperature of the troposphere decreases with height due to a decrease in energy transfer as height increases, and therefore saturation vapour pressure decreases strongly as temperature drops. This layer contains about 85-90% of the mass in the atmosphere. It is often dynamically unstable with rapid vertical exchanges of energy and mass being associated with convective activity. Globally, the time constant for vertical exchanges is of the order of several weeks. The World Meteorological Organization (WMO) defines the tropopause as the lowest level at which the rate of fall of temperature with height decreases to 2 K per km or less, and the lapse rate averaged between this level and any level within the next 2 km, does not exceed 2 K per km (Holton et al., 1995).

1.2.1.2. The stratosphere

The stratosphere is very stable and the second major layer of the Earth (Figure 1.2). It extends from altitudes of 12 km up to 50 km (the stratopause). It is stratified in temperature, which increases with altitude and produces a slow vertical mixing on time-scales from months to years (Brasseur et al., 1999). The temperatures in the upper and lower stratosphere are about −3°C, just slightly below the freezing point of water, and -52°C, respectively. Warmer layers above cooler layers prevent convection; which causes that weather systems be confined to the troposphere (Seinfeld and Pandis, 2006). The stratosphere is virtually cloudless due to the limited vertical transport of water vapour. Material injected into the lower stratosphere has a residence time between one to three years. The stratosphere contains about 90% of the atmospheric ozone. Ozone (O_3) absorbs high energy UVB and UVC energy waves from the Sun, which causes the vertical stratification.

1.2.2. General circulation in the troposphere

The irregular distribution of radiative heating on the Earth generates a meridional circulation of air (Figure 1.3). Air masses flow towards the Equator rising at low latitudes and sinking at mid- and high latitudes. In the tropics, the zonal-mean wind is characterised by rather weak easterlies. The circulation in the west-east direction (zonal flow) is deviated by orographic features on the surface of the planet (e.g. mountains). The meridional turnover of air masses is modified substantially by the Earth's rotation (Brasseur et al., 1999). The transport of chemical constituents is driven by transport processes generated by such dynamic disturbances. The mean

winds everywhere tend towards zero at the surface of the planet, which denotes the strong influence of friction at the ground.

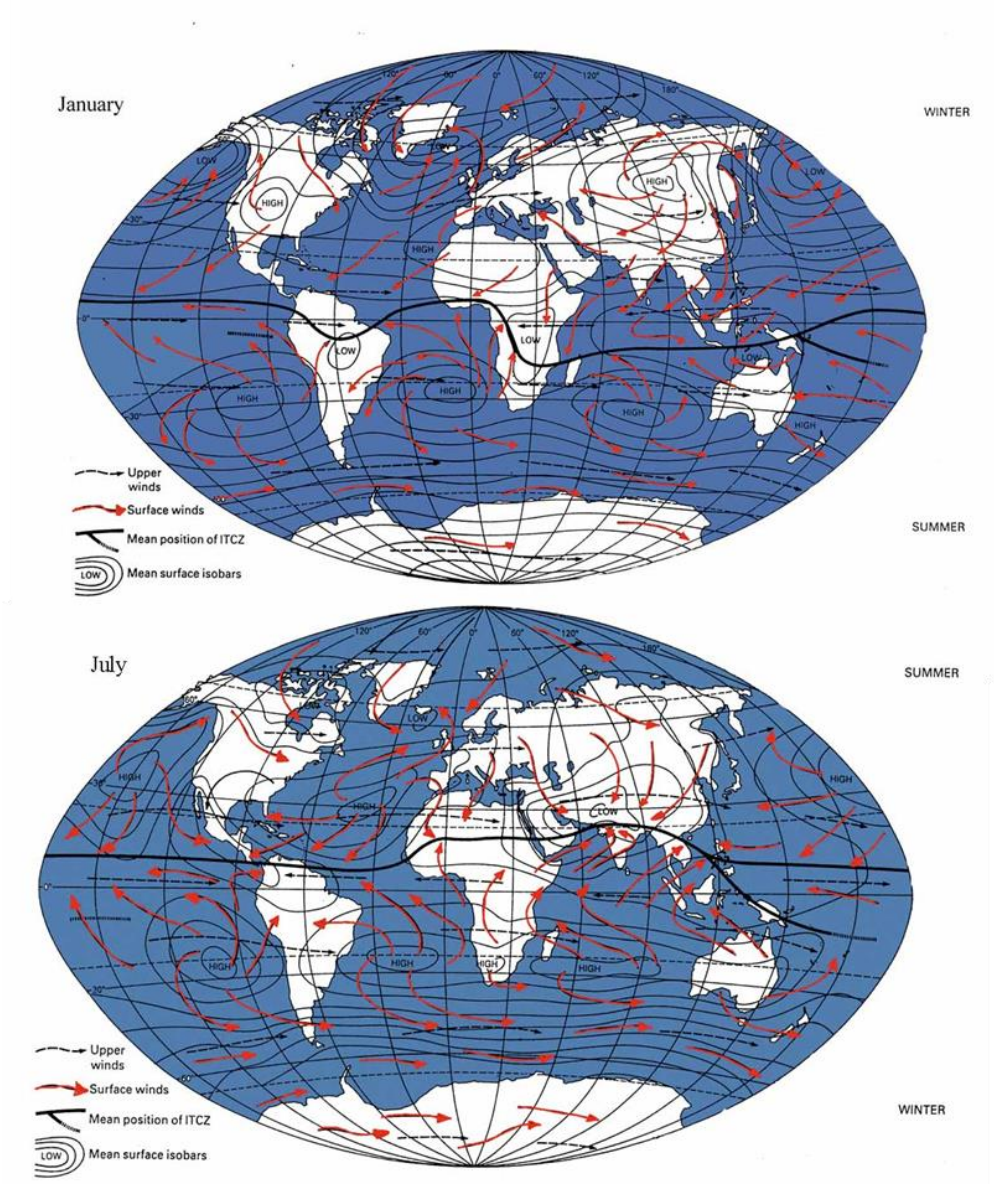

Figure 1.3. Average global circulation during January (northern hemisphere winter) and during July (northern hemisphere summer). ITCZ means Inter-tropical Convergence Zone. *Source: Available at http://www.st-andrews.ac.uk/~dib2/GE1001/atmosphere2.html*

Baroclinic disturbances dominate the circulation between 30° and 60° of both hemispheres. These regions are very well mixed vertically and horizontally as result of the highly variable surface winds. Precipitation is commonly associated with air rising above the warm fronts, as well as the passage of the cold fronts (Brasseur et al., 1999). The weather regime towards the equator, from about 30°, is different from that moving polewards. The weather is characterised by air descending slowly. A rapid rising motion occurs in the vicinity of the equator, along the Inter-Tropical

Convergence Zone (ITCZ). Figure 1.3 shows the southern shift in January and the northern shift in July of the ITCZ. In this region, there is abundant rainfall due to deep convective clouds.

1.2.3. The planetary boundary layer

The Planetary Boundary Layer (PBL) is the region adjacent to the surface. It develops through the depth of the atmosphere affected by the Earth's surface. Its depth is of the order of 0.2-1.5 km but varies significantly with the time of the day and meteorological conditions (Figure A1.1). The PBL height has a seasonal and diurnal dependency. Figure 1.4 shows the seasonal variation of the PBL in the UK over a year. A deep PBL develops during daytime, which allows efficient vertical mixing (PORG, 1997; NOAA/ESRL, 2014). In contrast, a shallow PBL exists during the night, which reduces the vertical mixing causing large vertical gradients (Hunt et al., 1988).

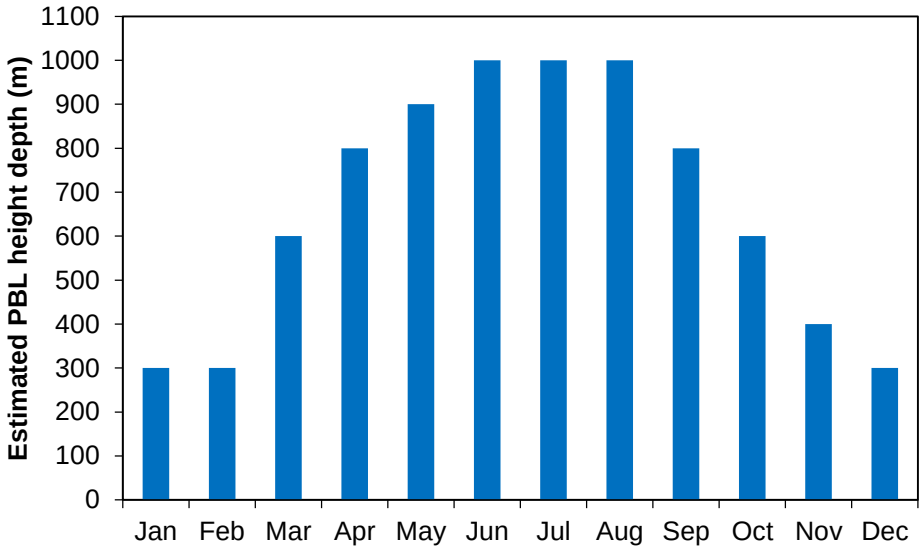

Figure 1.4. Average depth of the PBL depth across the UK. *Source: PORG, 1997.*

The stability of the PBL drives the exchange of chemical compounds between the surface and the free troposphere. Typical time scales range from several hours to a few days for transport out or into the boundary layer. Entrainment velocities into the PBL range between 0.01 to 0.20 m s^{-1} and typical layer heights from 100 m to 2 km (Brasseur et al., 1999). Active convection can vent the PBL much more rapidly (less than one hour). Stable boundary layers occur over the continents during winter

when the land surface is cold and during summer under large continental stable air masses.

1.2.4. Spatial and temporal scales of variability

In the atmosphere, motion takes place at spatial and temporal scales simultaneously. Interaction between scales is always important. The global atmospheric lifetime (in years) for example, characterises the time required to turn over the global atmospheric burden. It is defined as the burden (Tg) divided by the mean global sink (Tg/yr) for a gas in steady state. Figure 1.5 shows lifetimes of several chemical species in the atmosphere. When in a steady state (i.e., source strength = sink strength), the atmospheric burden of a gas equals the product of its lifetime and its emissions. The atmospheric lifetime is a scale factor relating (i) constant emissions (Tg/yr) to a steady-state burden (Tg), or (ii) an emission pulse (Tg) to the time-integrated burden of that pulse (Tg/yr). The lifetime is often additionally assumed to be a constant, independent of the sources; and it is also taken to represent the decay time (e-fold) of a perturbation (IPCC, 2007).

Spatial and temporal variability of chemical species are inversely related to their chemical lifetime. The intricate coupling between lifetimes and the atmospheric scales of motion set the spatial scales of several phenomena, such as urban and regional air pollution (Figure 1.5). The spatial scales of motion in the atmosphere range 9 orders of magnitude from microscale to synoptic and global scale (Gifford, 1982). Seinfeld and Pandis (1998) defined four categories of motion:

1. Microscale: Lifetime spans from seconds to minutes and distance less than 1 km.
2. Mesoscale: Lifetime spans from minutes to hours and distance from 1 km to 1,000km.
3. Synoptic: Lifetime spans from days to weeks and distance from 1,0000 km to 4,000km.
4. Planetary (Global scale): Lifetime spans from weeks to seasons and distance >4,000 km.

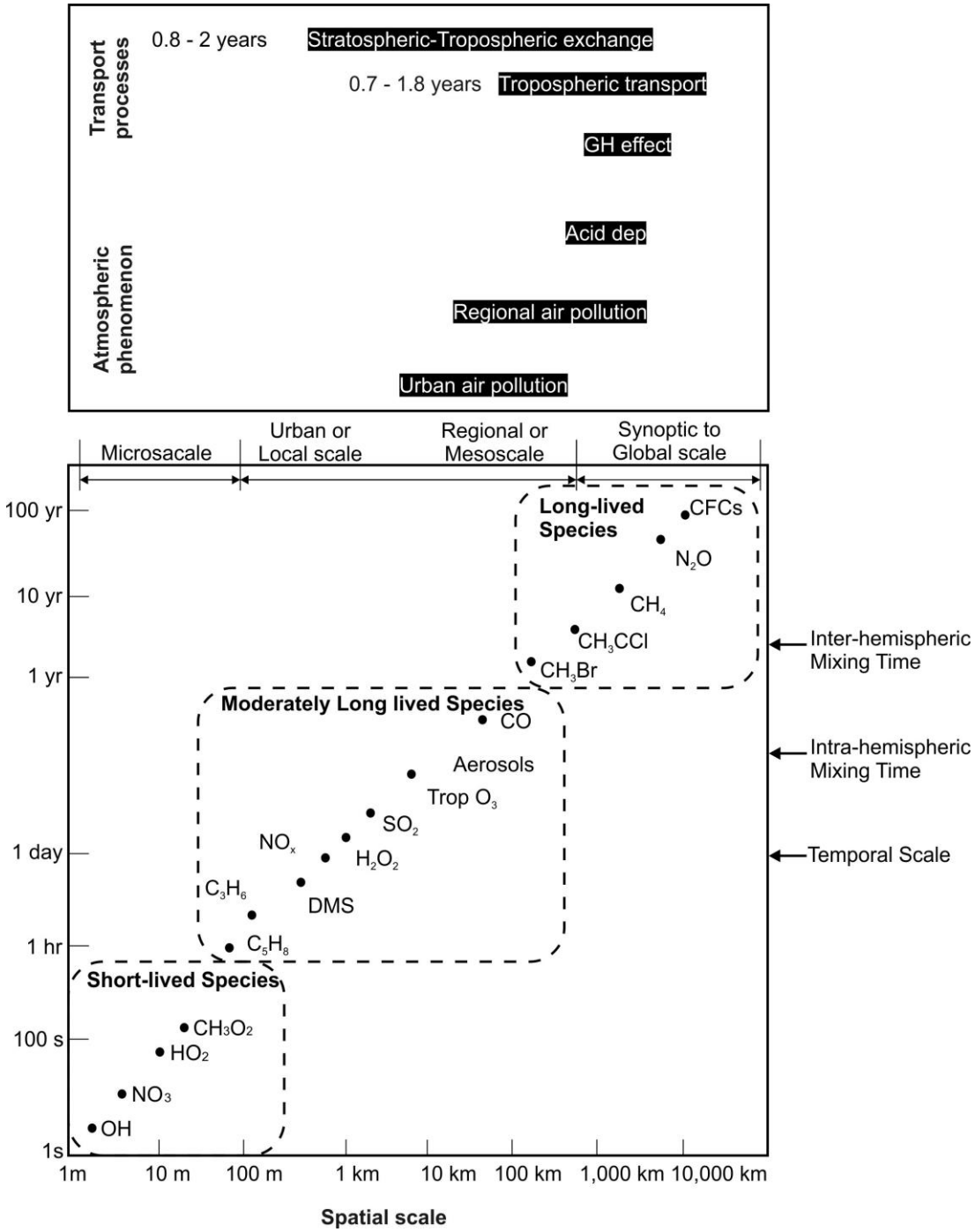

Figure 1.5. The temporal and spatial scales of variability in the atmosphere. *Source: Adapted from Seinfeld and Pandis, 1998 and Brasseur et al., 1999.*

1.3. The Concept of Air Pollution

Air pollution is defined as “the presence of substances in the ambient atmosphere, resulting from the activity of man or from natural processes, causing adverse effects to man and to the environment” (Weber, 1982). Build-up of air pollutants can cause direct or indirect damage to plants, animals, other life forms, ecosystems, structures

and works of art (Jacobson, 2002). Air pollution is not a modern issue as concerns have been well documented since ancient times. However, it was not until the twentieth century when the Great London Smog caused around 4,000 deaths in five days in 1952, and damage to agricultural crops was observed in the Los Angeles basin, that air pollution gained the attention of environmental authorities (Finlaysson-Pitts and Pitts, 2000). Since then, air quality policies and legislation have been issued to mitigate and abate air pollutant emissions.

The state of the air in the environment is defined as air quality. Air quality is a measure of gaseous pollutant concentrations and particulate matter. A good air quality is referred to clean, clear and unpolluted air and is essential to maintain the delicate balance of life on the earth (LAQN, 2014).

1.3.1. Health Associated Air Pollutants

Air quality has experienced drastic changes worldwide in the last two centuries due to industrialisation. During the nineteenth century, air pollution was considered to some extent as a symbol of growth and prosperity. However, a drastic change occurred when the presence of photochemical air pollutants was detected in the Los Angeles basin in 1940s, and moreover, after the large number of deaths experienced during the London great smog in 1952 (Finlaysson-Pitts and Pitts, 2000). Those events attracted the attention of authorities to control air pollutants emissions and consequently to improve air quality. Air quality issues effect some of the most populated cities in world. Table 1.1 shows the severity of air quality problems in 20 so-called megacities worldwide.

The length of exposure to air pollutants is strongly correlated with the level of worsening health. Air pollutants can have significant negative effects on the respiratory system (airways and lungs) and on the cardiovascular system (heart function and blood circulation). Some illnesses increase with the prolonged exposure to air pollutants. Exposure to nitrogen dioxide (NO_2) from gas cooking has been associated with respiratory symptoms (Schwela, 2000).

It has also been observed that such exposure is related to a decrease in lung function, chronic cough, bronchitis and conjunctivitis. Sulphur dioxide (SO_2) appears to be related to daily mortality and morbidity. Particulate matter (PM) has been found to cause other diseases as emphysema, asthma, angina, heart failure and

arrhythmia (Anderson et al., 2001). Diabetes also appears to worsen, perhaps due to its close relationship with heart disease. Therefore air pollution control is essential to protect public health.

Table 1.1. Air pollutants in some Megacities.

City	Pollutant					
	SO_2	CO	NO_2	O_3	Pb	PM
Bangkok	x		x	x	xx	xxx
Beijing	xxx	x	x	xx	x	xxx
Bombay	x	x	x		x	xxx
Buenos Aires					x	xx
Cairo		xx			xxx	xxx
Calcutta	x		x		x	xxx
Delhi	x	x	x		x	xxx
Jakarta	x	xx	x	xx	xx	xxx
Karachi	x				xxx	xxx
London	x	x	x	x	x	x
Los Angeles	x	xx	xx	xxx	x	xx
Manila	x				xx	xxx
Mexico City	xxx	xxx	xx	xxx	xx	xxx
Moscow		xx	xx		x	xx
New York	x	xx	x	xx	x	x
Rio de Janeiro	xx	x			x	xx
São Paulo	x	xx	xx	xxx	x	xx
Seoul	xxx	x	x	x	x	xxx
Shanghai	xx					xxx
Tokyo	x	x	x	xx		x

Source: Adapted from Finlaysson-Pitts and Pitts, 2000; Anderson et al., 2001; LAQN, 2014.
*Blank spaces mean not enough data are available.
X: WHO guidelines are normally met.
XX: WHO guidelines were exceeded by up to a factor of two.
XXX: WHO guidelines were exceeded by more than a factor of two.

1.4. Carbon monoxide (CO)

Out of the six air pollutant listed in Table 1.1, this thesis will only address the importance of CO as an air pollutant and as an indirect GHG. CO is a trace gas in the atmosphere. It is detrimental to human health if exposure is prolonged. In urban areas, the highest 1-hour concentrations are recorded during morning and evening rush hours (Schwela, 2000). In European cities, large concentrations are recorded in the proximity of highly loaded roads (Bigi and Harrison, 2010; von Schneidenmesser et al., 2010). In environments with adequate ventilation, population exposure to harmful CO concentrations is not enough to cause health

damage. However in closed environments like tunnels, car parks and buildings, the population is frequently exposed to high CO concentrations that can affects their health.

High indoor CO concentrations are caused by large emissions from domestic heaters (largely used during winter), tobacco smoke and carbon-based appliances mostly used in developing countries. CO uptake from the environment is only carried out by the lungs. It diffuses quickly across alveolar, capillary and placental membranes. From 80% to 90% of the total CO absorbed binds with haemoglobin to produce carboxyhemoglobin (COHb). COHb displaces oxygen and reduces oxygen delivery to the body's organs and tissues (Varon and Marik, 1997). Severe hypoxia from CO poisoning may cause reversible, shot-lasting, neurological deficits and severe, often delayed, neurological damage. The neurobehavioral comprise impaired coordination, tracking, driving ability, vigilance, and cognitive performance at COHb levels from 5% to 8% (Schwela, 2000). Vision impairment has been found to start at COHb levels above 18%.

CO is a trace gas in the atmosphere that plays a central role in tropospheric chemistry via its reaction with the OH radical (Waibel et al., 1999). CO does not absorb enough terrestrial infrared radiation to be considered as GHG, however it affects indirectly the CH_4 atmospheric burden by changing OH concentrations in the troposphere. CO global burden is estimated around 360 Tg (highly uncertain*)* (IPCC, 2007). CO has a short lifetime in the atmosphere, around two months. Because of its short lifetime, CO does not reach complete mixing in the atmosphere and produces large concentration gradients which are illustrated in Figure 1.6 and 1.7 (NOAA/ESRL, 2013).

1.4.1. Sources of CO

CO is mostly released as by-product of incomplete combustion of fossil fuels and biomass burning, (Equation 1.1; Zhang et al., 2001). In the atmosphere, it is produced by the oxidation of methane (Equation 1.2) and other hydrocarbons (Equation 1.3). The exhaust from light-duty motor vehicles is the major source in urban areas in the northern hemisphere. Secondary sources are the emissions by vegetation and microorganisms on land and by photochemical oxidation of

dissolved organic matter in the oceans (Hewitt and Jackson, 2003). Table 1.2 summarizes the IPCC estimates for CO sources.

$$C_xH_y + zO_2 \rightarrow aCO_2 + bCO + cH_2O + dH_2 \quad \text{(Eq. 1.1)}$$

$$CH_4 \rightarrow CO + H_2 + H_2O + 2O_2 \quad \text{(Eq. 1.2)}$$

$$H_2CO \xrightarrow{h\nu} H + HCO \quad \text{(Eq. 1.3)}$$

Table 1.2 Global budget for carbon monoxide.

Sources	Magnitude (Tg yr^{-1})
Biomass burning[a]	300 – 900
Fossil fuel burning[a]	300 – 600
Vegetation[a]	50 – 200
Oceans[a]	6 – 30
Methane oxidation[b]	400 – 1000
NMHC* oxidation[b]	300 – 1000
Total	***1400 – 3700***

Adapted from Khalil and Rasmussen, 1994; Brasseur et al., 2003; IPCC, 2007.
**Non-methane hydrocarbons. [a]Primary sources. [b]Secondary sources.*

1.4.2. Sinks of CO

The major loss of carbon monoxide is through its reaction with OH radicals in the atmosphere, Equation 1.4 (Levy, 1972). Other minor sources are the soil uptake and stratospheric oxidation. Due to its reactivity, CO sink estimations carry large uncertainties. Table 1.3 lists the main sinks of CO and their magnitudes.

$$OH + CO \rightarrow H + CO_2 \quad \text{(Eq. 1.4)}$$

$$H + O_2 + M \xrightarrow{h\nu} HO_2 + M \quad \text{(Eq. 1.5)}$$

Table 1.3. Sinks for carbon monoxide.

Sinks	Magnitude (Tg yr^{-1})
Chemical loss (OH)	1400 – 2600
Soil uptake	250 – 390
Stratospheric oxidation	80 – 140
Total	***1730 – 3130***

Adapted from Khalil and Rasmussen, 1994; Brasseur et al., 2003; IPCC, 2007.

1.4.3. Spatial variations of CO

Figure 1.6 highlights the importance of anthropogenic CO emissions over urban and industrial regions. Most remarkably are the large concentrations observed at equatorial regions due to high photochemical activity in spring and autumn. High CO concentrations over the northern Atlantic Ocean are ascribed to the oxidation of long lifetime hydrocarbons as ethane, and their oxidation products (Figure 1.6). They can be transported and further oxidised far from the location of their emissions. Those regions contrast with the relatively unpolluted ones observed at the both North and South poles.

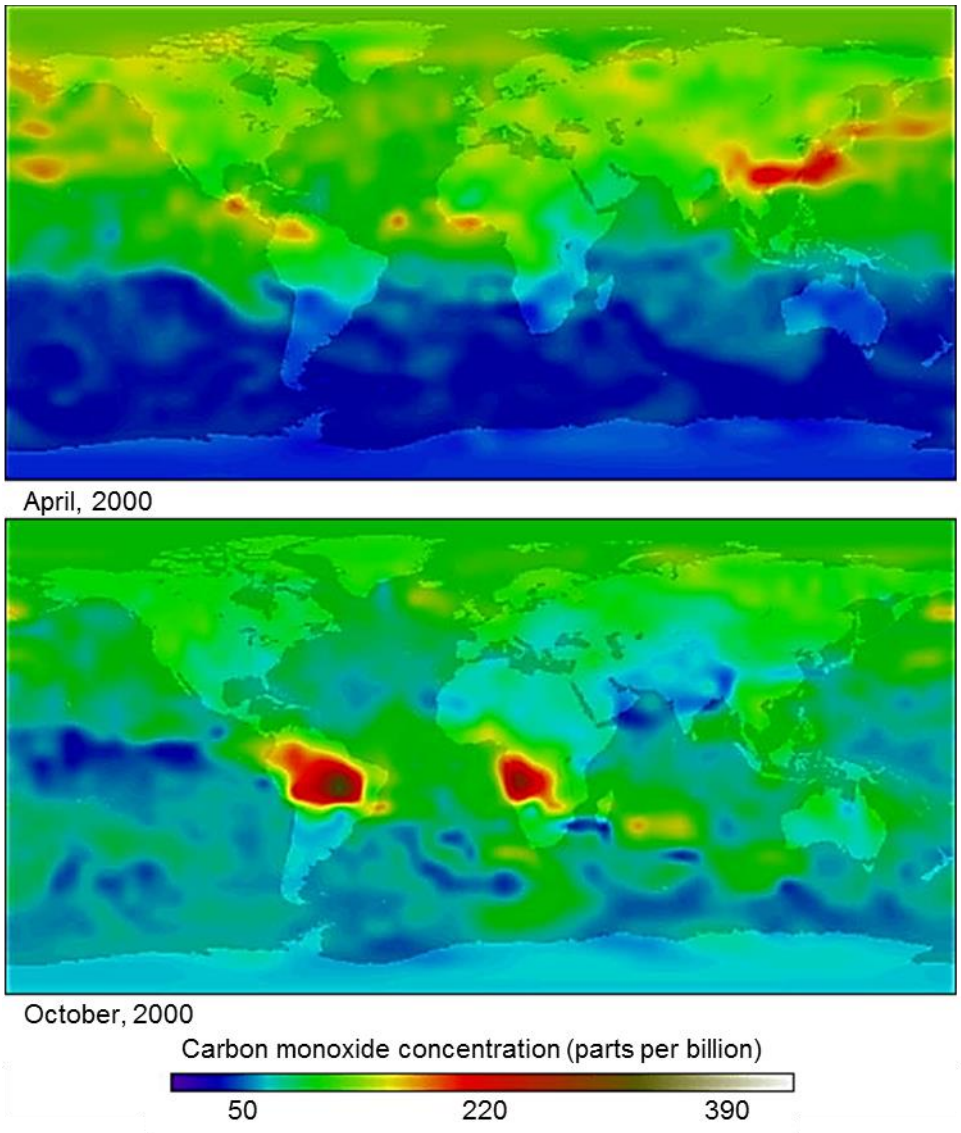

Figure 1.6. Measurements of CO in the lower atmosphere made by the MOPITT sensor aboard NASA's Terra satellite. CO concentrations are represented by the colour scale ranging from about 50 parts per billion (blue pixels), to 220 parts per billion (dark brown pixels), to 390 parts per billion (red pixels). *Source: Available at: http://www.wmo.int/pages/prog/arep/gaw/reactive_gases.html#monoxide*

In the high northern latitudes, CO concentrations vary from ~60 ppb during summer to 200 ppb in winter (Figure 1.7). Much higher concentrations can be observed in urban and industrial areas where CO emissions are intense, such as Europe, eastern US and eastern US (Grant et al., 2010; Kim and Shon, 2011). At the South Pole, it varies between about 30 ppb in summer and 65 ppb during winter.

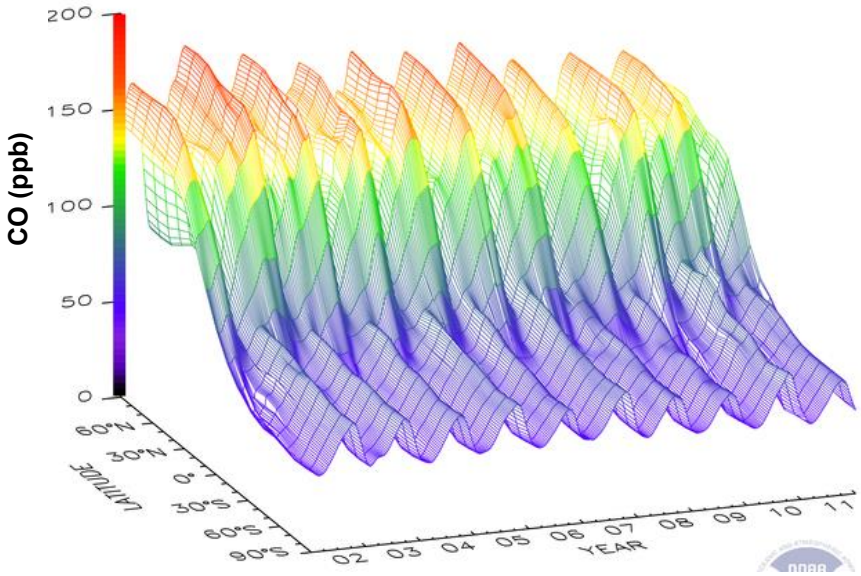

Figure 1.7. Three-dimensional representation of the latitudinal distribution of atmospheric CO during 2002-2011. Data from the Carbon Cycle cooperative sampling network were used. The surface represents data smoothed in time and latitude. *Source: Available at http://www.esrl.noaa.gov/gmd/Photo_Gallery/GMD_Figures/ccgg_figures/co_surface_color.png*

1.4.4. Temporal variations of CO

Global monitoring suggests that atmospheric CO concentrations increased during the nineteenth century until the late 1980s and then declined considerably (Khalil and Rasmussen, 1984; Zander et al. 1989). Such decline was possibly due to decreased automobile emissions, as result of the catalytic converter introduction, and reduction in biomass burning (Bakwin et al., 1994; Novelli et al., 1994). During the 1990s, a global decline in CO levels was observed a rate about 2% yr^{-1} (Novelli et al., 1998) but increased again during 1998-2000 (NOAA/ESRL, 2014).

During 2000s, CO declined globally at rates between 1% and 25% yr^{-1}, the larger decline rates were seen mostly in urban areas of megacities including London, Seoul, Mexico city, Los Angeles and others (Kuebler et al., 2001; Zhang et al., 2001; Cofala et al., 2007; Monks et al., 2009; von Schneidenmesser et al., 2010). Figure

1.8(a) shows the global average decreasing trend during 20-years of records calculated from the Carbon cycle co-operative air sampling network. During the measurement period, the global growth rate has oscillated from -13 to 14 ppb yr^{-1} (Figure 1.8(b); NOAA/ESRL, 2014.)

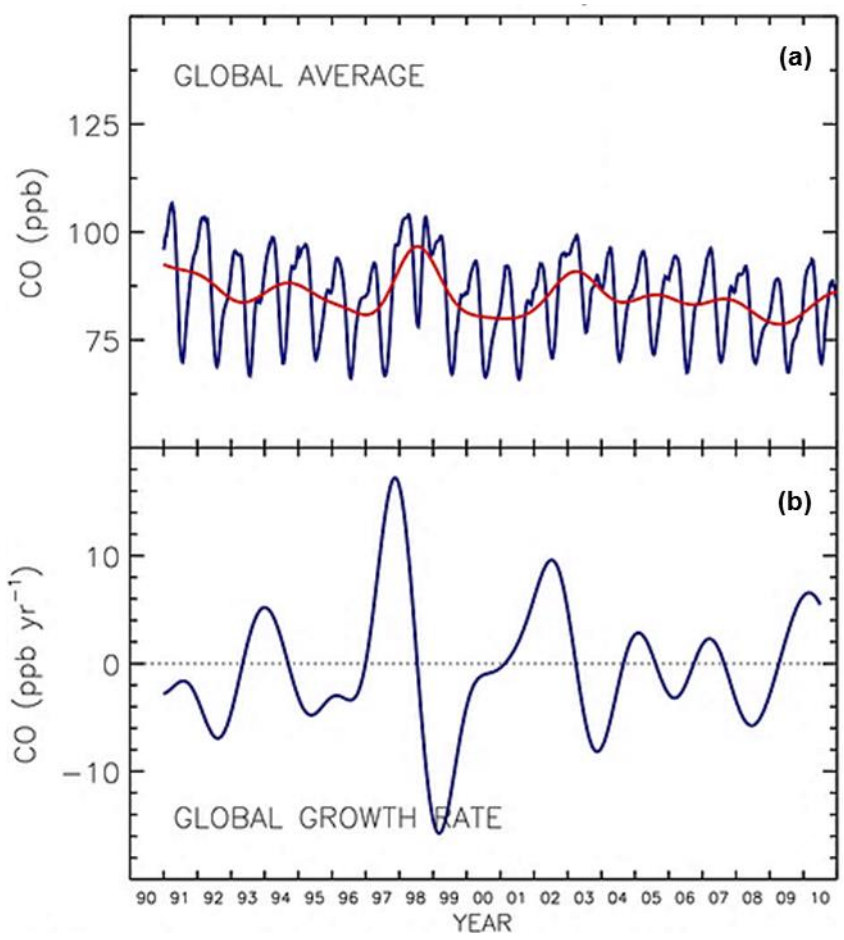

Figure 1.8(a). Global average atmospheric concentrations of CO calculated from measurements of the Carbon Cycle cooperative air sampling network during 1990-2010. The red line represents the long-term trend; **(b)** Global average growth rate for CO. *Source: Available at http://www.esrl.noaa.gov/gmd/Photo_Gallery/GMD_Figures/ccgg_figures/co_tr_global.png*

1.5. Greenhouse Gases (GHGs)

GHGs can absorb and emit long wave radiation within the thermal infrared range but not radiation in/or near the visible spectrum. GHGs are divided into primary and secondary gases. The primary GHGs in the atmosphere are water vapour, CO_2, CH_4, nitrous oxide (N_2O) and ozone (O_3) (IPCC, 2013). Nitrogen oxides (NO_x), CO, Non-Methane Volatile Organic Compounds (NMVOC) and sulphur oxides (SO_x) are considered secondary GHG. GHG concentration in the atmosphere together with

other trace gases (mostly argon) hardly ever rises above 0.001%. The remaining 99.99% is composed of nitrogen and oxygen (Hewitt et al., 2003).

GHGs warm the Earth's surface and the atmosphere via the greenhouse effect. Despite GHGs small proportion in the atmosphere, they are important for the thermal equilibrium of the planet. Small changes in GHGs atmospheric concentration can change rainfall patterns across the globe, increase ice caps melting and sea level (IPCC, 2007; 2013). Variations in the net incoming solar radiation and the outgoing long wave radiation can lead to unprecedented events on the planet.

The Earth's averaged global and annual energy balance is shown in Figure 1.9. Over the long term, the amount of incoming solar radiation incident on the upper layer of the atmosphere (342 Wm^{-2}, global average), 107 Wm^{-2} (31.2%) is reflected back to space by clouds and the Earth's surface. 168 Wm^{-2} (49.1%) of the total radiation is absorbed by the Earth and 67 Wm^{-2} (19.6%) by the atmosphere. Of the 390 Wm^{-2} emitted by surface radiation 324 Wm^{-2} (83%) are reflected back by greenhouse gases in the atmosphere and lately absorbed by the surface (IPCC, 2007).

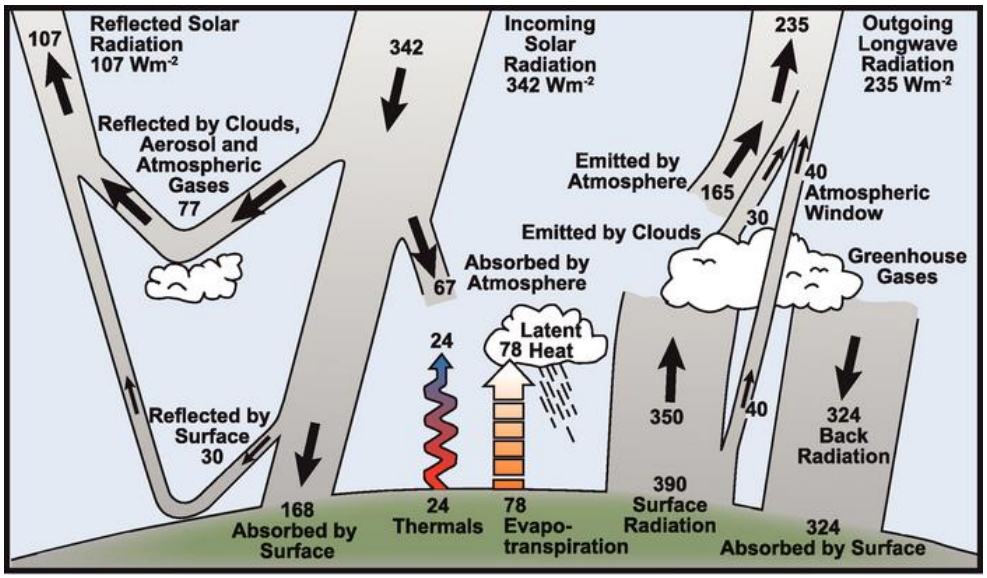

Figure 1.9. Estimate of the Earth's annual and global average energy balance. *Source: IPCC, 2007; 2013.*

Humans enhance the greenhouse effect directly by emitting large quantities of GHGs (Table 1.4). Additionally, other air pollutants such as CO, volatile organic

compounds (VOC), NO_x and SO_2, which by themselves are negligible GHGs, have indirect effects on the greenhouse effect by altering, through atmospheric chemical reactions, the abundance of important gases to the amount of outgoing LWR such as CH_4 and O_3, and/or by acting as precursors of secondary aerosols (IPCC, 2013).

Table 1.4. Increase in atmospheric concentration of CO_2 and CH_4, change in radiative forcing and global warming potential.

GHG*	Global averaged concentration (2011)	Increase in concentrations (1750-2011)	Radiative forcing due to 1750-2011 increase (W m^{-2})	Mean atmospheric lifetime (years)	Global warming potential (100 years)
CO_2	390.5 ppm	40%	1.82	5 - 200[a]	1
CH_4	1750 ppb	142%	0.48	12[b] / 8.4[c]	23

Source: Adapted from IPCC (2013)
**Greenhouse gas.*
[a]*Different rates of uptake by different removal processes, hence variable lifetime.*
[b]*Perturbation lifetime, takes into account the indirect effect of the gas on its own residence time.*
[c]*Global mean atmospheric lifetime.*

1.6. Carbon dioxide (CO_2)

CO_2 is considered the most important greenhouse gas, which contributes ~70% of the enhanced greenhouse gas effect experienced to date (IPCC, 2013). The CO_2 global average mixing ratio in 2013 was calculated as 395.31 ppm (global average concentration; NOAA/ESRL, 2014). CO_2 plays an important role both in biological and chemical processes. As part of the carbon cycle, CO_2 is used together with water to photosynthesize carbohydrates by plants, algae and cyanobacteria, with the consequent release of oxygen. It is naturally exhaled in the breath of humans and other land animals.

The turnover of carbon is vast, processed via photosynthesis and respiratory processes via ocean-atmosphere exchange (Hewitt et al., 2003). Current observations of the carbon cycle show a net global average increase in the atmospheric loading of CO_2 (NOAA/ESRL, 2014; WMO, 2014). Concerns over the current and future effects of this increased loading have led to a need for better quantification of the sources and sinks of CO_2.

1.6.1. Sources of CO_2

CO_2 is produced both from natural and anthropogenic processes. Natural sources include organic matter decomposition, ocean release and respiration, and volcanic eruptions (Figure 1.10). Anthropogenic emissions come mostly from fossil fuel combustion, cement production and biomass burning. Almost all fossil fuel combustion is related to the production of energy for human needs (Hewitt et al., 2003; IPCC, 2013). Anthropogenic sources are recognised as those governing the balance of the carbon cycle over natural sources. Figure 1.10 shows the most important natural and anthropogenic sources of CO_2. Fossil fuel combustion represents 87% of CO_2 anthropogenic emissions, with land use change 9% and industrial processes 4% (Le Quéré et al., 2013). The IPCC (2013) estimates the emissions from fossil fuels as 7.8 ± 0.6 PgC yr^{-1}, whilst the net land use change as 1.1 ± 0.8 PgC yr^{-1} (Figure 1.11).

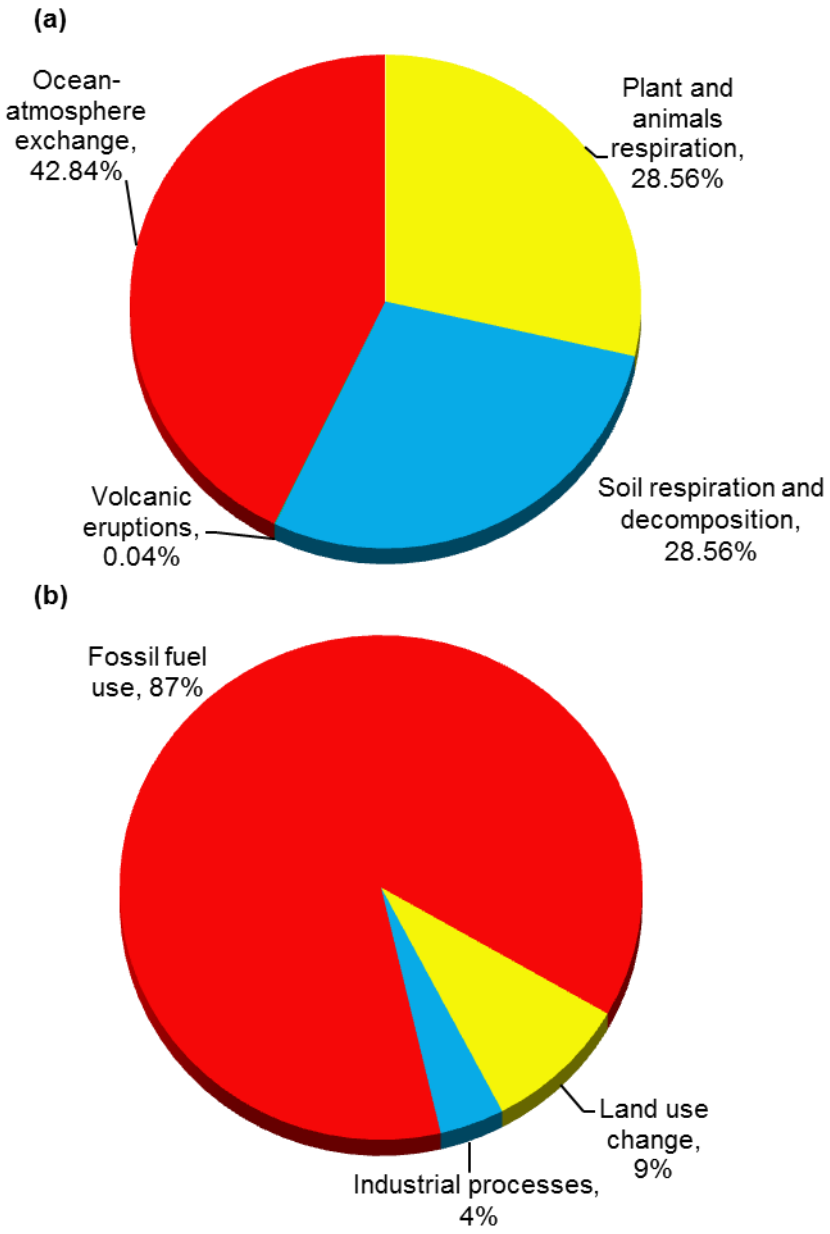

Figure 1.10(a). Natural; **(b).** Anthropogenic sources of CO_2. *Source: Adapted from IPCC, 2007; Le Quéré et al., 2013.*

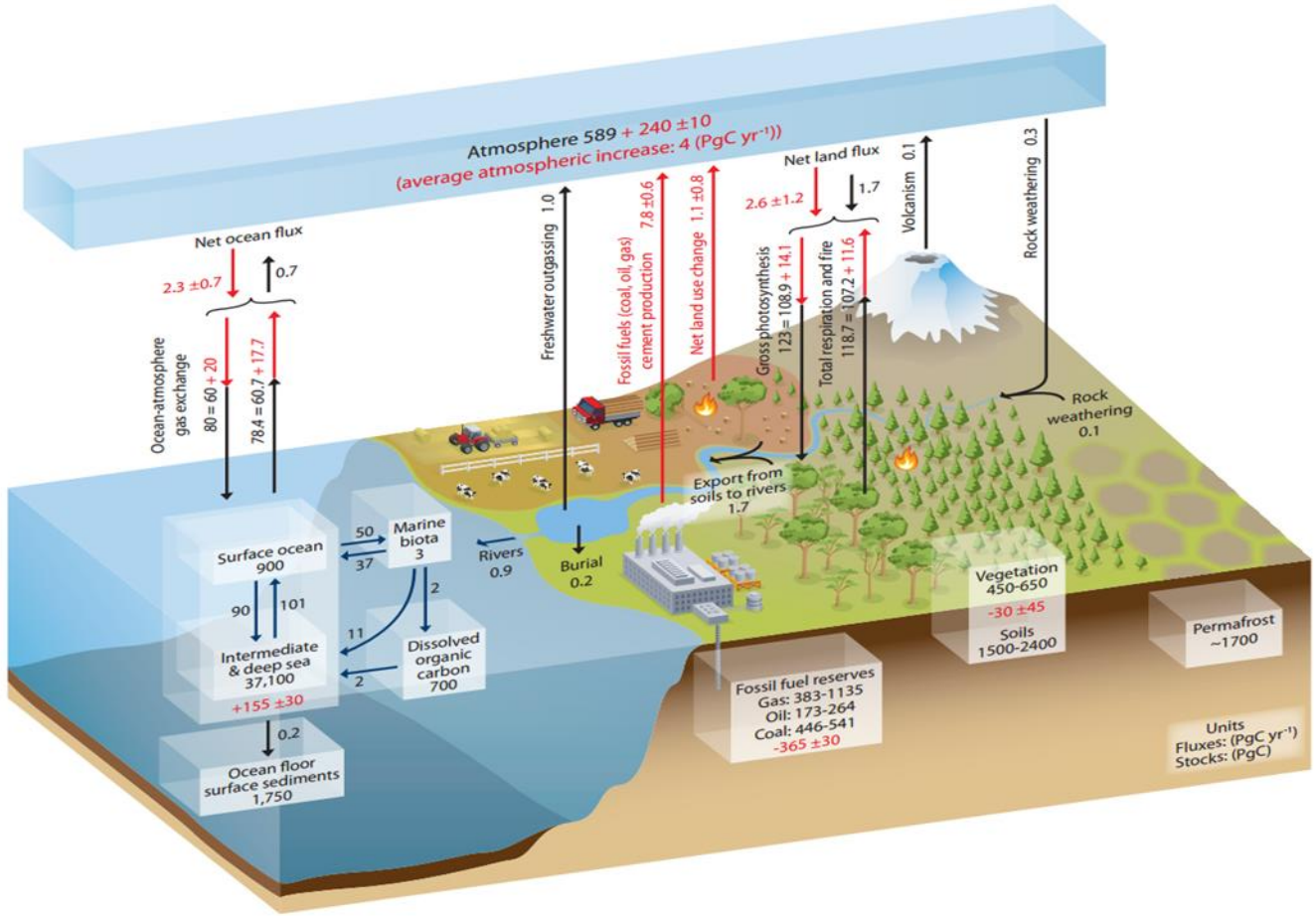

Figure 1.11. Simplified schematic of the global carbon cycle. Numbers represent carbon stocks in PgC (1 PgC = 10^{15}gC) and annual carbon exchange fluxes (in PgC yr^{-1}). Black numbers and arrows indicate reservoir mass and exchange fluxes estimated for the time prior to the Industrial Era, about 1750. Red arrows and numbers indicate annual 'anthropogenic' fluxes averaged over the 2000–2009 time period. These fluxes are a perturbation of the carbon cycle during Industrial Era post 1750. *Source: IPCC AR5 (2013).*

1.6.2. Sinks of CO_2

Carbon sequestration is the process by which CO_2 is removed from the atmosphere. CO_2 sinks can be both natural and artificial, although natural sinks are much larger than artificial sinks. The natural sinks are the oceans, which absorb CO_2 via physicochemical and biological processes, and photosynthesis by terrestrial vegetation (Equation 1.6; IPCC, 2007). Figure 1.11 shows estimated net fluxes reported in the IPCC (2013). Oceans are the largest active carbon sink on the planet. CO_2 dissolves in three different forms in the ocean: carbon dioxide form, bicarbonate and carbonate ions (Equation 1.7). The net CO_2 absorption by the oceans is 2.3 ± 0.7 PgC yr^{-1}. Forests and soils are net active sinks mostly during the growing season. The net uptake by land ecosystems is estimated in 2.6 ± 1.2 PgC yr^{-1} by gross photosynthesis (IPCC, 2013).

$$6CO_2 + 6H_2O \rightarrow C_6H_{12}O_6 + 6O_2 \quad \text{(Eq. 1.6)}$$

$$CO_2 + H_2O \leftrightarrow HCO_3^- + H^+ \quad \text{(Eq. 1.7)}$$

The net ocean and land negative fluxes have been perturbed by anthropogenic CO_2 emissions (from fossil fuel burning, cement production and land use change) since the beginning of the Industrial Era. Estimations of annual CO_2 fluxes averaged during 2000-2009 show significant changes in the negative fluxes of the carbon cycle compared with those prior to 1750. Figure 1.11 shows the most important variations in CO_2 fluxes, i.e. uptake of CO_2 by the ocean and terrestrial ecosystems (IPCC, 2013). Increases in CO_2 concentrations in the atmosphere may slightly reduce oceanic pH, which leads to a small increase in CO_2 uptake. However, increases in the ocean average temperature can reduce the solubility of CO_2. It may lead to ocean stratification and then to a global reduction in oceanic CO_2 uptake (Brasseur et al., 1999; Hewitt et al., 2003).

1.6.3. Spatial variations of CO_2

CO_2 exhibits seasonal and interannual variations that are shown in Figures 1.12 and 1.13, and which are caused by seasonal cycles in vegetation cover. The CO_2 annual cycle is made-up of a frequency of 1 cycle yr^{-1}, with the peak of the cycle in winter and the trough in summer. Figure 1.12 shows the seasonal cycle at mid-northern latitude retrieved from CO_2 records at MLO station. High winter CO_2 mixing ratios

are caused by the low height of the planetary boundary layer (PBL) and low photosynthetic activity (Dettinger and Ghil, 1998; Randerson et al., 1999). Low summer CO_2 mixing ratios are caused by the strong turbulent conditions and the high height of the PBL together with large respiration rate of vegetation. Figure 1.12 shows that the CO_2 seasonal cycle is stronger in the northern hemisphere.

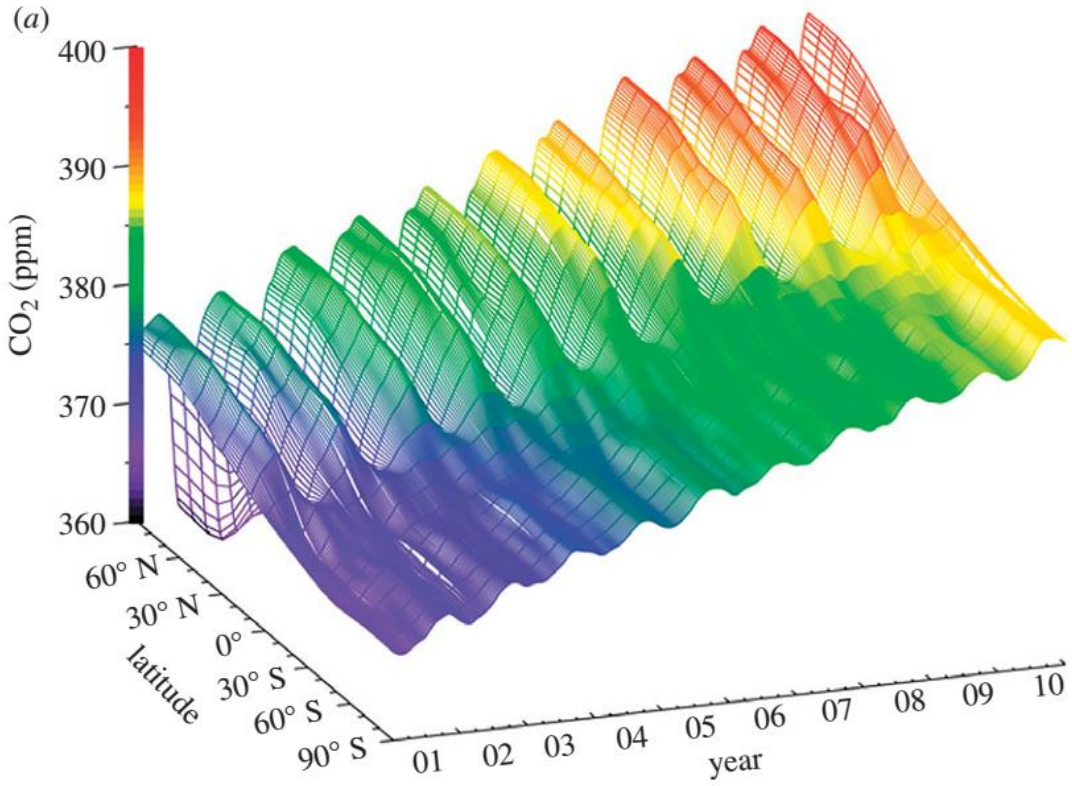

Figure 1.12. Three-dimensional representation of the latitudinal distribution of atmospheric CO_2 in the marine boundary layer, from the US NOAA/ESRL/GMD programme. Data from the Carbon Cycle cooperative global air sampling network were used. The surface represents data mathematically smoothed in time and latitude (Tans et al., 2012; NOAA/ESRL/GMD Carbon Cycle Greenhouse Gases Group, Boulder, CO, USA). *Taken from: http://www.esrl.noaa.gov/gmd/Photo_Gallery/ GMD_Figures/ccgg_figures/).*

1.6.4. Temporal variations of CO_2

The CO_2 atmospheric concentration has increased about 40% since the beginning of the Industrial Era (Table 1.4). It increased from approximately 277 ppm in 1750 (Le Quéré et al., 2013 and references therein) to 395.31 ppm in 2013 (NOAA/ESRL, 2014). Moreover, measurements of air trapped in Antarctic ice cores have indicated that atmospheric CO_2 concentrations fluctuated between 200 and 280 ppm during

the past 200,000 years, until the nineteenth century (IPCC, 1995; Brasseur et al., 1999). The CO_2 atmospheric increase was caused mostly by the release of carbon to the atmosphere from fossil fuel combustion, and to a lesser extent, deforestation and land use change (IPCC; 2001; Ciais et al., 2013).

Direct measurements of atmospheric CO_2 were started by Professor Charles Keeling of the Scripps Institution of Oceanography in March of 1958 at a facility of the National Oceanic and Atmospheric Administration at Mauna Loa (MLO), Hawaii (Keeling et al., 1976). The National Oceanic and Atmospheric Administration (NOAA) started to measure CO_2 at MLO in May of 1974, and more recently at other monitoring stations across the globe (Figure A1.2). At MLO, CO_2 daily averages over 400 ppm were recorded for the first time in May 2013 (NOAA/ESRL, 2014). Figure 1.13(a) shows the global average of atmospheric CO_2 using measurements from the Carbon Cycle cooperative air sampling network. It spans from 1979 to 2010.

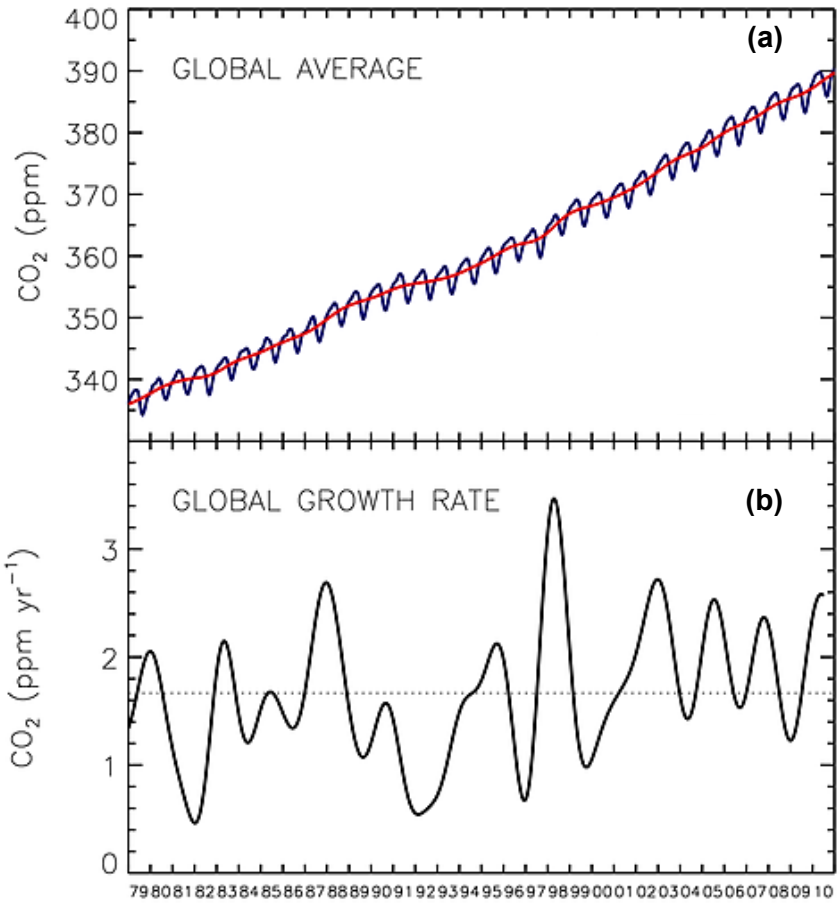

Figure 1.13(a). Global average atmospheric CO_2 concentrations determined from measurements carried out by the Carbon Cycle cooperative air sampling network. The red line represents the long-term trend; **(b).** Global average growth rate for CO_2 *Source: Available at http://www.esrl.noaa.gov/gmd/ccgg/trends/ index.html*

Figure 1.13(b) illustrates the global average growth rate of CO_2. Global growth rates during the period represent have ranged from 0.4 to 3.6 ppm yr^{-1} (NOAA/ESRL, 2014), and are in good agreement with records at MLO, where annual increases of CO_2 have ranged from 0.28 (1964) to 2.93 (1998) ppm yr^{-1}. Similarly, at the South Pole (SPO) monitoring station, CO_2 growth rates during 1976-2012 ranged from 0.84 (1992) to 2.45 ppm yr^{-1} of CO_2 (1997) (NOAA/ESRL, 2014), and corroborate the linear increasing trend of atmospheric CO_2 observed worldwide.

1.7. Methane (CH_4)

CH_4 is the second most important GHG in the atmosphere after CO_2. It is 23 times more efficient than CO_2 at trapping the outgoing long wave radiation, on a 100 years time-scale (IPCC, 2007). This makes the additional radiative forcing due to methane (~0.5 W/m^2) around 1/3 of that due to CO_2 in the atmosphere. CH_4 is the most abundant VOC in the atmosphere and has a significant effect on atmospheric chemistry (Hewitt et al., 2003). It affects the oxidising capacity of the atmosphere and acts as precursor of tropospheric ozone.

The average atmospheric lifetime of CH_4 is estimated to be 12.4 years (IPCC, 2013). During 1990s and 2000-2005, atmospheric CH_4 increase dropped, but since 2006 it has been increasing constantly (NOAA/ESRL, 2014). To understand the CH_4 budget and current trend it is important to study and monitor its concentration and evolution over different time scales.

1.7.1. Sources of CH_4

CH_4 can be produced by natural and anthropogenic processes. Natural sources account for about 30% of the global CH_4 emissions. Tropical and subtropical wetlands are the largest natural source of CH_4 on the planet. Other minor natural sources of CH_4 are the oceans and lakes and rivers. Anthropogenic sources account for 50 to 65% of CH_4 total emissions (IPCC, 2013). These include agriculture, landfills, livestock farming, and production, transportation and use of fossil fuels (Figure 1.14). From these, fossil fuels use is the largest CH_4 source (29%) followed by ruminants (27%) and landfills (23%).

About 95% of animal CH_4 emissions are produced by domestic ruminants via microbial digestion in the digestive tract and from microbial degradations of excreted residues in manure (Johnson et al., 2000). Rice cultivation contributes with 11% of the total CH_4 emissions; the majority of them in the 15-35° N region. These are thought to have contributed importantly to current CH_4 atmospheric levels during the last century though its rate of increase slowed in the 1990s (IPCC, 1996; Neue et al., 1997).

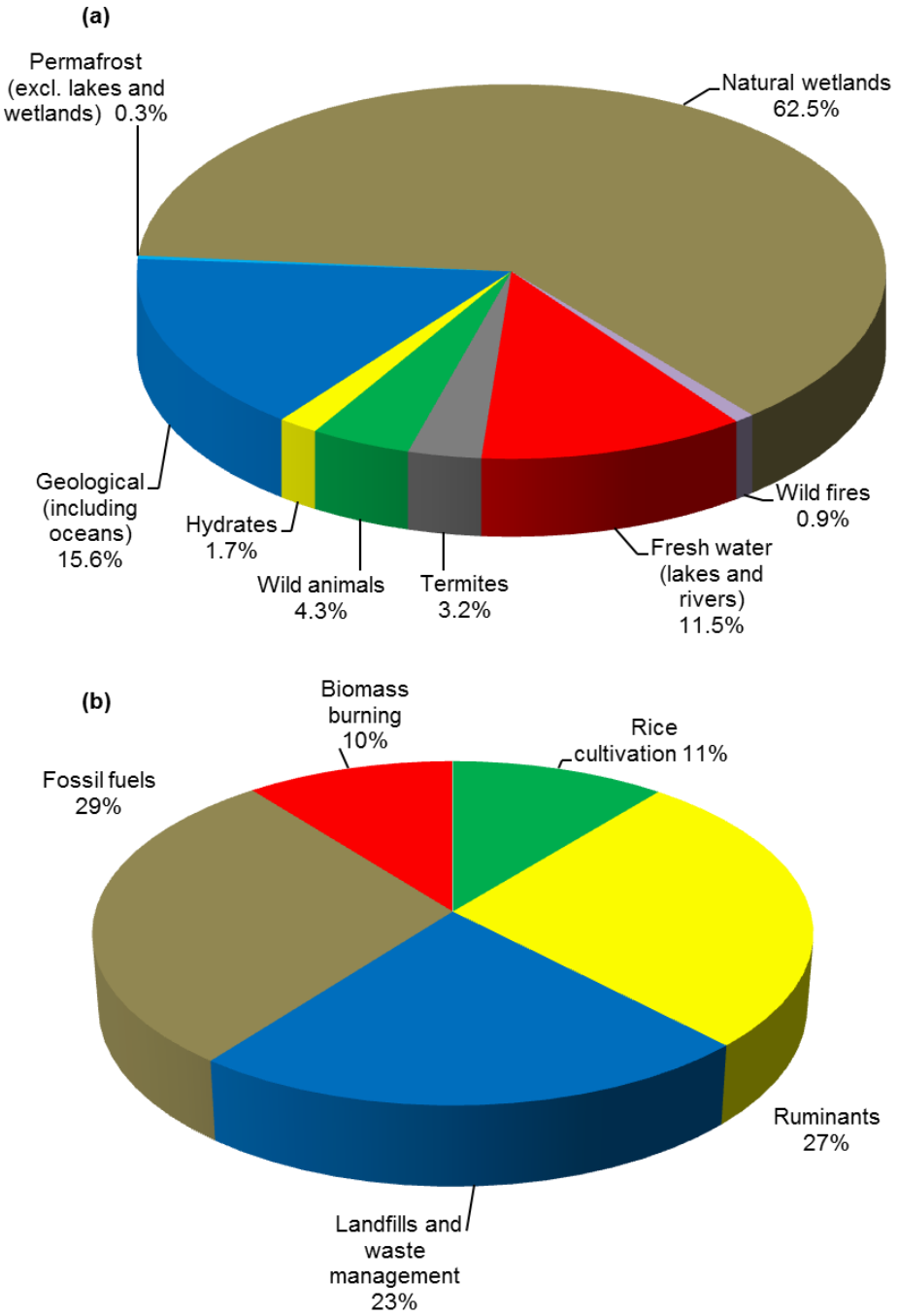

Figure 1.14(a). Natural; **(b).** Anthropogenic sources of CH_4. *Source: IPCC, 2013.*

1.7.2. Sinks of CH_4

The primary sink for atmospheric CH_4 is oxidation by hydroxyl radicals (OH), mostly in the troposphere. It accounts for about 90% of the global CH_4 sink (Levy, 1972; 1973a,b). These series of reactions generate formaldehyde as the first stable product. To produce OH radicals, an important process of radical initiation in the troposphere is required. It is the photolysis of O_3 and the reaction of the resulting excited oxygen radical $O(^1D)$ with H_2O (Reaction 1.9).

$$O_3 \xrightarrow{h\nu} O_2 + O(^1D) \qquad \text{R 1.8}$$

$$O(^1D) + H_2O \rightarrow 2OH \qquad \text{R 1.9}$$

OH radicals have a very short lifetime in the order of one second, and most of the OH radicals are used up in the reaction with CO (Hobbs, 2000).

$$CO + OH \rightarrow CO_2 + H \qquad \text{R 1.10}$$

$$H + O_2 + M \rightarrow HO_2 + M \qquad \text{R 1.11}$$

The species that removes the excess of energy and stabilises the HO_2 radical is represented by M, but does not participate in the reaction. In urban areas, where a rich environment in NO_x concentrations exist, reactions of HO_2 with NO produce OH radicals and lead to net ozone production (Equation 1.12-13). Low concentrations of NO_x cause ozone destruction by reacting with the OH_2 radical (Equation 1.14).

$$HO_2 + NO \rightarrow OH + NO_2 \qquad \text{R 1.12}$$

$$NO_2 + O_2 \xrightarrow{h\nu} NO_2 + O_3 \qquad \text{R 1.13}$$

$$O_3 + HO_2 \rightarrow O_2 + OH \qquad \text{R 1.14}$$

NO_x is crucial to determine the recycling of HO_2 and CH_3O_2 to OH. Under high NO_x concentrations, the series of reactions yield CH_2O and CH_3OH.

$$CH_3O_2 + HO_2 + M \rightarrow CH_3O_2H + O_2 + M \qquad \text{R 1.15}$$

$$CH_3O_2 + CH_3O_2 + M \rightarrow CH_2O + CH_3OH + O_2 + M \qquad \text{R 1.16}$$

Additional oxidation sinks include methanotrophic bacteria in aerated soils (~4%), reactions with chlorine radicals and atomic oxygen radicals in the stratosphere (~3%), and reactions with chlorine radicals from sea salt in the marine boundary layer (~3%) (Johnston and Kinnison, 1998; Kirschke et al., 2013).

$$CH_4 + 2O_2 \rightarrow CO_2 + 2H_2O \quad \text{R 1.17}$$

$$CH_4 + Cl_2 \rightarrow CH_3Cl + HCl \quad \text{R 1.18}$$

1.7.3. Spatial variations in CH_4 concentrations

CH_4 atmospheric concentrations are largely influenced by variations in natural and anthropogenic emissions. The larger sources of CH_4 are located in the northern hemisphere, which causes a marked inter-hemispheric gradient in atmospheric CH_4 concentrations. On average, CH_4 concentrations in the northern hemisphere are about 100-150 ppb higher than in the southern hemisphere (Wahlen, 1993; Dlugockenky et al., 2011; NOAA/ESRL, 2014). Time series records of CH_4 at different latitudes uncover a seasonal cycle in atmospheric CH_4 concentrations. Figure 1.15 reveals the dominance of the CH_4 northern sources. The plot shows a seasonal cycle with larger amplitudes in the northern hemisphere (Manning et al., 2011).

In the northern hemisphere the seasonal cycle is mainly determined by variations in the source strengths during the year. In contrast, in the southern hemisphere the cycle is driven by the oxidation of CH_4 by OH, i.e. loss. The amplitudes of the CH_4 seasonal cycles in the northern hemisphere range between 40-60 ppb and diminish towards the equator. In the southern hemisphere, CH_4 seasonal amplitudes are smaller about 30 ppb and opposite in phase to those at northern latitudes (Dlugokencky et al., 2011).

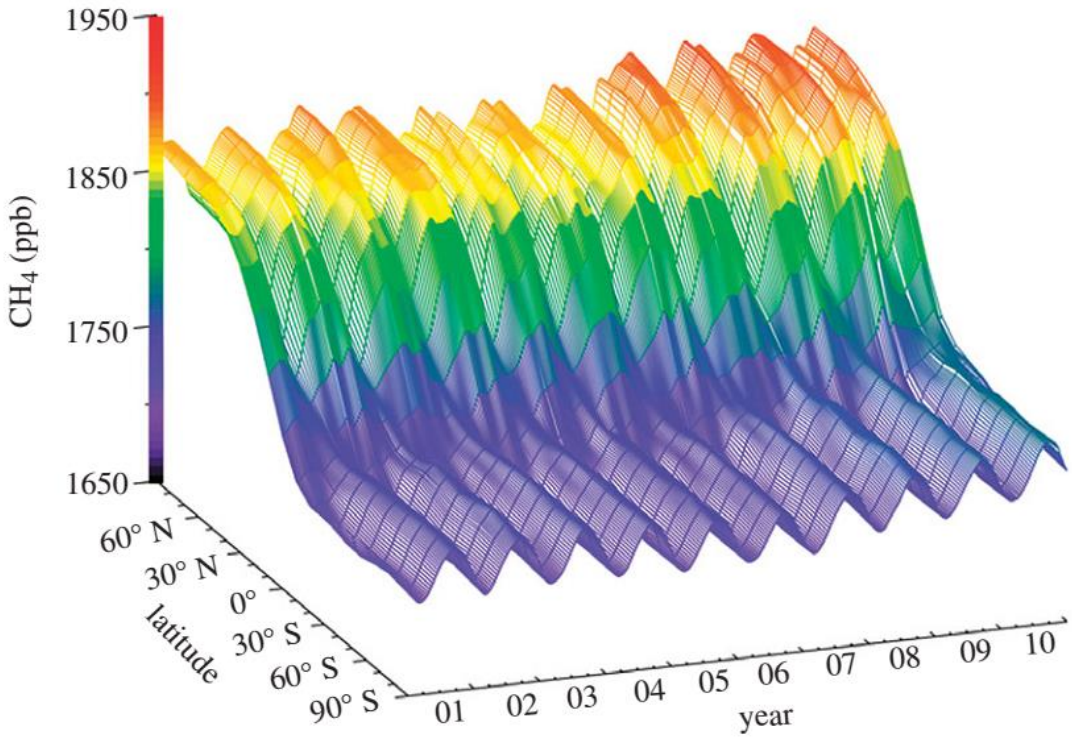

Figure 1.15. Three-dimensional representation of the latitudinal distribution of atmospheric CH_4 in the marine boundary layer, from the US NOAA/ESRL/GMD programme. Data from the Carbon Cycle cooperative global air sampling network were used. The surface represents data mathematically smoothed in time and latitude (Dlugokencky et al, 2011; NOAA/ESRL/GMD Carbon Cycle Greenhouse Gases Group, Boulder, CO, USA). *Source: Available at http://www.esrl.noaa.gov/gmd/Photo_Gallery/GMD_Figures/ccgg_figures/).*

1.7.4. Temporal variations of CH_4

Reconstructions of CH_4 atmospheric concentrations for the last 420,000 years have been made from air bubbles trapped in the Vostok ice core in Eastern Antarctica (Petit et al., 1999). The data reveal that CH_4 concentrations have naturally oscillated between 300-700 ppb due to variations in the orbit of the Earth around the sun. However since the industrial revolution, CH_4 levels have increased exponentially from about 850 ppb to 1819 ppb in 2012 (WMO, 2014; Table 1.4; Figure 1.16(a)). It is widely accepted that such an increase is due to large CH_4 emissions from anthropogenic activities, linked to increases in the industry and agriculture (IPCC, 2013).

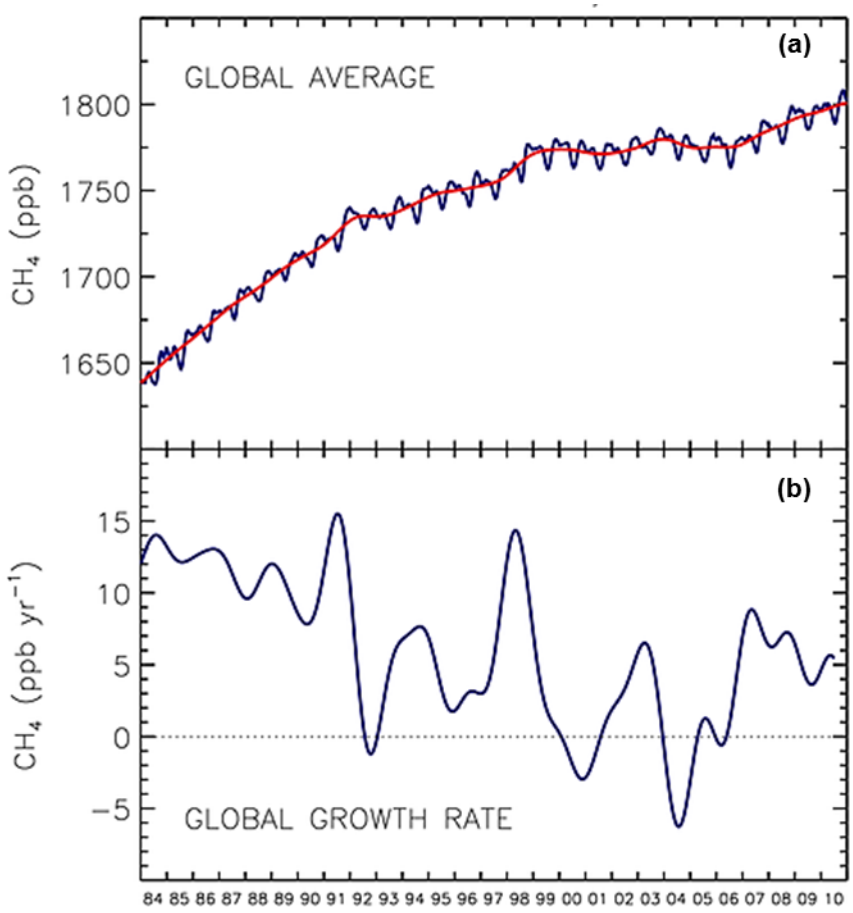

Figure 1.16(a). Global average atmospheric CH_4 concentrations determined from measurements carried out by the Carbon Cycle cooperative air sampling network. The red line represents the long-term trend; **(b).** Global average growth rate for CH_4. *Source: Available at http://www.esrl.noaa.gov/gmd/ccgg/trends/index.html*

Continuous data recorded since 1978 reveal that during the 1980s there was a sustained increase of atmospheric CH_4 concentrations (12 ± 6 ppb yr^{-1}). Then, during 1990s a slowdown in growth was observed, and steady concentrations were seen from 1999 to 2006 (Rigby et al., 2008a; Dlugokencky et al., 2011). But since 2007, CH_4 concentrations have increased again and reached 1819 ppb in 2012 (NOAA/ESRL, 2014; Figure 1.16). This increment reveals a recent imbalance between sources and sinks, which is not yet completely understood. Therefore, to understand this imbalance it is important to interpret regional CH_4 records.

1.8. The Air Quality Strategy and The UK Climate Change Act

1.8.1. The Air Quality Strategy

The 1995 Environment Act requires the UK Government and the devolved administrations for Scotland and Wales to produce a national air quality strategy containing standards, objectives and measures for improving ambient air quality and

to keep these policies under review. Air quality in the UK has improved since 1997 when the first Air Quality Strategy was adopted. In January 2000, it was replaced by the Air Quality Strategy for England, Scotland, Wales and Northern Ireland. It established the framework for achieving further improvements in ambient air quality in the UK to 2003 and beyond. The strategy identified actions at local, national and international level to improve air quality. It was followed by an Addendum in February 2003 (Defra, 2007).

The air quality objectives in the Air Quality Strategy are a statement of policy intentions or policy targets. The aim was a steady decrease in ambient levels of pollutants towards the objectives over the period of implementation, and to sustain the improvement. Social considerations and economical goals were considered to determine the appropriate levels of such objectives. For CO, the objective set was to achieve 10 mg m^{-3} as maximum daily 8-hour running mean. The 31st of December 2003 was the date fixed to achieve the objective and has been maintained since then. This concentration is the same stated in the EU Ambient Air Quality Directive of 10 mg m^{-3}.

An evaluation of the Air Quality Strategy was performed in January 2005. Air quality policies in the road transport and electricity generation sectors were assessed to verify their effectiveness in achieving air quality improvements. Such evaluation reported major positive impacts in the road transport and the electricity generation sectors in reducing air pollutants emissions. The fitting of catalytic converts to motor vehicles and the increased use of gas to generate electricity were particularly important. However the most important benefit was the improvement of human health (Defra, 2007).

1.8.2. The UK Climate Change Act

The Kyoto Protocol to the United Nations Framework Convention on Climate Change (UNFCCC) was established in 1997 in response to the threat of dangerous climate change. Under it, the UK agreed to an emissions reduction target of -12.5% on 1990 levels, to be achieved during the first commitment period of the Protocol, which ran from 2008 to 2012 (Climate Change Act, 2008).

The UK Climate Change Act became part of UK law in November 2008. It introduced a new and more ambitious and legally binding target for the UK to

reduce GHG emissions to 80% below base year levels by 2050. This will be implemented by way of legally binding five year Carbon Budgets. In May 2009, the UK Government set the levels of the first three five-year carbon budgets, which cover the periods 2008-12, 2013-17 and 2018-22.The fourth carbon budget which covers the period 2023-27, was set in June 2011. In December 2011, the UK's Carbon Plan, which sets out plans for achieving the first four carbon budgets, superseded the UK's Low Carbon Transition Plan, which was published in July 2009. The Annual statement of emissions is published by 31st March each year, it reports to the UK Parliament the progress towards these Carbon Budgets. Finally, the fourth Annual Statement, in relation to the 2011 reporting year, was published in March 2013 (Climate Change Act 2008; DECC, 2014).

1.8.3. The UK Greenhouse Gas Inventory

The UK ratified the United Nations Framework Convention on Climate Change (UNFCCC) in December 1993, and the Convention came into force in March 1994. Parties to the Convention are committed to develop, publish and regularly update national emission inventories of GHGs. The UK's National Inventory Report (NIR) submitted in April 2013, contains GHG emissions estimates for the period 1990 to 2011, and describes the methodology on which the estimates are based. The UK GHG inventory aims to include all anthropogenic sources of GHGs.

The UK Greenhouse Gas Inventory contains estimates for emissions of six categories:

1. Energy
2. Industrial Processes
3. Solvent and Other Product Use
4. Agriculture
5. Land Use, Land Use Change and Forestry Emissions
6. Waste

The inventory covers the six direct greenhouse gases under the Kyoto Protocol. These are as follows:

- Carbon dioxide (CO_2)
- Methane (CH_4)
- Nitrous oxide (N_2O)

- Hydrofluorocarbons (HFCs)
- Perfluorocarbons (PFCs)
- Sulphur hexafluoride (SF_6)

The inventory also reports four indirect greenhouse gases:

- Nitrogen dioxide (NO_2)
- Carbon monoxide (CO)
- Non-Methane Volatile Organic Compounds (NMVOC)
- Sulphur oxides (SO_2)

The research in this thesis will only assess data concerning CO_2, CH_4 and CO emissions. Total emissions of direct greenhouse gases have decreased by about 26% between 1990 and 2012 (Table 1.5). Such decline is driven predominantly by a decrease in emissions from the energy sector and particularly from power stations. Since 1990, emissions from the energy sector have declined by about 24%. In 2011, this contributed 84% to the total emissions. Such decline has been driven predominantly by the shift towards use of combined cycle gas turbine (CCGT) stations rather than conventional steam stations burning coal or oil. Differences in efficiency between CCGT (which operate at 47.7%) and coal-fired stations (which operate on-average at 36%) with larger requirements of coal/oil to generate (therefore larger CO_2 emissions) the same quantity of energy that CCGT could explain that decrease. The calorific value of natural gas per unit mass carbon is higher than that of coal and oil. A slight increase in electricity generated from non-fossil fuels energy sources could also contribute to the decline observed in CO_2 emissions (GGI, 2014; NAEI, 2014).

Table 1.5. Emissions by sector in 1990 and 2011, the emissions trend and share of the total.

Sector	Emissions (Mt CO_2e)		Trend	Share	
	1990	2011	1990-2011	1990	2011
Energy	610.76	465.95	-24%	79%	84%
Industrial Processes	54.40	26.47	-51%	7%	5%
Solvent and Other Product Use	-	-	N/A	0%	0%
Agriculture	58.15	46.67	-20%	8%	8%
LULUCF*	4.02	-3.31	-182%	1%	-1%
Waste	47.48	17.36	-63%	6%	3%
Grand Total	774.81	553.15	-29%	100%	100%

**Land Use and Land Use Change and Forestry. Source: Adapted from UK Greenhouse Gas Inventory, 2013.*

1.8.4. Trends in CO_2, CH_4 and CO emissions and UK Greenhouse Gas and National Emissions Inventory

1.8.4.1. Trends in CO_2 emissions

Total CO_2 emissions in the UK in 2011 were recorded at 460.7 Mt CO_2 equivalent. These are 22.4% below the 1990 level. The declining trend in CO_2 emissions is shown in Figure 1.17. Figure 1.18 shows that total emissions of CO_2 are dominated by the energy sector, which is the main driver for the declining trend in emissions (UK GHGI, 2013). In contrast, CO_2 emissions from industrial processes remained almost constant during the period. Land Use and Land Use Change and Forestry (LULUFC) and waste CO_2 emissions are considered negligible.

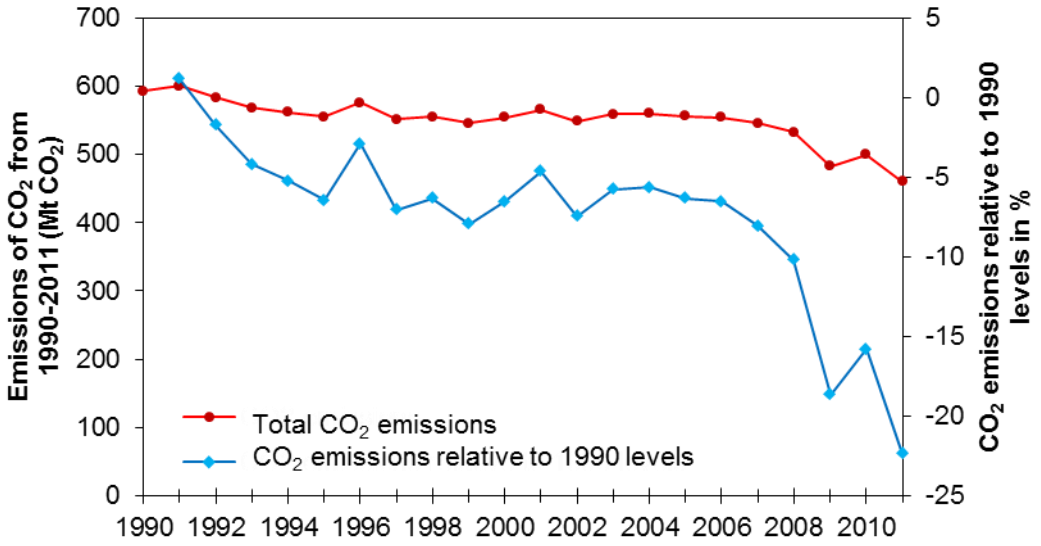

Figure 1.17. Trend in UK CO_2 emissions from 1990 to 2011. *Source: Adapted from UK Greenhouse Gas Inventory, 2013.*

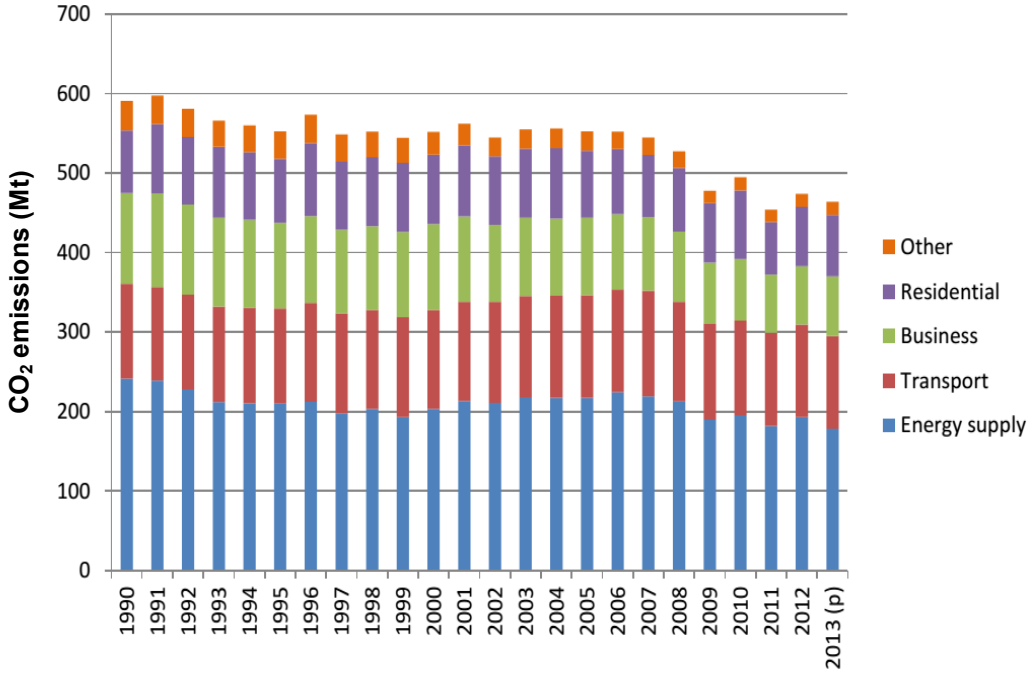

Figure 1.18. UK CO_2 emissions trend by source from 1990 to 2011. *Source: Adapted from UK Greenhouse Gas Inventory, 2013.*

1.8.4.2. Trends in CH_4 emissions

In the UK, CH_4 is the second most emitted GHG after CO_2. The main sources of CH_4 are agriculture, waste management and disposal, leakage from the gas distribution system and coal mining (Figure 1.19). The LULUCF and industrial processes sectors are considered not significant in terms of CH_4 emissions compared to the other sectors. CH_4 emissions in 2011 were recorded at 42 Mt CO_2 equivalent (UK GGI, 2014). These emissions represent 57.3% of the total CH_4 emissions in 1990 (Figure 1.20). The observed decline in emissions since 1990 has three main reasons:

- In the energy sector, emissions have decreased about 73.4% due to a reduction in coal mining activity, and improvements to the gas distribution network. This decrease represents a reduction about 39.9% of the total CH_4 emissions in the UK.
- In the waste sector, a decrease of 64.7% has been observed due to the implementation of CH_4 recovery and utilisation systems at landfill sites. Since 1990, a decrease of 51.6% of the total CH_4 emissions is ascribed to the reduction from this sector.
- In the agriculture sector, since 1990 CH_4 emissions have decrease about 20.6%. It is related to the declining trend of livestock numbers.

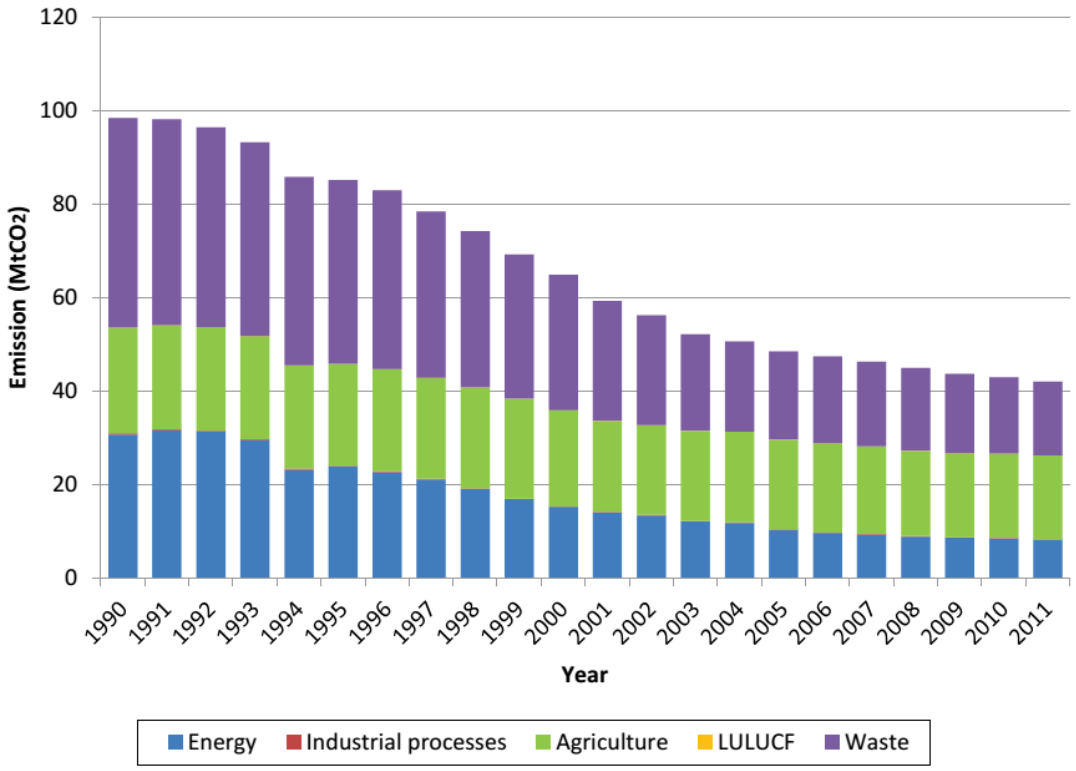

Figure 1.19. UK CH_4 emissions trend by source from 1990 to 2011. *Source: Adapted from UK Greenhouse Gas Inventory, 2013.*

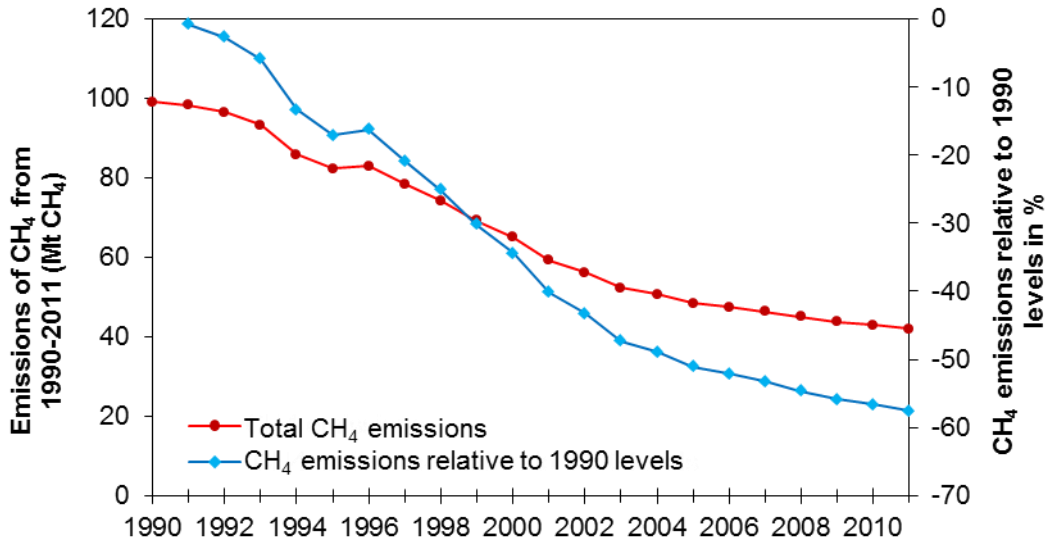

Figure 1.20. Trend in UK CH_4 emissions expressed as Mt $CO_{2\ eq}$ from 1990 to 2011. *Source: Adapted from UK Greenhouse Gas Inventory, 2013.*

1.8.4.3. Trends in CO emissions

In the UK, the largest source of CO emissions is the energy sector. CO emissions have decreased by 76% since 1990. Figure 1.21 shows the CO emissions trend

during 1990-2011. In 2011, the total emissions of CO were 2,015 kt. During this year, CO emissions from the energy sector contributed 93% to overall UK emissions. Of that, 40% of emissions correspond to the transport sector. Regarding this, emissions have declined by 87% since 1990 (UK NAEI, 2013). It is mainly due to the increased use of the three way catalysts, and to a lesser extent to the switch in fuel from petrol to diesel cars. Emissions from biomass combustion and petrol use in off-road vehicles within the manufacturing, industry and combustion contributed 31% to overall emissions of CO in 2011.

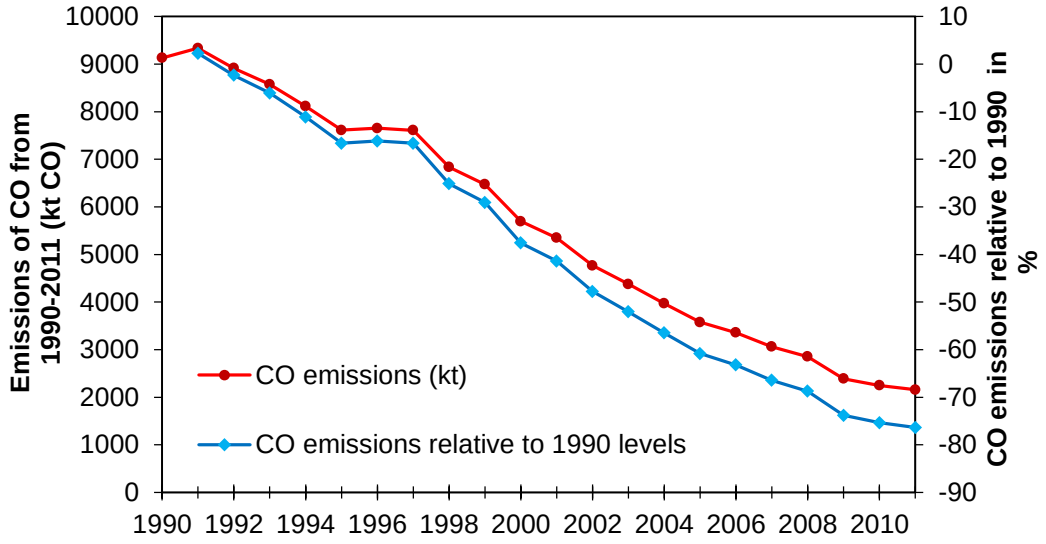

Figure 1.21. Trend in UK CO emissions from 1990 to 2011. *Source: Adapted from UK Greenhouse Gas Inventory, 2013.*

1.9. Aims and Objectives of this Research

1. To interpret EGH data for the period 2000 to 2012 on hourly, daily, weekly, monthly, seasonal and long-term scales of CO_2, CO and CH_4.

2. To evaluate sources and trends of CO_2, CO and CH_4.

3. To understand the origins of high concentrations of CO_2, CO and CH_4 in the SW of London, and to predict changes in response to measures to control their emissions.

2. METHODOLOGY

2.1. Site Location

Measurements of atmospheric CO_2, CO and CH_4 were made from 2000 to 2012 (and continuing) at the Greenhouse Gas Laboratory of the Earth Sciences Department (GGLES) at Royal Holloway University of London (RHUL). RHUL (i.e. the EGH site) is situated in Egham Surrey, UK (51°25'35.99" N, 0°33'39.66" W; Figure 2.1(a)), 32 km WSW of the City of London on the first significant incline to the west of the conurbation (Figure 2.1(b)). The laboratory is about 45 m mean above sea level, and 30 m above the level of the nearby Thames Floodplain. Figure 2.1(c) shows the air inlet, which is located approximately 15 m above ground level, above the roof of the Earth Sciences building. This single length of Synflex ½-inch OD tubing enters the lab and is connected to a KNF-Neuberger pump which pulls the air through the inlet at 20 litres / min. After the pump the airline splits and feeds all of the measurement instruments.

The EGH site is approximately 7 km SW of the London Heathrow Airport perimeter. Windsor Great Park is located around 2 km west of the site, and covers an area of 30 km^2. To the SW is a predominantly sub-urban area of clusters of housing interspersed with woodland and the Surrey heathlands. The E sector is dominated by the London conurbation (Lowry et al., 2001). It makes EGH ideal for local, regional, and background studies.

2.2. Meteorology

The climate at the EGH site is mild and maritime, with widely varying wind directions. Southwesterly and northwesterly winds are most common, as depressions track across the United Kingdom, but easterly winds are frequent in anti-cyclonic conditions. Northeasterly winds occur regularly in spring and autumn. Relatively clean air arrives at the sampling site from the SW. In background conditions air pollutant concentrations should be similar to the contemporary Atlantic background control samples from Mace Head, Ireland. Thus the seasonal background variation can be well constrained. In contrast, easterly air trajectories pass over the whole London urban area before arrival at EGH.

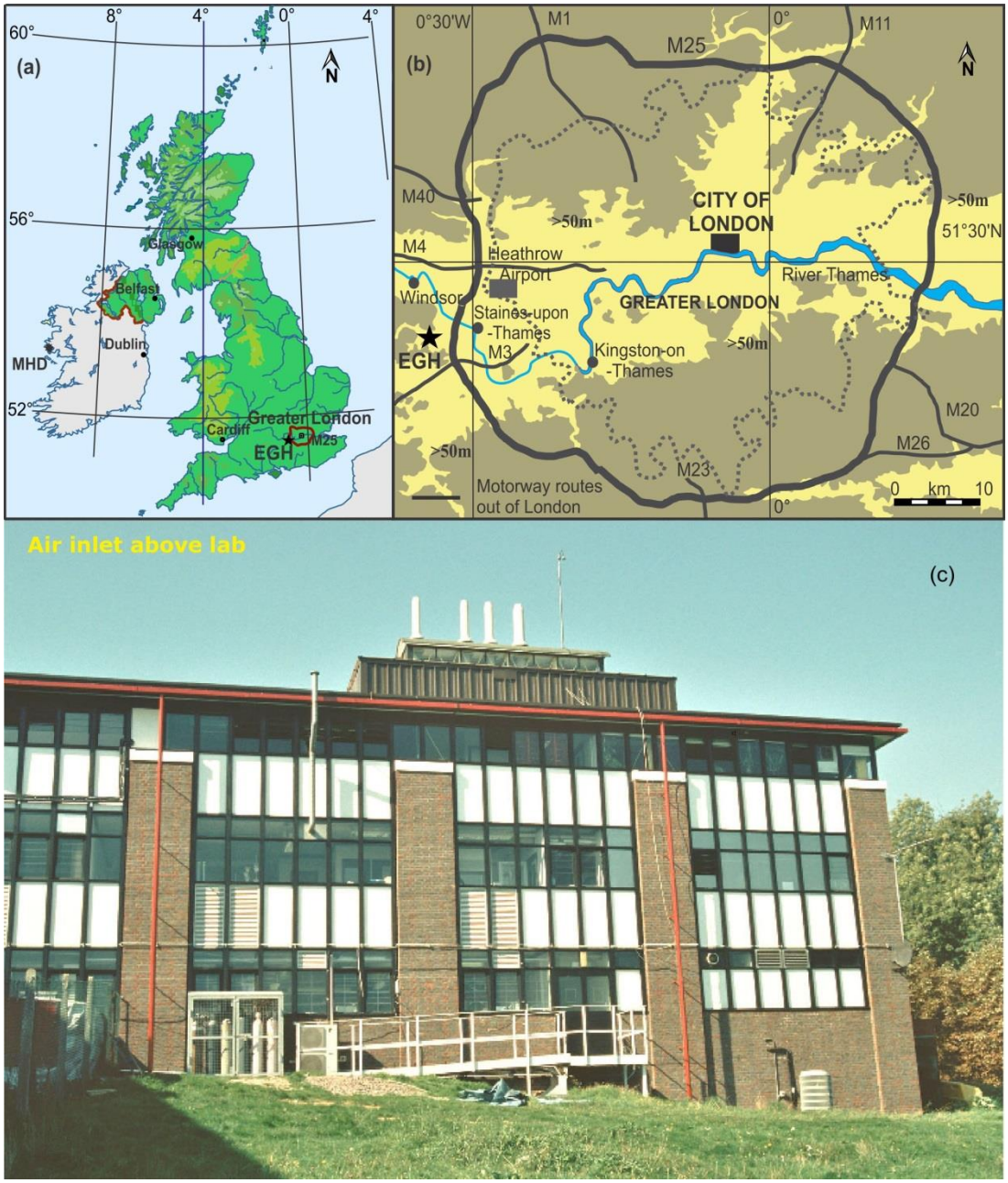

Figure 2.1(a). The EGH site, M25 motorway and greater London area in the national context; **(b).** The EGH site at RHUL in relation to central London and the Greater London motorway network; **(c).** Physical location of the air inlet on the roof of the department of Earth Sciences at RHUL.

During slow-moving anti-cyclonic air conditions in winter and early spring, the initial relatively clean air is augmented by emissions from the London basin and continental Europe. Such widespread conditions may persist for several days or more, with primary air pollutants accumulating as the blanketing temperature inversion rises and falls (Lowry et al., 1998), and thus CO_2, CO and CH_4 data

recorded at EGH may be regarded as a broad proxy for air quality in the London area.

Trajectories for south-westerly air streams typically approach above the English Channel and descend over 80-100 km of rural and sub-urban areas before reaching EGH. Air masses from the NE often pass over the North Sea from Arctic regions, then over 80-100 km of rural East Anglia before reaching NW London and on to EGH (Lowry et al., 2001).

2.3. Sampling, instrumentation and calibrations

2.3.1. CO_2 measurement methodology, instrumentation and calibration

CO_2 was measured in air continuously drawn in through the air inlet located approximately 15 m above ground level, on the roof of the Earth Sciences building (Figure 2.1(c)). CO_2 was measured continuously at the EGH site at time-intervals of 5 mins to 10 secs during January 1st 2000 to December 31st 2012. Between 2000 and 2009, a LiCor 6252 non dispersive infrared analyser was used to measure CO_2 (Table 2.1). This instrument was operated in absolute mode with the reference cell filled with zero air and scrubbed with soda lime to maintain 0 ppm CO_2 in the cell. Before 2007, data were logged at 5-min intervals, but after 2007 data were logged at 1-minute intervals to be more consistent with European stations in the GeoMon project (GeoMon, 2014).

During 2009, a Picarro G1301 cavity ringdown spectrometer (CRDS) was run in direct comparison with the LiCor instrument, before becoming the primary instrument to measure CO_2 from 2010 to the present. The CRDS outputs a CO_2 measurement at approximately 10-second intervals and these are 1-minute averaged. Both instruments were calibrated using NOAA calibration gases. From 2000 to 2007 two standards of 372.1 and 420.1 ppm CO_2 were analysed daily to account for drift and span corrections. In 2008 the 372.1 ppm CO_2 standard was replaced by a 378.9 ppm calibration gas, and in 2010 the 420.1 ppm standard replaced by a 415.4 ppm calibration gas. The CRDS was calibrated during 2010 and 2011 using the replacement NOAA gases. Since 2012, air standards with 380.3, 394.9 and 420.1 ppm CO_2, that were prepared at MPI-Jena and calibrated against NOAA standards as part of the IMECC project (IMECC, 2014), have been analysed weekly.

Table 2.1. Instrumentation used to measure CO_2, CO and CH_4, precision, frequency and periods of operation during 2000-2012 at the EGH site.

Gas	Period	Instrument	Precision	Measurement frequency
CO_2	1999-2009	Licor 6252	± 0.1 ppm	1999-2006 (every 5 min) 2007-2009 (every 1 min)
	2010-2012	Picarro G1301	± 0.05 ppm	2010-2012 (every 10 sec)
CH_4	1995-2009	HP 5890 GC-FID	± 4 ppb	1995-2009 (every 30 min)
	2010-2012	Picarro G1301	± 0.3 ppb	2010-2012 (every 10 sec)
CO	1996-2007	Trace Analytical RGD-2	± 2 ppb	1996-2007 (every 30 min)
	2008-2012	Peak Performer 1	± 1 ppb	2008-2012 (every 5 min)

2.3.2. CO measurement methodology, instrumentation and calibration

CO, like the other carbon gases was measured on air drawn in through the roof top inlet (Figure 2.1(c)). Until the end of 2012, CO measurements were made every 30-minutes by a Trace Analytical RGD-2 instrument, coupled to a HP-5890 GC, using 2 1/8" columns packed in series: a Unibeads 1S and a Molecular Sieve 5A, with zero air as the carrier gas (Table 2.1). A working standard was measured with each ambient air measurement and used to derive the CO mole fraction. Working standards were calibrated twice per month using a suite of NOAA-filled and measured cylinders of ambient air having mole fractions ranging from 164 to 309 ppb.

Since July 2007, measurement of CO has been by improved by installation of a Peak Laboratories Performer 1 (PP1) instrument (Reduced compound photometer), with similar columns and carrier gas to the RGD-2. Measurement is every 5 minutes with a precision of better than ±1 ppb, A working standard is measured twice daily with twice monthly calibration checks using a suite of NOAA-filled and measured cylinders of ambient air having mole fractions ranging from 186 to 300 ppb. A target gas has been measured daily on both instruments since September 2008. During the 2008 period of instrument overlap there was very good agreement between the two instruments in the range from 80-600 ppb CO (post-calibration offset of 0 ± 5 ppb). The PP1 has been the primary source of CO data since 2008.

2.3.3. CH_4 measurement methodology, instrumentation and calibration

CH_4 was also measured in air continuously drawn in through the roof top inlet (Figure 2.1(c)). CH_4 was measured at EGH at 30-minute intervals by HP-5890-FID Gas Chromatograph until 2010 (Table 2.1). A working standard was measured with each ambient air measurement and used to derive the methane mole fraction. Working standards were calibrated using a suite of NOAA-filled and measured cylinders of ambient air having mole fractions ranging from 1834 to 1965 ppb. During January to April 2009 a Picarro G1301 was operational and sampled from the same ambient air line in direct comparison with the GC, before becoming the primary instrument for CH_4 measurement from 2010 to present.

The Picarro sends a CH_4 measurement via the serial output at approximately 10-second intervals and these are 1-minute averaged. The Picarro G1301 was calibrated during 2010 and 2011 using a suite of NOAA-filled and measured cylinders of ambient air having mole fractions ranging from 1831 to 1975 ppb. Since 2012 air standards have been used that were filled at MPI-Jena and calibrated against NOAA standards as part of the IMECC project. These have CH_4 mole fractions of 1809, 1912 and 2092 ppb and are measured weekly.

2.4. Wind speed, wind direction and temperature measurements

Wind direction, wind speed and temperature were recorded at the EGH site from 2000 to 2006 using a MJP Geopacks PC weather station located on the roof of the Earth Sciences bldg (Figure 2.2). It was replaced in 2007 by a Geopacks WS-200 MK-III weather station, which has been operational since 2007 at the same location.

Figure 2.2. Location of the weather station on the roof of the Earth Sciences building.

2.5. Definition of wind sectors and seasons

To carry out wind-sector analyses, the data set was divided into 8 wind sectors of 45° starting from 0° ± 22.5° (Figure 2.2(a,b); Worthy et al., 1994; Bousquet et al., 1996; Fleming et al., 2012). To avoid data duplicity, the lower bound of each sector was established by adding 0.5° as shown in Table 2.2. To carry out seasonal analyses, 4 seasons were defined according to temperature records in the northern hemisphere: winter (December to February), spring (March to May), summer (June to August) and autumn (September to November) (Fisher, 2006; Lowry et al., in preparation 2014).

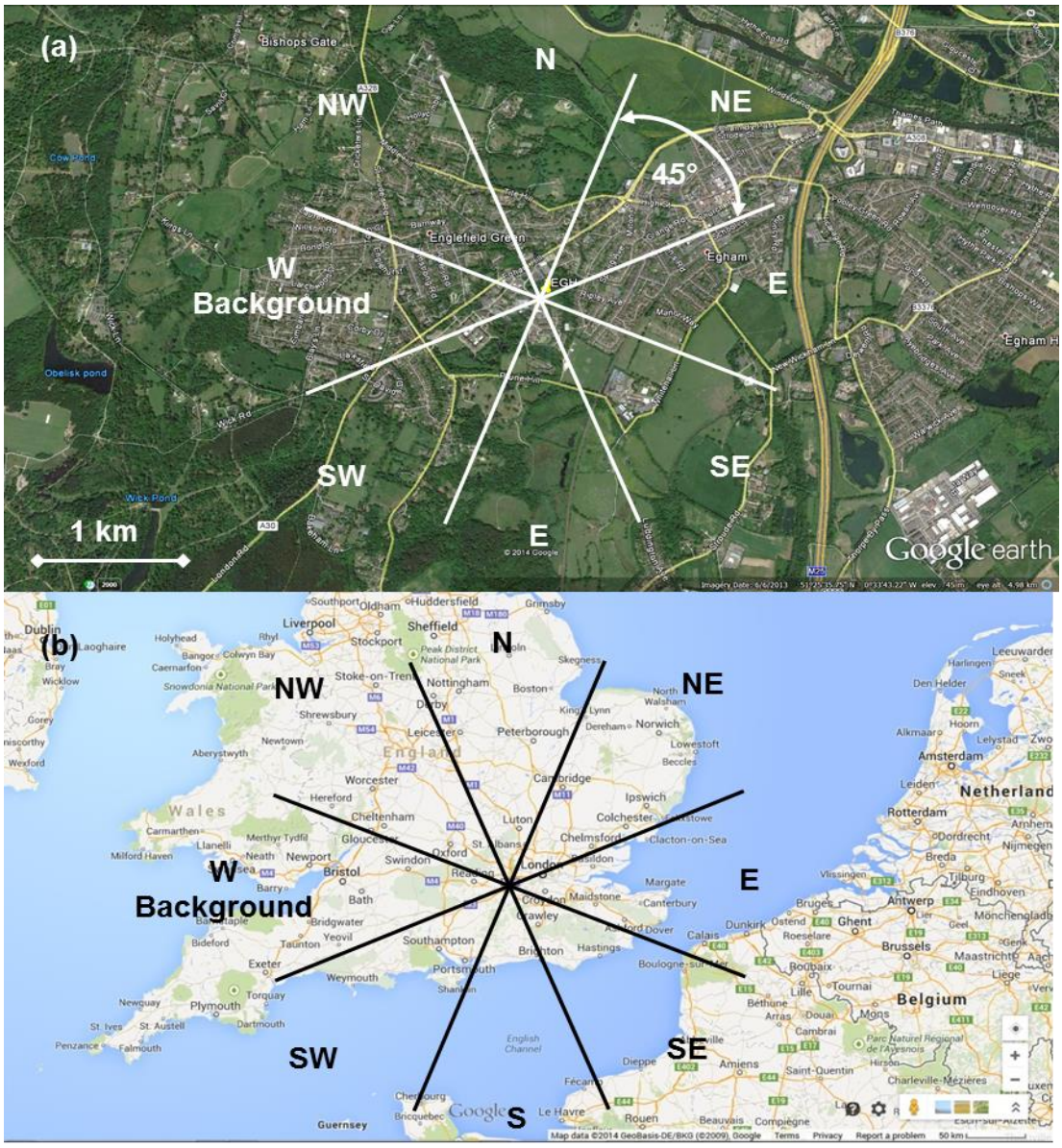

Figure 2.3(a). Wind sectors definition at EGH in the local context; **(b).** EGH location in the regional context and wind sectors definition.
Source: https://www.google.co.uk/maps/@51.4227486,-0.5429014,14z

Table 2.2. Wind sectors definition and span.

Sector	Degrees
North (N)	338° to 22.5 °
Northeast (NE)	23° to 67.5 °
East (E)	68° to 112.5°
Southeast (SE)	113° to 157.5
South (S)	158° to 202.5
Southwest (SW) *background*	203° to 247.5°
West (W)	248° to 292.5
Northwest (NW)	293° to 337.5°

2.5.1. Definition of background atmospheric conditions

2.5.1.1. Mace Head Research Station and data

The Mace Head station (MHD, Figure 1.1(a)) samples Atlantic background air (53°20' N, 9°54' W) for much of the year. MHD is situated on the Atlantic Ocean coastline of Ireland to monitor CO_2 concentrations and quantify European and trans-Atlantic sources and sinks of CO_2 (Bousquet et al., 1996; Derwent et al., 2002; Messager et al., 2008). It receives clean maritime air masses from across the Atlantic Ocean, and under anti-cyclonic conditions, air masses from the UK and continental Europe (Derwent et al., 2002). The MHD CO_2 continuous data set is maintained by the Climate and Environment Sciences Laboratory (LSCE), which belongs to the Institut Pierre Simon Laplace, and was obtained from the WMO Global Atmosphere Watch programme web site (http://ds.data.jma.go.jp/gmd/wdcgg). The data set spans continuous, hourly, measurements of CO_2 from January 1992 to December 2011.

Flasks monthly averages for CO_2, CO and CH_4 data recorded at MLO and MHD stations were obtained from the Earth System Research Laboratory (Global Monitoring Division) web site (Carbon Cycle Cooperative Global Air Sampling Network http://www.esrl.noaa.gov/gmd/) (Dlugokencky et al., 2014).

2.5.1.2. Background conditions definition at EGH

CO_2, CO and CH_4 concentrations can be affected positively or negatively by local perturbations such as changes in meteorological conditions and pollution episodes, therefore data affected must be removed from the data set (Bousquet et al., 1996; Derwent et al., 2002). Lowry et al. (2001) observed that during the advection of "clean air at the EGH site, CH_4 concentrations were between 25-30 ppb above MHD baseline. They reported that when CH_4 monthly averages recorded at EGH were compared with monthly averages at MHD, such difference decreased to <10 ppb CH_4 and ascribed the excess to local inputs of CH_4 nearby EGH. On such basis, the SW sector at EGH (203° - 247.5°, Figure 2.3) is considered as the background sector to perform background analyses for CO_2, CO and CH_4 data in this thesis.

2.6. Data quality and data capture criterion

Although occasional instrument breakdowns caused data gaps, the data capture varied between 76-100% of maximum possible yearly measurements, except for wind speed in 2005 when only 67% of the total possible data was recorded. Figure 2.4 shows total percentage coverage for CO_2, CO, CH_4, wind direction, wind speed and temperature data at the EGH site during 2000-2012. A minimum data capture threshold of 75% was used to consider data valid and representative (Zellweger et al., 2009; Hernandez-Paniagua et al., 2014a; LAQN, 2014). 30-min averages were used to calculate daily averages. Monthly averages were calculated from daily averages, whereas yearly averages were calculated from monthly averages.

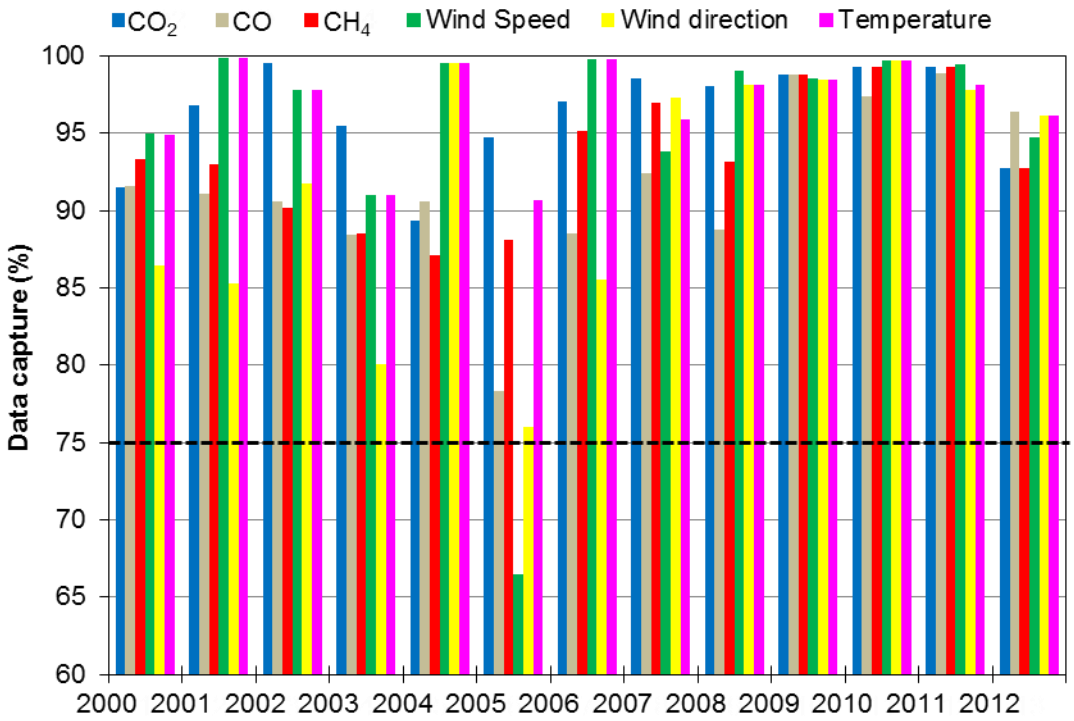

Figure 2.4. Data capture of 30-min averages recorded for CO_2, CO, CH_4, wind speed, wind direction and temperature during 2000-2012 at EGH. Dotted line shows the threshold of 75% data capture.

2.7. Mathematical analyses

The dataset was analysed extensively with the *openair* package (Carslaw and Ropkins, 2012; Carslaw and Beevers, 2013; Carslaw, 2014) for R software (R Core Team, 2013). Table 2.3 summarises functions and codes used in *openair* package to analyse the EGH data set. Long-term trends were computed with the MAKESENS 1.0 macro, which performs two types of statistical analysis. Firstly, the presence of a monotonic increasing or decreasing trend is tested with the non-parametric Mann-Kendall test. Secondly, the slope of a linear trend is calculated with the nonparametric Sen's method. At EGH, MAKESENS used the normal approximation test for n = 13 to test the presence of a statistically significant trend using the Z value. A positive Z value indicates an upward trend, whereas a negative value indicates a downward trend. To test either an upward or downward monotone trend, a two-tailed test, at α level of significance, H_0 is rejected if the absolute value of Z is greater than $Z_{1-\alpha/2}$, where $Z_{1-\alpha/2}$ is obtained from the standard normal cumulative distribution tables. MAKESENS tests significance levels for α of 0.001, 0.01, 0.05 and 0.1 (Salmi et al., 2002).

Table 2.3. Summary of calculations and plots made with the *openair* package, and commands and codes used.

Calculation	Command	Code	Chapter*
Loading data	read	read	4
Formatting date	as.POSIXct	format = "%d/%m/%Y %H:%M", tz = "GMT"	4
Exporting data	write	write	
Summary	summary	summary()	4
Hourly averages (week-long cycle)	means, aggregate	%w-%H	4
Daily averages	means, aggregate	%Y-%j	4
Weekly averages	means, aggregate	%Y-%W	4
Monthly averages	means, aggregate	%Y-%m	4
Monthly averages (year-long cycle)	means, aggregate	%m	4
Annual averages	means, aggregate	%Y	4
Classifying data	cutData	type=("season"); type=("ws"); type=("wd"); type=("year"); type=("daylight")	11
Wind speed and wind direction	windRose	type=("year"); type("season")	12
Frequency of data by wind direction and wind speed	polarFreq	type=("year"); type("season"); type=("month")	14
Bivariate polar plot	polarPlot	pollutant=" "; type=("year"); type("season"); type=("mc	15
Cluster analysis	polarPlot	pollutant=" "; n.clusters=" "	15
Calendar plot	calendarPlot	pollutant= " "; year=" "; month=" "; annotate=" "	18

**Chapter in openair manual (Carslaw, 2014)*

Sen's method is used where the trend is assumed to be linear and can be represented by a slope and a constant *Q* and *B*, respectively. To calculate *Q*, first the slopes of all data values are calculated in pairs. For *n* values x_j in the time series, $N = n(n-1)2$ slope estimates are obtained Q_i. The Sen's estimator of slope is the median of these *N* values of Q_i. Then, the *N* values of Q_i are ranked from the smallest to the largest. A 100(1-α)% two-sided confidence interval about the slope estimate is obtained by the nonparametric technique based on the normal distribution. The method is valid for *n* as small as 10 unless there are many gaps. MAKESENS computes the confidence interval at two different confidence levels; α = 0.01 and α = 0.05, resulting in two different confidence intervals. To obtain an estimate of B, the *n* values of differences $x_i - Qt_i$ are calculated. The median of these values gives an estimate of B (Salmi et al., 2002).

The Seasonal-Trend Decomposition technique (STL) was used to decompose the time-series into trend, seasonal and residual components (Cleveland et al., 1990). STL consists of two recursive procedures: an inner loop nested inside and outer loop. In each of the passes through the inner loop, the seasonal and trend components are updated once; each complete run of the inner loop consists of $n_{(i)}$ such passes. Each pass of the outer loop consists of the inner loop followed by a computation of the robustness weights; these weights are used in the next run of the inner loop to reduce the influence of transient, aberrant behaviour on the trend and seasonal components. An initial pass of the outer loop is carried out with all robustness weights equal to 1, and then $n_{(0)}$ passes of the outer loop are carried out.

Statistical analyses were performed with the computational software SPSS 19.0 for Windows. Linear regression analyses were performed with the Microsoft Excel computer software 2010. Redmond, Washington. In order to asses differences in long-term trends, linear regression analyses performed with Microsoft Excel were compared with the computer software SigmaPlot Version 12.2 (Systat Software, San Jose, CA).

3. INTERPRETATION AND ANALYSIS OF METEOROLOGICAL RECORDS FOR THE EGH SITE FROM 2000 TO 2012

Meteorological conditions influence the concentrations of air pollutants in the environment. Parameters that have been widely monitored to help understand air pollutant dynamics include: temperature, wind speed, wind direction and PBL height. They have important impacts upon air pollutant dispersion. Air mass back-trajectory analyses are also used to track air mass origins to identify potential sources of air pollutants. Previous studies have shown that air pollutants are subject to long-rage transport from their source origin transported to different latitudes and longitudes in some cases (Higuchi et al., 1987; Trivett et al., 1989; Kanawade et al., 2012) and forming discrete layers at different altitudes in the troposphere. For example, Trivett et al. (1989) reported short-term increases of CO_2 and CH_4 at Alert, Canada, that were greatly influenced by long-range transport of anthropogenic emissions from the industrial regions in Europe and Russia.

More recently, Adame et al. (2012) reported a big increase in CO and PM_{10} concentrations in the southwest of the Iberian Peninsula (western Andalusia) during the advection of northerly air masses. They ascribed the high levels of CO and PM_{10} observed to long-range transport of air masses which accumulated high loading of pollutants from wildfires in the northwest of the Iberian Peninsula (Galicia and Portugal). Therefore, it is important to analyse and interpret meteorological parameters together with air pollutant records.

3.1. Temperature records during 2000-2012 at EGH

Ambient air temperatures recorded from January 2000 to December 2012 at EGH were summarised as 30-min averages. Data capture during the period was 97.6%. The minimum temperature recorded was -8.9°C on February 11th 2012, while the maximum was 38.1°C on August 10th, 2003. The average temperature was 12.7°C with a median of 12.1°C and standard deviation of 6.2°C. Daily averages were calculated from 30-min averages.

Figure 3.1 shows the daily averages from 2000 to 2012. Temperature shows a harmonic cycle with frequency made up by 1 cycle yr^{-1}. Seasonality is observed with warmer temperatures in summer and colder temperatures during winter. A

malfunction in the instrument was detected in April 2005 and then it was recalibrated. After the recalibration, a shift in daily averages is noticed. In order to ratify the trend, monthly averages were calculated from daily averages and then compared with monthly averages from the Heathrow meteorological station of the Met Office (officially the Meteorological Office until 2000). Monthly averages of temperature data recorded at Heathrow were obtained from the Met Office web site (http://www.metoffice.gov.uk/climate/uk/stationdata/heathrowdata.txt).

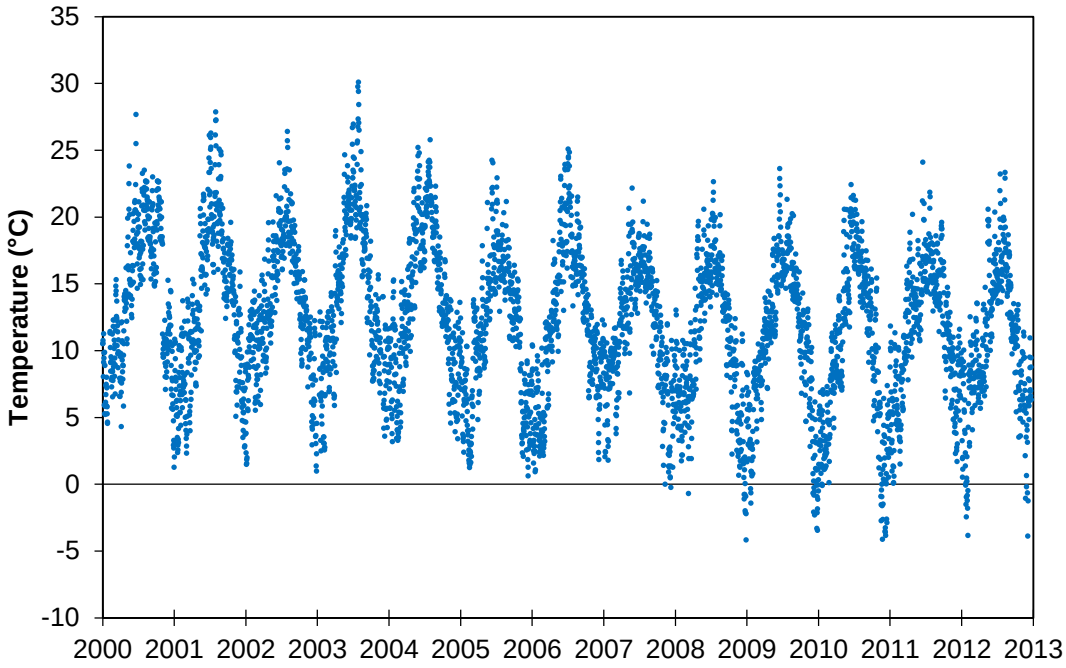

Figure 3.1. Daily averages of temperature records at EGH during 2000-2012.

Figure 3.2(a) shows a comparison for monthly averages and 3.2(b) for annual averages. During 2000-2004, higher temperatures (~2°C) were recorded at EGH than at Heathrow. After 2005, when the instrument was recalibrated the differences decreased (<1 °C). Annual averages show more clearly the differences between the two records (Figure 3.2b). It is clear that after 2005, the differences observed were negative (EGH-Heathrow averages) and decreased in magnitude. Slightly colder temperatures at EGH than at Heathrow are due to its location on a hill. The lower seasonal differences since 2007 observed are due to the more accurate weather station installed in 2007. Thus, the downward trend observed at EGH (-2.3° yr^{-1}, r=0.88) was not detected at Heathrow (-1.6° yr^{-1}, r=0.19) and it is attributed to the recalibration of the instrument in April 2005 and to the replacement of the weather station in 2007.

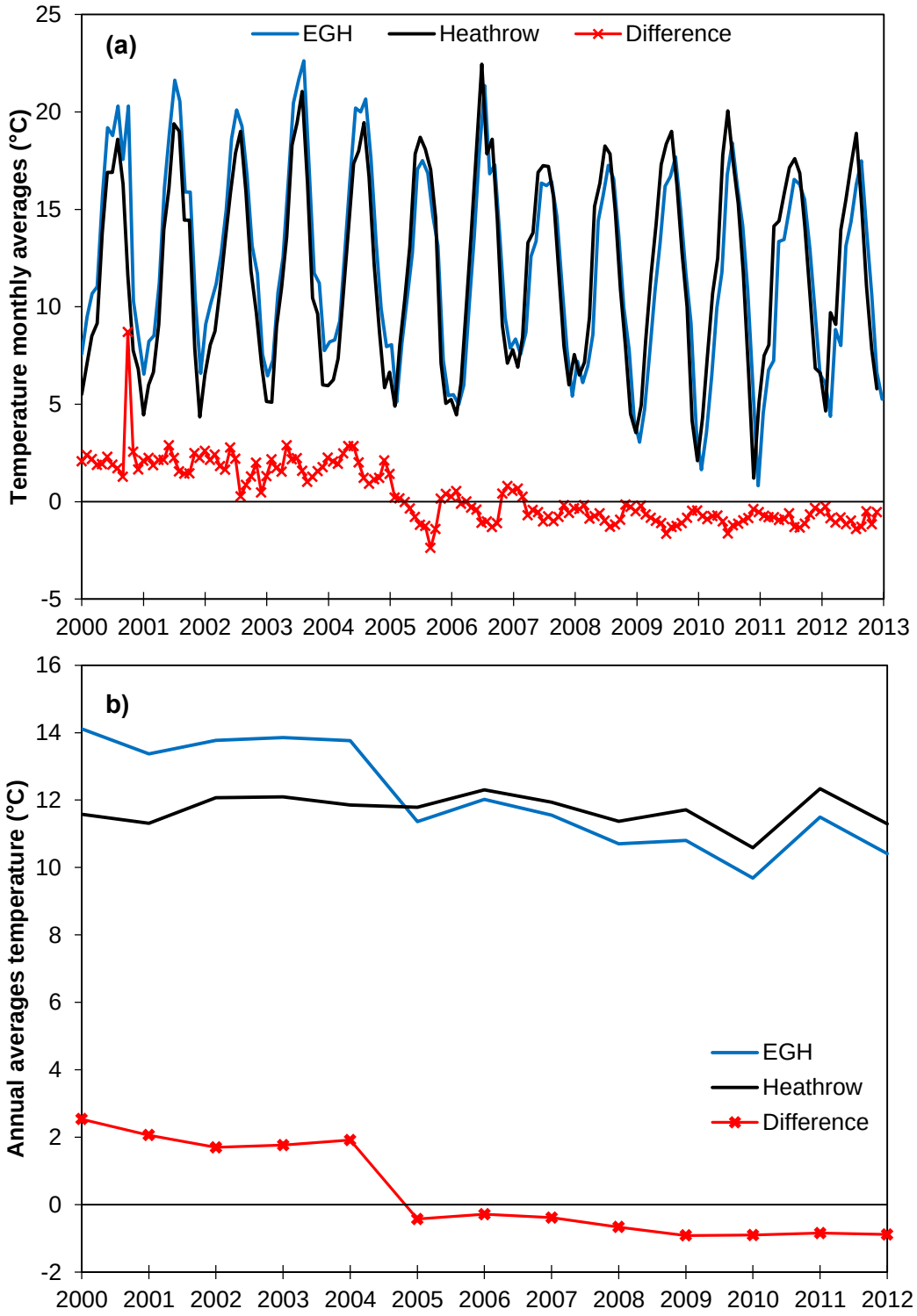

Figure 3.2(a). Monthly-averaged temperatures at EGH calculated from daily averages and monthly averages at Heathrow meteorological station during 2000-2012. The difference is calculated by subtracting the average at Heathrow from the EGH average; **(b).** Temperature annual averages at EGH and Heathrow calculated from monthly averages during 2000-2012. Differences were calculated by subtracting the annual average at Heathrow from the EGH average.

3.2. Analysis of wind speed and wind direction records for the EGH site during 2000-2012

Wind speed records at EGH during 2000-2012 span 90.4% of all possible data. Data capture was over 85% during the period except for 2004, 2005 and 2007 when it was 85%, 66% and 52% respectively. Data were categorized from 0-1, >1-2, >2-3, >3-4, >4-5, >5-6, >6-7 and >7 m s^{-1}. Figure 3.3 shows relative frequencies by category at EGH. The highest frequency was for the 0-1 m s^{-1} category (51%) and decreased with the increase of wind speed. The 13-years wind speed average was 1.4 m s^{-1} and median 1.0 m s^{-1}.

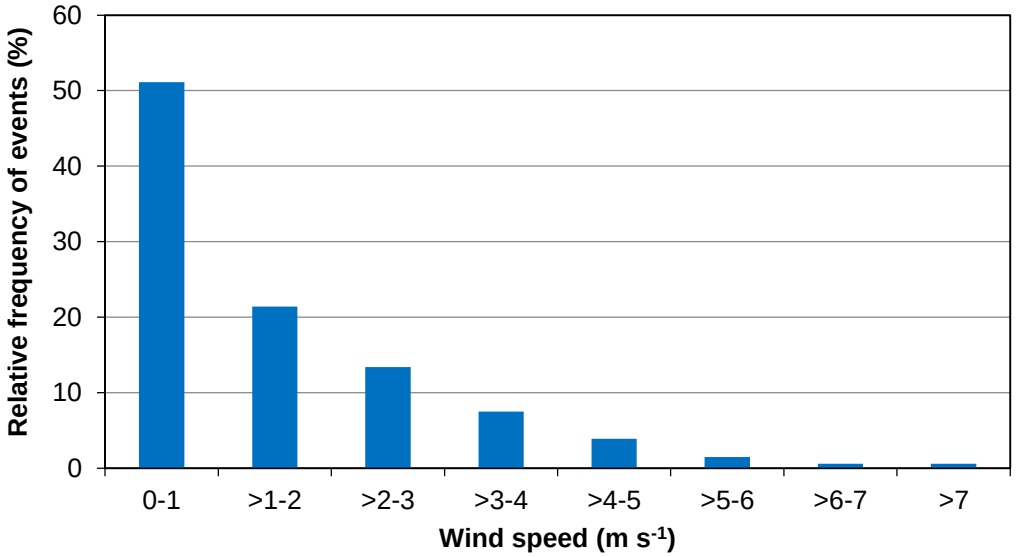

Figure 3.3. Relative frequency of wind speed records at the EGH site during 2000-2012.

3.2.1. Yearly profile of wind speed at the EGH site during 2000-2012

Figure 3.4 shows the yearly cycle of wind speed records at EGH during 2000-2012. No significant difference (p>0.05) was observed between monthly averages and medians for wind speed records. Wind speed monthly averages ranged between 0.9 m s^{-1} and 2.14 m s^{-1}, whereas median values ranged from 0.6 m s^{-1} to 1.8 m s^{-1}. The highest averaged wind speed is in February and the lowest in August. The largest spread of values was observed in February, whereas the lowest spread was recorded in August.

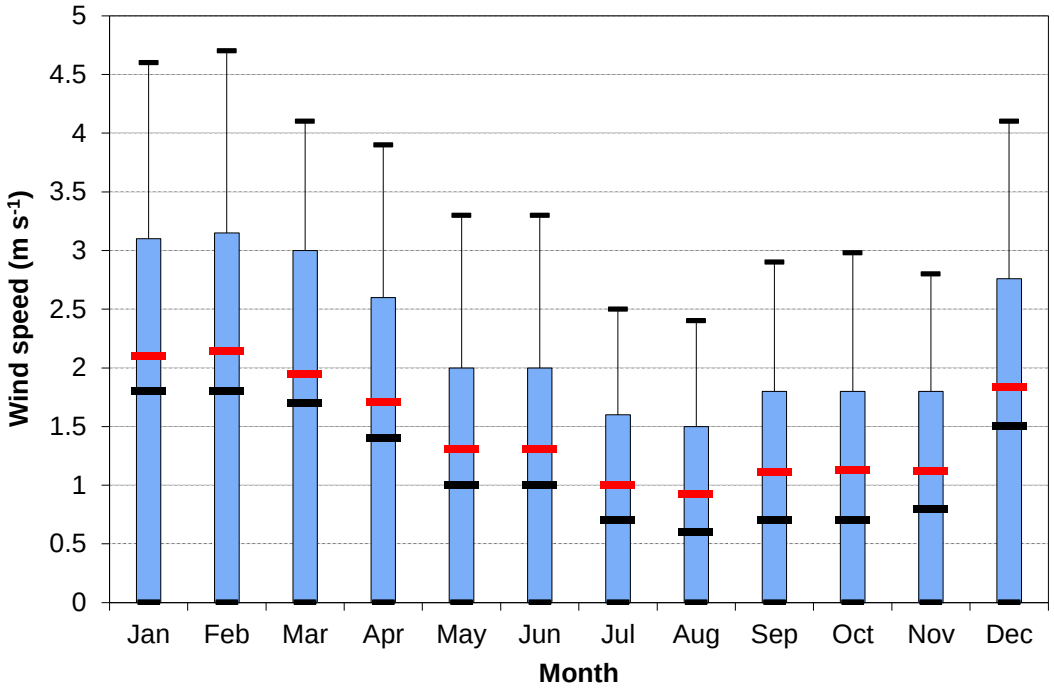

Figure 3.4. Averaged yearly cycle for wind speed records at the EGH site from 2000 to 2012. Black and red lines represent the median and average respectively. Vertical bars (whiskers) correspond to the 10th and 90th percentiles.

3.2.2. Yearly profile of wind direction and speed by wind sector at EGH

Wind speed frequency varied as function of wind sector and across the year. Prevailing wind directions were SW-W-NW-E (occurrence 25.1%, 16.5%, 12.2% and 9.6%). Calm conditions (wind speed ≤ 0.1m s^{-1}) occurred 9.7%. The lowest occurrence was observed for SE (3.7%). Figure 3.5 shows monthly wind roses during 2000-2012 at EGH. SW (background sector) shows the highest monthly occurrence during the year clearly. Higher frequencies of high wind speeds were observed mostly from December to March (Winter). By contrast, high wind speeds are rare in July and August.

Data for wind direction and wind speed were studied by season. Figure 3.6 shows seasonal wind roses for data recorded at EGH from 2000 to 2012. Wind frequencies varied from season-to-season. Wind roses in winter and spring are similar, likewise the ones for summer and autumn also. SW dominates in all seasons, however in winter the occurrence in order of prevalence was SW-W-NW-S whereas in spring it was SW-W-E-NW. By contrast, in summer and autumn the prevalence was SW-W-NW-E. The higher frequency of large wind speeds was seen in winter while in summer it was minimal. Calm also varied, in winter was observed the lowest occurrence (11.5%) while in autumn the higher (23.1%).

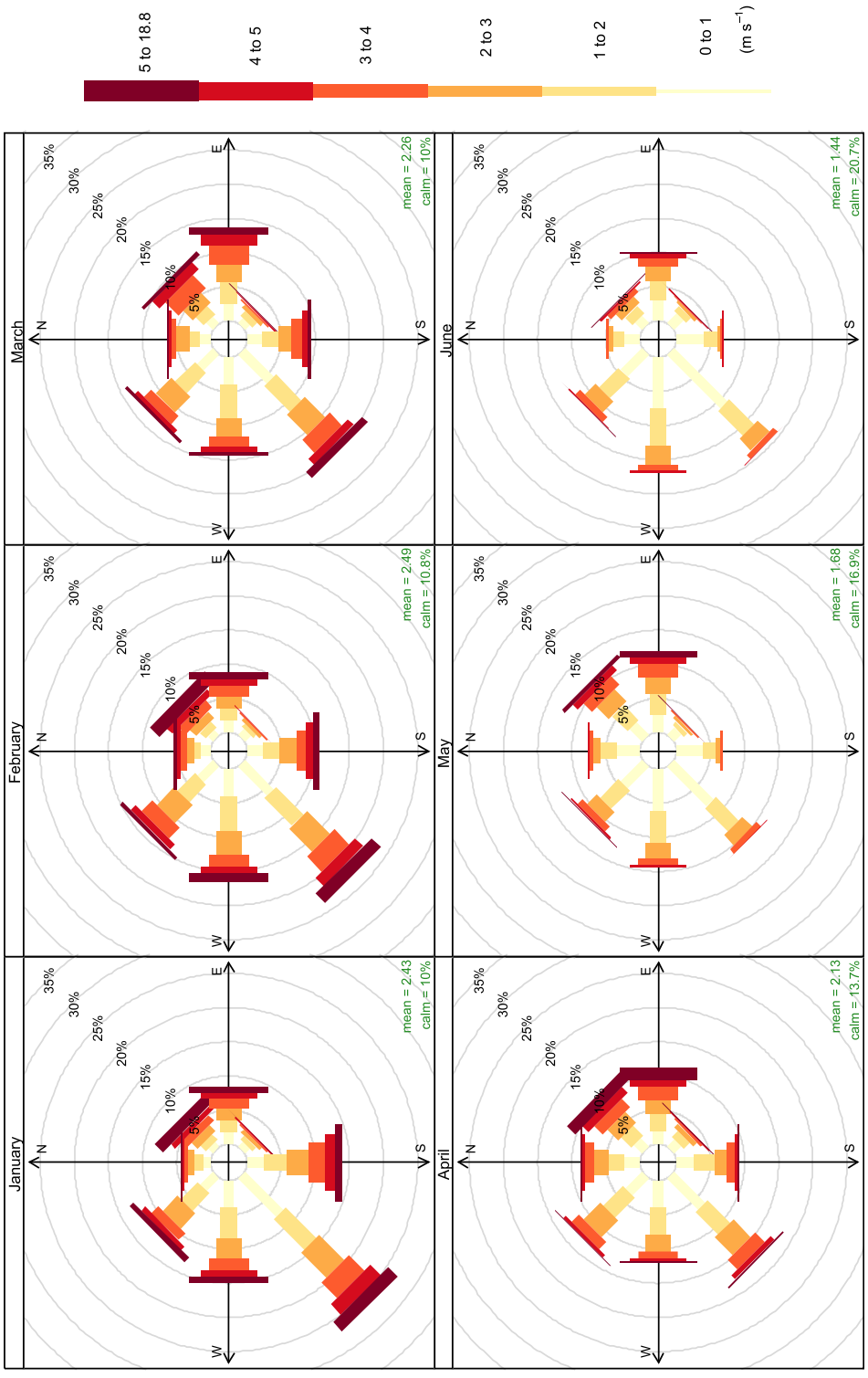

Figure 3.5. Yearly profile of wind occurrence at EGH during 2000-2012. Calm occurred when wind speed was zero. Frequency of counts by wind direction is expressed in %.

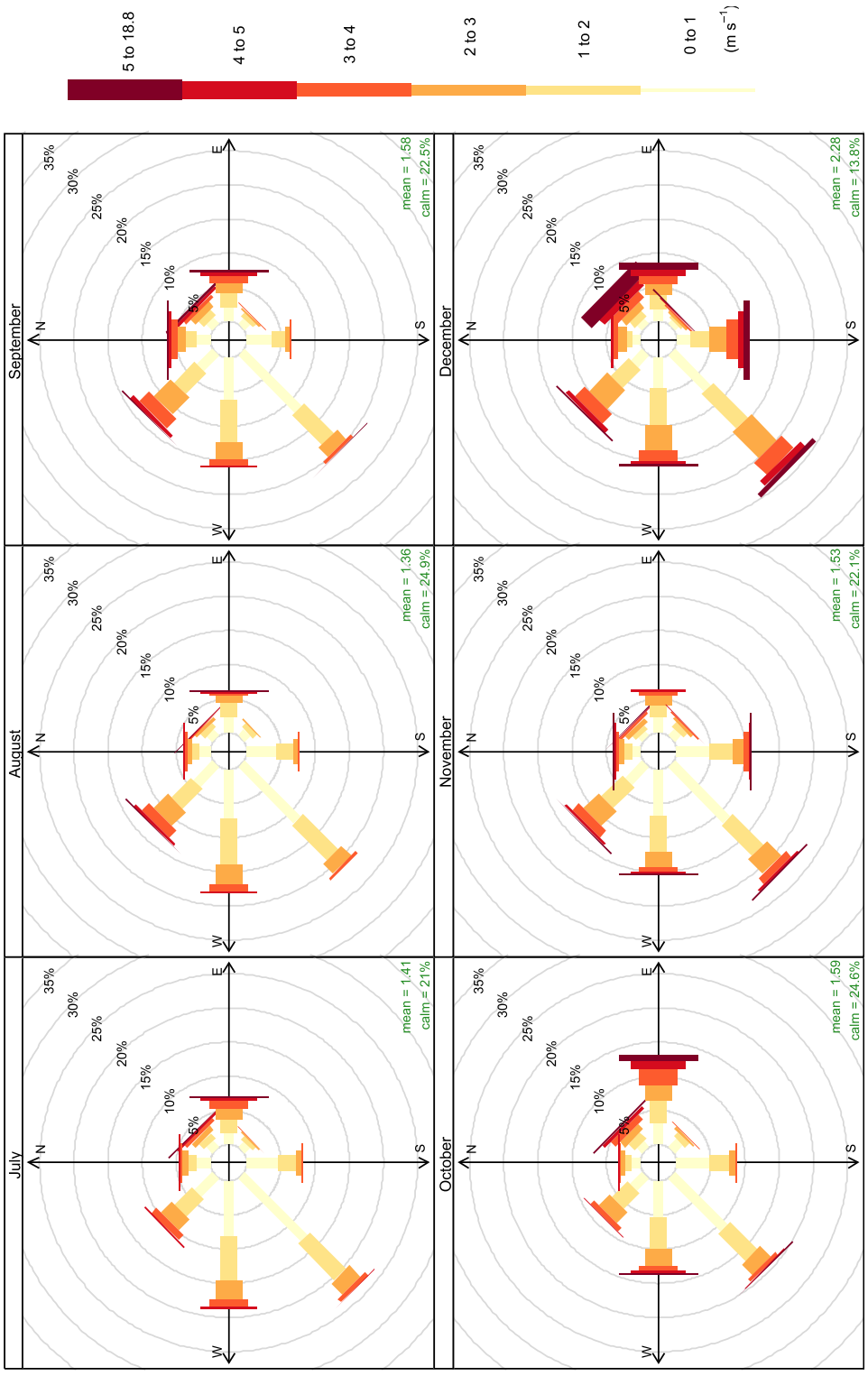

Figure 3.5. (Continuation) Yearly profile of wind occurrence at EGH during 2000-2012. Calm occurred when wind speed was zero. Frequency of counts by wind direction is expressed in %.

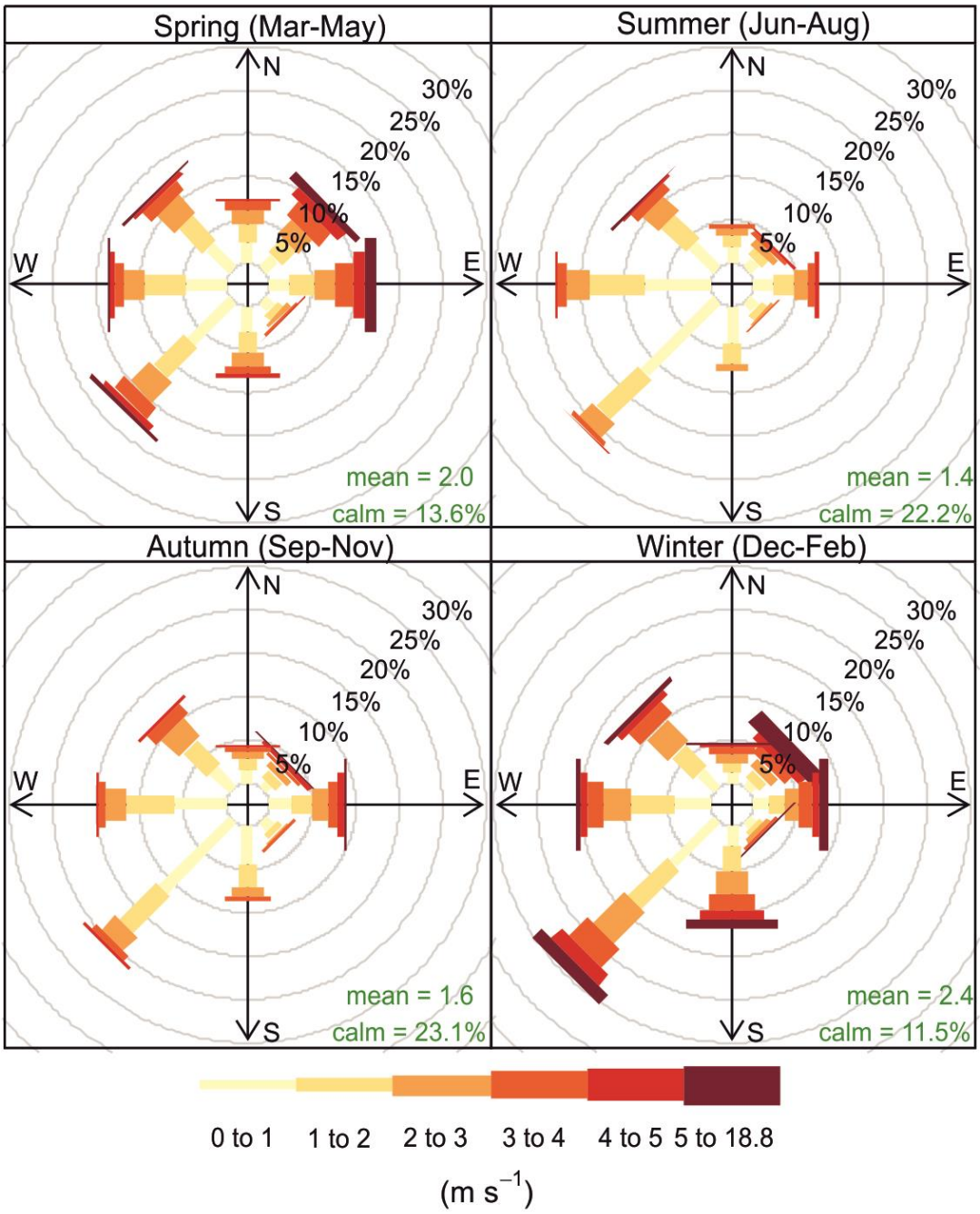

Figure 3.6. Wind roses by season for data recorded at EGH during 2000-2012. Frequency of counts by wind direction is expressed in %.

4. ANALYSIS AND INTERPRETATION OF AMBIENT DATA FOR CO_2 RECORDED AT THE EGH SITE DURING 2000 TO 2012

The first continuous measurements of atmospheric CO_2 date back to March 1958 when Professor Charles Keeling started to measure CO_2 at the Mauna Loa Observatory in Hawaii, which is the longest CO_2 record existing. Keeling was the first to calculate the global CO_2 background value, ca. 315 ppm CO_2 in 1958, from measurements at the Pacific coast in USA, Mauna Loa observatory and Antarctica. He also noticed a rapid rise in CO_2 atmospheric concentrations, today ascribed to CO_2 emissions mainly from fossil fuels burning. CO_2 measurements at the Mauna Loa observatory since 1958 represent the Keeling curve (Figure 4.1; NOAA/ESRL, 2014).

Nowadays, CO_2 is continuously measured at many monitoring stations located around the world, which are part of different cooperative networks (Global Atmosphere Watch programme of the World Meteorological Organization, Global Monitoring Division of the Earth System Research Laboratory of the National Oceanic and Atmospheric Administration, US). These global monitoring networks record in-situ measurements at observatories, tall towers, and air samples collected aboard small aircraft for atmospheric CO_2, CH_4, N_2O and CO; Figure A2.1 shows different monitoring stations and measurements. The most recent estimate of the global CO_2 average by NOAA/ESRL (2014) indicates an atmospheric concentration of 395.3 ppm CO_2 for 2013. This is 80.3 ppm CO_2 more than the first global estimation made by Keeling in 1958, and supposes an increment of 25.5% during the period. Although, the Keeling curve shows periods of steep increases and dips in CO_2 annual averages (Figure 4.1), the overall upward trend is persistent caused by the burning of fossil fuels (IPCC, 2013).

The contribution to CO_2 emissions from urban, suburban and rural areas has been widely assessed using in-situ, tall tower and sampling bag measurements since around 1980. Table 4.1 summarises studies for CO_2 atmospheric analyses and CO_2 fluxes at different locations around the world. It shows also some different techniques that have been developed for such purpose and some of the results reported. Studies span CO_2 measurements at both hemispheres and different longitudes.

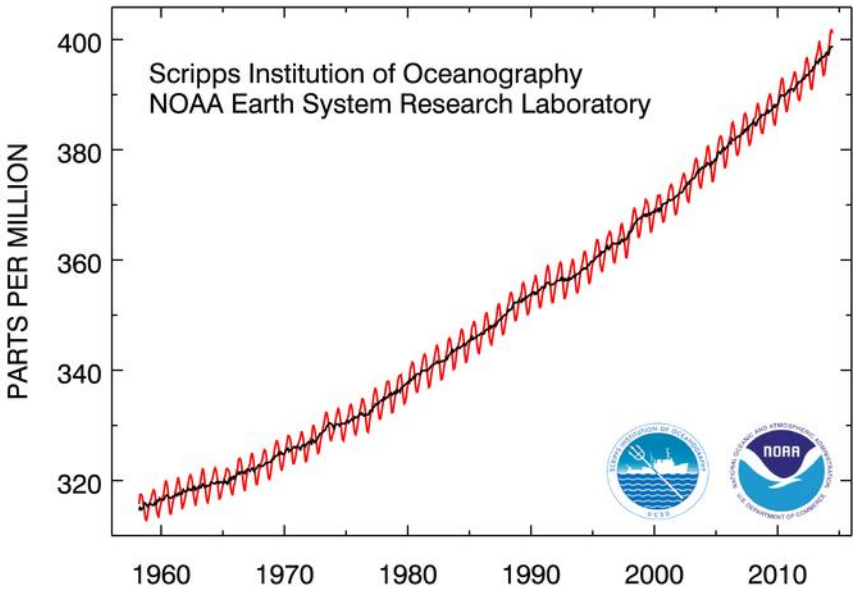

Figure 4.1. Monthly average atmospheric CO_2 concentrations recorded at Mauna Loa Observatory, Hawaii during 1958-2014. *Source: Available at http://www.esrl.noaa.gov/gmd/ccgg/trends/*

At the EGH site, atmospheric CO_2 measurements started in July 1999, however in this thesis only records from 2000 onwards are considered, when meteorological data started to be recorded. Continuous, high-frequency (5 min) and high-precision (±0.1 ppm) in-situ measurements of atmospheric CO_2 have been made at the EGH site, in Surrey, UK from 2000 to 2012. Data were analysed on 30-minute, daily, weekly, monthly, seasonal and yearly time scales. CO_2 data recorded at the EGH station are compared with data from the MHD station to test whether they fit the global observed trend.

4.1. Aims

The aims of this chapter are:

1. To interpret on hourly, daily, weekly, monthly, seasonal and long-term scales data for CO_2 recorded at the EGH site during 2000-2012.
2. To evaluate local sources of CO_2 by comparing spatial variations in data recorded at EGH with data recorded at MHD monitoring station during 2000-2012.

Table 4.1. Summary of previous studies of atmospheric CO_2 at different monitoring stations.

Reference	Sampling site	Type of site	Coordinates	Period studied	Type of analysis
O'Shea et al., 2014	Greater London area, UK	Urban	Over greater London area	Jul-12	Aircraft measurements, inventories verification
Aulagnier et al., 2010	Europe	Background	Europe	2001-2006	Long-term trend
Ramonet et al., 2010	CARBOEUROPE-IP[b], NOAA/ESRL[a]	Background, continental, aircraft	Europe	1997-2007	Seasonal cycle, long-term trend, inventories verification
Barichivich et al., 2012	NOAA/ESRL[a]	Background	Both hemispheres	1975-2010	Seasonal cycle, long-term trend
Keeling et al., 2011	NOAA/ESRL[a]	Background	Both hemispheres	1957-2003	Seasonal cycle, differences between hemispheres
Nakazawa et al., 1991a	Route Tokyo-Anchorange, Tokyo-Sydney	10-12 km altitude	Both hemispheres	1984-1985	Seasonal cycle, differences between hemispheres
Randerson et al., 1997	NOAA/ESRL[a]	Background	Both hemispheres	1981-1995	Seasonal cycle, inventories verification, differences between hemispheres
Trivett et al., 1989	Alert, Canada	North Pole	82.52°N, 62.28°W	1981-1987	Seasonal, long-term trend, pollution
Worthy et al., 1994	Alert, Canada	North Pole background	82.52°N, 62.28°W	1988-1993	Daily cycle, seasonal cycle, long-term trend, sectorial analysis
Ugglieti et al., 2008	Junfgraujoch, Switzerland	Background	56.55°N, 7.59°E	2005-2007	Seasonal cycle, pollution episodes
Valentino et al., 2008	Junfgraujoch, Switzerland	Background	56.55°N, 7.59°E	2001-2006	Seasonal cycle, long-term trend
Rigby et al., 2008b	EGH, UK	Semi-rural, sub-	54.42°N, 0.55°W	2006-2008	Daily cycle, seasonal cycle
Bousquet et al., 1996	Mace Head, Ireland	Background	53.31°N, 9.9°W	1992-1994	Seasonal cycle, sectorial analysis
Derwent et al., 1998a	Mace Head, Ireland	Background	53.31°N, 9.9°W	1993-1996	Sectorial analysis
Helfter et al., 2011	BT Tower, Central London, UK	Suburban	51.52°N, 0.14°W	2006-2008	Daily cycle, inventories verification

Table 4.1. Continuation.

Reference	Sampling site	Type of site	Coordinates	Period studied	Type of analysis
Rigby et al., 2008b	Queen's Tower, South Kensington, London, UK	Urban	51.5°N, 0.59°W	2006-2007	Daily cycle, seasonal cycle
Vogt et al., 2006.	Basel, Switzerland	Urban	47.56°N, 7.59°E	Jun-2002	Daily cycle
Haszpra and Barcza, 2010	Hegyhátsál, Hungary	Rural, regional background	46.95°N, 16.65°E	1994-2009	Daily cycle, seasonal cycle, long-term trend, inventories verification
Hazspra et al., 2008	Hegyhátsál, Hungary	Rural, regional background	46.95°N, 16.65°E	1981-2008	Daily cycle, seasonal cycle, long-term trend
Zhang and Zhou, 2013	Waliguan, China	Background	36.28°N, 100.90°E	1995-2008	Seasonal cycle, long-term trend, pollution episodes
Zhang et al., 2013.	Waliguan, China	Background	36.28°N, 100.90°E	1995-2008	Daily cycle, seasonal cycle, ssectorial analysis
Zhou et al., 2003	Waliguan, China	Background	36.28°N, 100.90°E	1991-2000	Seasonal cycle, long-term trend, sectorial analysis
Jin et al., 2010	Gosan, Korea	Background	33.17°N, 126.15°E	2004-2005	Seasonal cycle, pollution episodes
Graven et al., 2012	La Jolla, California, US	Background	32.87°N, 117.25°W	1992-2008	Seasonal cycle, long-term trend (^{14}C)
Cleveland et al., 1990	Mauna Loa, Hawaii, US	Background	19.53°N, 155.57°W	1974-1986	Seasonal cycle, long-term trend
Dettinger and Ghil, 1998	Mauna Loa, Hawaii, US	Background	19.53°N, 155.57°W	1958-1994	Seasonal cycle, long-term trend
Thoning et al., 1989	Mauna Loa, Hawaii, US	Background	19.53°N, 155.57°W	1974-1985	Daily cycle, seasonal cycle, long-term trend
Nakazawa et al., 1991b	Syowa, Antarctica	South Pole background	69.00°S, 38.58°E	1984-1988	Seasonal cycle, long-term trend, sectorial analysis
Morimoto et al., 2003	Syowa, Antarctica	South Pole background	69.00°S, 38.58°E	1984-2001	Daily cycle, seasonal cycle, long-term trend
Dettinger and Ghil, 1998	South Pole, Antarctica	Background	90.00°S, 0.00°W	1957-1994	Seasonal cycle, long-term trend

Superscripts correspond to the abbreviations of the full name of cooperative networks.

[a]National Oceanic and Atmospheric Administration/Earth System Research Laboratory

[b]Integrated Project CarboEurope-IP

4.2. Continuous observations of CO_2 at EGH from 2000 to 2012

CO_2 continuous measurements recorded at different frequencies as shown in section 2.4 have been summarised as 30-min averages. Figure 4.2(a) shows CO_2 30-min averages from January 1st, 2000 to December 31st, 2012 recorded at EGH and Figure 4.2(b) shows a histogram for 30-min averages in 5 categories. CO_2 30-min averages ranged from 347.1 to 669.0 ppm CO_2, recorded in August 8, 2001 and October 4, 2012, respectively. The largest frequency of CO_2 30-min averages was observed for values between 347.1 and 400 ppm CO_2 (64.9%), a frequency of 32.7% was recorded for averages >400-550 ppm CO_2, whereas very low frequencies were observed for averages >450-50, >500-550 and >550 ppm CO_2, 2.1%, 0.23% and 0.05%, respectively.

The data set for CO_2 at EGH seasonal cycles, summer and winter pollution episodes, and an increasing, which are typical of CO_2 datasets (Antonovsky et al., 1991; Navascues et al., 1991; Nakazawa et al., 1991a; Lintner et al., 2006; Hazspra et al., 2008; Ramonet et al., 2010; Zhang et al., 2013). The presence of a peak and a trough generates an amplitude value (AV) in the CO_2 cycles that can be daily (AV_d), weekly (AV_w) or seasonal (AV_s). The AV is defined as the difference between the largest and the lowest value recorded and can represent the difference between sinks and sources, and is dependent on the location of the monitoring site. Thus, the largest CO_2 AV_s are recorded at northern latitudes, where the most important CO_2 sources and major vegetated areas are located (Barichivich et al., 2013). By contrast, the lowest CO_2 AV_s are observed at high southern latitudes (Nakazawa et al., 1991a; Morimoto et al., 2003).

At EGH, the seasonal cycle shows the largest CO_2 mixing ratios in winter and the lowest in late summer. This cycle arises from a combination of CO_2 uptake by photosynthesis (Dettinger and Ghil, 1998), which is enhanced during summer when the lowest CO_2 concentrations are recorded, and increased emissions from fossil fuel burning for heating during winter. The CO_2 seasonal cycle in the northern hemisphere is enhanced strongly by fossil combustion, whereas at the South Pole relatively minor sources influence the CO_2 seasonal cycle (Nakazawa et al., 1991a,b).

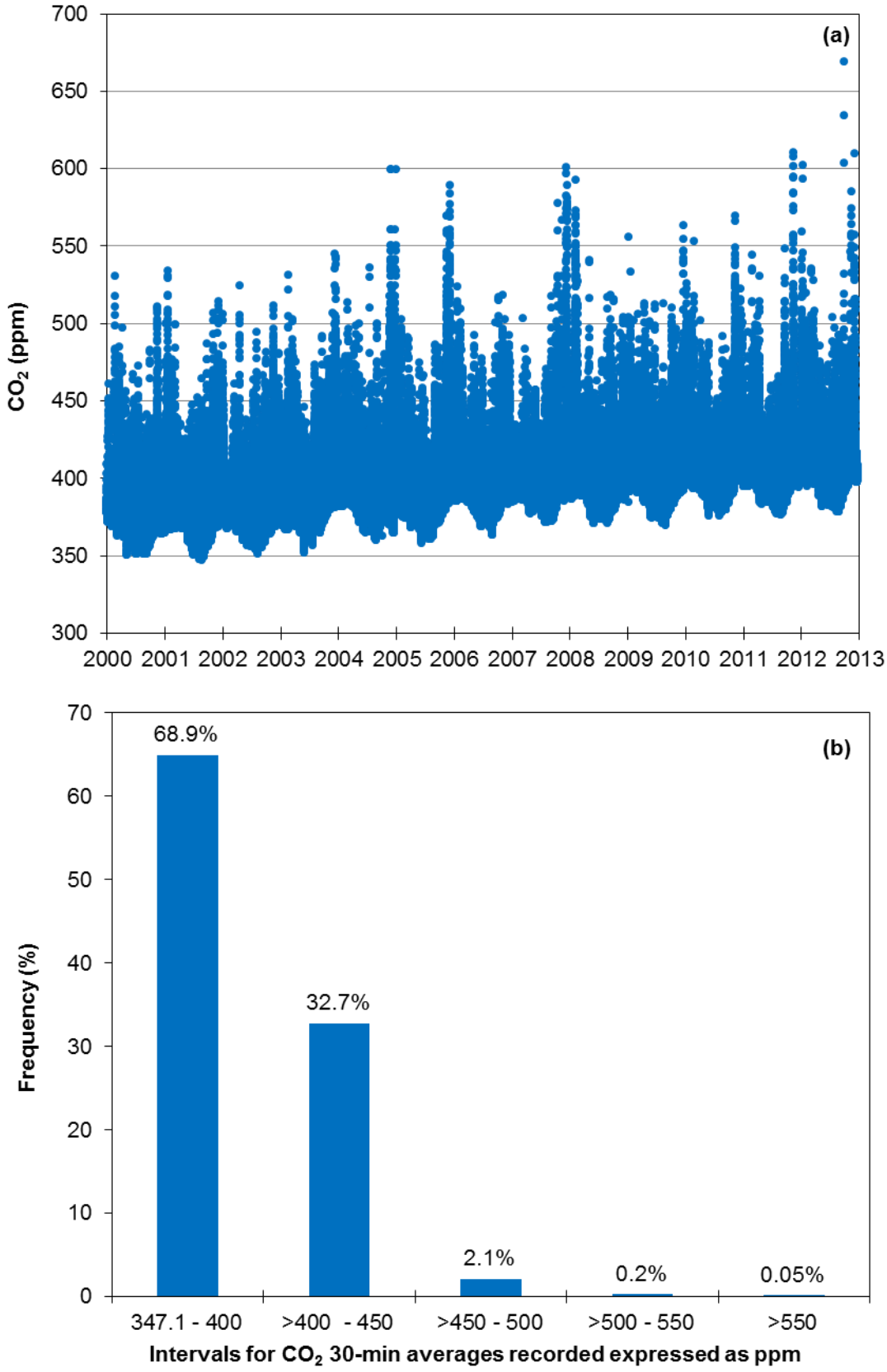

Figure 4.2(a). CO_2 30-min averages; **(b).** histogram for 30-minutes averages of CO_2 at the EGH site from January 2000 to December 2012.

The pollution episodes shown in Figure 4.2(b) can be divided into: a) summer episodes, b) winter episodes and c) long-range transport episodes, and are analysed in Section 7.2. The summer episodes are due to chemical reactions of mixtures of air pollutants emitted by automobiles, fuel burning and solvent usage, which are accelerated by the sunlight and high summerly temperatures. The winter pollution episodes are caused by strong surface radiation inversion trapping local emissions; the breakdown of this inversion with subsequent transport of CO_2 from aloft to the surface. Nakazawa et al. (1991b) observed at the Syowa monitoring station in Antarctica, that large CO_2 concentrations were recorded when low wind speed prevailed, which avoided the CO_2 dispersion generated by local sources keeping their emissions close to the sources. The long-range transport episodes are caused by the transport of pollutants from highly industrialized areas in Europe and occasionally North Africa. Winterly and summerly episodes were occasionally recorded at the EGH site during 2000-2012. When pollution episodes occurred, CO_2 levels reached several times up to 200% the 13-year though their frequency decreased along the period.

The secular trend observed in Figure 4.2(b) shows persistent annual increases in CO_2 levels, which are caused by the combustion of fossil fuels (IPCC, 2013). The increasing overall trend is in accordance with that observed worldwide and is studied in Section 4.5 (Ramonet et al., 2010; Tans et al., 2014).

4.3. Analyses of CO_2 records on daily and weekly time-scales

CO_2 daily averages were calculated from 30-min averages and are plotted in Figure 4.3(a). CO_2 daily averages ranged from 356.8 to 533.0 ppm CO_2, recorded in August 15, 2001 and December 13, 2007, respectively. Figure 4.3(b) shows frequencies of CO_2 daily averages in 4 categories. The largest frequency of CO_2 daily averages averages was observed for values between 356.8 and 400 ppm CO_2 (64.2%), a frequency of 34.5% was recorded for averages >400-450 ppm CO_2, whereas very low frequencies for averages >450-500 and >500 ppm CO_2 were observed, 1.1% and 0.09%, respectively.

Figure 4.3(a) shows clearly the seasonal cycle, pollution episodes and the secular trend. The largest CO_2 concentrations were observed during winter, when also the largest CO_2 daily averages were recorded due to the occurrence of pollution episodes and poor dispersion conditions. Such episodes were recurrently observed

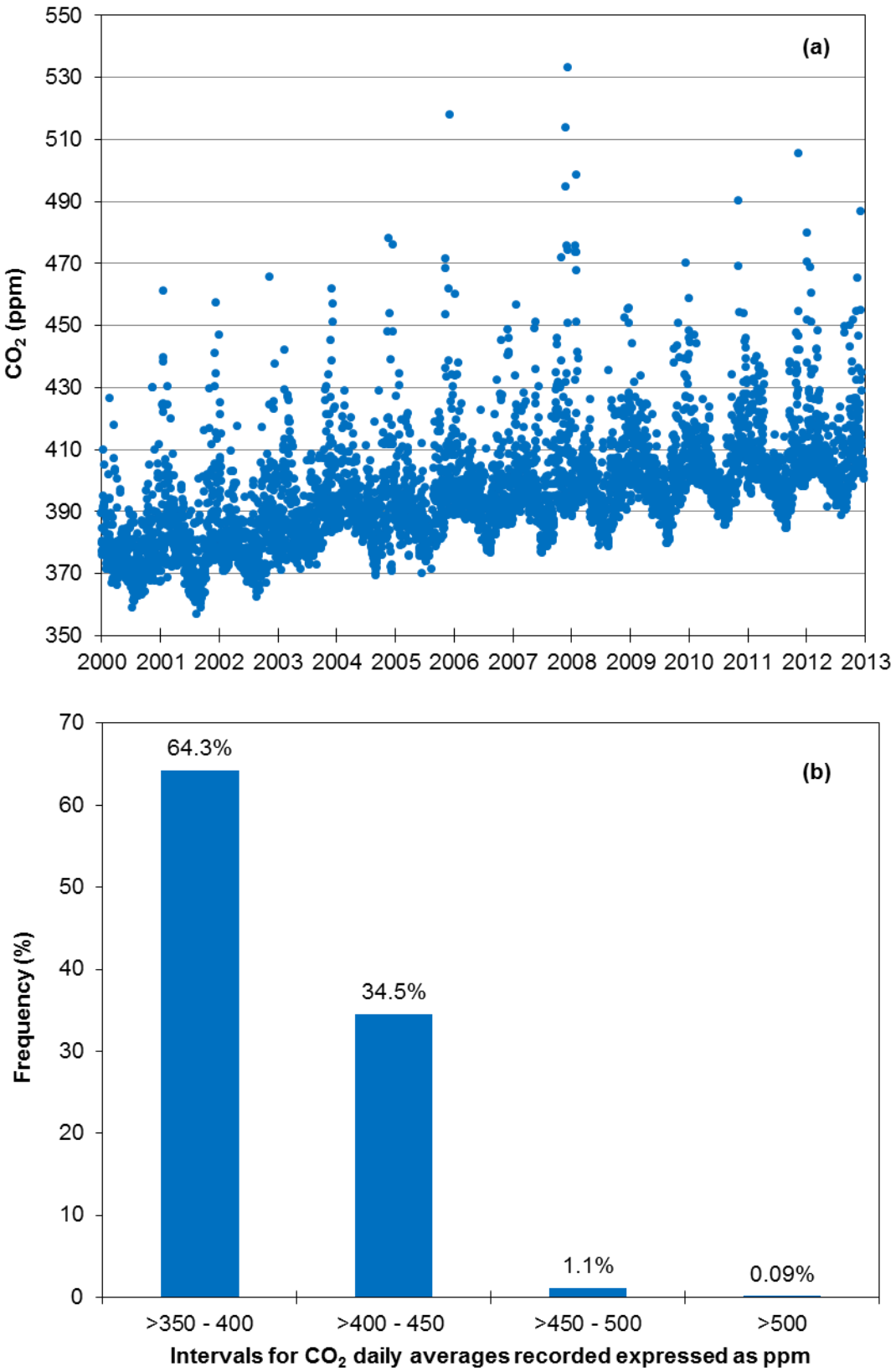

Figure 4.3(a). CO_2 daily averages calculated from 30-min averages; **(b)** Histogram for daily averages of CO_2 recorded at the EGH site during January 2000-December 2012.

by early February each year. CO_2 concentrations decrease by mid-March, which is ascribed to the beginning of leaves growing, net sink of CO_2 (Piao et al., 2008;

Barichivich et al., 2012). The lowest concentrations CO_2 concentrations are recorded during summer, when the vegetation activity is enhanced (Barichivich et al., 2013). CO_2 concentrations increase after summer, from early September and during autumn up to winter, when the peak of the seasonal cycle is observed.

CO_2 weekly averages were calculated from daily averages (Figure B1). CO_2 weekly averages show more clearly seasonality, pollution episodes and the secular trend. The CO_2 seasonal cycles at EGH are consistent with CO_2 seasonal cycles reported previously at other monitoring stations in the northern hemisphere (Table 4.1), with the peaks of the cycles in winter and the troughs in summer. As reported previously, these cycles show the important role in driving seasonally CO_2 concentrations by vegetation (Piao et al., 2008; Barichivich et al., 2012; 2013). The high CO_2 averages observed during winter are caused by the occurrence of pollution episodes (duration of one week).

4.3.1. CO_2 diurnal cycle at the EGH site

Diurnal variations were calculated using normalised daily cycles derived from average diurnal cycles by subtracting or adding daily averages in order to remove the impacts of long-term trends (Zhang and Zhou, 2013). The overall diurnal cycle is plotted in Figure 4.4, whereas diurnal variations split by seasons are plotted in Figure 4.5. The CO_2 diurnal cycle arises from a combination of several factors such as photosynthesis and respiration, changes in emissions from automobiles and domestic heating, and changes in meteorological conditions (Zhou et al., 2003; Haszpra et al., 2008; Zhang et al., 2013).

The CO_2 diurnal cycle observed at EGH is similar in shape to CO_2 cycles observed both at urban and rural stations (Vogt et al., 2006; Rigby et al., 2008b; Haszpra et al., 2008; Haszpra and Barcza, 2010;s Zhang et al., 2013), with the largest concentrations recorded during nighttime due to a stable nocturnal boundary layer followed by a decrease after sunrise caused by the enhancement of mixing processes during morning (Rigby et al., 2008b).

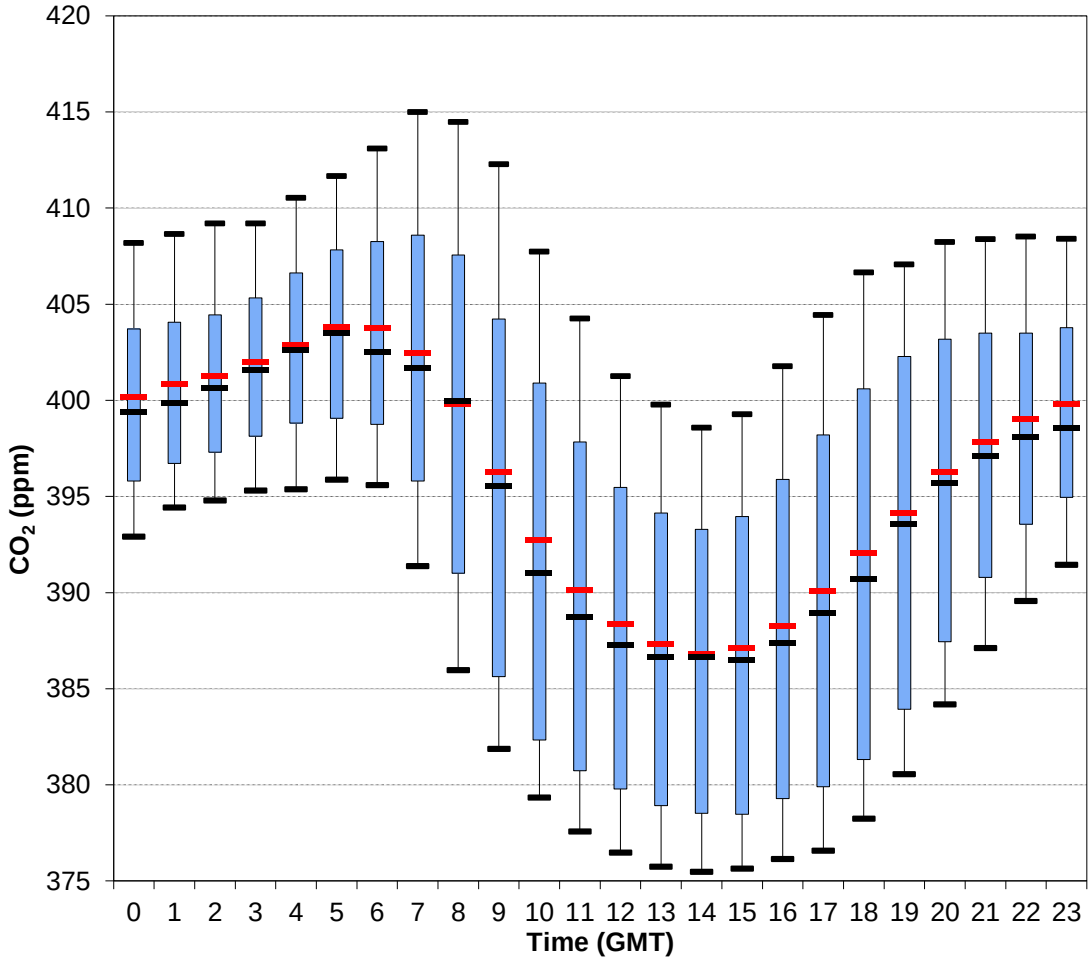

Figure 4.4. Averaged daily cycle for CO_2 records at EGH from 2000 to 2012. Black and red lines represent the median and average respectively. Vertical bars (whiskers) correspond to the 10th and 90th percentiles.

Figure 4.4 shows that the largest CO_2 hourly averages are recorded during nighttime due to the stability of the boundary layer and poor mixing processes. By contrast, the lowest CO_2 concentrations are recorded at mid-afternoon, as combination of enhanced mixing processes and photosynthetic uptake decreases the ambient CO_2 (Haszpra et al., 2008). CO_2 concentrations increase constantly during afternoon when larger dispersion of data is observed due to seasonal variability and contrasts with consistent data recorded in nighttime. No significant difference was found between averages and median values (p>0.05), therefore in this thesis CO_2 averages are used to describe the diurnal variations.

4.3.2. CO_2 diurnal cycles on a week time basis at the EGH site

At EGH, the largest daily amplitude value (AV_d) of 26.3 ppm CO_2 occurs in summer with a peak at 05:00 GMT and trough at 14:00 GMT; the smallest AV_d of 10.2 ppm CO_2 is in winter with a peak at 09:00 GMT and a trough at 14:00 GMT (Figure 4.5).

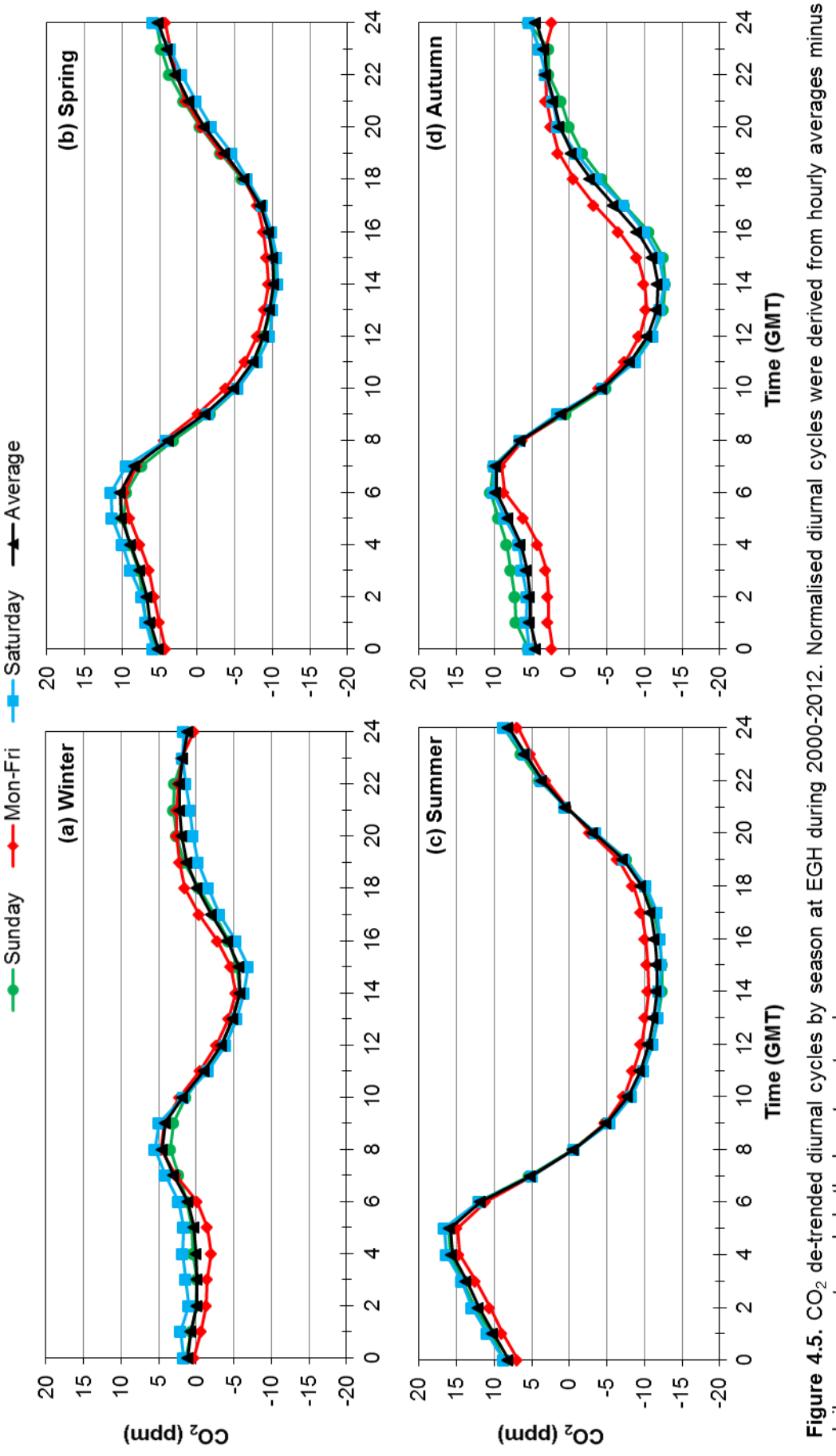

Figure 4.5. CO_2 de-trended diurnal cycles by season at EGH during 2000-2012. Normalised diurnal cycles were derived from hourly averages minus daily averages to exclude the long-term trend.

The larger AV_d in summer is due to an enhanced biological (photosynthesis-respiration) system with more abundant vegetation in the 'green belt' around EGH. By contrast, in winter, the predominance of deciduous trees and slower growth of vegetation produces the smallest diurnal AV_ds. The morning peak of CO_2 on top of the daily cycle, particularly in winter, highlights the contribution of combustion sources (particularly transport and domestic heating) of CO_2 to the biological system. Table B1-4 list standard deviations for CO_2 hourly averages by season.

At EGH, an average AV_d of 17.0 ppm CO_2 was calculated for the 13-year averaged daily cycle. A similar winter AV_d of 7 ppm CO_2 was recorded at the rural site of Hegyhátsál, Hungary (Haszpra et al., 2008). However at EGH, the summer AV_d of 26 ppm CO_2 is half of 52 ppm CO_2 calculated in summer by Haszpra et al. (2008), which highlights differences in the biological system in the continental interior and the maritme-moderated climate of EGH. At an urban location in Basel, Switzerland, the summer AV of 61 ppm CO_2 reported by Vogt et al. (2006) is much higher than that at EGH. The Basel station is greatly affected by traffic load and wind speed conditions leading to a higher variability than at EGH, but has also a greater annual temperature variation to exacerbate the biological system.

The normalised daily cycle shows the largest CO_2 concentrations at EGH before sunrise (Figure 4.), the earliest being at 05:00 GMT in summer and the latest at 09:00 GMT in winter. The peaks in the CO_2 cycle appear before the biological system becomes a net CO_2 sink and are enhanced by shallow night-time boundary layers (Haszpra et al., 2008; Larson and Volkmer, 2008). Also, vegetation respiration contributes to atmospheric CO_2 as maximum biological activity occurs before sunrise, hence the peak in the CO_2 cycle follows the timing of sunrise during the year. Boundary layer break up, vertical mixing after sunrise and the onset of net biological CO_2 uptake enhance the AVs and leading to cycle minima at EGH at 14:00 GMT due to the biological system. This is observed clearly in summer when the vegetation uptake reaches its maximum activity (Haszpra et al., 2008).

4.3.3. CO_2 diurnal and weekly cycles at the EGH site on wind direction basis

The build-up of atmospheric CO_2 is not constant and changes day-to-day producing a weekly cycle. Wind speed and direction also play an important role driving diurnal and weekly CO_2 cycles. Seasonal changes in meteorology also have significant effects driving diurnal and weekly CO_2 cycles. As described in Section 2.5, eight

wind sectors of 45° starting from 0° ± 22.5° were defined to perform the analysis of wind occurrence at EGH.

Figure 4.6 shows CO_2 weekly cycles by season for the eight wind sectors defined. The CO_2 weekly cycle responds mostly to changes in emissions from transport, domestic heating and, to a lesser extent, industrial activities. Those activities differ from weekdays to weekends depending on season and meteorological conditions. The CO_2 weekly cycle is largely dependent on the rush hour, as large CO_2 emissions are recorded (Helfter et al., 2011). The EGH site is close to the A30 and M25 motorways, the latter the most crowded motorway in southeast England. The observed appears to be affected both by the CO_2 emissions during the rush hour during mornings and evenings and by the dispersion processes within the boundary layer (Monni and Syri, 2011).

Figure 4.6 shows that CO_2 highest concentrations were recoded when air masses arrived at the EGH site from the SE, E and NE sectors, whereas the lowest CO_2 concentrations were observed in air masses origins from S and SW (background sector) in all seasons. The largest variability was also observed for the weekly cycle of the SE sector. For the NE wind sector, where Heathrow airport is located CO_2 concentrations were slightly lower than the largest in SE air masses. Interestingly, CO_2 concentrations for E air masses, where Greater London is located were not the largest observed.

In winter, the highest CO_2 concentrations were recorded arriving from E and SE wind sectors. There is no pattern between wind sectors and largest concentrations, since during some days largest CO_2 concentrations arrived from the SE sector and others from NE. Interestingly, the CO_2 lowest concentrations were identified in air masses arriving from the S and SW, consistently with the cleanest sectors. Over night-time the CO_2 lowest concentrations arrived in winds from SE, whereas in daytime from SW. Also differences between seasons patterns were observed. For example, in winter the highest CO_2 concentrations coincided with air masses from the SE and NE, whereas in spring arrived only from the SE.

Surprisingly, in spring the E sector showed CO_2 concentrations even lower than the background sector (SW). Overnight, the lowest CO_2 concentrations arrived from the S, whereas in daytime from the E. It contrasts with the fact that the SW sector, the

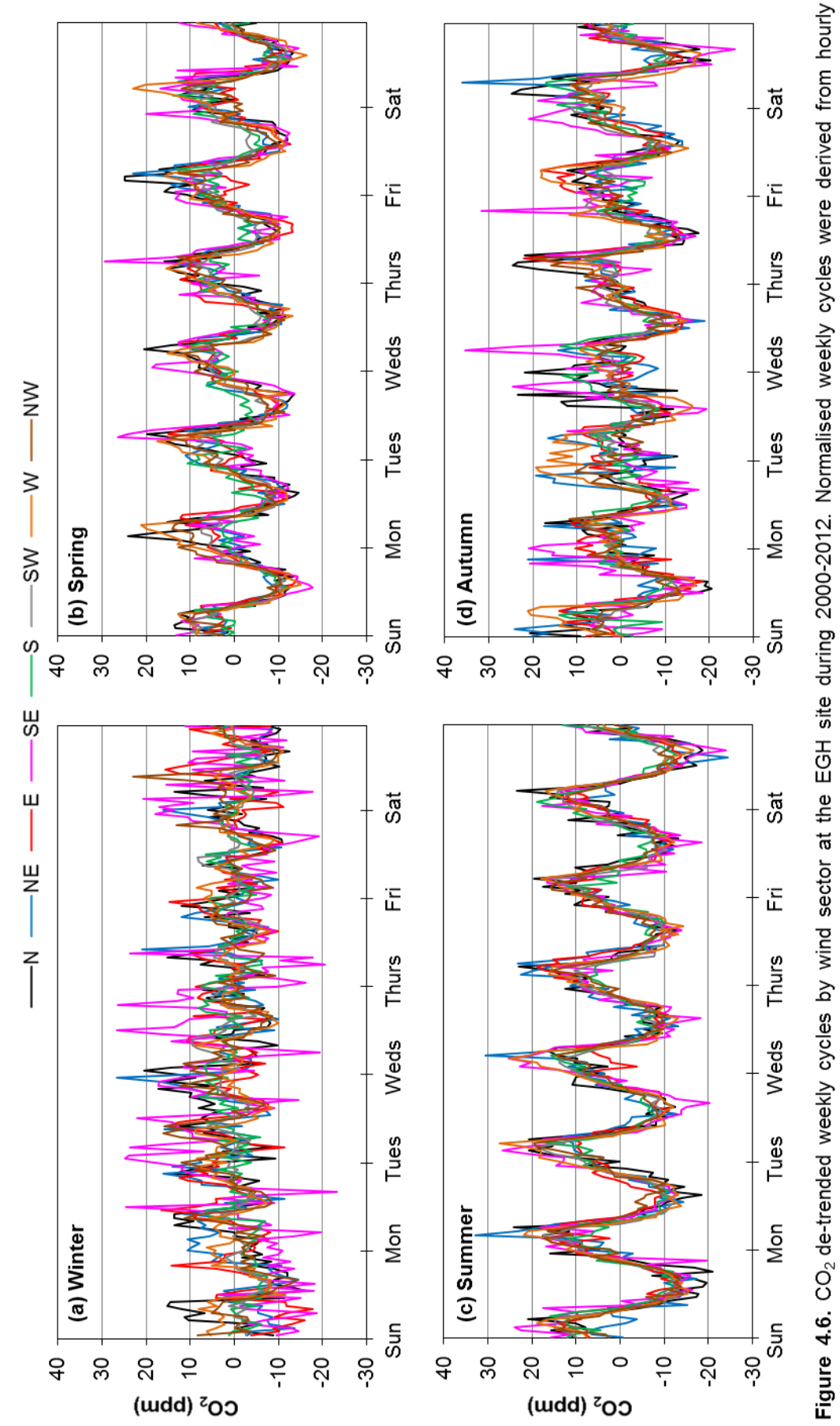

Figure 4.6. CO_2 de-trended weekly cycles by wind sector at the EGH site during 2000-2012. Normalised weekly cycles were derived from hourly averages minus weekly averages to exclude the long-term trend.

background, was not the cleanest sector and air masses did not show the lowest CO_2 concentrations (Figure 4.6b). Minor variability in the CO_2 weekly cycle was observed in summer compared with the other seasons. Although, the CO_2 largest concentrations were recorded in air masses from the SE and NE, no significant difference (p>0.05) among all the sectors was seen. Indeed, some wind sectors showed lowest CO_2 concentrations that the background.

In autumn, the CO_2 greatest concentrations arrived from different sectors: on Monday, Tuesday Wednesday and Friday from the SE, whereas in weekends from the NE. The largest peak of CO_2 was identified from the N sector on Thursday like in spring, and also the cleanest sector over daytime was the E, whereas on nighttime was the S, and only during Tuesday was the N sector. For the rest of the sectors no defined pattern was observed.

Weekdays showed larger CO_2 concentrations and larger variability than weekends in all the wind sectors, which is due to human behaviour. Larger CO_2 concentrations corresponding to the daily cycle peaks were greater during weekdays than weekends, whereas the lower CO_2 values correspond to the troughs of daily cycles during weekends. Automobile emissions lead to larger CO_2 concentrations during weekdays than weekends; however the AVs for weekdays and weekends are mostly dependent on the vegetation respiration process rather than automobile emissions (Haszpra et al., 2008).

Seasonality influences the highest and lowest CO_2 concentrations timing in the weekly cycle. CO_2 weekly cycles show maximum concentrations before the morning rush hour began and were recorded daily by 5:00 and 6:00 GMT in spring, summer and autumn, and by 8:00 and 9:00 GMT in winter. Only during winter, the CO_2 largest values coincided with the morning rush hour, which highlights that automobile emissions are not the main factor driving the CO_2 weekly cycle. Although, the same profile was observed for all the seasons, AVs ranging from 9.4 to 26.1 ppm CO_2 during weekdays and from 9.3 to 28.4 ppm CO_2 over weekends were calculated. Despite different the AV_ds, no significant difference (p>0.05) was found between daily and weekly CO_2 AV_ds in all the seasons. Thus, the CO_2 weekly cycle can be seen as the combination of changes in emissions but also in sinks due to seasonality.

4.4. CO_2 seasonal cycles at the EGH site

CO_2 seasonal cycles respond to changes in temperature, vegetation extent, combustion emissions and meteorology. As consequence, CO_2 seasonal cycles vary from site-to-site, spatial variations, and from year-to-year, inter-annual/temporal variations (Keeling et al., 1989; Thoning and Tans, 1989; Dettinger and Ghil, 1998; Piao et al., 2008). Seasonal cycles were obtained by filtering the data set with STL at EGH (Figure 4.7a). The shape of the cycles is similar each year, with winter maxima and summer minima. Maxima, are observed in January in 2000 and 2001, in December from 2002 to 2009, and in November from 2010 to 2012. By contrast, apart from 2003 (June) and 2006 (July), minima are consistently seen in August. Shoulders in the cycles are observed in February due to the prevalence of higher W wind speeds than in January and March. The advection of background westerly air masses generates convective conditions that disperse local emissions, and dilute the CO_2 accumulated by mixing it with clean air.

The averaged CO_2 yearly cycle at EGH was calculated by averaging each month (data filtered with STL) during 200-2012. Figure 4.7(b) shows the averaged CO_2 yearly cycle; data are relative to the overall yearly average. The largest CO_2 concentrations are observed in winter, whereas the lowest in summer. The peak of the cycles appears in December and the trough in August. After the winterly peak, CO_2 decreases constantly with the beginning of the growing season in spring, when vegetation becomes a net sink of CO_2. Then CO_2 concentrations are the lowest during July and August, and start to increase with the beginning of the fall season. From September onwards, CO_2 increases constantly until December. The largest variations are observed during winter and summer, where standard deviations are larger during than in spring. This is may be caused by year-to-year within the seasons, and can be ascribed mostly to vegetation (Barichivich et al., 2012).

The average seasonal amplitude value (AV_s) was calculated using STL for the 13-year record as 21.7 ± 3.4 (1SD) ppm CO_2. The lowest AV_s was 17.0 ppm in 2003 with the largest of 27.1 ppm in 2008. Despite annual variability in the AV_s, an annual growth rate of 0.64 ppm CO_2 yr^{-1} in AV_s was obtained (Figure 4.7(c)). This observed growth rate is statistically significant (*p=0.005*). Variable AV_s and an increasing trend agree with several previous studies (Cleveland et al., 1983; Thoning and Tans, 1989; Dettinger and Ghil, 1998; Zhang and Zhou, 2013). AV_s growth rates are due to increases in fossil fuel combustion, changes in the growing vegetation

season (Barichivich et al., 2012; 2013), and changes in surface ocean and land temperatures (Cleveland et al., 1983; Dettinger and Ghil, 1998).

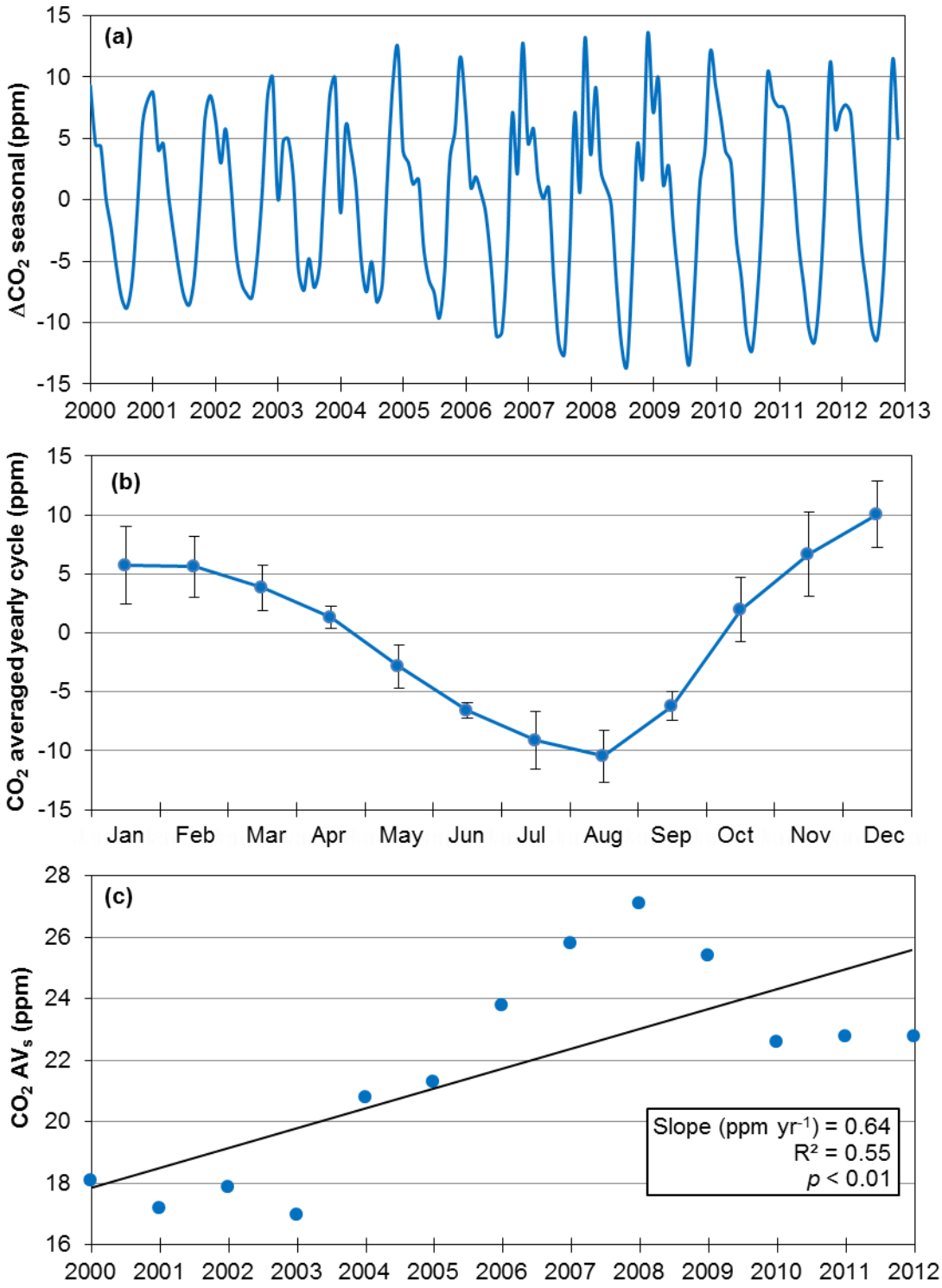

Figure 4.7(a). De-trended seasonal cycles of CO_2 at EGH during 2000-2012 calculated by filtering the monthly averages with the STL technique; **(b).** yearly averaged cycle of atmospheric CO_2 calculated from the filtered values with STL, error bars represent 1SD; **(c).** upward trend in CO_2 seasonal amplitudes (AV_s). AV_s is defined as the difference in ppm CO_2 from peak-to-trough within one-seasonal cycle.

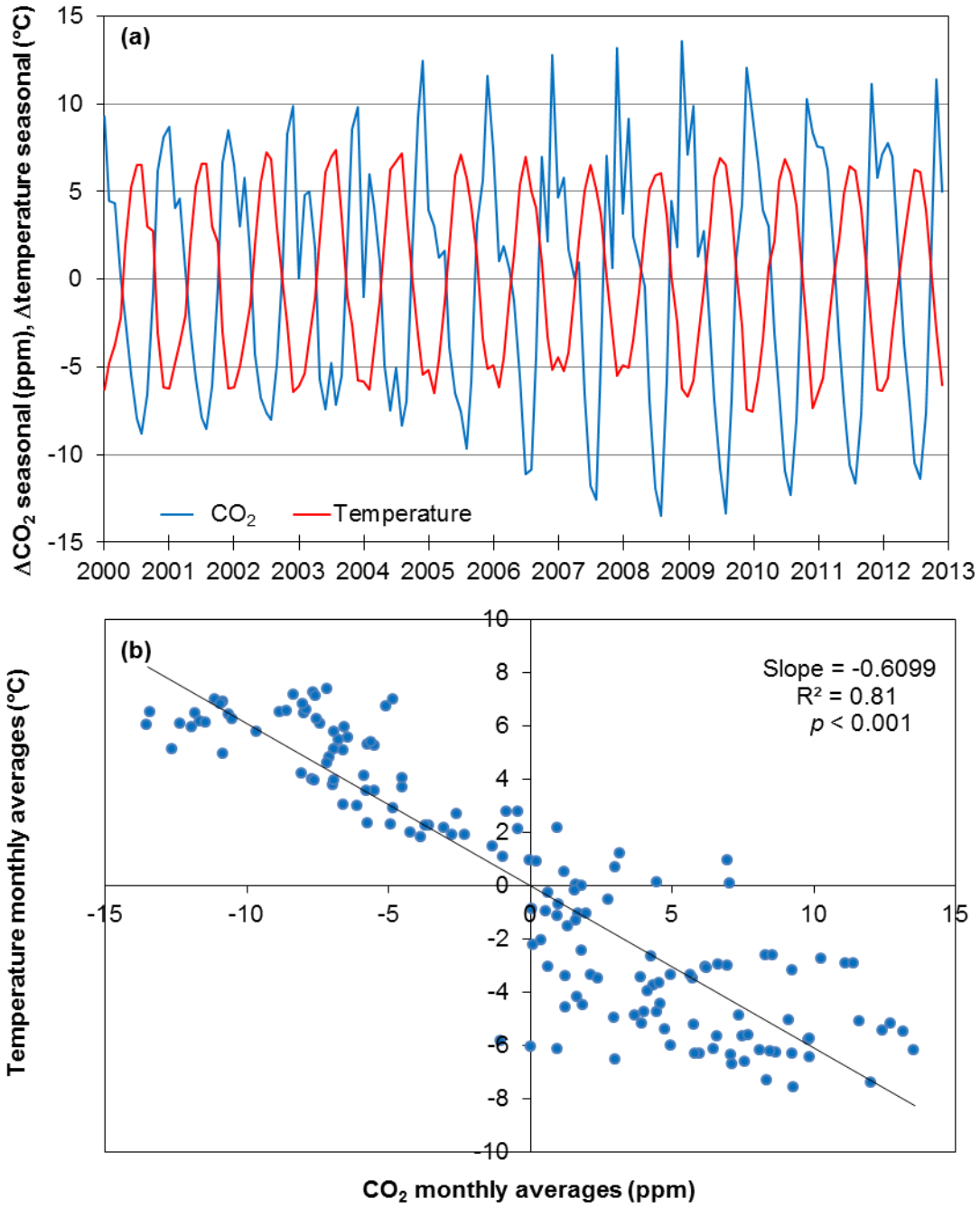

Figure 4.8(a). CO_2 and temperature seasonal cycles; **(b).** linear regression for CO_2 and temperature monthly values of the seasonal cycles from 2000 to 2012 obtained by filtering monthly averages with the STL technique.

The onset of the growing season in the northern hemisphere, and thus CO_2 uptake are strongly coupled with temperature (Haszpra and Barcza, 2010; Barichivich et al., 2012; 2013). Monthly de-trended averages of CO_2 and temperature were obtained from the dataset using the STL filtering technique (Figure 4.8(a)). Results show a strong anti-phase relationship of the seasonal cycles of CO_2 and temperature with linear regression analysis confirming a negative correlation with an r^2 value of 0.81 and significance of *p<0.001* for 156 monthly averages (Figure

4.8(b)). Temperature increases also modify the CO_2 AV_s by increasing respiration rates, enhancing CO_2 release, and prolonging the growing season and thereby increasing CO_2 uptake from the atmosphere (Piao et al., 2008). However at EGH, no local effect of the temperature was associated with increasing AV_s of CO_2, which confirms that the AV_s is due to factors other than temperature variations, such as changes in traffic flows.

4.4.1. Comparison of CO_2 seasonal cycles and AVs from filtered data with STL and unfiltered data

CO_2 seasonal cycles and AV_s at EGH from unfiltered and data filtered with STL are compared in order to investigate possible differences (Figure B2, Table 4.2). Differences in the maxima and minima of the CO_2 seasonal cycles were observed as shown in Table 4.2. For unfiltered data, maxima occurred mostly in December, whereas for STL data maxima showed larger variability. Interestingly, the minima for unfiltered data coincided with STL data mostly in August. This makes clear that the trend component in unfiltered data can obscure inter-annual variations as has been reported (Cleveland et al., 1990; Dettinger and Ghil, 1998). It also highlights the importance of using an adequate technique to filter the CO_2 data in order to study properly the seasonal cycles and variations, which can improve the accuracy and quality of the analysis, especially for monitoring sites where the trend component is strong.

Differences in seasonal AV_s (unfiltered minus STL) were also observed, and ranged from -4.2 ppm CO_2 (2006) to 11.7 ppm CO_2 (2007). Whereas minimum significant difference (p<0.01) was found for the growth rate of AV_s calculated from filtered data with STL, no significant difference was found for the growth of AVs for unfiltered data (p>0.05).

4.4.2. CO_2 seasonal cycles by wind sector

CO_2 seasonal cycles and averaged yearly cycles by wind sector were calculated from STL filtered data. Analyses show that the SE sector has the largest AV_s (34.7 ppm CO_2), whereas the SW, the background, the lowest AV_s (14.8 ppm CO_2). The CO_2 AV_s for all wind sectors are listed in Table 4.3. Data show that the maxima of the cycles was observed mostly in December for all the sectors, and only in the E sector was in November. By contrast, the minima of the cycles was seen in August

Table 4.2. Comparison between AV_s of CO_2 from unfiltered data and STL data from 2000 to 2012 at the EGH site.

Year	2000	2001	2002	2003	2004	2005	2006	2007	2008	2009	2010	2011	2012
Unfiiltered	14.1	24.3	19.9	23.6	21.8	30.8	19.6	37.5	32.6	24.5	28.7	29.3	19.8
STL	18.1	17.2	17.9	17.0	20.8	21.3	23.8	25.8	27.1	25.4	22.6	22.8	22.8
ΔUnfiltered-STL	-4.0	7.1	2.0	6.6	1.0	9.5	-4.2	11.7	5.5	-0.9	6.1	6.5	-3.0
Max Unfiltered	Jan	Jan	Dec	Dec	Feb	Dec	Jan	Dec	Feb	Dec	Dec	Nov	Feb
Max STL	Jan	Jan	Dec	Dec	Dec	Dec	Dec	Dec	Dec	Dec	Nov	Nov	Nov
Min Unfiltered	Aug	Aug	Jul	May	Sep	Jul	Aug	Jul	Aug	Aug	Aug	Aug	Aug
Min STL	Aug	Aug	Aug	Jun	Aug	Aug	Jul	Aug	Aug	Aug	Aug	Aug	Aug

CO_2 AVs expressed in ppm.

(N, E, S, SW and NW) and in July (for NE, SE and W). Differences in CO_2 AV_s are due to a combination of seasonal changes in traffic, human behaviour at regional scale and to the substantial human transformation of the land surface, especially in rural and semi-rural areas (Randerson et al., 1997). Chase et al. (1996) observed that the main human-induced changes in surface roughness, albedo, and leaf area have the potential to change the humidity, wind speed, planetary boundary layer height and the general circulation of the atmosphere, which have been observed that affect strongly the atmospheric mixing ratio.

Table 4.3. CO_2 seasonal cycles of wind sector for STL data averages from 2000 to 2012.

Sector	N	NE	E	SE	S	SW	W	NW
AV_s	28.5	21.4	34.7	30.8	17.4	14.8	17.1	24.6
Maxima	Dec	Dec	Nov	Dec	Dec	Dec	Dec	Dec
Minima	Aug	Jul	Aug	Jul	Aug	Aug	Jul	Aug

**Maxima and minima correspond to the average seasonal CO_2 cycle from STL data.*
***AVs expressed in ppm CO_2.*

4.4.3. Influence of the PBL height on CO_2 yearly cycle

The relationship between CO_2 monthly averages for each month calculated from 13-years of measurements at the EGH site and the estimated PBL height at the UK reported in the Fourth Report of the Photochemical Oxidants Review Group (PORG, 1997) is shown in Figure 4.9. Linear regression from least squares shows that there is significant relation between CO_2 concentrations and PBL height (p<0.01). The largest CO_2 concentrations correspond to low PBL heights recorded during winter (300 m). By contrast, the lowest CO_2 concentrations coincide to the largest height of the PBL (1000 m), which occur during summer (July and August).

During winter, the stable boundary layer caused by low wind speeds and cold temperatures keep the CO_2 emissions close to the ground and avoid their dispersion (Worthy et al., 1994; Netcen, 2003). By contrast, the enhanced mixing processes during summer promote the dispersion of CO_2 emissions, which is also coupled with the advection of clean air masses from the background sector that can dilute the CO_2 build-up.

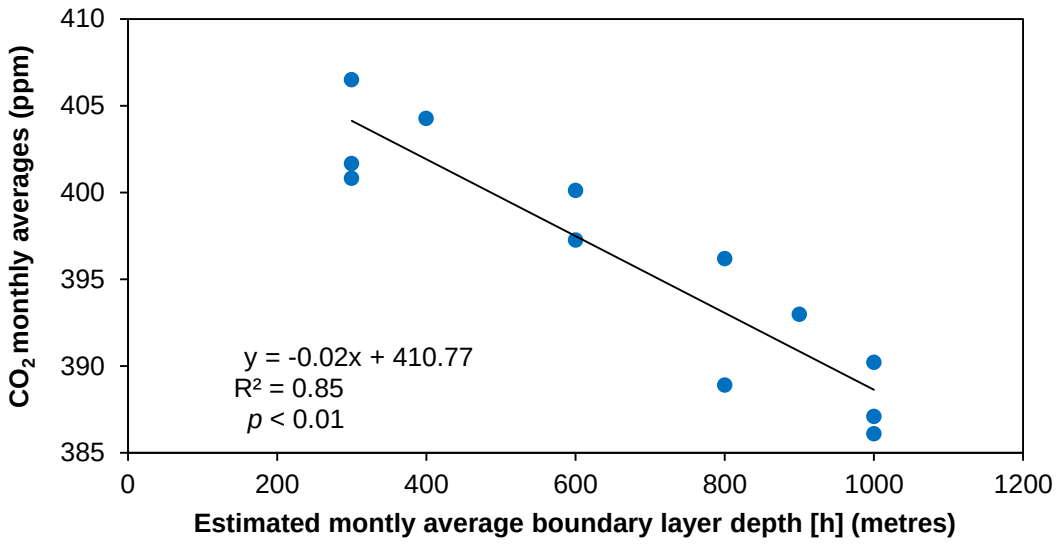

Figure 4.9. Relationship between PBL depth and monthly averages of the CO_2 averaged yearly cycle at EGH from 2000 to 2012. Monthly averages span the same month during 13-years of measurements.

4.5. Long-term trends of CO_2 at the EGH site during 2000-2012

4.5.1. CO_2 monthly averages and filtered trend computed with STL

CO_2 monthly averages were calculated from daily averages recorded at the EGH site from 2000 to 2012. Monthly averages were calculated using the criteria previously established of 75% data capture to consider averages as valid. During 13-years measurements, 156 monthly averages were calculated from daily averages, which represent 100% of coverage. Monthly standard deviations were calculated from daily averages. Figure 4.10(a) shows unfiltered monthly averages and 1SD from 2000 to 2012. CO_2 monthly averages ranged from 370.0 ppm CO_2 in August 2001 to 425.4 ppm CO_2 in November 2001. By contrast, SDs ranged from 3.1 ppm CO_2 to 37.6 ppm CO_2 in December 2007. No relationship was observed between the timing for the largest CO_2 monthly averages and the largest SDs.

Figure 4.10(a) shows the typical features of a CO_2 data set from the northern hemisphere, such as the largest CO_2 concentrations during winter and the lowest CO_2 concentrations in summer. The seasonal component (Section 4.4) and the upward trend (secular trend) can be also observed. The greatest variability occurs during winter and can be clearly seen from the standard deviation bars in Figure 4.10(a). As shown in Section 4.4, the CO_2 seasonal cycles show the largest concentrations in winter and lowest concentrations during summer as reported by Dettinger and Ghil (1998), Derwent et al. (2002), Haszpra et al. (2008) and Haszpra

and Barcza (2010). Calm conditions promote the development of a stable layer which traps the pollutants close to the ground and avoid their dispersion leading to large CO_2 concentrations during winter.

The CO_2 secular trend was calculated with the STL technique from unfiltered monthly averages at the EGH site from 2000 to 2012. The smoothed line in Figure 4.9b represents secular trend computed with the STL technique (Cleveland et al., 1990). The smoothed curve shows persistent increases in the CO_2 concentrations with declines in 2004 and 2008. The observed trend is in good agreement with other observations of an increasing build-up in CO_2 at the northern hemisphere during the same period (Aulagnier et al., 2009; Ramonet et al., 2010). The trend is also consistent with observations made by different cooperative networks for CO_2 observations (NOAA/ESRL/GMD), which have reported an increase of atmospheric CO_2 of 24.3 ppm during 2000-2012 (Tans and Keeling, 2014).

Residuals represent irregular variations beyond the seasonal cycles and secular trend (Figure 4.10(b)). The declines at EGH both coincide with observations from monitoring stations across the globe (Tans and Keeling, 2014), and are explained by two factors. A global increase in temperatures during 2003 and 2004, which may have led to increased uptake by vegetation and high oil prices during 2008 which caused a 50% reduction in the annual increase in global emissions of CO_2.

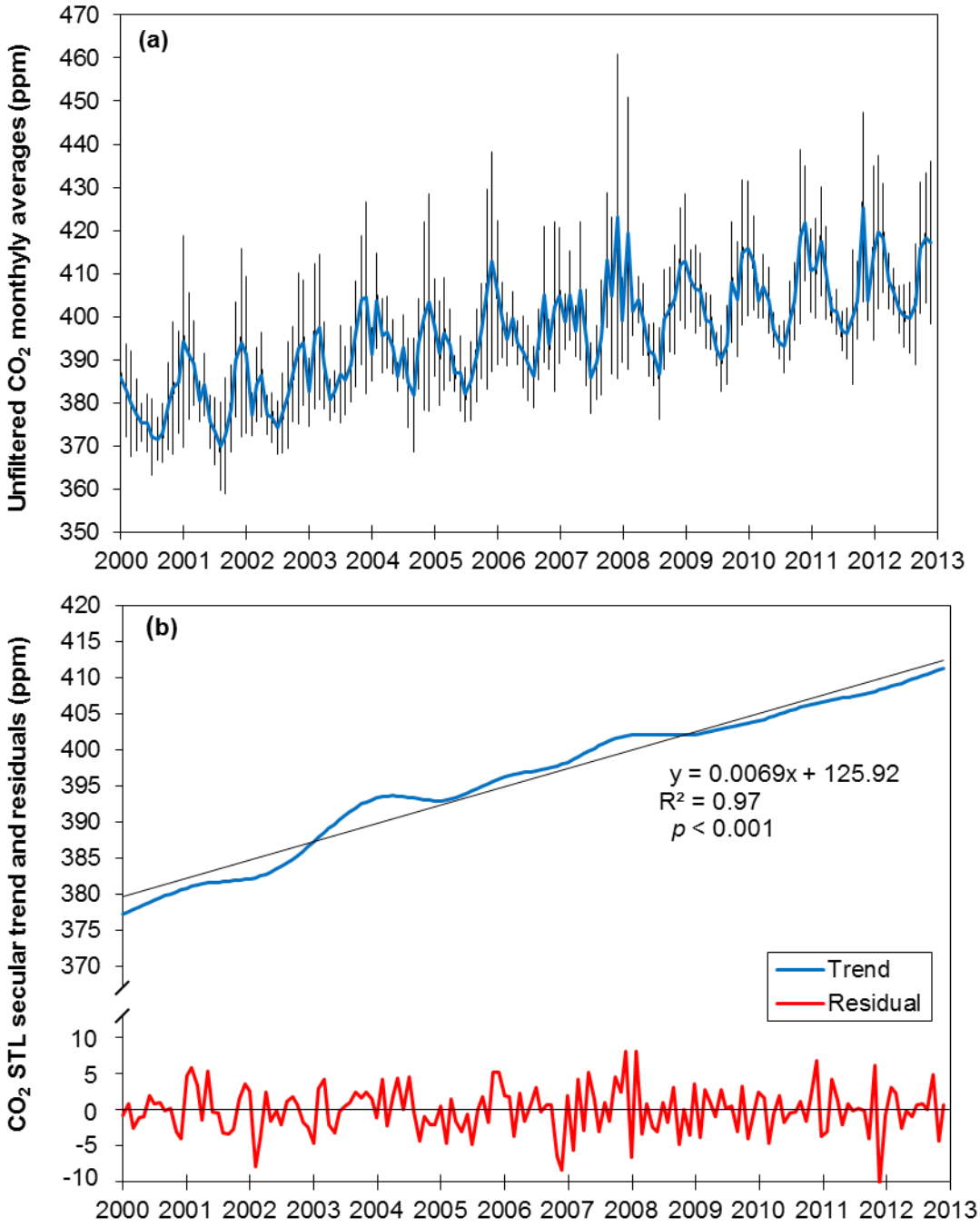

Figure 4.10(a). Unfiltered CO_2 monthly averages ± 1SD calculated from daily averages; **(b).** STL filtered CO_2 long-term trend and residuals observed at EGH during 2000-2012. The residuals represent the remaining CO_2 beyond the trend and seasonal components as defined by Cleveland et al. (1990).

4.5.2. *CO_2 long-term trend observed at EGH during 2000-2012*

CO_2 annual averages at the EGH site during 2000-2012 were calculated from monthly averages. Figure 4.11 shows the CO_2 annual averages at the EGH site from 2000 to 2012. Overall, a total increment of 31.8 ppm CO_2 is observed at EGH.

Annual variability is evident: at EGH annual changes in annual averages (ΔCO_2) range from -0.6 (2006-2007) to 7.8 ppm CO_2.

The Mann-Kendall test and Sen's estimate (Salmi et al., 2002) were used to calculate trends in annual averages at EGH, as shown in Figure 4.11. A statistically significant (p<0.01) average growth rate of 2.45 ppm yr^{-1} CO_2 was calculated at EGH. Annual residuals, defined as the difference of annual averages minus the Sen's estimates, ranged from -2.9 ppm CO_2 (2000) to 3.1 ppm CO_2 (2007). The largest residual observed is 3.1 ppm CO_2 in 2007, whereas the lowest residual at is -2.9 ppm CO_2 in 2000.

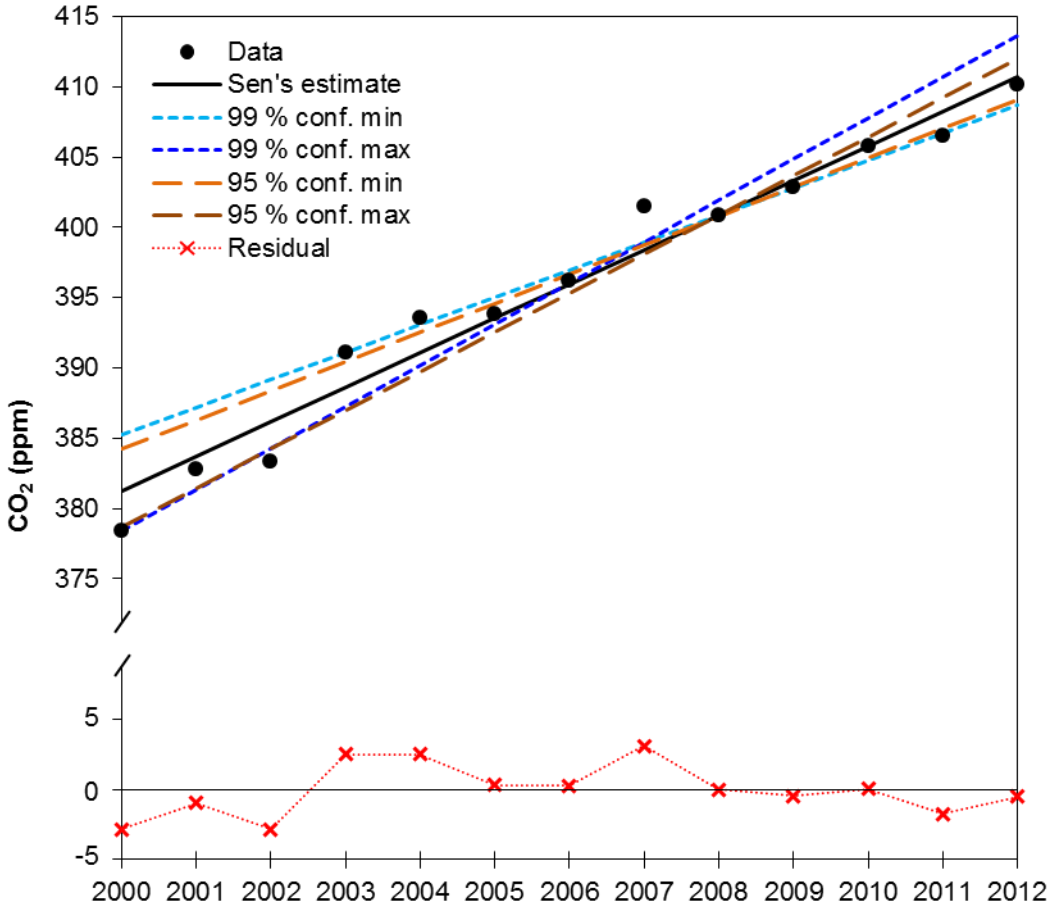

Figure 4.11. Annual averages and upward trend for atmospheric CO_2 at EGH over 2000-2012 calculated with the Mann-Kendall test and Sen's estimate, and annual residuals.

The Mann-Kendall and Sen's estimate method was compared with the least squares linear regression method in the Excel and SigmaPlot statistical software to verify the growth rate observed at EGH from 2000-2012. Annual CO_2 averages calculated from filtered data in order to remove seasonality are also compared with

Table 4.4. Comparison between Mann-Kendall and Sen's estimate tests for unfiltered and STL filtered data of CH_4 at EGH during 2000-2012.

CO_2 data	Test Z	Significance	Q[a]	Qmin99	Qmax99	Qmin95	Qmax95	B[b]	Bmin99	Bmax99	Bmin95	Bmax95
Unfiltered	4.6	***	2.45	2.0	2.9	2.1	2.8	381.3	385.2	378.4	384.2	378.7
STL filtered	4.7	***	2.46	2.1	3.0	2.1	2.7	380.8	384.6	378.5	384.0	379.0

Slopes and series data are expressed in ppm CO_2

°Test Z is performed when n≥10. The absolute value of Z is compared to the standard normal cumulative distribution to define if there is a trend or not at the selected level α of significance. A positive (negative) value of Z indicates an upward (downward) trend.

[a]True slope of linear trend

[b]First data of the series

The following symbols are used for the four tested significance levels α with which the Mann-Kendall trend shows that the null hypothesis of no trend should be rejected:

*** if trend at a = 0.001 level of significance

** if trend at a = 0.01 level of significance

* if trend at a = 0.05 level of significance

+ if trend at a = 0.1 level of significance (no symbol if a is greater than 0.1).

Qmin99: the lower limit of the 99 % confidence interval of Q (α= 0.1)

Qmax99 the upper limit of the 99 % confidence interval of Q (α= 0.1)

Qmin95: the lower limit of the 95 % confidence interval of Q (α= 0.05)

Qmax95: the upper limit of the 95 % confidence interval of Q (α= 0.05)

Bmin99: estimate of the constant Bmin99 for 99% confidence level of linear trend

Bmax99: estimate of the constant Bmax99 for 99% confidence level of linear trend

Bmin95: estimate of the constant Bmin95 for 95% confidence level of linear trend

Bmax95: estimate of the constant Bmax95 for 95% confidence level of linear trend

Table 4.5. CO_2 upward trends calculated by three different methods at the EGH site during 2000-2012.

Year	Unfiltered annual averages	STL annual averages	Unfiltered Sen's estimate	STL Sen's estimate	Unfiltered least squares Excel	STL least squares Excel	Unfiltered least squares SigmaPlot	STL least squares SigmaPlot
2000	378.4	379.0	381.3	380.8	380.8	380.7	380.8	380.7
2001	382.7	381.5	383.7	383.2	383.3	383.2	383.3	383.2
2002	383.3	383.9	386.2	385.7	385.9	385.8	385.8	385.7
2003	391.1	390.4	388.6	388.2	388.4	388.3	388.3	388.3
2004	393.6	393.3	391.1	390.6	390.9	390.9	390.8	390.8
2005	393.8	394.2	393.5	393.1	393.4	393.4	393.3	393.3
2006	396.2	397.0	396.0	395.5	395.9	395.9	395.8	395.9
2007	401.5	400.3	398.4	398.0	398.4	398.5	398.4	398.4
2008	400.9	402.0	400.9	400.5	400.9	401.0	400.9	400.9
2009	402.9	402.9	403.3	402.9	403.5	403.5	403.4	403.5
2010	405.8	405.3	405.8	405.4	406.0	406.1	405.9	406.0
2011	406.5	407.4	408.2	407.8	408.5	408.6	408.4	408.5
2012	410.2	409.9	410.7	410.3	411.0	411.1	410.9	411.1
Slope (ppm CO_2 yr^{-1})	N.A.	N.A.	2.45	2.46	2.51	2.54	2.51	2.54
Increase in CO_2 (ppm)	31.8	30.9	29.4	29.5	30.2	30.4	30.2	30.4
% increase in CO_2 (13-years)	8.4	8.2	7.7	7.7	7.9	8.0	7.9	8.0
Significance (*p*)	N.A.	N.A.	<0.001	<0.001	<0.001	<0.001	<0.001	<0.001

Annual averages and data series are expressed in ppm CO_2.

N.A.: *Not applicable*

unfiltered annual averages. Table 4.4-5 list upwards trends and growth rates calculated with the different methods.

No significant difference was found between CO_2 annual averages calculated from unfiltered monthly averages and from STL filtered monthly averages (p>0.05). Interestingly, though there is a difference in the total increase during the period of 0.9 ppm, between unfiltered and filtered annual averages, it is not significant. Similarly, the increase differs by 0.2%, which represents a total difference of 2% between both calculations. When analysed the growth trends calculated by the Sen's estimate for filtered and unfiltered data, also no significant difference was found (p>0.05).

Calculations for made with least squares regression in Excel and SigmaPlot showed exactly the same results as shown in Table 4.5. Similarly to Sen's estimations, no significant differences were found between filtered and unfiltered data for the upwards trends calculated with the linear squares regression tests included in Excel and Sigmaplot (p>0.05). In those, the total increase appears to be underestimated compared to unfiltered data by 1.6 ppm CO_2. A difference of 2% in the growth rate was obtained when the least squares methods were compared with the Sen's estimate.

The CO_2 growth is not constant and shows annual variability, which has been seen previously by Haszpra et al. (2008) and Ramonet et al. (2010). This is might be caused by different phenomena such as changes in temperature patterns due to the north Atlantic oscillation (Piao et al., 2008; Barichivich et al., 2013), which cause changes on the biosphere, annual hotter years can lead to increments in the uptake rate by vegetation and soil (Barichivich et al., 2012). Ramonet et al. (2010) attribute the observed upward trends in CO_2 to two possible causes: boundary layers becoming more shallow, and regional changes in CO_2 emissions within 500 km of the measurement locations, which account for 32% and 27%, respectively, of the trends. By contrast, Aulagnier et al. (2009) suggest a combination of the more shallow boundary layers and changes in wind speed.

4.5.3. CO_2 of long-term trends by wind sector at EGH during 2000-2012

CO_2 annual averages by wind sector and calm were calculated from unfiltered monthly averages in order to assess the variability recorded at EGH during 2000-2012 considering that no significant difference (p>0.05) was observed between filtered and unfiltered data (Section 4.5.2). Figure 4.12 shows the CO_2 upward trends by wind sector at EGH. CO_2 growth rates by wind sector were calculated using the Mann-Kendall test and Sen's estimate from unfiltered annual averages. Table 4.6 summarises growth rates, % of increase and significance for each wind sector.

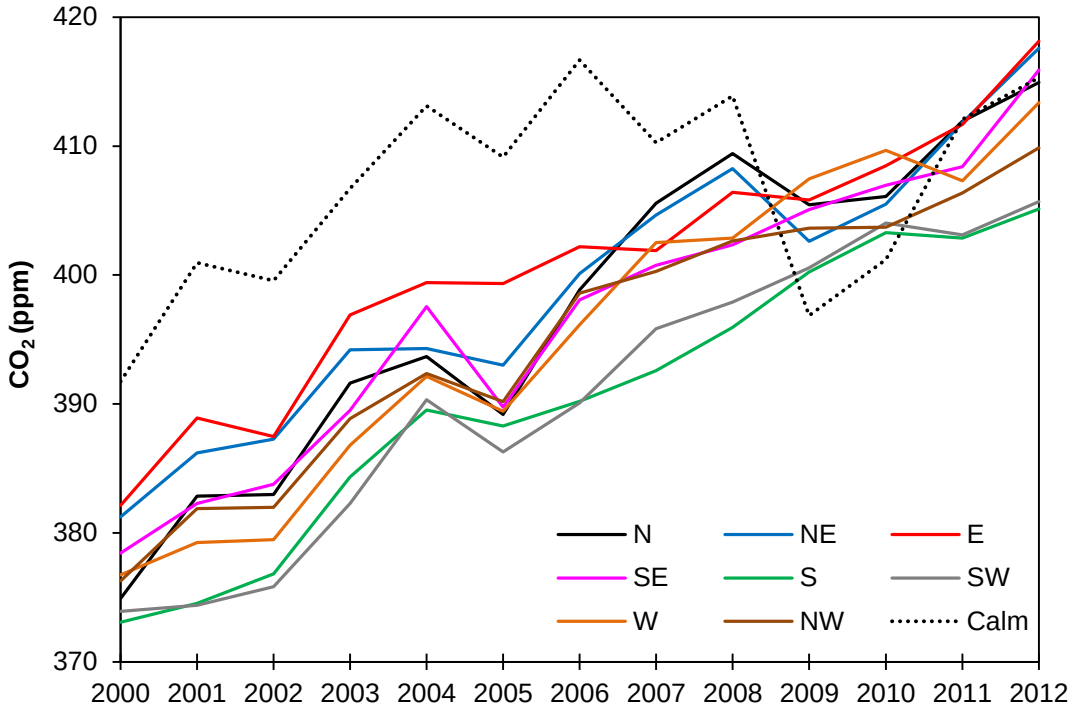

Figure 4.12. CO_2 annual averages and upwards trends for atmospheric CO_2 measured at EGH during 2000-2012 by wind sectors and calm. Annual averages were calculated from unfiltered data in order to maintain the variability recorded.

CO_2 growth rates ranged from 2.56 ppm CO_2 yr^{-1} for E sector to 3.26 ppm CO_2 yr^{-1} for W sector with a significance of p<0.01 obtained for all wind sectors. No significant differences (p>0.05) were found between growth rates calculated with Mann-Kendall and Sen's estimate and least squares linear regression. Interestingly, the sector with the largest growth rate was the W may be due to new combustion sources in that sector. It highlights the appearance of new CO_2 local sources close to the EGH site. CO_2 local sources are studied in Section 7.1. The calm sector shows an annual growth rate of 1.16 ppm CO_2 yr^{-1}, which is attributed to the sustained decrease of important CO_2 local sources in the vicinity of EGH. This is in

Table 4.6. CO_2 Mann-Kendall test and Sen's estimates for wind sectors at the EGH site during 2000-2012.

Wind sector	Test Z	Significance	Q[a]	Qmin99	Qmax99	Qmin95	Qmax95	B[b]	Bmin99	Bmax99	Bmin95	Bmax95
N	4.09	***	3.2	2.1	4.1	2.5	3.9	376.7	385.4	374.8	383.6	375.1
NE	4.09	***	2.8	1.9	3.5	2.2	3.3	383.2	386.7	380.1	385.5	380.6
E	4.21	***	2.6	1.7	3.2	1.8	2.9	385.9	391.1	381.2	390.1	383.1
SE	4.58	***	2.9	2.1	3.5	2.3	3.2	379.4	385.7	376.6	384.2	377.6
S	4.45	***	2.8	2.1	3.3	2.3	3.2	373.5	377.9	370.3	377.4	371.4
SW	4.33	***	2.9	2.0	3.5	2.5	3.5	373.5	381.2	368.9	376.0	369.4
W	4.33	***	3.3	2.5	3.9	2.6	3.7	376.7	381.4	372.5	380.4	374.0
NW	4.58	***	2.7	1.9	3.4	2.1	3.1	379.2	384.8	375.7	383.6	376.3
Calm	1.89	+	1.2	-0.8	3.5	-0.2	2.9	401.4	413.2	391.7	409.9	391.7

Slopes and series data are expressed in ppm CO_2
[a]True slope of linear trend
[b]First data of the series
The following symbols are used for the four tested significance levels α with which the Mann-Kendall trend shows that the null hypothesis of no trend should be rejected:
*** if trend at a = 0.001 level of significance
** if trend at a = 0.01 level of significance
* if trend at a = 0.05 level of significance
+ if trend at a = 0.1 level of significance (no symbol if a is greater than 0.1).
Qmin99: the lower limit of the 99 % confidence interval of Q (α= 0.1)
Qmax99 the upper limit of the 99 % confidence interval of Q (α= 0.1)
Qmin95: the lower limit of the 95 % confidence interval of Q (α= 0.05)
Qmax95: the upper limit of the 95 % confidence interval of Q (α= 0.05)
Bmin99: estimate of the constant Bmin99 for 99% confidence level of linear trend
Bmax99: estimate of the constant Bmax99 for 99% confidence level of linear trend
Bmin95: estimate of the constant Bmin95 for 95% confidence level of linear trend
Bmax95: estimate of the constant Bmax95 for 95% confidence level of linear trend

good agreement with data reported in the UK GGI (2014). Annual variations in CO_2 growth rates can be caused by changes in CO_2 local fluxes mostly from fossil fuel combustion and domestic heating (Zimnoch et al., 2010; Helftner et al., 2011, O'Shea et al., 2014).

4.6. Comparison of CO_2 records at EGH and MHD

4.6.1. CO_2 weekly cycles at EGH and MHD during 2000-2012

Normalised weekly cycles were calculated using hourly averages relative to the weekly mean. Figure 4.13 shows the normalised weekly cycles at EGH and MHD with larger amplitudes (peak-to-trough) seen at EGH. Daily amplitudes range from 15.2 to 19.3 ppm CO_2 at EGH and from 2.0 to 2.3 ppm CO_2 at MHD. Significant variability at EGH was observed at EGH between weekdays and weekends (2.3 ppm CO_2 difference on average) but was not observed at MHD. It is clear that during weekdays CO_2 emissions in the sub-urban area are greater than at weekends. The process of respiration/uptake by vegetation does not change during the week in the normalised cycles; the higher concentrations are thought to be caused by combustion gases emitted (e.g. heating) near to EGH, in Greater London and on the very busy motorways and main road network (Kotthaus and Grimmond, 2012).

As with the daily cycle, the day of week peaks coincide with sunrise (between 04:00 and 08:00 GMT depending on the season) with the trough in early afternoon (14:00 GMT). By contrast, the daily cycle at MHD does not show significant changes between different days of the week. The small variations observed in clean sector data at MHD indicate that the site is not influenced by major CO_2 sources or sinks and the CO_2 cycle from local vegetation is clean sector data dampened by the reduced development of inversion conditions at this coastal site (Dettinger and Ghil, 1998; Derwent et al., 2002; Haszpra and Barcza, 2010). Variations in seasonal cycles of CO_2 have been reported for sites with local vegetation and combustion sources, whereas more remote locations normally show more harmonic cycles (Nakazawa et al., 1991a,b; Dettinger and Ghil, 1998).

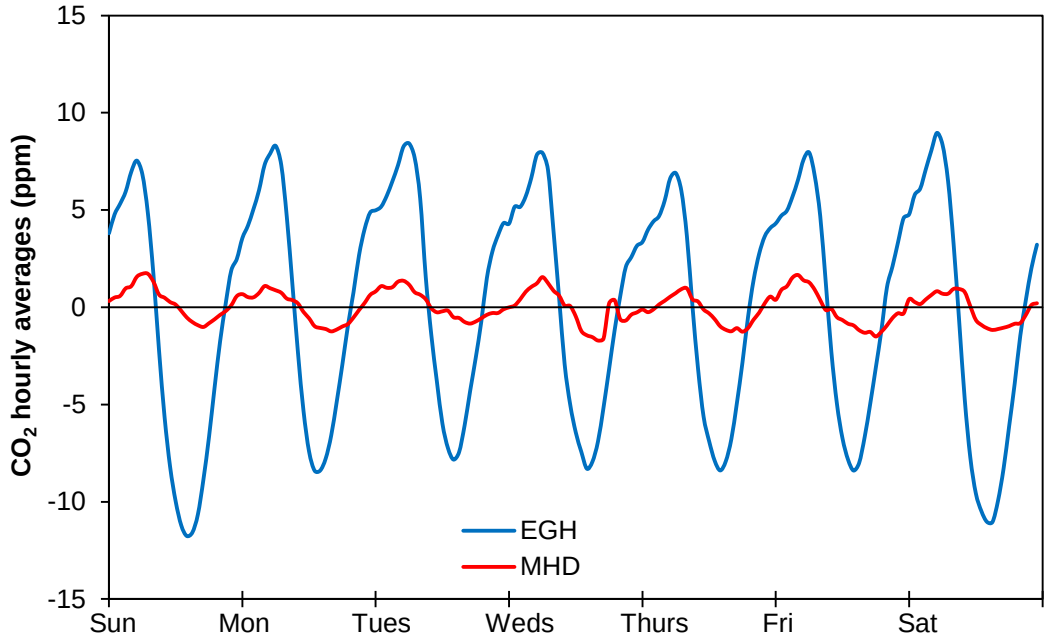

Figure 4.13. Normalised weekly cycles constructed from hourly averages of CO_2 for EGH and MHD during 2000-2011.

4.6.2. CO_2 monthly averages comparison

Figure 4.14 compares unfiltered monthly averages of CO_2, calculated from daily averages, at EGH and MHD for 2000-2011. The relatively high EGH results are due to local emissions and air masses from Greater London, whereas the MHD observations show mostly background and Atlantic Ocean levels. Differences in monthly averages between the two sites ranged from 0.2 to 36.1 ppm CO_2. The smallest differences are always observed in late spring and early summer, which coincides with the onset of the growing season at EGH when vegetation becomes a net sink for CO_2 (Haszpra et al., 2008, Barichivich et al., 2013). By contrast, the biggest differences are always found in winter, when the largest monthly CO_2 concentrations are observed at EGH due to increased combustion sources and frequency of anti-cyclonic weather conditions (Worthy et al., 1994).

To investigate the correlation between CO_2 records at EGH and MHD, a linear regression analysis for unfiltered CO_2 southwesterly monthly averages and CO_2 monthly averages at MHD during 2000-2011 was performed. Figure 4.15 shows the linear regression analysis and significance. CO_2 southwesterly monthly averages at EGH show strong correlation (p<0.001) with CO_2 records at MHD. It shows that during the advection of southwesterly air masses CO_2 concentrations at both sites are similar as shown above, and that the background sector at EGH represents well Atlantic background CO_2 levels.

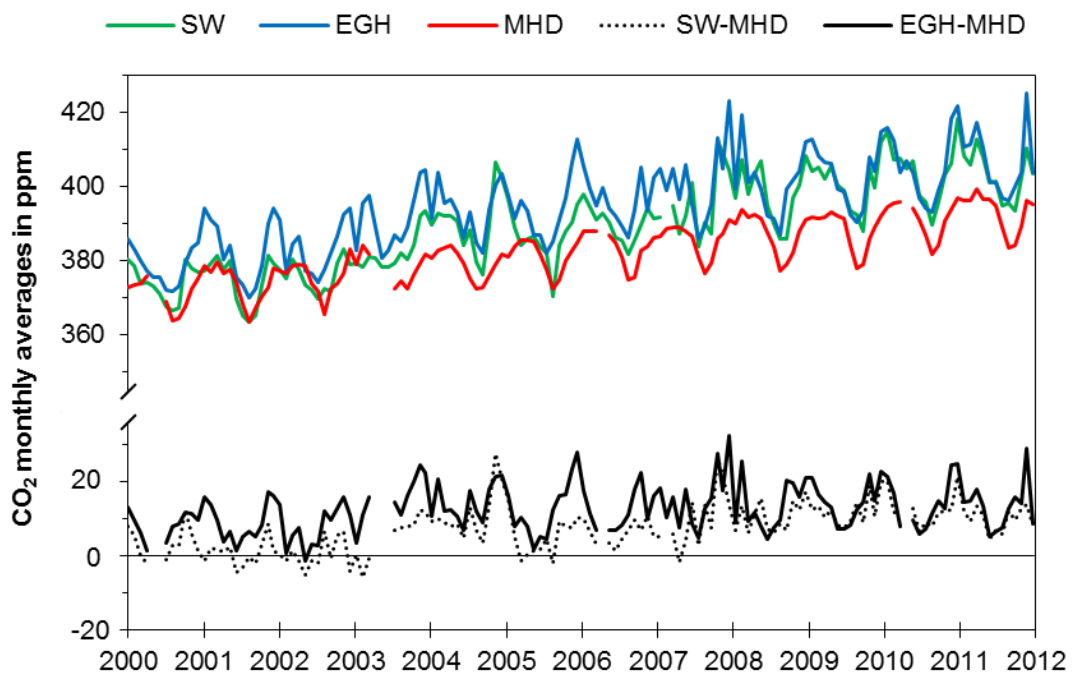

Figure 4.14. Comparison of CO_2 overall and background monthly averages at EGH with CO_2 monthly averages at MHD, Ireland during 2000-2012. Differences between overall and background CO_2 monthly averages are also shown.

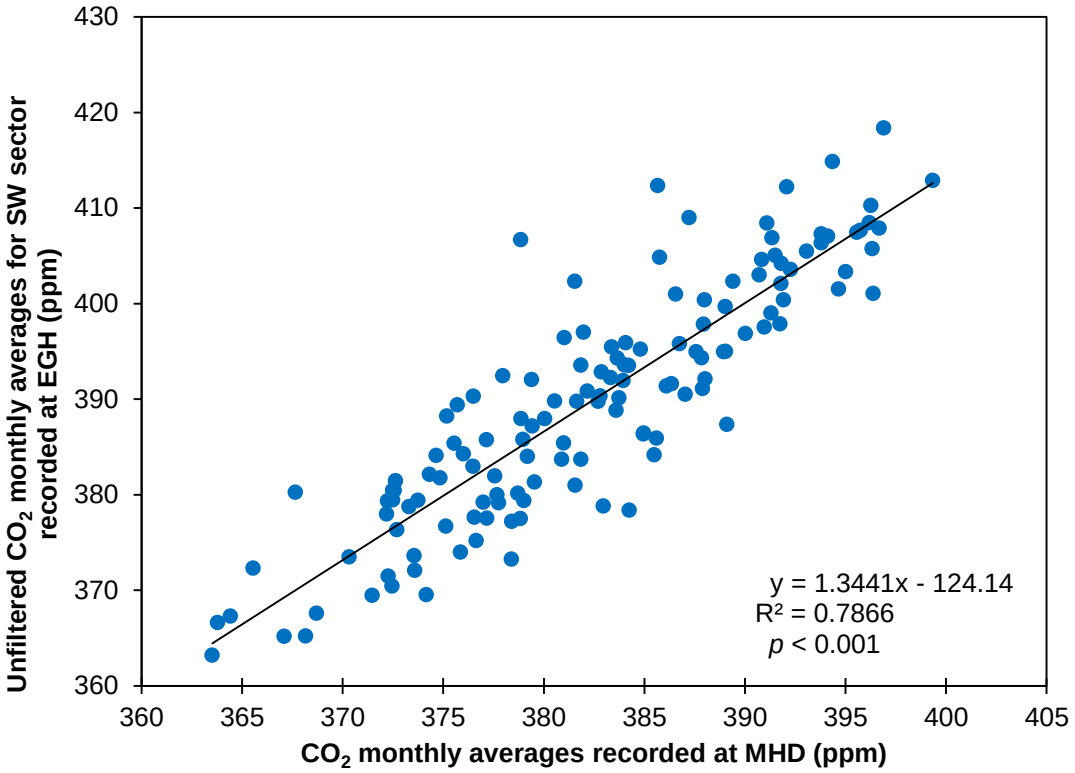

Figure 4.15. Linear correlation observed between CO_2 unfiltered southwesterly monthly averages at EGH and CO_2 monthly averages at MHD during 2000-2012. The correlation is significant for n=156 at level of 99.9% of confidence.

4.6.3. CO_2 seasonal cycles comparison

Seasonal cycles for CO_2 at MHD were computed from monthly averages using the STL technique (Cleveland et al., 1990), and are shown in Figure 4.16(a). The annual cycles remained almost constant with much less variability than at EGH. An anomaly or small trough at the maximum of the cycle occurred each February in 2000 to 2004, and is attributed to dilution by air masses with relatively high wind speeds. The averaged CO_2 yearly cycle at MHD is similar in shape to that at EGH, though with a smaller AV (Figure 4.16(b)). At MHD, the largest CO_2 concentrations are seen in April, which contrasts with the largest CO_2 averages observed in December at EGH. Both cycles show the trough of the yearly cycle in August, but at MHD low concentrations are recorded also in September, whereas at EGH are much larger.

CO_2 AV_s ranged from 12.9 to 14.6 ppm CO_2 (Figure 4.16(c)). There is no trend in the CO_2 AV_s during 2000-2011 at MHD whereas at EGH a linear increasing of 0.64 ppm CO_2 yr^{-1} was found. This increase is related to new local CO_2 combustion sources, which increase CO_2 in winter, and enhanced uptake of CO_2 by vegetation during summer.

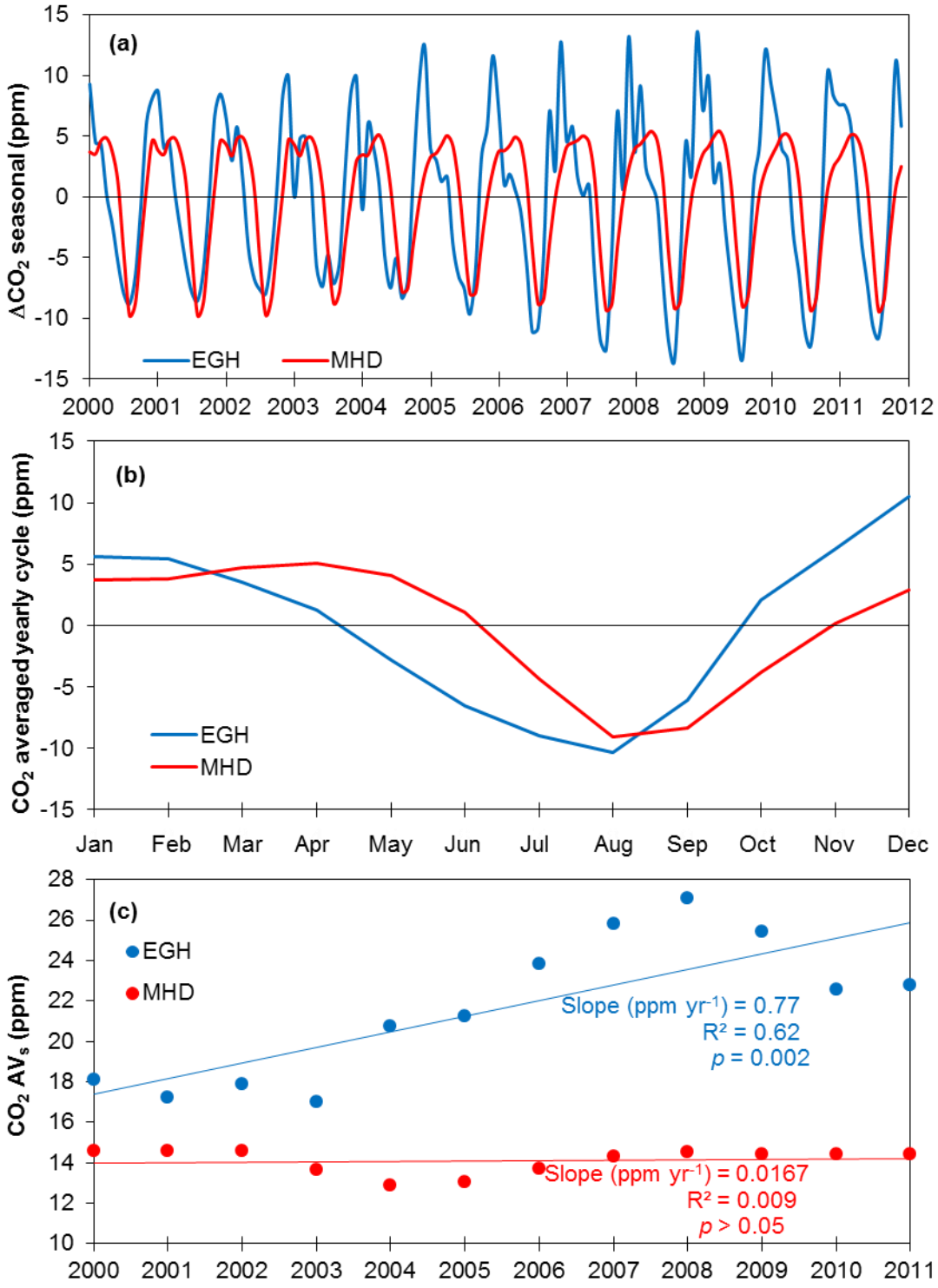

Figure 4.16(a). STL seasonal cycles; **(b).** yearly cycle averaged calculated; **(c).** seasonal amplitudes peak-to-trough of each seasonal cycle and trends at EGH and MHD during 2000-2011.

4.6.4. CO_2 long-term trends at EGH and MHD from 2000 to 2011

Annual CO_2 averages at MHD were calculated from unfiltered monthly averages and are plotted in Figure 4.17. Overall, a total increment of 22.4 ppm is observed at MHD. As for EGH, annual variability is also evident at MHD. ΔCO_2 ranges from 1.0 (2007-2008) to 3.1 ppm CO_2 (2000-2001). Interestingly, the largest ΔCO_2 at EGH

and MHD coincide (in 2000 to 2001), but the smallest ΔCO_2 at MHD does not coincide with that at EGH.

As for EGH CO_2 annual averages, CO_2 annual averages from filtered and unfiltered data were compared statistically. Similarly to EGH data, no significant differences (p<0.05) were found between annual averages calculated from filtered data and unfiltered data. Also the Mann-Kendall test and Sen's estimate was compared with least square regression methods in Excel and SigmaPlot software (Table 4.7). Excel and SigmaPlot calculations were identical as for EGH. No significant differences were found for growth rates calculated from filtered and unfiltered annual averages. No significant difference was found between Mann-Kendall and Sen's estimate and Excel and SigmaPlot analysis. In this thesis, growth rates calculated with Mann-Kendall and Sen's estimate are used to discuss CO_2 increases.

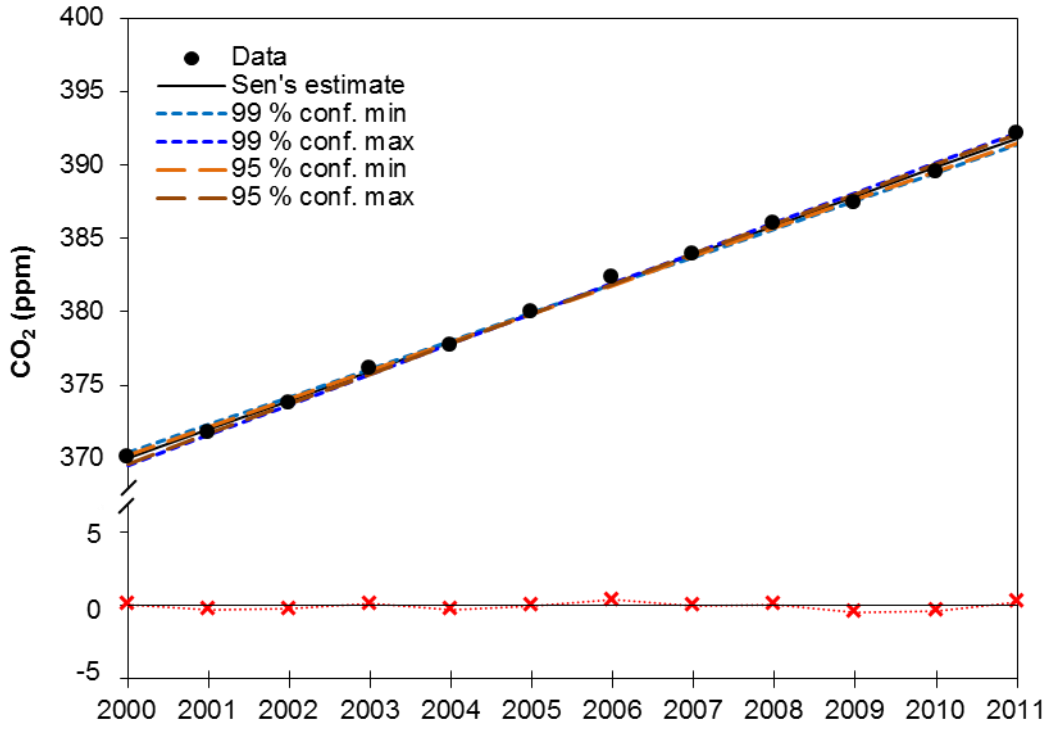

Figure 4.17. CO_2 annual averages and upward trend calculated with the Mann-Kendall test and Sen's estimate at MHD during 2000-2011.

The Mann-Kendall test and Sen's estimate for data at MHD is shown in Figure 4.17 and 4.18. Statistically significant (p<0.01) average growth rates of 2.45 and 1.95 ppm CO_2 yr^{-1} were calculated at EGH and MHD, during 2000-2012 and 2000-2011, respectively. Annual residuals, defined as the difference of annual averages minus the Sen's estimates, ranged from -2.9 ppm CO_2 (2000) to 3.1 ppm CO_2 (2007) at EGH, and from -1.0 ppm CO_2 (2000) to 0.7 ppm CO_2 (2002) at MHD (Figure 4.18).

The largest residuals observed at EGH and MHD are 3.1 ppm CO_2 in 2007 and 0.7 ppm CO_2 in 2002, respectively, whereas the lowest residuals at EGH of -2.9 ppm CO_2 and at MHD of -1.0 ppm CO_2 coincided in 2000.

The increasing trends in CO_2 annual averages observed at EGH and MHD agree well with those at other monitoring stations, and confirm the rate of increasing CO_2 concentrations around the globe (Haszpra et al., 2008; Ramonet et al., 2010; Barichivich et al., 2013; Zhang and Zhou, 2013; Tans and Keeling, 2014).

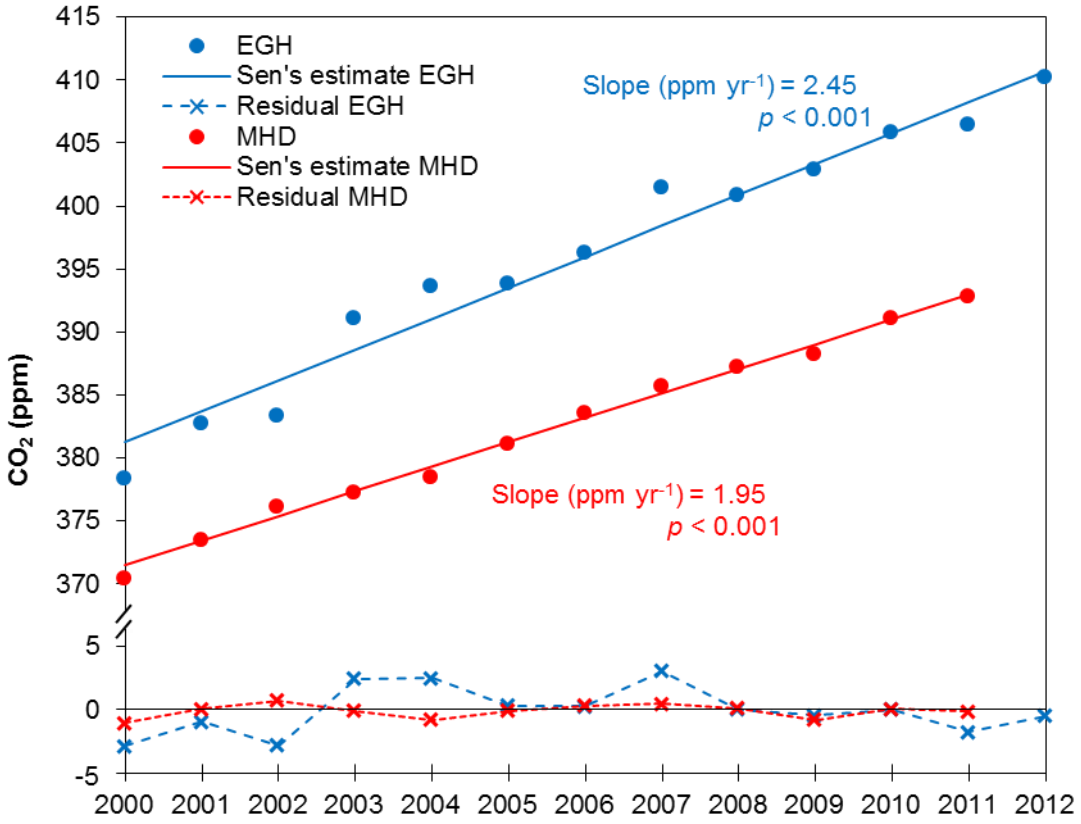

Figure 4.18. Linear trends calculated using annual averages with Sen's estimate at EGH from 2000 to 2012 and MHD from 2000 to 2011.

Table 4.7. CO_2 upward trends calculated by different methods at MHD station during 2000-2011.

Year	Unfiltered annual averages	STL annual averages	Unfiltered Sen's estimate	STL Sen's estimate	Unfiltered least squares Excel	STL least squares Excel	Unfiltered least squares SigmaPlot	STL least squares SigmaPlot
2000	370.5	370.1	371.5	370.0	371.3	370.0	371.4	370.1
2001	373.5	371.8	373.5	372.0	373.3	372.0	373.3	372.0
2002	376.1	373.8	375.4	374.0	375.3	373.9	375.3	374.0
2003	377.3	376.1	377.4	376.0	377.2	375.9	377.2	376.0
2004	378.5	377.7	379.3	378.0	379.2	377.9	379.2	378.0
2005	381.2	379.9	381.3	379.9	381.2	379.9	381.2	380.0
2006	383.5	382.3	383.2	381.9	383.1	381.9	383.1	382.0
2007	385.7	383.9	385.2	383.9	385.1	383.8	385.1	383.9
2008	387.2	386.0	387.1	385.9	387.0	385.8	387.1	385.9
2009	388.2	387.4	389.1	387.9	389.0	387.8	389.0	387.9
2010	391.1	389.5	391.0	389.8	391.0	389.8	391.0	389.9
2011	392.8	392.1	392.9	391.8	392.9	391.8	393.0	391.9
Slope (ppm CO_2 yr^{-1})	N.A.	N.A.	1.95	1.98	1.97	1.98	1.97	1.98
Increase in CO_2 (ppm)	22.4	22.0	21.4	21.8	21.6	21.8	21.6	21.8
% increase in CO_2 (13-years)	6.0	5.9	5.8	5.9	5.8	5.9	5.8	5.9
Significance (p)	N.A.	N.A.	<0.001	<0.001	<0.001	<0.001	<0.001	<0.001

Annual averages and data series are expressed in ppm CO_2.

N.A.: *Not applicable*

4.7. Comparison with the UK National Emissions Inventory (UK NAEI)

The UK NAEI reports that during 2000-2012, CO_2 emissions decreased by ca.14.2% (NAEI, 2014). By contrast, the EGH data show that during the period 2000-2012, atmospheric CO_2 increased by 8.4%. For comparison, during the slightly shorter 2000-2011 period, CO_2 at Mace Head rose by 6%, which agrees with upward trends recorded at several locations in Europe during 2000-2005 (Ramonet et al., 2010).

All other factors being equal, this would imply that in the London region, CO_2 emissions have risen in excess of the increase in the regions contributing to the Atlantic background values (i.e. global but particularly USA). Interestingly, airborne CO_2 measurements in the Greater London Area suggest that the UK NAEI underestimates CO_2 emissions by a factor of 2.3 (O'Shea et al., 2014), whereas annual estimates of net exchange of CO_2 above Central London agree with the UK NAEI estimates (Helfter et al., 2011).

4.8. Summary

CO_2 concentrations varied on time scales ranging from minutes to inter-annual and annual cycles. The diurnal cycle of CO_2 varies with patterns of atmospheric transport and biologically with length of daylight. Weekly cycles are strongly influenced by anthropogenic emissions during weekdays when fossil fuel burning and combustion processes are higher than at weekends. CO_2 seasonal cycles are driven by temporal variations in human behaviour, atmospheric transport and in photosynthesis. Annual cycles at EGH exhibit maxima and minima in winter and late summer. The smallest seasonal amplitude of CO_2 observed at EGH was 17.0 ppm in 2003, with the largest of 27.1 ppm in 2008. This underlies an increasing trend in seasonal amplitudes observed at other northern hemisphere locations.

The greatest CO_2 concentrations were recorded when air masses arrived at EGH from the E and SE sectors. Such concentrations represent CO_2 emissions transported from the London region and continental Europe. The lowest concentrations were observed for the S and SW sectors, which are close to background Atlantic levels.

The growth rate observed at EGH (2.45 ppm yr^{-1}; p<0.05) was larger than at MHD (1.9 ppm yr^{-1}; p<0.05) during 2000-2012 and 2000 and 2011, respectively, and was

due to local and regional increases in CO_2 emissions from fossil fuel combustion that are not recorded in the MHD data set. The decreasing trend in CO_2 emissions reported in the UK NAEI is opposite to the CO_2 upward trend observed at EGH.

5. ANALYSIS AND INTERPRETATION OF AMBIENT CO DATA MEASURED AT THE EGH SITE DURING 2000 TO 2012

CO is released to the atmosphere as a result of combustion processes. Large-scale biomass burning, automobile emissions and biofuel combustion are recognized as the most important sources, while contributions from industrial processes to the global burden are considered almost negligible (Lin et al., 2008). During the last century, the atmospheric concentrations of CO varied from one decade to the next. From 1950 to 1980, CO atmospheric levels increased due to industrialisation in western nations with a growth rate between 1 and 2 ppb CO yr^{-1} (Zander et al., 1989; Yurganov et al., 1999). By contrast, in the last couple of decades atmospheric CO has decreased, most notably from observations in urban areas. Kuebler et al. (2001) reported a decline between 20 and 50% in atmospheric levels of CO during 1987-1998 at urban areas in Switzerland. Most recently, Lin et al. (2008) observed at decline of CO of 240 ppb CO yr^{-1} in central Taiwan during 1994-2006. In Central London von Schneidemesser et al. (2010) reported a decrease in CO concentrations of 12% yr^{-1} during 1998-2008.

Lower rates of decline of atmospheric CO concentrations have been observed for rural and semi-rural areas. Simmonds et al. (1997) found a decline rate of 0.17 ppb CO yr^{-1} from 1990 to 1994 at the MHD station. Such slower decline rates have been observed at monitoring stations which are not directly exposed to on-road CO emissions. Lin et al. (2008) observed a decline rate of CO of 8 ppb CO yr^{-1} at a background station in central Taiwan during 1994-2006, which contrasted with the decline observed at an urban station (240 ppb CO yr^{-1}). This is due to the fact that air quality policies implemented have had a positive effect on the abatement of CO emissions, which has been clearly observed at urban stations (Kuebler et al., 2001; Lin et al., 2008; von Schneidemesser et al., 2010).

As result of “The Air Quality Strategy” implemented in 1997 in the UK, CO levels have decreased significantly across the whole country but most notably in central London as reported in the UK NAEI and by the London Air Quality Network. Measurements of ambient CO carried out at the Marylebone Road urban monitoring station, showed a decreasing rate of 12% yr^{-1}, from 1.6 ppm CO in 1998 to 0.53 ppm CO in 2008 (von Schneidemesser et al., 2010). Table 5.1 summarises studies of atmospheric CO made at different monitoring stations around the world.

Table 5.1. Summary of previous studies of atmospheric CO at different monitoring stations.

Reference	Sampling site	Type of site	Coordinates	Period studied	Type of analysis
Kuebler et al., 2001	NABE[b], Switzerland	Background, rural, urban	Switzerland	1985-1998	Seasonal cycle, long-term trend, inventories verification
Kim and Shon, 2011	South Korea	Background, urban	South Korea	1998-2008	Seasonal cycle, long-term trend, inventories verification
Azmi et al., 2010	Klang Valley, Malaysia	Urban, urban background	Kuala Lumpur suburbs,	1997-2006	Diurnal cycle, long-term trend,
Granier et al., 1996	ECMWF[a]	Intermediate Model of the Annual and Global Evolution of Species	Both hemispheres	1989-1993	Spatial variations, inventories verification
Law, 1999	GIM/IGAC[c]	Background	Both hemispheres	1990-1993	Diurnal cycle, seasonal cycle,
Novelli et al., 1998	NOAA[d]/CMDL[e]	Background, marine	Both hemispheres	1988-1995	Seasonal cycle, spatial variations
Zhang et al., 2001	ECMWF[a]	Global two-dimensional chemical model	Both hemispheres	1840-2020	Seasonal cycle, long-term trend, spatial variations, inventories verification
Makarova et al., 2011	Peterhof, St. Petersburg, Russia	Urban	59.88°N, 29.83°E	1995-2009	Seasonal cycle, long-term trend, inventories verification
Zander et al., 1989	Junfgraujoch, Switzerland	Background	56.55°N, 7.59°E	1950-1951, 1985-1985	Seasonal cycle, long-term trend
Zellweger et al., 2009	Junfgraujoch, Switzerland	Background	56.55°N, 7.59°E	1996-2007	Diurnal cycle, seasonal cycle, long-term trend
Yurganov et al., 1999	Zvenigorod, Russia	Background	55.70°N, 38.60°E	1970-1996	Seasonal cycle, long-term trend
Derwent et al., 1998a	Mace Head, Ireland	Background	53.31°N, 9.9°W	1990-1994	Seasonal cycle, spatial variations
Simmonds et al., 1997	Mace Head, Ireland	Background	53.31°N, 9.9°W	1987-1995	Diurnal cycle, seasonal cycle, spatial variations, long-term trend, sectorial analysis

Table 5.1. (Continuation) Summary of previous studies of atmospheric CO at different monitoring stations.

Reference	Sampling site	Type of site	Coordinates	Period studied	Type of analysis
Bigi and Harrison, 2010	London, UK	Urban background	51.52°N, 0.21°W	1996-2008	Diurnal cycle, seasonal cycle, long-term trend
von Schneidemesser et al., 2010	London, UK	Urban	51.52°N, 0.15°W	1998-2008	Seasonal cycle, long-term trend
Yver et al., 2011a	Trainou, France	Background	47.96°N, 2.11°E	2008-2010	Diurnal cycle, seasonal cycle
Meghea et al., 2012	Bucharest, Romania	Urban	44.41°N, 26.13°E	2004-2005	Diurnal cycle, sectorial analysis
Meng et al., 2009	Shangdianzi, China	Background	40.63°N, 117.12°E	2003-2006	Diurnal cycle, seasonal cycle,
Li and Liu, 2011	Beijing, China	Urban	40.28°N, 116.22°E	2000-2010	Diurnal cycle, seasonal cycle, long-
Xu et al., 2011	Wuqing, China	Sub-urban	39.38°N, 117.01°E	2009-2010	Diurnal cycle, sectorial analysis
Hossain and Easa, 2012	Dhaka City, Bangladesh	Urban	23.76°N, 90.38°E	2004	Diurnal cycle, seasonal cycle
Lin et al., 2008	Central Taiwan Basin, Taiwan	Urban, urban background	22.8-24.7°N, 120.4-121.0°E	1994-2006	Diurnal cycle, seasonal cycle, long-term trend, sectorial analysis

Superscripts correspond to the abbreviations of the full name of cooperative networks

[a]European Center Medium-Range Weather Forecast

[b]Swiss National Air Pollution Monitoring Network

[c]Global Integration and Modelling/International Global Atmospheric Chemistry

[d]National Oceanic and Atmospheric Administration

[e]Climate Monitoring and Diagnostics Laboratory

High-precision and high-frequency in-situ measurements of atmospheric CO were made at the EGH site during 2000-2012. These measurements were standardised using NOAA calibration gases as described in Section 2.3. CO trends are compared against MHD data to test if EGH trends are consistent with current global observations, and to identify and understand discrepancies.

5.1. Aims

The aims of this chapter are:

1. To interpret on hourly, daily, weekly, monthly, seasonal and long-term scales data for CO recorded at the EGH site during 2000-2012.
2. To evaluate local sources of CO by comparing spatial variations in data recorded at EGH with data recorded at MHD during 2000-2012.

5.2. Continuous observations of CO at EGH from 2000 to 2012

The continuous records of CO measurements at EGH were summarised as 30-min averages during 2000-2012. Figure 5.1(a) shows 30-min averages calculated at EGH during the recorded period. Figure 5.1(b) shows the histogram for 30-min averages of CO at EGH during 2000-2012 classified in five 250 ppb categories. The largest frequency of CO averages observed was from 66 to 250 ppb CO (69.6%). The frequency of higher concentrations of CO decreased inversely with increasing CO concentration. Thus, frequencies of 22.7%, 4.5%, 1.55 and 1.6% 30-min averages of CO were observed for concentrations from >250-500 ppb CO, >500-750 ppb CO, >750-1000 ppb CO and >1000 ppb CO, respectively.

Figure 5.1(a) shows a decreasing trend both in the daily average and maximum atmospheric CO concentrations recorded mostly during winter pollution episodes. More frequent high concentrations of CO were observed at the beginning of the measurements in the early 2000s and decreased across the period. The apparent decline in CO levels can be divided into three periods as seen in Figure 5.1(a): 2000-2003, 2004-2007 and 2008-2012. During the first period, CO concentrations were as high as 3,760 ppb, recorded during pollution episodes in winter. In the second period, 2004-2007, the CO largest concentration recorded was 2,630 ppb CO, whilst in the third period the largest concentration decreased to 1,334 ppb CO, which is about 50% of the largest concentration during the second period and 33% of the largest recorded during the first period.

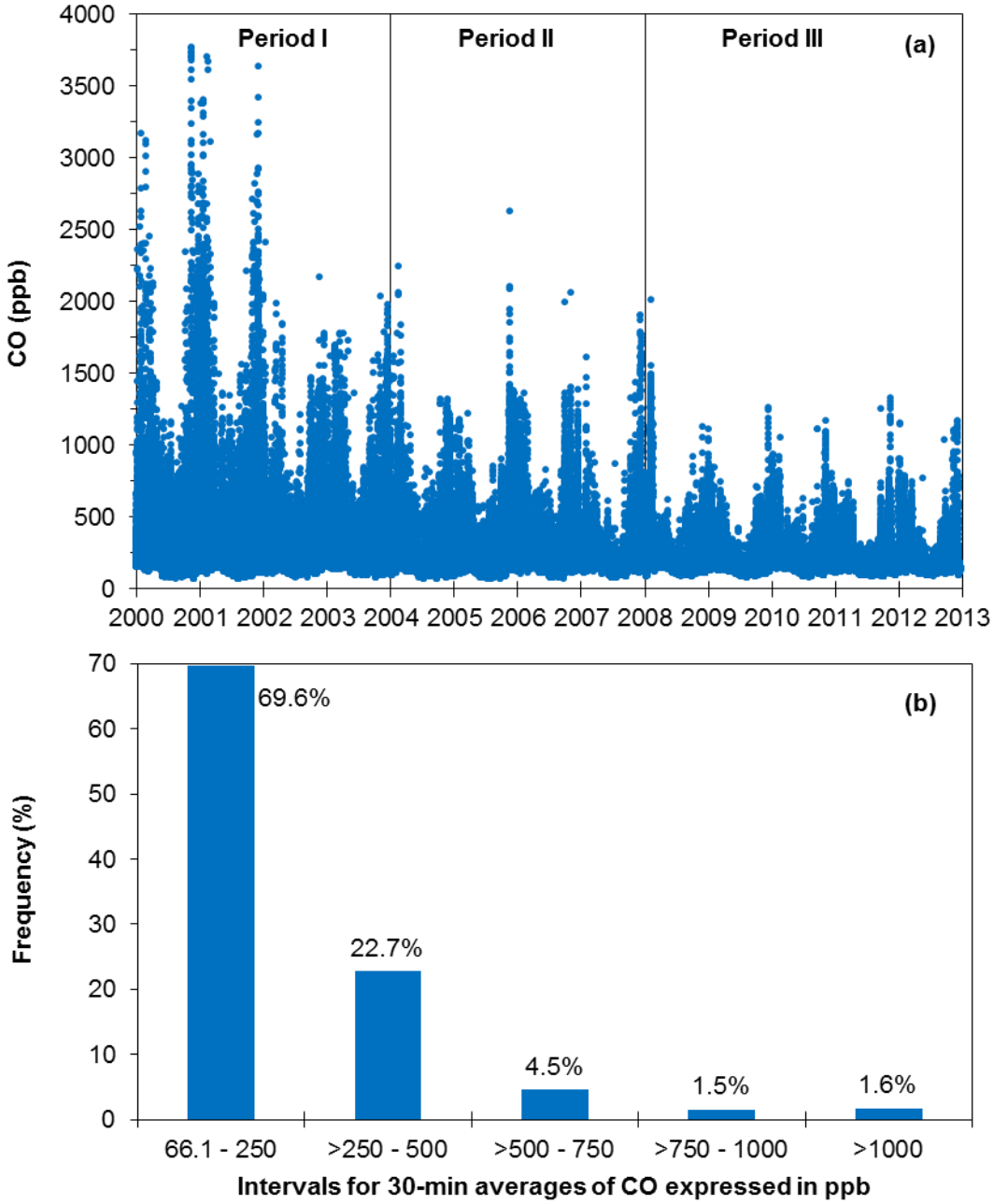

Figure 5.1(a). 30-min averages of CO recorded at EGH from January 2000 to December 2012; **(b).** histogram for 30-min averages of CO classified into 250 ppb categories.

The largest CO concentration recorded at EGH, 3,760 ppb CO, is larger than the overall average for the 13-years of measurements (253 ± 213 (SD) ppb CO) at EGH by a factor of 15, which shows the notable large concentrations of CO at the beginning of the measurements and during winter. The CO concentrations observed at EGH are similar to those recorded at urban and suburban stations in Central London, also similar to CO records at several cities in Switzerland and in China but are larger than CO concentrations recorded at background monitoring stations, and

rural and semi-rural stations in the northern hemisphere (Table 5.1). The largest CO concentration at EGH is 10-times higher than the CO average measured at the Taiwan basin from 1994 to 2006 at a background site located on a small hill (380 ± 80 ppb CO), and 4-times higher than the Taiwanese urban site (940 ± 210 ppb CO; Lin et al., 2008). By contrast, the largest CO concentrations at EGH were similar to the highest value of CO of about 3 ppm recorded in central London at the beginning of measurements (von Schneidemesser et al., 2010). The magnitude of CO decrease is similar to that observed at EGH.

The CO continuous records at EGH show seasonal cycles, with the highest CO concentrations in winter and the lowest concentrations in summer. In particular, the highest CO winter concentrations were recorded during 2000-2002. By contrast, the lowest CO concentrations in winter were seen in 2012, at the end of the recorded period. CO summer concentrations also showed significant variations during the sampled period. The highest CO concentrations during summer were recorded in early 2000s and decreased across the measurement period until the end of 2012. Interestingly, the frequency of high CO summer concentrations decreased similarly along the period and were almost absent by the end of the measurements.

The decline in CO concentrations observed at EGH during summer and winter was previously reported in central London by von Schneidermesser et al. (2010) and in an earlier study in Europe by Kuebler et al. (2001). In general terms, the decline in CO atmospheric levels is ascribed to the success of environmental policies implemented to improve the air quality in the UK and EU.

5.3. Analysis of CO records at daily and weekly time scales

CO daily averages at EGH during 2000-2012 were calculated from 30-min averages. Figure 5.2(a) shows daily averages during the period and Figure 5.2(b) shows the histogram for five concentration categories. The biggest frequency of 49.1% CO daily averages was observed for concentrations from 89.4 to 200 ppb CO, whereas 39.3% of daily averages fell into the range between >200 and 400 ppb CO. Frequencies decreased as CO daily averages increased, with 7.2% of data between 400 and 600 ppb, 2.4% and 1.9% of data were in the 600-800 and >800 ppb ranges, respectively.

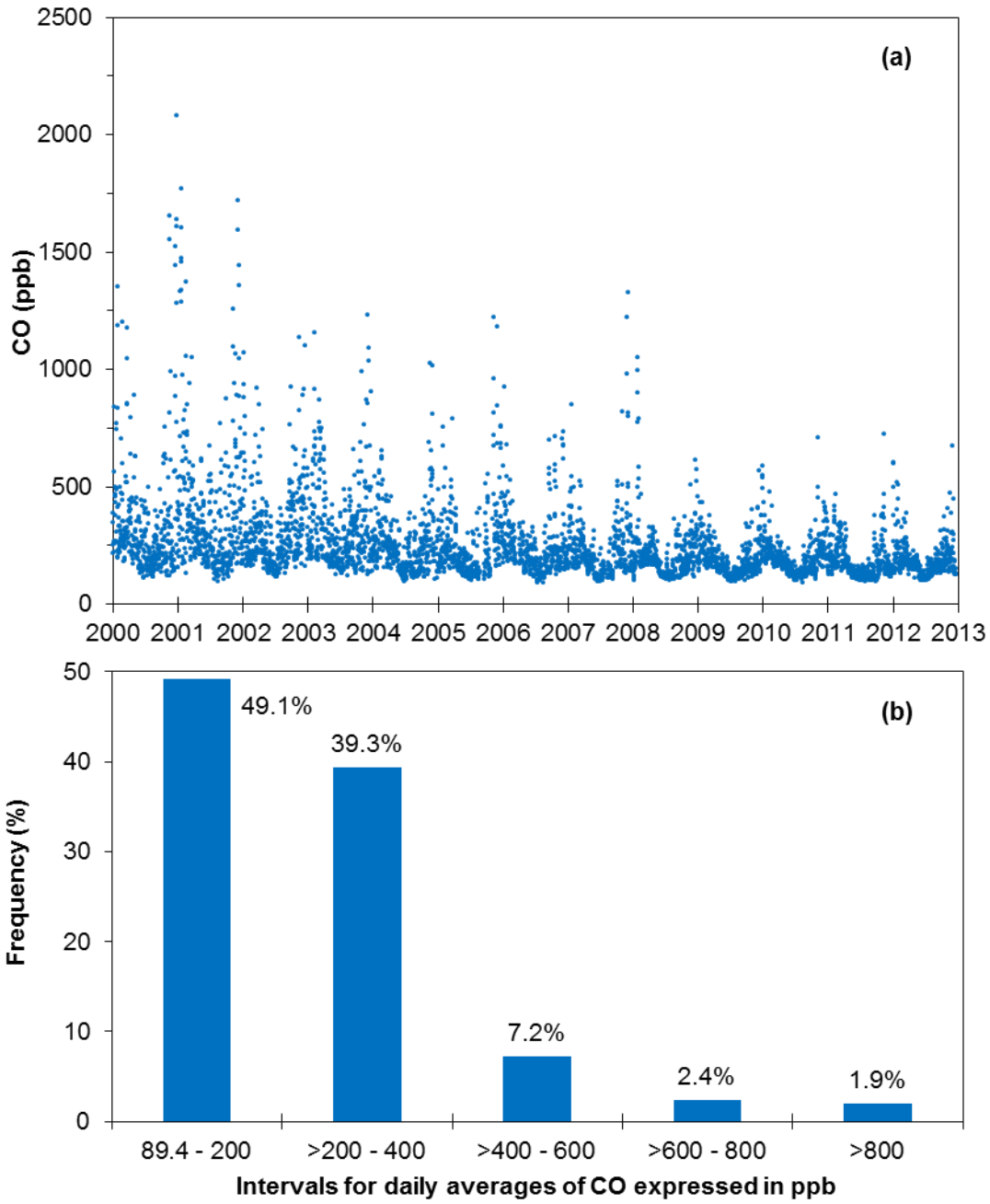

Figure 5.2(a). CO daily averages calculated from 30-min averages at the EGH site from January 2000 to December 2012; **(b).** histogram of CO concentration intervals.

During the measurement period, a consistent decrease in the daily averaged CO concentration is noticeable. The decline in CO is dramatic and sustained during 2000-2003. Then, the decline rate of CO is smaller but also consistent from 2004 to 2008. A lower decline is observed after 2008 but is still persistent. During 2000-2003, the largest CO daily average was 2,081 ppb, whereas in 2004-2008 largest daily average was 1,326 ppb CO, which is 64% of the largest concentration during the first period. By contrast, the largest CO daily average recorded after 2008 was

725 ppb, 54.7% of the largest daily average recorded during the second period and 34.8% of the largest daily average recorded during the whole sampled measured.

CO daily averages calculated for the measurement period show that the greatest CO concentrations were recorded at the beginning and that concentrations are higher during winter. This behaviour is related to the seasonal cycle of CO, which is discussed in Section 5.4. The daily CO averages show the seasonal cycle with higher concentrations during winter and lower in summer. The daily averages also show that during pollution episodes in winter the largest concentrations became less frequent and less extreme as measurements progressed. Similarly, the CO concentrations observed in summer also decreased across the period

Two possible reasons that could explain the observed decline in CO concentrations are: a) the reduction in CO anthropogenic emissions due to the implementation of air quality policies worldwide and b) increasing concentration of OH, the major sink for CO, due to the decrease of stratospheric ozone (Zhang et al., 2001).

5.3.1. CO diurnal cycle at the EGH site

CO diurnal variations are dependent upon multiple factors such as changes in emissions from combustion sources especially during the rush-hour, wind speed and wind direction, and the height of the boundary layer (Grant et al., 2010; von Schneidemesser et al., 2010; Hossain et al., 2012). The averaged daily cycle for CO at EGH during 2000-2012 was constructed by averaging 30-min records into hourly averages for the 24-hour cycle. Figure 5.3 shows the results of this, showing two peaks and two troughs. The peaks occur during the early morning (08:00-09:00) and mid-evening (21:00). The troughs of the cycle are observed before the sunrise (04:00) and at mid-afternooon (14:00). The CO cycle is similar in shape to daily cycles observed at the urban monitoring stations in North Kensington, London (Bigi and Harrison, 2010), three monitoring stations in the Klang valley of Malaysia (Azmi et al., 2010), Beijing, China (Lin and Liu, 2011) and at Dhaka city in Bangladesh (Hossain and Easa, 2012). It is also similar to the CO daily cycle reported at background monitoring stations in Shangdianzi in northeast Beijing (Meng et al., 2009), Trainou, France and MHD, Ireland (Yver et al., 2011).

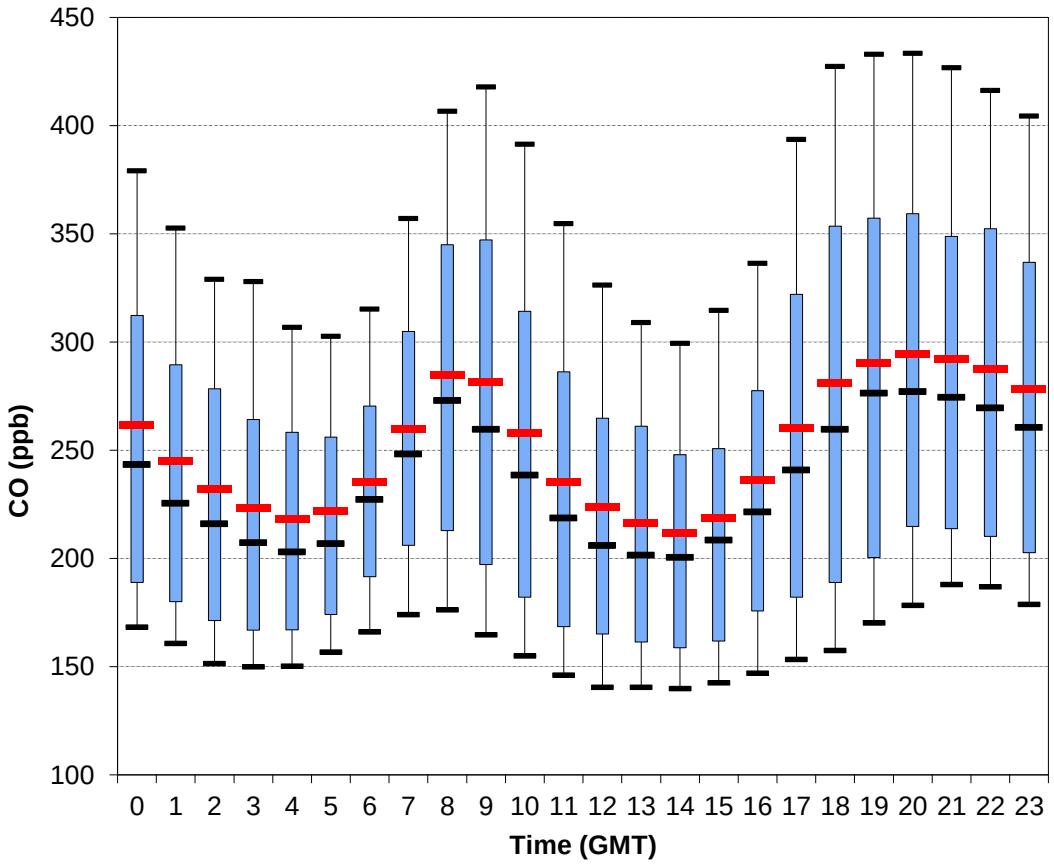

Figure 5.3. Averaged daily cycle for CO records at EGH from 2000 to 2012. Black and red lines represent the median and averages, respectively. Vertical bars (whiskers) correspond to the 10th and 90th percentiles.

Interestingly, the CO daily cycle at EGH differs from that reported by Xu et al. (2011), which only shows one peak and one trough for measurements made at Wuqing monitoring station. That monitoring station is situated in between Beijing and Tianjin and receives high concentrations of CO from urban emissions, which could explain the difference in the shape of the daily cycle. CO emissions from the power generation sector shows a single CO daily cycle, whereas the transportation CO daily cycle shows two peaks and two troughs, as observed in records of urban monitoring stations. Since the CO emissions from the transportation sector are among the most important contributors to the CO build-up, temporal variations exist when CO daily cycles for weekends are compared with CO cycles for weekdays (Grant et al., 2010; Bigi et al., 2012).

The observed decline in the CO before the sunrise is thought to be caused by dispersion and, to a lesser extent, dry deposition of CO, combined with weaker emissions from combustion sources overnight (Grant et al., 2010; An et al., 2013). The morning rise of CO concentrations has been reported previously in urban,

suburban and background monitoring stations (Table 5.1). Bigi and Harrison (2010) found that the morning CO peak was related to high traffic volume and poor dispersion conditions at North Kensington in London. Grant et al. (2010) observed the morning-peak by 09:00-10:00 at an urban station in Bristol, UK. They saw a delay of one-hour due to mixing-time required for emissions to raise the average and then travel to the measurement site.

At EGH, no significant delay was observed between the morning-peak and rush hour. This could be explained by the proximity of the sampling site to the M25 motorway, which is very busy especially on weekdays, since emissions of CO from automobiles are the major source during the morning. Also favourable wind direction could bring the CO emissions from M25 motorway and close conurbations to EGH. The effect of lighter traffic can be more clearly appreciated during weekends where the morning-peak is less intense as discussed in Section 5.3.2 (Bigi and Harrison, 2010).

A decline in CO concentrations was observed in the early afternoon at 14:00. This is influenced by photochemical depletion via oxidation by OH radicals which reaches the maximum production by early afternoon (Brasseur et al., 1999). The light traffic and consequently lower CO emissions together with enhanced dispersion conditions can also contribute to this depletion (Bigi and Harrison, 2010; An et al., 2013). The evening-peak appeared later than the rush hour. Therefore poor dispersion conditions would facilitate stable CO concentrations overnight (Bigi and Harrison, 2010). Xu et al. (2011) also observed a poor CO dispersion due to the stability of the boundary layer overnight. The timing of inversion development and lowering of the PBL also influences the occurrence and timing of this evening peak at the EGH site.

5.3.2. CO diurnal cycles over the weekly period at the EGH site

To interpret the CO short-term changes observed at EGH during 2000-2012 CO daily cycles were divided by season and by day of week. At EGH, CO average diurnal cycles were derived by subtracting CO daily averages to CO hourly averages in order to remove the impacts of long-term trends (Zhang et al., 2013). Figure 5.4 shows the averaged CO diurnal variations by season and day of the week at EGH during 2000-2012.

The daily cycles of CO at EGH during weekdays and weekends divided by season are made-up by a frequency of 2 d^{-1}, which is two peaks and two troughs. The first trough and peak are observed in the morning, and the others during the afternoon and evening, respectively. The timing of the troughs and peaks was variable, depending on the day of the week and season. Seasonal variations in the daily cycles result from differences in CO emissions of domestic heating during winter, which contrast with the emissions of CO in summer when the domestic heating is not used.

The largest variations in the CO diurnal cycles are observed between winter and autumn and summer when the lowest variability is seen (Figure 5.4). Spring is observed as the transition season between the stable conditions in winter with recurrent development of inversion events and the strong convective conditions in summer. In winter, the morning-trough is observed by 05:00 during weekdays and shifts to 06:00 and 07:00 on Saturday and Sunday, respectively. Then, CO concentrations increase during the early morning and show the first peak of the cycle by 09:00 weekdays and Saturday and by 10:00 on Sunday. During spring, the morning trough on weekdays is seen by 04:00 and 05:00 on Sunday, whereas it varies from 03:00 to 05:00 on Saturday. The first CO peak is observed by 07:00 on Saturday, and at 08:00 in weekdays and Sunday.

During summer the differences in the first trough of the CO daily cycle are less pronounced and is observed between 03:00 and 04:00 for all days, whereas in autumn it is also observed at 04:00 on weekdays but at 05:00 and 06:00 on Saturday and Sunday, respectively. Interestingly in summer, the first peak of CO is seen by 05:00 in Sunday and between 07:00 and 08:00 on weekdays and Saturday.

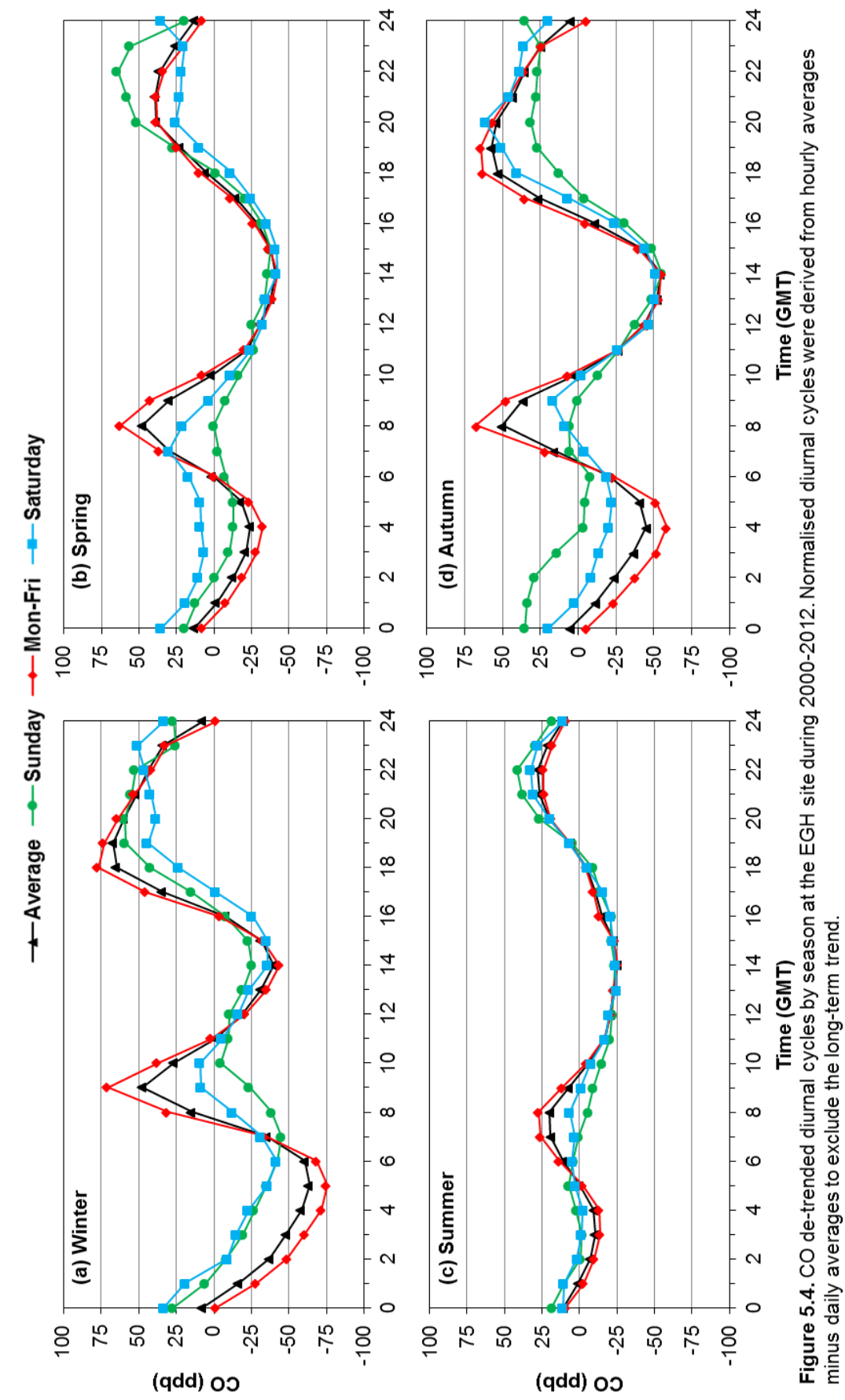

Figure 5.4. CO de-trended diurnal cycles by season at the EGH site during 2000-2012. Normalised diurnal cycles were derived from hourly averages minus daily averages to exclude the long-term trend.

It contrasts with the timing of the first trough of the CO cycle in winter, which is by 5:00. In autumn, the first peak of CO is seen at 7:00, 8:00 and 9:00 in Sunday, weekdays and Saturday, respectively. The differences observed in the present work for the timing of the CO morning trough and peak were also observed by Bigi and Harrison (2010) in Central London. They observed in winter the trough and peak between 06:00 and 08:00 and at 09:00, respectively. There is a difference between the timing of the trough of one hour but the peak coincides with the results in the present work.

By contrast, Bigi and Harrison (2010) did not observe a trough during the Sunday morning but on weekdays it was observed between 04:00 and 06:00, which is the same timing that was observed at EGH. However, there was a difference for the timing of the morning peak during weekdays, they reported it at 09:00, whilst at EGH was seen by 08:00. Such differences can be ascribed to the different environments around the stations, as at North Kensington, high loading of vehicles is normal during morning and the topology of the area affects the dispersion of the emissions. The M25 near EGH is already extremely busy by 07:00.

The afternoon trough of the CO daily cycle did not change in any season and is always observed at 14:00 during weekdays and weekends. This can be explained by the increase in the height of the PBL and high rate of dispersion due to the enhanced convective conditions during early afternoon. Such conditions did not change despite the season at EGH. Xu et al. (2011) observed that at the Wuqing suburban station in China, the boundary layer height reaches the maximum between 14:00 and 15:00 local time, when the lowest concentrations were recorded. This is in good agreement with the strong convective conditions observed at EGH.

The evening CO peak shows large variability in timing. During weekdays, in winter and autumn it is observed by 18:00, whereas it occurs by 21:00 in spring and summer. By contrast, on Sunday it is seen by 19:00 in winter, 22:00 in spring and summer and at 00:00 in autumn. Bigi and Harrison (2010) also observed a later peak in summer than in winter which can be thought due to larger evening-nighttime traffic. It is clearly appreciated during weekends and especially during summer when the peak is more intense due to increased late evening vehicular activity. Xu et al. (2011) also observed a weaker evening-peak during summer due to the later lowering of the boundary layer compared to winter and autumn. The same peak observed on Saturday night in winter was reported by Grant et al. (2010) for the

Bristol site. They related this peak timing at 23:00-24:00 to the stable nocturnal conditions that concentrate CO overnight.

Large differences in the AV_d were observed between weekends and weekdays and between morning and evening AV_ds. Table C1-4 list standard deviations for CO hourly averages by season at EGH. Overall, morning AV_d were smaller than evening AV_d. During the morning, the smallest AV_d was observed on Sunday (4.2 ppb CO), while the largest was seen on weekdays (90.8 ppb CO). The largest evening AV_d was 85.5 ppb CO on weekdays, whereas the lowest was 74.9 ppb CO on Saturday. No significant difference (p>0.05) was found between morning and evening AV_ds. Grant et al. (2010) explained that evening CO peaks are more stable and drop off more slowly due to the stability of the PBL overnight. Meng et al. (2009), also observed larger AV_ds in winter than in summer at the Shangdianzi background station. However, they observed only one peak and trough in the CO daily cycles, which is attributable to the environmental conditions as that station is not directly exposed to CO emissions from conurbations and fossil fuel burning. It highlights the importance of combustion sources to the CO build-up and to the seasonal variations in the diurnal cycles.

5.3.3. Wind direction analysis of CO diurnal cycles by day of week and season

CO daily cycles vary by day of the week depending on the season. This is due to the oscillations in CO emissions ascribed to human activities but also influenced by seasonal changes in wind direction and wind speed. Xu et al. (2011) observed that large variations of wind speed across the year at the Shangdianzi background station produce different CO daily cycles. Simmonds et al. (1997) reported that air masses with different frequencies of wind direction and at different speeds carrying important pollution loading affected greatly the CO concentrations recorded at MHD, Ireland, background observatory. High wind speeds increase the turbulence and dilute pollutants in the atmosphere by bringing clean air masses, which can mix with polluted urban and suburban air (Grant et al., 2010). It highlights the importance of performing analysis and interpretation of CO daily cycle by day, season and wind direction.

To study seasonal variations in CO daily cycles by wind sector, CO de-trended cycles were derived from hourly averages minus weekly averages to exclude the long-term trend (Zhang et al., 2013). Figure 5.5 shows daily cycles by day of week

for each season and wind direction sector during 2000-2012. At EGH, very different CO cycles were observed from season-to-season as function of the wind direction. The biggest differences were observed between winter and summer CO cycles, whereas in spring and autumn the CO cycles were similar. The largest concentrations of CO were recorded for easterly air masses during winter and ranged from ~300 to ~800 ppb CO. By contrast, during summer CO concentrations ranged from ~150 to 350 ppb CO. In winter such large CO values can be explained by the high frequency observed for easterly air masses, which likely may transport CO emissions of vehicle exhausts and domestic heating from the suburban area nearby EGH and from the local motorways. However in winter, the largest CO concentrations were not observed at any specific time, as large concentrations were recorded both during mornings and evenings, though high and similar CO peaks between 600 and 800 ppb were seen from Monday to Saturday, but were lower on Sunday ranging from 400 to 500 ppb CO.

During summer, CO peaks usually reached 300 ppb both in morning and evening. Similarly to winter, the largest CO concentrations were observed in easterly air masses but also from northeasterly, which contributes importantly to the build-up from Wednesday to Saturday morning. Only one peak of CO was observed on Thursday in air masses from the NE sector, which was over 400 ppb CO. Although the background south and west sectors did not show significant differences from weekdays to weekends in any season, variations were more pronounced in winter and autumn than in summer and spring. This can be explained since no large CO sources are located in those wind sectors together with the advection to EGH of westerly and southwesterly air masses, clean air masses that can dilute air pollutants (Lowry et al., 2001).

Figure 5.5 shows the frequency of 2 peaks and 2 troughs per day in daily cycles of CO. Bigi and Harrison (2010) observed the same frequency in central London with lower peaks at weekends during winter due to different traffic regimes. In the present work, lower peaks of CO are only observed in Sunday probably due to high traffic density from Monday to Saturday on the motorways around EGH. Grant et al. (2010) reported in a study for a one-week period made at an urban station in Bristol,

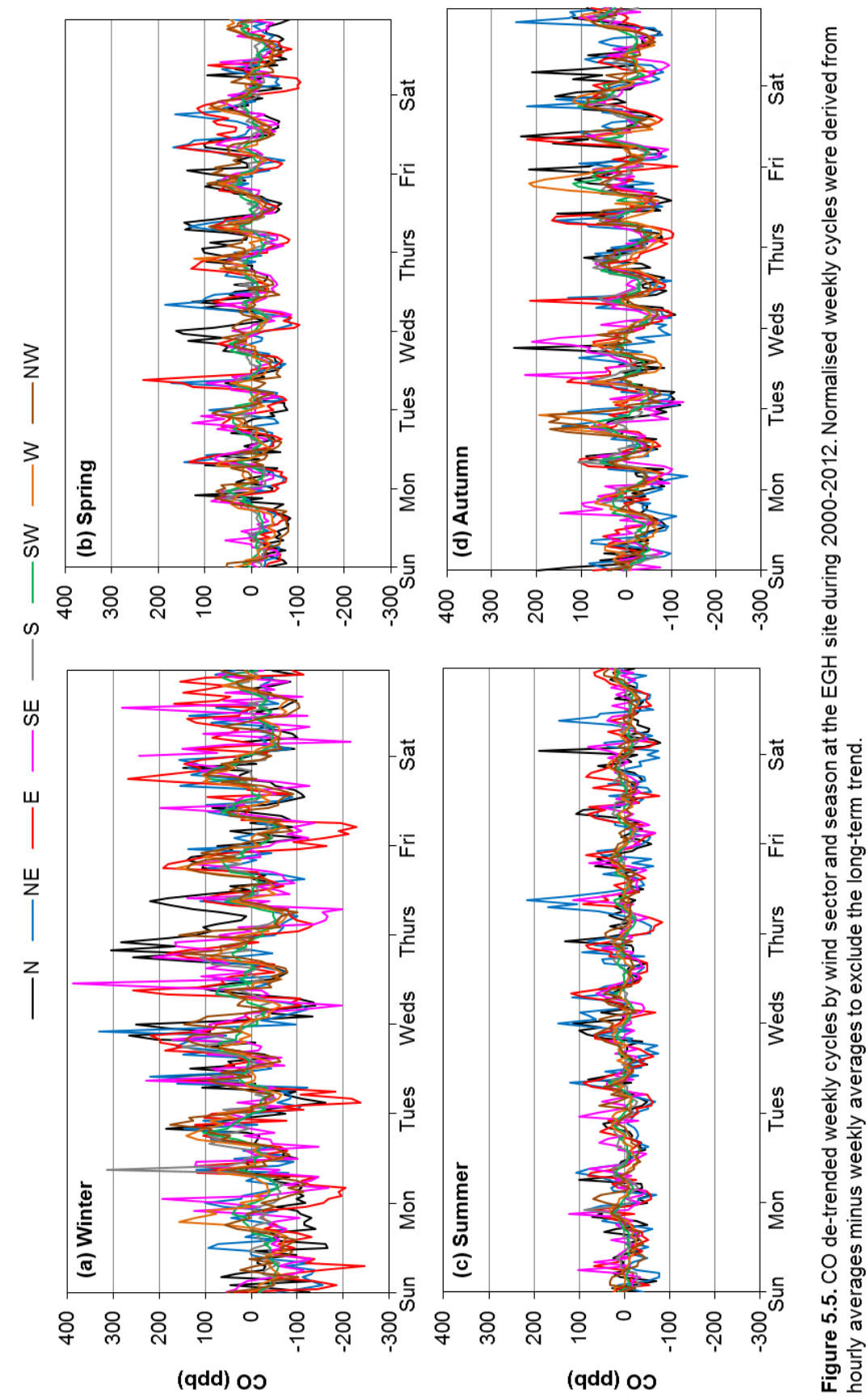

Figure 5.5. CO de-trended weekly cycles by wind sector and season at the EGH site during 2000-2012. Normalised weekly cycles were derived from hourly averages minus weekly averages to exclude the long-term trend.

that Saturday nightlife contributed substantially to the CO build-up observed in the data. This is in good agreement with data at EGH, where afternoon and evening emissions from automobiles can explain the CO peak on Saturday evening in easterly air masses, the sector with the highest density of habitation. On the other hand, Meng et al. (2009) observed that at Shangdianzi observatory (China) the CO cycle in autumn is less strong than in winter but more than in summer and spring, which was also seen at EGH. Furthermore, no noticeable differences between weekdays and weekends were observed in air masses passing over important pollution areas (E and SE wind sector). Finally, the background sector showed the same profile like other northern backgrounds stations with low variations among season and day of week as seen previously by Meng et al. (2009) and Xu et al. (2011).

5.4. CO annual cycle at the EGH site

The CO annual cycle is driven by seasonal changes in OH concentration, together with changes in anthropogenic emissions of CO, and meteorological conditions (Novelli et al., 1998; Kim and Shon, 2011). In the northern hemisphere, the peak of the CO seasonal cycle occurs during late winter/spring, whereas the trough occurs in summer (Simmonds et al., 1997; Derwent et al., 1998a; Bigi and Harrison, 2010). However, the timing of both can change slightly depending on the latitude. In an early study of the seasonal behaviour of CO at different latitudes Novelli et al. (1998) observed that in the NH, the peak of the CO seasonal cycle occurs several months after the OH minimum, as response to the transport of anthropogenic CO emissions. Other reports have shown similar behaviour in the NH. In a study of St. Petersburg, Russia during 1995-2009 Makarova et al. (2011) observed the peak between February and March, and the trough between July and August. Kim and Shon (2011) in a study made at several urban and background monitoring stations in several cities in South Korea (NH) found the peak in late winter, whereas the tough was observed in summer.

To study the annual cycle of CO at EGH during 2000-2012, monthly averages of CO were calculated from daily averages and then were filtered with the STL technique. CO monthly averages were calculated if at least 75% of daily averages were resent. In total 156 CO monthly averages were calculated, which represent 100% of all possible data during the recorded period. Figure 5.6(a) shows the CO seasonal cycles at EGH from 2000 to 2012.

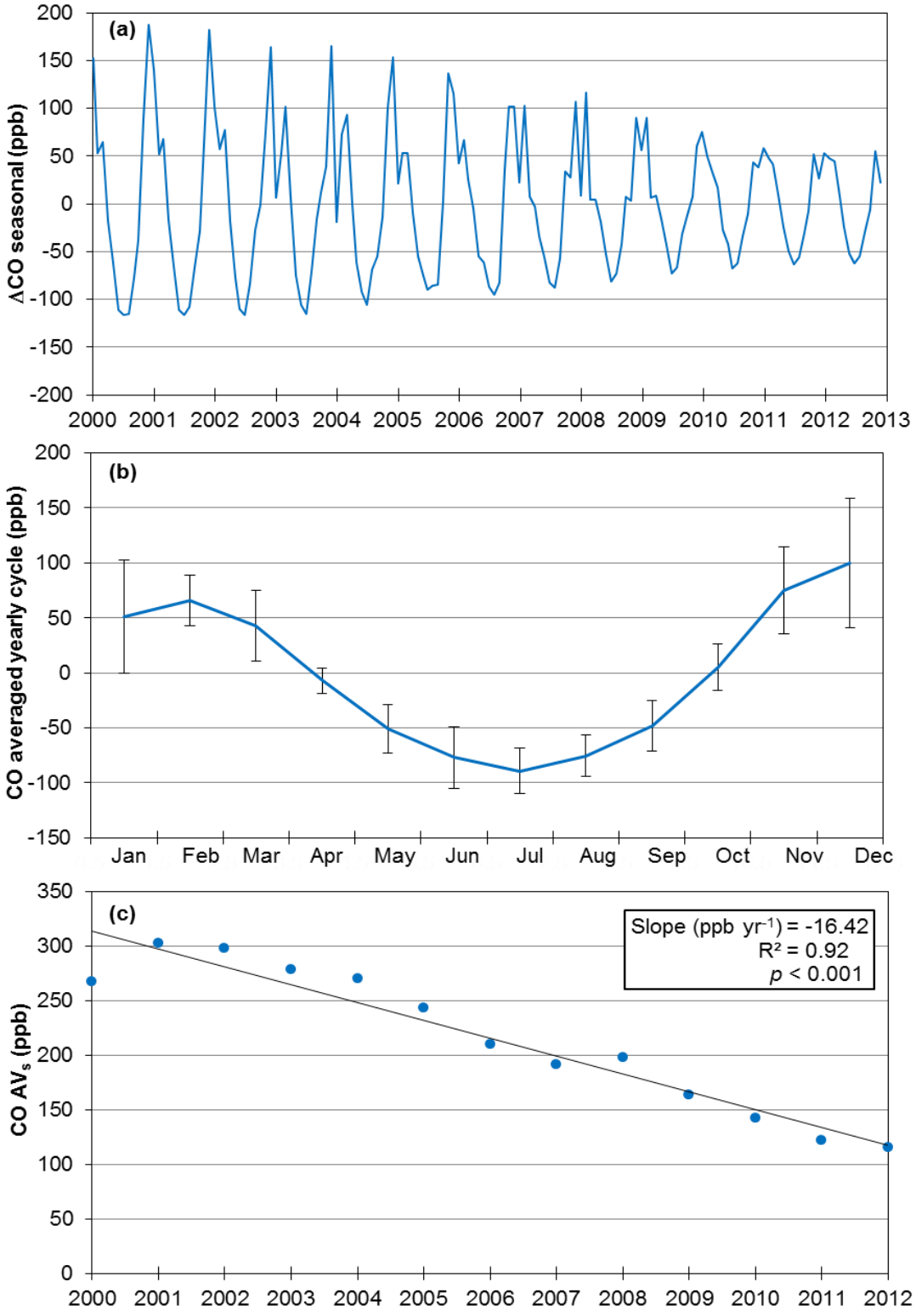

Figure 5.6(a). De-trended seasonal cycles of CO at EGH during 2000-2012 calculated by filtering the monthly averages with the STL technique; **(b).** yearly averaged cycle of atmospheric CO calculated from the filtered values with STL, error bars represent 1SD; **(c).** decreasing trend in CO seasonal amplitudes (AV_s). AV_s is defined as the difference in ppb CO from peak-to-trough within one-seasonal cycle.

The CO seasonal cycle is strong and overall the maxima occur in winter and the minima in summer. The CO peak was observed mostly in December (2000-2005),

in January (2007-2009) and February (2010-2012). This is slightly different to the CO cycle observed in North Kensington, London by Bigi and Harrison (2010) where the peak of the cycle was in November. Such differences are ascribed to the variable meteorological conditions, mostly wind direction and speed (good dispersion).

During winter, increased occurrence of southeasterly air masses was recorded at EGH, which possibly transported significant CO loading to EGH from the urban areas nearby and caused the peak observed. Interestingly, a sharp decline in the CO seasonal cycles is observed in January almost each year. Bigi and Harrison (2010) also observed a similar decline in some cycles during measurements from 1996 to 2008 at North Kensington.

Although, vehicular CO emissions main remain fairly constant throughout the year, increases in CO emissions from domestic heating during winter can contribute to the large concentrations observed. Another important factor that could explain the largest concentrations in winter is the stable condition of the PBL. By contrast, the advection of clean air masses from the background sector passing over large green areas can contribute also to dilute the CO emissions together with the enhanced convective conditions in summer (Grant et al., 2010). Rain fall during summer can produce the wash-out effect and lead to lower concentrations (Hossain and Easa, 2012).

The CO averaged yearly cycle was calculated by averaging the monthly filtered values for a period of one year. The averaged CO yearly cycle is showed in Figure 5.6(b). The largest CO concentration is observed in winter, in December. Then a sharp decline in concentrations is observed from March to June, and then the lowest concentration of CO is recorded in July. After, concentrations increase persistently during autumn and winter. Variations in the monthly CO averages (1SD) ranged from 11.5 to 58.9 ppb CO. The largest variations were observed in December and January (1SD = 58.9 and 51.4 ppb CO, respectively), whereas the lowest were observed in April and August (1SD=11.5 and 18.9 ppb CO, respectively).

During the recorded period, a decreasing trend in AV_s of CO is observed (Figure 5.6c). The declining trend was calculated from individual annual amplitudes peak-to-trough based on STL filtered values. The largest AV_s was observed in 2001 (302.9

ppb CO), whereas the lowest AV_s was in 2012 (115.6 ppb CO). The decline rate was calculated as 16.4 ppb CO yr^{-1} with R^2=0.93 (p<0.001), however it must be pointed out that the first cycle is not complete for the winter season. Thus, if the first AV_s is not considered the decline rate is calculated as 18.5 ppb CO yr^{-1} and the R^2=0.98 (p<0.001). Even so, the decreasing trend in the AV_s from 2000 to 2012 is clear and is explained by the decline in CO emissions mostly from fossil combustion due to the effective implementation of air quality policies in the UK (NAEI, 2014).

5.4.1. Comparison of CO annual cycles and AV_s from filtered data with STL and unfiltered data

CO annual cycles and AV_s at EGH from filtered data with STL and unfiltered data were compared to investigate differences. Table 5.2 lists differences in CO AV_s at EGH and in the occurrence of the maxima and minima between STL filtered seasonal cycles and unfiltered seasonal cycles during 2000-2012. Differences in CO AV_s ranged from -12.9 to 96.8 ppb CO in 2007 and 2001, respectively. Although more variation in the occurrence of the CO peak for unfiltered data than for STL filtered data was observed, no MSD was found between both data (p>0.05). Thus, for STL filtered data, the CO peak was observed in December (2001-2006), January (2000, 2010-2012) and February (2007, 2008), whereas for unfiltered data was observed in December (2002-2005, 2011), in January (2000, 2001, 2006, 2009, 2010) and in February (2007, 2008, 2012).

The occurrence of the CO peak occurred in December from 2002 to 2005, in January for 2000 and 2010 and in February in 2007 and 2008. By contrast, more coincidences in the occurrence of the trough of the cycles were found. For STL filtered data, the trough is observed in July (2000-2005, 2008-2012) and in August (2006, 2007) and coincided with the trough of the unfiltered data during 2002-2004, 2006, 2009, 2010 and 2012. Interestingly, in 2005 the trough of the cycle for unfiltered data was recorded in September, which highlights the importance of using a filtering technique to remove the trend component that may obscure inter-annual variations.

Table 5.2. Comparison between AV_s of CO from unfiltered data and STL data from 2000 to 2012 at the EGH site.

Year	2000	2001	2002	2003	2004	2005	2006	2007	2008	2009	2010	2011	2012
Unfiltered	263.5	399.7	314.9	311.3	269.7	288.5	253.7	178.3	271.5	165.5	168.5	141.9	110.3
STL	268.1	302.9	298.6	279.1	270.7	243.3	210.2	191.2	198.0	163.6	142.5	121.9	115.6
ΔUnfiltered-STL	-4.6	96.8	16.3	32.2	-1.0	45.2	43.6	-12.9	73.5	1.9	25.9	19.9	-5.3
Max Unfiltered	Jan	Jan	Dec	Dec	Dec	Dec	Jan	Feb	Feb	Jan	Jan	Dec	Feb
Max STL	Jan	Dec	Dec	Dec	Dec	Dec	Dec	Feb	Feb	Feb	Jan	Jan	Jan
Min Unfiltered	Aug	Oct	Jun	Jul	Jul	Sep	Aug	Jul	Aug	Jul	Jul	Aug	Jul
Min STL	Jul	Jul	Jul	Jul	Jul	Jul	Aug	Aug	Jul	Jul	Jul	Jul	Jul

**CO AV_s expressed in ppb.*

5.4.2. CO annual cycles by wind sector

CO seasonal cycles and the CO averaged yearly cycles by wind sector at EGH were calculated from STL filtered data. Data show that largest AV_s for the yearly averaged cycle was recorded for the E (390.0 ppb CO), whereas the lowest AV_s was for the SW (107.0 ppb CO), the background sector. Table 5.3 summarises AVs for yearly averaged cycles and the occurrence of the peak and trough by wind sector. The occurrence of the peak was in November for W, December for NE, E and SE, January for N and NW, and in February for S and SW. Interestingly the clean sectors, show the latest occurrence of the peak, which can be related to the advection of clean air masses and the highest wind speeds recorded during the period.

Table 5.3. CO seasonal cycles of wind sector for STL data averages from 2000 to 2012.

Sector	N	NE	E	SE	S	SW	W	NW
AV	199.8	225.0	390.0	261.8	115.2	107.0	158.4	189.3
Maxima	Jan	Dec	Dec	Dec	Feb	Feb	Nov	Jan
Minima	Jun	Jun	Jul	Jul	Aug	Jul	Jul	Aug

Maxima and minima correspond to the average seasonal CO cycle from STL data.
AV expressed in ppb CO.

By contrast, only small variation was observed for timing of the trough occurrence of the CO seasonal cycle. The largest frequency observed for the occurrence was for July in the E, SE, SW and W, June for the N and NE, and in August for the S and NW. Differences in the occurrence can be ascribed to changes in meteorological conditions and in the emissions mostly from automobiles in the areas nearby.

5.4.3. Influence of the PBL height on CO yearly cycle

Unfiltered monthly CO averages at EGH during 2000-2012 were used to investigate the relationship between concentrations and the estimated PBL height at the UK (PORG, 1997). The linear regression test from least squares performed shows a strong and significant relationship (p<0.001) between PBL height and CO concentrations recorded (Figure 5.7). The highest CO concentrations are recorded when the lowest height (300 m) of the PBL is estimated during winter. By contrast, the lowest CO averages coincide with the largest height of the PBL (1000 m).

Highest concentrations of CO are due to the low level of the PBL during winter. Cold weather may form a stable PBL and lead to poor dispersion conditions, which can

trap the CO emissions close to the ground (Netcen, 2003). During summer, the enhanced mixing due to large convective processes can disperse and dilute the CO emissions. This is coupled with the advection of clean air masses from the background sector which contain low loading of CO.

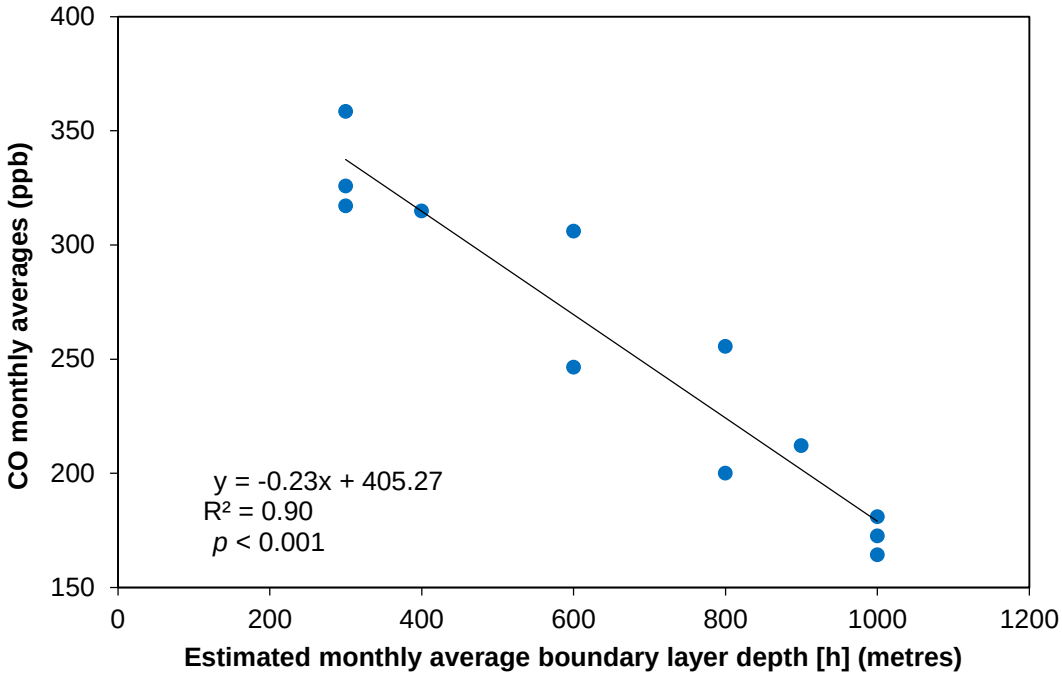

Figure 5.7. Relationship between PBL depth and 13-year monthly averages of the CO yearly cycle at EGH from 2000 to 2012.

5.5 Long-term trend of CO at the EGH site during 2000-2012

5.5.1. CO monthly averages and filtered trend computed with STL interpretation

In the last two decades, reports have shown that global atmospheric levels of CO have decline considerably (Novelli et al., 1998, Kuebler et al., 2001; von Schneidemesser et al., 2010; Table 5.1). Such a large decrement has been mostly observed in urban areas (Kuebler et al., 2001; Bigi and Harrison, 2010; Li and Liu, 2011). In the UK, the long-term decline in CO concentrations is the outcome of the implementation of successful policies to improve the air quality. Since 1990, the decline in CO levels has been driven by reductions in emissions from: road transport, agricultural field burning and the domestic sectors (NAEI, 2013). Despite this, CO emissions from road transport sector still remain important. The UK National Emissions Inventory (2013) report that in 2010, CO emissions from the road transport were 38% of the total CO emitted in UK. It also reports for 2011 a

total emission of CO of 1,625 kt, which means a decline of 77% relative to CO emissions in 1990.

The long-term trend of CO records at EGH during 2000-2012 was calculated by filtering CO monthly averages with STL. Unfiltered monthly averages for CO records at EGH during 2000-2012 and 1SD are shown in Figure 5.8(a), Figure 5.8(b) shows the long-term trend of CO calculated with STL and the residual beyond the trend and seasonal components. A decreasing trend is noticeable, which indicates that there has been a marked decline at EGH in the CO levels. The data show some small increases through the recorded period especially in winter, which may be ascribed to increases in CO emissions from the residential sector due to domestic heating use (NAEI, 2013).

Overall, the decline in CO levels is more pronounced from 2000 to 2003, and then the slope decreases. At North Kensington, London, Bigi and Harrison (2010) also observed a marked decline in CO concentrations during 1996-2008. However, they mentioned that according to the UK NAEI, CO emissions have decreased gradually within the recorded period, which do not explain the strong decline observed from 2000 to 2003. They also suggested that annual variations in meteorological conditions drive the changes in CO concentrations observed, especially during long-range transport events from Western Europe to the UK. In this thesis, such transport events are discussed and analysed in section 7.3.

Figure 5.8(b) shows large monthly residuals of CO during winter, which ranged from -125.6 to 144.0 ppb CO. CO residuals were greater during the first years of measurements (2000-2003) and increase also during winter up to 2008. Then, CO residuals did not show important increases even during winter except in 2012. The smaller CO residuals were observed in summer and decreased across the recorded period.

The declining trend of CO seems to halt after 2009 and remained constant until 2012. Indeed, a slight increment in CO concentrations is observed after summer 2012. The halt in the CO trend observed between 2009 and 2010 could be related to the cold weather experienced in 2010, which triggered CO emissions from domestic heating use (NAEI, 2013). The further increases after 2011 may reflect increases in recent years in biomass use for industrial combustion, which have increased four-times since 2008 according to the UK National Emissions Inventory.

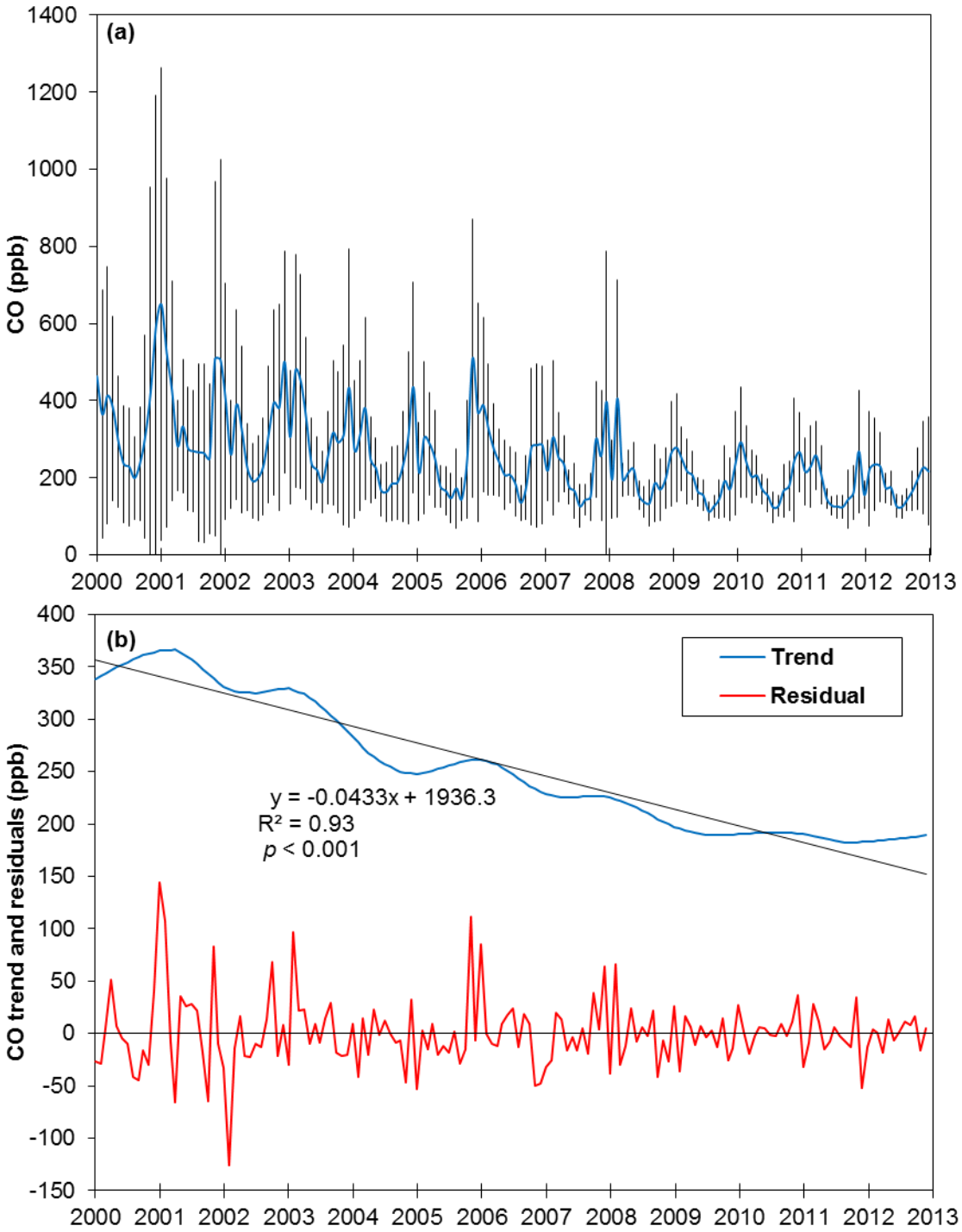

Figure 5.8(a). Unfiltered CO monthly averages ± 1SD calculated from daily averages; **(b).** STL filtered CO long-term trend and residuals observed at RHUL during 2000-2012. The residuals represent the remaining CO beyond the trend and seasonal components as defined by Cleveland et al. (1990).

5.5.2. CO decline rate observed at RHUL during 2000-2012

To calculate the magnitude of the decline rate observed at EGH, annual CO averages were calculated from monthly averages. Then, the non-parametric Mann-Kendall test was applied to test the trend existence and the nonparametric Sen's

method was to calculate the magnitude. Decline rates in CO were calculated from unfiltered and filtered data in order to investigate differences. The CO decline rates were compared with those calculated by least squares linear regression in the Excel and SigmaPlot software.

In order to analyse the variations recorded in ambient CO data at EGH, annual averages of CO were calculated from unfiltered monthly averages (Table 5.4). Figure 5.9 shows the Mann-Kendall analysis and Sen's estimate for CO annual averages at EGH during 2000-2012. A decline rate of -15.3 ppb CO yr^{-1} was calculated from unfiltered annual averages, whereas the decline was -15.6 ppb yr^{-1} from STL filtered annual averages. No significant difference (p>0.05) was found between the decline rates from filtered and unfiltered data. Table 5.5 lists decline rates of CO at EGH calculated using Mann-Kendall and Sen's estimate and least square linear regressions for filtered and unfiltered data calculated with Excel and SigmaPlot.

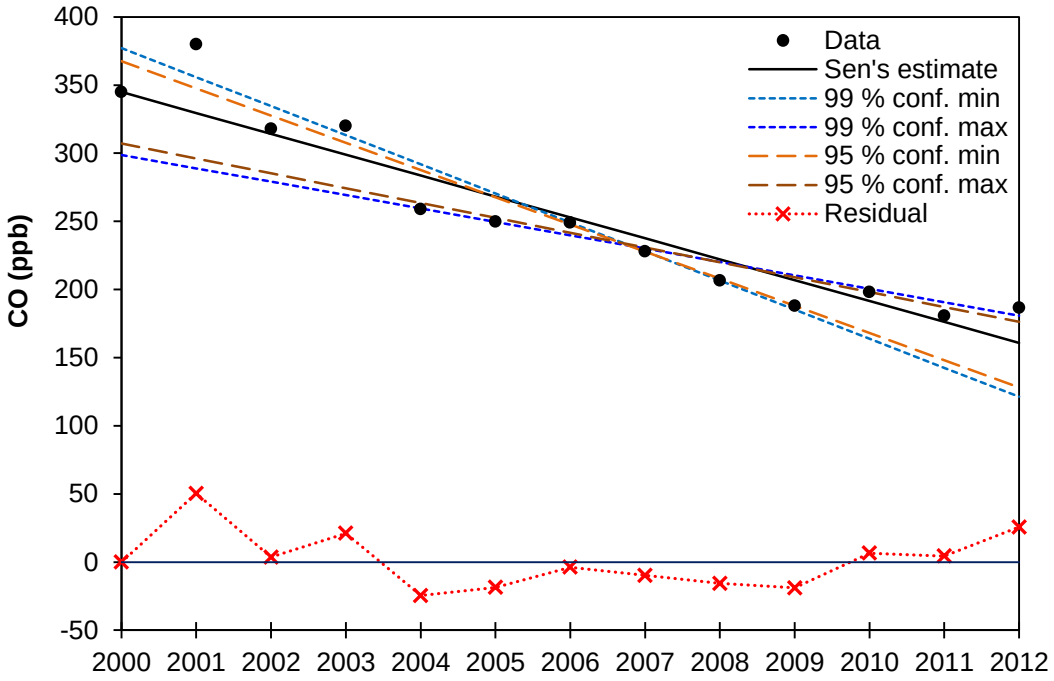

Figure 5.9. Annual averages and decline trend for atmospheric CO at EGH during 2000-2012 calculated with the Mann-Kendall test and Sen's estimate, and annual residuals.

Table 5.4. Comparison of long-term trends of CO from unfiltered data and STL data during 2000 to 2012 at the EGH site.

CO data	Period	Test Z	Significance	Q[a]	Qmin99	Qmax99	Qmin95	Qmax95	B[b]	Bmin99	Bmax99	Bmin95
Unfiltered	2000-2012	-4.2	***	-15.3	-21.3	-9.8	-19.9	-10.9	344.9	377.2	298.7	367.5
STL filtered	2000-2013	-4.5	***	-15.6	-20.2	-10.8	-19.4	-11.7	347.2	373.3	309.0	365.9

Slopes and series data are expressed in ppb CO

°Test Z is performed when n≥10. The absolute value of Z is compared to the standard normal cumulative distribution to define if there is a trend or not at the selected level α of significance. A positive (negative) value of Z indicates an upward (downward) trend.

[a]True slope of linear trend

[b]First data of the series

The following symbols are used for the four tested significance levels α with which the Mann-Kendall trend shows that the null hypothesis of no trend should be rejected:

*** if trend at a = 0.001 level of significance

** if trend at a = 0.01 level of significance

* if trend at a = 0.05 level of significance

+ if trend at a = 0.1 level of significance (no symbol if a is greater than 0.1).

Qmin99: the lower limit of the 99 % confidence interval of Q (α= 0.1)

Qmax99 the upper limit of the 99 % confidence interval of Q (α= 0.1)

Qmin95: the lower limit of the 95 % confidence interval of Q (α= 0.05)

Qmax95: the upper limit of the 95 % confidence interval of Q (α= 0.05)

Bmin99: estimate of the constant Bmin99 for 99% confidence level of linear trend

Bmax99: estimate of the constant Bmax99 for 99% confidence level of linear trend

Bmin95: estimate of the constant Bmin95 for 95% confidence level of linear trend

Bmax95: estimate of the constant Bmax95 for 95% confidence level of linear trend

Table 5.5. Comparison between CO trends calculated with Mann-Kendall and Sen's tests and Excel and SigmaPlot least squares linear regression.

Year	Unfiltered annual averages	STL annual averages	Unfiltered Sen's estimate	STL Sen's estimate	Unfiltered least squares Excel	STL least squares Excel	Unfiltered least squares SigmaPlot	STL least squares SigmaPlot
2000	344.9	352.4	344.9	347.2	351.6	349.3	350.4	349.2
2001	379.9	355.4	329.5	331.6	335.4	333.4	334.4	333.4
2002	317.9	327.1	314.2	316.1	319.2	317.6	318.4	317.6
2003	320.0	312.7	298.9	300.5	303.0	301.8	302.4	301.7
2004	258.9	261.5	283.5	284.9	286.8	286.0	286.4	285.9
2005	249.6	254.9	268.2	269.3	270.6	270.1	270.4	270.1
2006	249.1	247.8	252.9	253.7	254.4	254.3	254.4	254.3
2007	227.8	226.4	237.5	238.1	238.2	238.5	238.3	238.5
2008	206.6	213.5	222.2	222.6	222.0	222.7	222.3	222.6
2009	188.0	191.7	206.9	207.0	205.8	206.8	206.3	206.8
2010	198.1	191.4	191.5	191.4	189.6	191.0	190.3	191.0
2011	180.6	185.3	176.2	175.8	173.5	175.2	174.3	175.2
2012	186.5	186.0	160.9	160.2	157.3	159.4	158.3	159.4
Slope (ppb CO yr^{-1})	N.A.	N.A.	-15.3	-15.6	-16.2	-15.8	-16.0	-15.8
Decrease in CO (ppb)	158.4	166.4	184.0	187.0	194.3	189.9	192.1	189.8
% decline in CO (13-years)	45.9	47.2	53.3	53.9	55.3	54.4	54.8	54.4
Significance (*p*)	N.A.	N.A.	<0.001	<0.001	<0.001	<0.001	<0.001	<0.001

Annual averages and data series are expressed in ppb CO

***N.A.**: Not applicable*

CO decline rates calculated with Excel and SigmaPlot ranged from -15.8 to -16.2 ppb CO yr^{-1}. No significant difference (p>0.05) was found between CO decline rates calculated with Mann-Kendall and Sen's estimate, and Excel and SigmaPlot tests. The CO observed decreasing trend at EGH is in good agreement with reports from at the Marylebone Road and at North Kensington, in London, which show a declining trend in CO levels from 1998 onwards. At EGH, the CO decline was 3.5% yr^{-1} (3.6% yr^{-1} for STL data) during 2000-2012, whereas von Schneidemesser et al. (2010) reported a decline of 12% yr^{-1} from 1998-2008 at the kerbside of Marylebone road. This is a decrease from 1600 ppb CO in 1998 to 530 ppb CO in 2008. Such decrease is 3.4 times larger than that observed at EGH and can be explained by the decline in CO emissions from automobiles (NAEI, 2013), which are the main source of CO near to the sampling site.

In North Kensington, Bigi and Harrison (2010) reported a lower decline rate in atmospheric CO levels, which decreased from 400-600 ppb CO in 1998 to 200-400 ppb CO in 2008. The different decline rates observed show the positive effects air quality policies which have led to a substantial decrease in CO emissions. Thus, while at Marylebone road the CO large decline rate is related to reduction in emissions mostly from automobiles, at north Kensington (urban background site) the influence of declining emissions from on-road sources is less strong, whereas at EGH the decline in CO results from the combination between decreases from on-road sources and from domestic combustion local sources.

Decline rates of ambient CO were calculated at the urban background sites of Bloomsbury and Westminster in London and Reading, UK during 2000-2012, 2001-2012 and 2003-2006, respectively. Data were obtained from the Automatic Urban and Rural Network (AURN) web site (http://uk-air.defra.gov.uk/data/; Defra, 2012). Table 5.6 summarises the calculated trends of CO with the Mann-Kendall and Sen's estimate. The largest decline rate was observed for the Reading station (36.4 ppb CO yr^{-1}; p>0.05), which is 2.0 and 2.1 times larger than the decline rates observed at EGH for unfiltered and filtered CO annual averages during 2003-2006. Decline rates of CO of 32.3 and 26.3 CO yr^{-1} (p<0.05) were calculated for Bloomsbury and Westminster stations. Such decline rates are 2.1 and 1.7 times larger than the decline observed at EGH during the same period for unfiltered and filtered CO data. Such decline rates are in good agreement with previous reports (Table 5.1), which have shown larger declines of CO at urban areas than at semi-rural and sub-urban areas.

Table 5.6. CO Mann-Kendall test and Sen's estimates for the urban background sites Bloomsbury and Westminster in London during 2000-2012 and 2001-2012, respectively, and for Reading during 2003-2006.

Site	n	Test S	Test Z	Significance	Q[a]	Qmin99	Qmax99	Qmin95	Qmax95	B[b]	Bmin99	Bmax99	Bmin95	Bmax95
Bloomsbury	*13*	N.A.	-3.7	***	-32.3	-52.1	-13.4	-48.8	-16.4	555.7	714.4	404.3	697.2	427.7
Westminster	*12*	N.A.	-2.1	*	-26.3	-49.4	13.9	-40.6	-5.0	558.7	648.9	231.6	597.9	383.1
Reading	4	-6.0	N.A.	+	-36.4	N.A.	N.A.	N.A.	N.A.	481.3	N.A.	N.A.	N.A.	N.A.

Slopes and series data are expressed in ppb CO
n: number of annual values
[◎]Test S is performed when n≤10. the absolute value of S is compared to the probabilities of the Mann-Kendall nonparametric test for trend to define if there is a monotonic trend or not at the level a of significance. A positive (negative) value of S indicates an upward (downward) trend.
[○]Test Z is performed when n≥10. The absolute value of Z is compared to the standard normal cumulative distribution to define if there is a trend or not at the selected level α of significance. A positive (negative) value of Z indicates an upward (downward) trend.
[a]Slope calculated by the Sen's estimate
[b]First data of the series
The following symbols are used for the four tested significance levels α with which the Mann-Kendall trend shows that the null hypothesis of no trend should be rejected:
*** if trend at α = 0.001 level of significance
** if trend at α = 0.01 level of significance
* if trend at α = 0.05 level of significance
+ if trend at α = 0.1 level of significance (no symbol if α is greater than 0.1).

In an earlier study in Switzerland, Kuebler et al. (2001) observed larger rates of CO decline at urban monitoring stations than at rural monitoring stations. They suggested that the large decline rates in CO levels observed were due to decreases in CO emissions mostly from automobiles, as urban records without the influence of local traffic showed no important changes. At Seoul, South Korea, Kim and Shon (2011) also observed larger CO decline rates at urban monitoring stations than at background stations. They reported CO decline rates at urban stations from 182 to 26 ppb CO yr^{-1}, whereas at background stations the decline rates observed ranged from 43 to 10 ppb yr^{-1}. According to this, the decline rate calculated at EGH corresponds to a semi-rural monitoring station, which under certain meteorological conditions can track polluted air masses passing over greater London and and urban areas nearby the station.

5.5.3. Sector analysis of CO long-term trends at EGH during 2000-2012

CO annual averages by wind sector were calculated from unfiltered monthly averages considering that no statistical difference (p>0.05) was observed between filtered and unfiltered data to assess the variability recorded at EGH during 2000-2012 (Section 5.5.2). The Mann-Kendall test and Sen's estimate were applied to the unfiltered annual averages to calculate the decline rates for each wind sector. Figure 5.10 shows the CO decline trends by wind sector. Table 5.7 summarises decline rates, % of decrease and significance for each wind sector.

CO decline rates ranged from -7.4 ppb CO yr^{-1} for S sector to -36.1 ppb CO yr^{-1} for the calm sector with a significance of p<0.01 for all wind sectors. Overall, the decline in CO levels is consistent. Data show that sustained reduction in the CO local emissions from larger sources at the beginning of the measurements, and then the reduction rate decreased as observed towards the end of the measured period. The largest decline rates in CO were observed for the calm and E sectors, -36.1 and -25.3 ppb CO yr^{-1}. This is a decrease of CO of 56.0% and 50.7% during 2000-2012. The E sector showed a sustained drop after 2001, whereas the calm shows a decrease from 2002 onwards. By contrast, the smallest CO declines were observed in the background sector, SW and S, -7.5 and -7.4 ppb CO yr^{-1}, which is an overall decline of CO of 36.25 and 32.9% during 2000-2012 for SW and S, respectively. Interestingly, only those sectors showed a consisted decrease in the CO levels through the overall recorded period.

Table 5.7. CO Mann-Kendall test and Sen's estimates for wind sectors at the EGH site during 2000-2012.

Wind sector	Test Z	Significance	Q[a]	Qmin99	Qmax99	Qmin95	Qmax95	B[b]	Bmin99	Bmax99	Bmin95	Bmax95
N	-3.1	**	-14.0	-23.2	-3.6	-20.3	-7.8	360.6	418.1	289.1	408.9	322.7
NE	-3.8	***	-21.8	-32.4	-7.2	-30.3	-11.3	448.6	504.1	331.0	489.0	356.0
E	-4.1	***	-25.3	-37.7	-14.6	-33.0	-17.5	503.9	573.5	397.4	531.6	423.1
SE	-3.5	***	-16.3	-26.1	-6.0	-23.2	-10.1	381.7	438.8	299.8	419.0	327.1
S	-3.8	***	-7.4	-9.5	-4.1	-9.0	-5.4	240.0	251.2	218.6	247.1	227.4
SW	-4.1	***	-7.5	-9.5	-5.3	-9.1	-5.8	238.8	252.1	225.1	249.5	227.1
W	-3.5	***	-9.3	-13.8	-5.2	-12.5	-7.3	278.4	312.3	252.0	303.1	266.6
NW	-3.7	***	-12.0	-18.8	-7.9	-16.2	-8.7	315.1	367.7	286.3	344.8	292.4
Calm	-3.2	**	-36.1	-54.7	-12.0	-50.2	-19.6	597.3	733.6	448.9	726.3	495.9

Slopes and series data are expressed in ppb CO

°Test Z is performed when n≥10. The absolute value of Z is compared to the standard normal cumulative distribution to define if there is a trend or not at the selected level α of significance. A positive (negative) value of Z indicates an upward (downward) trend.

[a]Slope calculated by the Sen's estimate

[b]First data of the series

The following symbols are used for the four tested significance levels α with which the Mann-Kendall trend shows that the null hypothesis of no trend should be rejected:

*** if trend at α = 0.001 level of significance

** if trend at α = 0.01 level of significance

* if trend at α = 0.05 level of significance

+ if trend at α = 0.1 level of significance (no symbol if α is greater than 0.1).

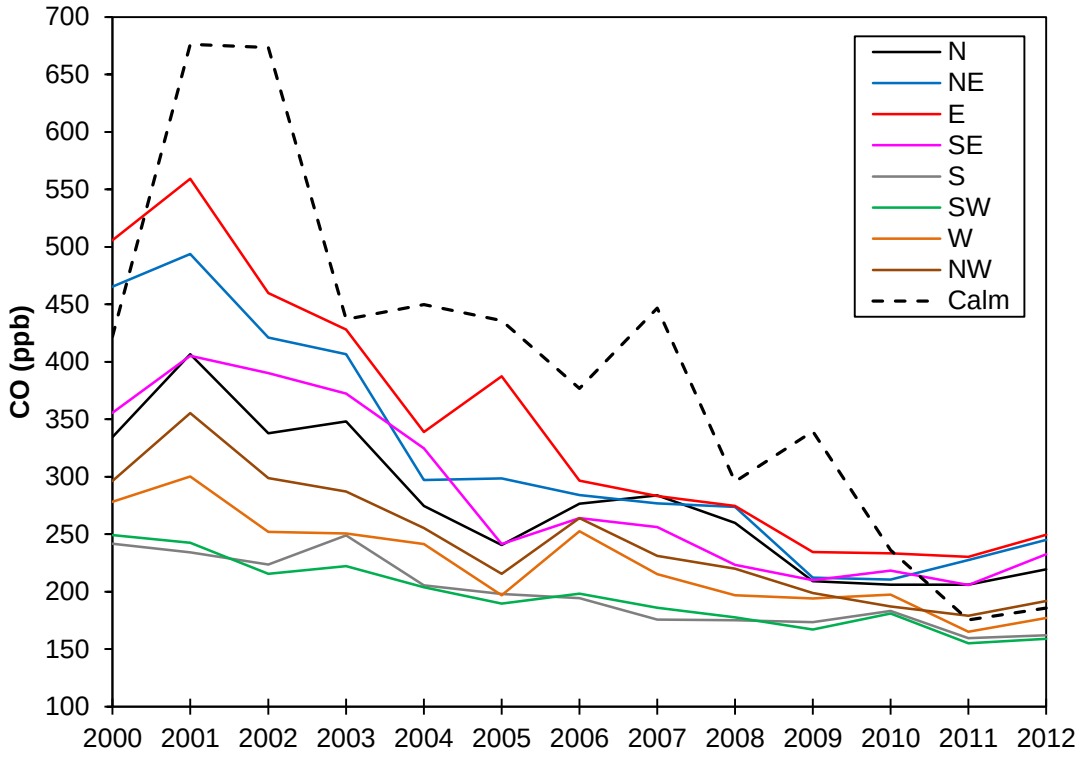

Figure 5.10. CO annual averages and decline trends for atmospheric CO measured at EGH during 2000-2012 by wind sectors and calm. Annual averages were calculated from unfiltered data in order to maintain the variability recorded.

The CO decline observed at EGH can be dominated by a reduction of global and local sources. Three possible sources of the declining CO levels are: a decline in the Atlantic background, a decline in local sources in London and SE England, and a decline in European sources. Previous studies in central Europe have shown a sustained drop in CO concentrations. Zellweger et al. (2009) observed a decline rate of -2.65 ± 0.04 ppb CO yr^{-1} from 1991-2004 in tropospheric CO at Jungfraujoch, Switzerland. A lower decline rate of -0.84 ± 0.95 ppb CO yr^{-1} was reported by Chevalier et al. (2008) at Zugspite, Germany during 1991-2004. Bigi and Harrison (2010) observed during the advection of easterly air masses from continental Europe to the UK, which passed over central London, that the levels of air pollutants increased and after the occurrence the CO levels decreased slowly.

At EGH, the lowest decline rates in CO levels are observed for the background SW and S sectors, where air masses which represent Atlantic CO levels arrived at the sampling station. SW and S sectors have very few CO sources after making landfall, which could explain the lowest decline rates observed and is ascribed to the abatement of local sources weaker than those observed for the urban sectors. Such behaviour was reported by Kuebler et al. (2001) whom observed larger CO decline rates at urban than at rural monitoring stations. This is in good agreement

with the UK National Emissions Inventory (2013), which shows larger declines for the transport sector, the main source at urban areas, than CO decline rates for the domestic and agricultural sectors.

5.6. Comparison of CO records at EGH and MHD

5.6.1. Comparison between monthly-averaged continuous measurements at EGH and flask measurements at MHD

Flask measurements of CO at MHD are made on a discrete frequency of 5-12 month^{-1}, and were obtained from the NOAA/ESRL/GMD web site (http://www.esrl.noaa.gov/gmd/dv/data/?parameter_name=Carbon%2BMonoxide&site=MHD&frequency=Discrete&type=Flask). The comparison of the overall CO monthly averages and the averages for the background sector at EGH with the monthly averages from MHD flasks can provide an idea of the principal CO sources close to EGH. Airflow from the east allows detection of CO emissions from the Greater London area, and from the SE sector during anti-cyclonic conditions can reveal the contribution from sources on the European continent.

Figure 5.11 shows the comparison between CO overall monthly averages and CO background averages at EGH with CO flask monthly averages at MHD 2000 to 2012. Figure 5.12 shows the linear regression analysis between monthly averages of CO for the SW sector at EGH with monthly averages from flask measurements at MHD. Differences between EGH and MHD ranged from 515.7 ppb CO (January 2001) to 21.1 ppb CO (May 2011). Such differences were larger at the beginning of the measurements and show a sustained decline during the measured period. Differences increased during winter due to meteorological conditions and to low height of the PBL as shown in section 5.4.3. Differences in summer were lower than differences in winter.

Interestingly, the differences between background CO averages and flask averages were larger by the middle of the sampled period in winter 2006 (248 ppb CO) but similarly to the overall averages decreased by the end of the measured period (23 ppb CO). The more pronounced decline trend for the EGH records can be related to the decline in CO emissions mostly from the transport sector as reported in the UK NAEI 2013 (Section 1.7). The CO decline observed is in good agreement with the

wind sector analysis shown in Section 5.5.3. At MHD, the CO decline was reported by Derwent et al. (2006) who studied continuous records of CO at Mace Head from 1990 to 2003. They suggested that the decline of background CO concentrations is the outcome of air quality policies issued worldwide to reduce CO emissions to improve the air quality.

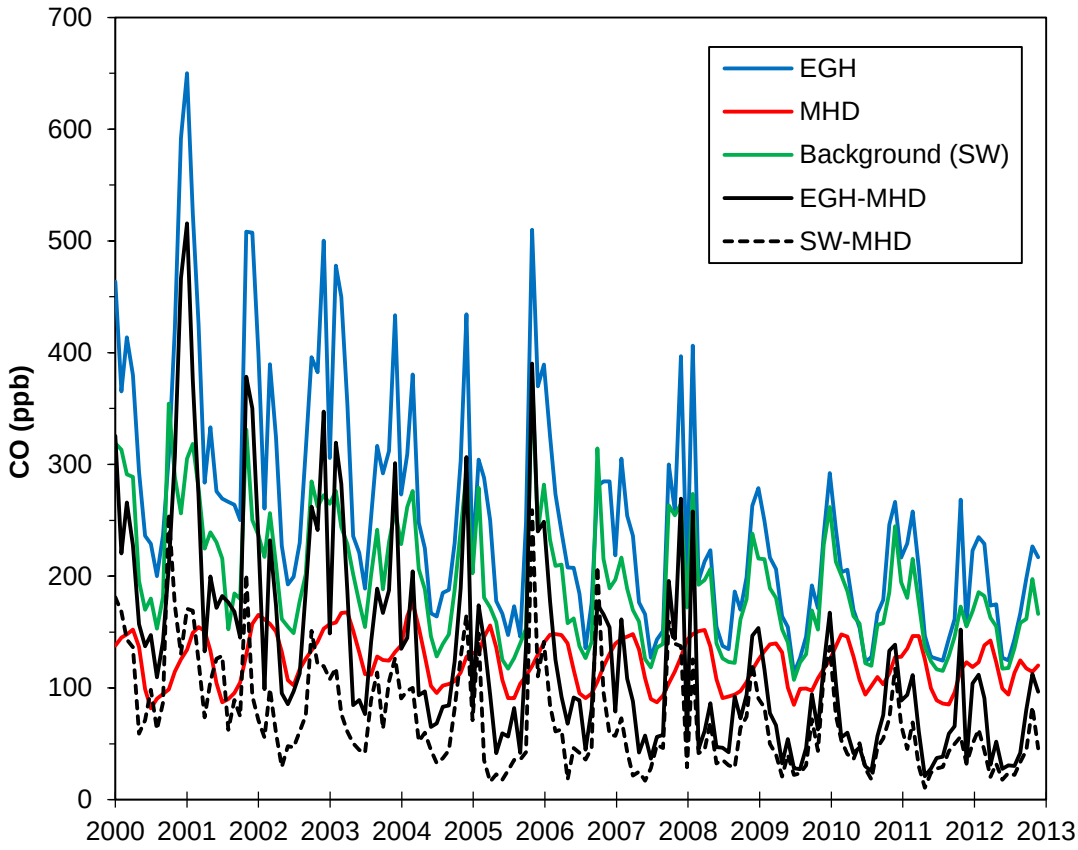

Figure 5.11. Comparison of CO overall and background monthly averages at EGH and monthly averages for flask measurements at MHD and differences between the two sites during 2000-2012.

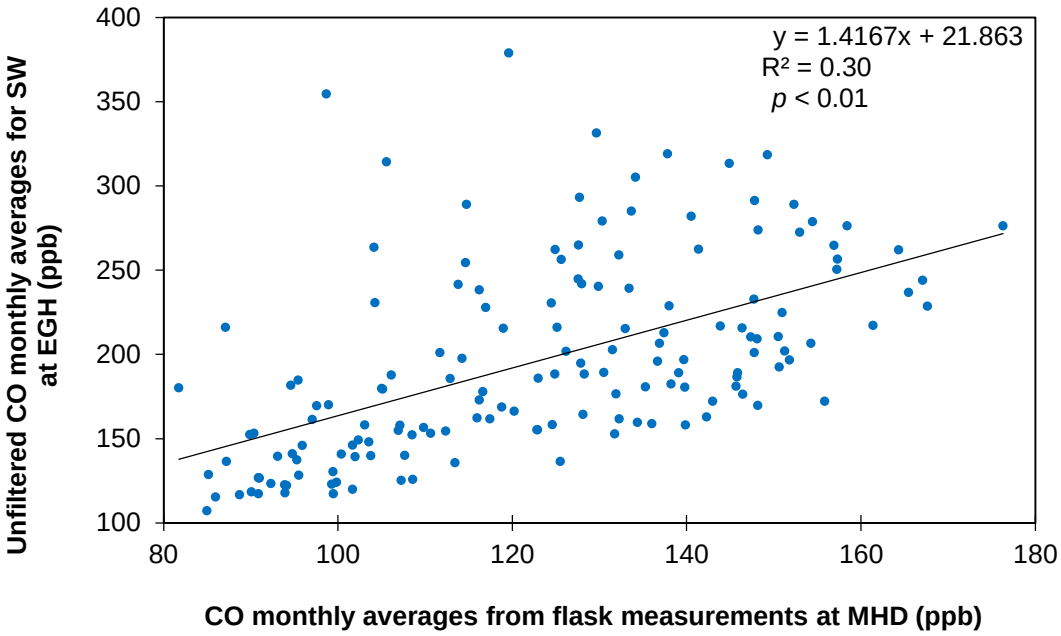

Figure 5.12. Linear correlation observed between unfiltered SW and flask measurements of CO monthly averages at EGH and MHD, respectively during 2000-2012. The correlation is significant for n=156 at level of 99% of confidence.

5.6.2. CO seasonal cycles comparison

The STL seasonal cycles for CO records at EGH are compared with the CO seasonal cycles at MHD during 2000-2012 in Figure 5.13(a). Both cycles show the maxima during winter and the minima in summer. Interestingly, at EGH a shoulder in the cycles is observed after the maxima in all years except 2010, whilst at MHD that shoulder is not present. This appeared in winter but varied in timing from December to February with no clear pattern. This is most likely the result of variable meteorological conditions, when prolonged periods of cyclonic conditions during winter bring Atlantic air masses to EGH and disperse the CO build-up.

Figure 5.13(b) shows the averaged CO annual cycle at EGH and MHD. The cycle at MHD was reported by Derwent et al. (2006), who observed the maxima of the cycle in March-April and the minima in July. Novelli et al. (1998) also observed the largest CO levels in late winter / early spring, whereas the minimum was reported in July. A difference of two months for the peak timing is observed for EGH, but it is most common in December. By contrast, the minima of the CO seasonal cycles at EGH and MHD is in July and coincides with the maximum activity of the OH radical.

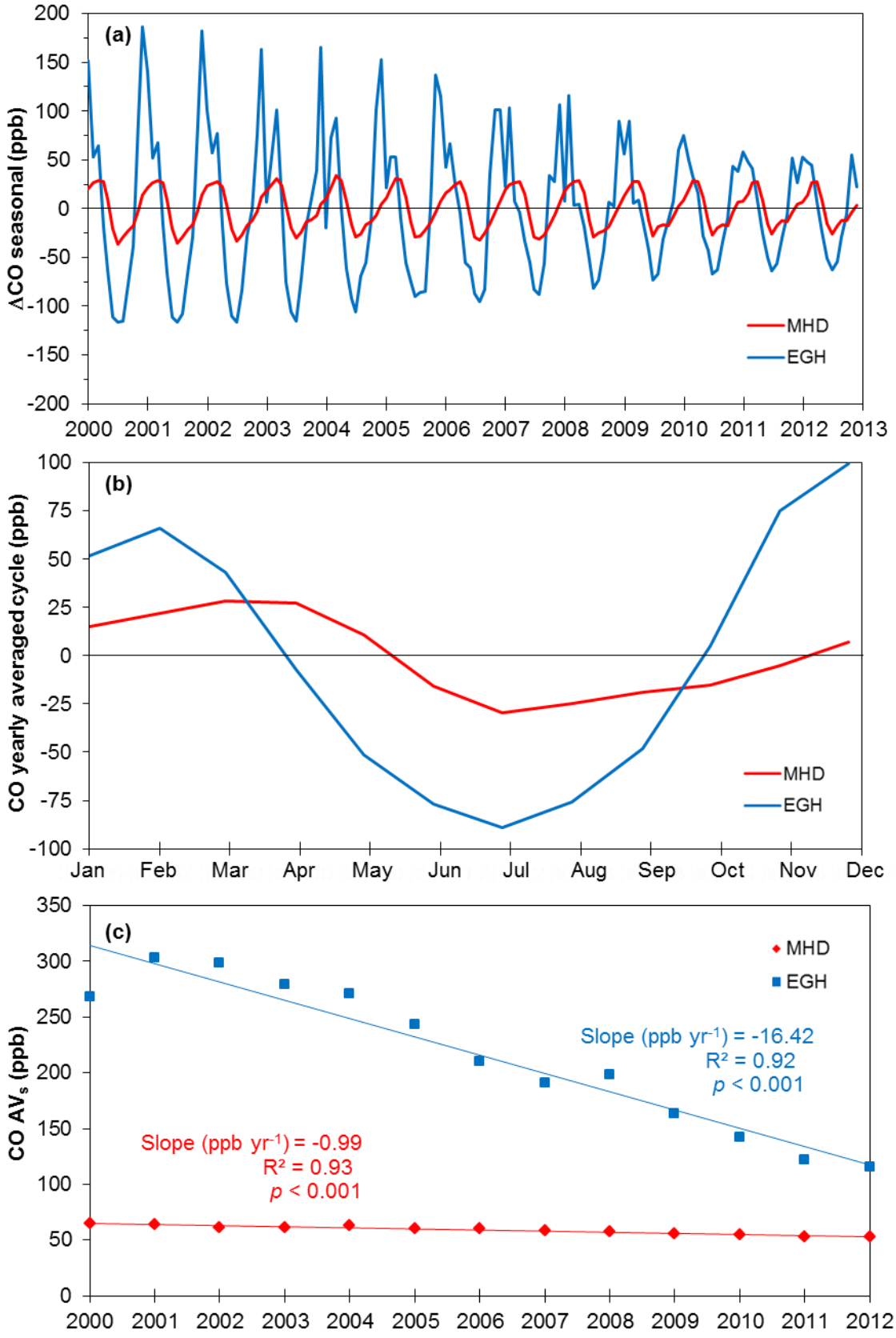

Figure 5.13(a). STL seasonal cycles; **(b).** CO averaged yearly cycles calculated from 13-years of measurements; **(c).** AVs peak-to-trough of each seasonal cycle and trend at EGH and MHD during 2000-2012.

Although the CO seasonal cycles show similar behaviour, larger AV_s are observed at EGH than at MHD. Figure 5.13(c) shows the amplitudes of the seasonal cycles and the trends calculated. Larger AV_s are produced by large variations of the CO concentrations, and at EGH these are ascribed to higher CO emissions during winter adding increased domestic heating-related emissions from the suburbs nearby and the effects of a lower than average PBL. The summer decrease in CO levels is due to the enhanced mixing of air masses and the maximum consumption via reaction with the OH radical. During winter the CO emissions from southeast England and Western Europe are transported during anti-cyclonic conditions and contribute to the large levels recorded at EGH. By contrast, the lower CO levels observed at MHD than at EGH are likely due to the few combustion sources nearby MHD.

Figure 5.13(c) shows a declining trend in the CO AV_s at EGH and MHD during 2000-2012, but a large difference between the rates is observed. At EGH the decline rate is calculated as 16.4 ppb CO yr^{-1}, whilst at MHD the decline rate was 1 ppb CO yr^{-1}. The contrasts are explained by the implementation of air quality policies that have abated important CO emissions in the urban environment.

5.6.3. CO long-term trends at EGH and MHD during 2000-2012

Annual averages at MHD were calculated from flask measurements during 2000-2012. The Mann-Kendall and Sen's estimate tests were used to calculate the decline trend (Table 5.8). Figure 5.14 shows the declining CO trends at EGH and MHD during 2000-2012. At EGH the decline rate was calculated as 15.3 ppb CO yr^{-1}, whereas at MHD the decline rate was 0.8 ppb CO yr^{-1}. The decline rate at EGH is 19.1 times larger than at MHD. It is thought to be due to the decline rate in CO levels worldwide, which has been highlighted since the implementation of air quality policies to reduce CO emissions. CO concentration declined by 1 to 6 ppb CO during 1990s (Novelli et al., 1994; Law, 1999). Moreover, the largest decline rates in CO levels were observed in urban conurbations. Kuebler et al. (2001) observed larger decline rates at urban monitoring stations than at rural stations in Switzerland. During the 2000s, the same behaviour was observed by Lin et al. (2008) in the central Basin of Taiwan.

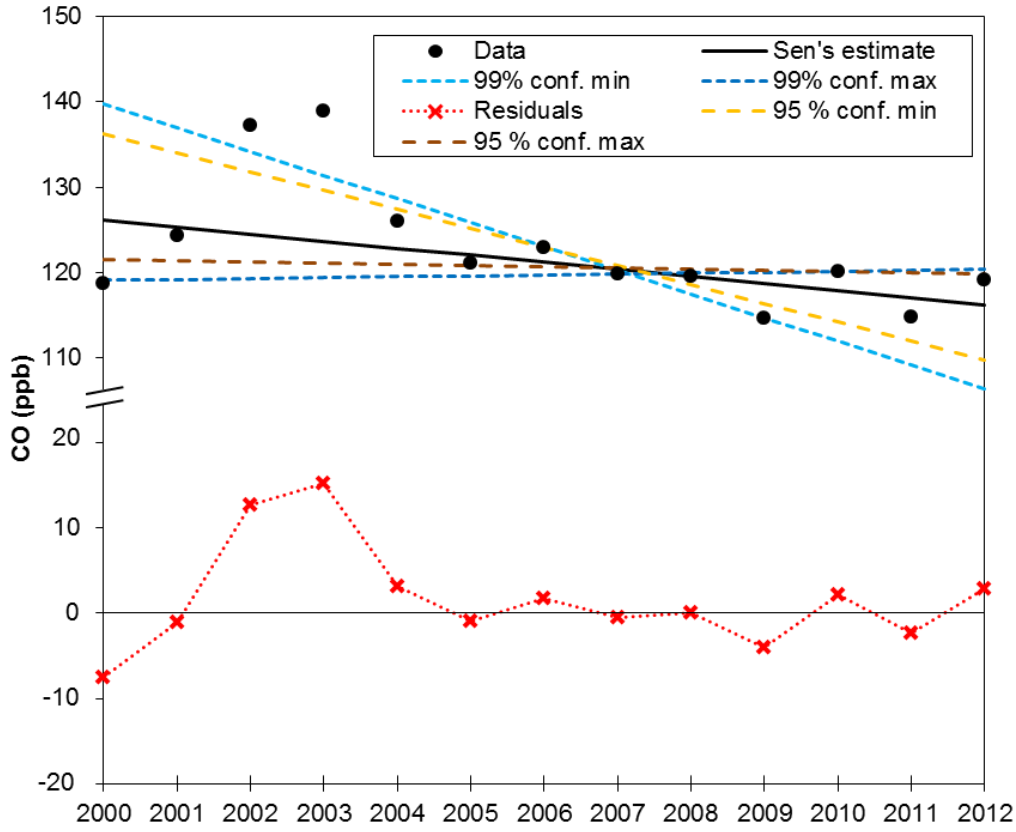

Figure 5.14. CO annual and declining trend calculated with the Mann-Kendall test and Sen's estimate at MHD during 2000-2012.

Reduction in CO emissions from on-road sources clearly have a much greater influence on the decline rate at urban stations than at semi-rural stations. The decline in CO concentrations observed is in good agreement with data reported by the UK NAEI (2013), which states that there has been a marked decline in CO emissions mostly from the transport sector since 1997. At EGH, a semi-rural monitoring station such changes are much more significant than at MHD, a station which tracks the Atlantic background CO levels during the advection of westerly Atlantic air masses. CO measurements at MHD provide insights into the northern hemisphere CO decline rate of ~1 ppb CO yr^{-1} (Novelli et al., 1998; Derwent et al., 2006). It can be concluded that CO measurements at EGH help to assess the continuing success of the air quality policies implemented in the UK and Western Europe. By contrast, CO measurements made at MHD provide significant information about CO in the Northern Hemisphere as a whole.

Table 5.8. CO Mann-Kendall test and Sen's estimates for flask measurements at MHD during 2000-2012.

Year	Data	Sen's estimate	99 % conf. min	99 % conf. max	95 % conf. min	95 % conf. max	Residual
2000	118.7	126.2	139.8	119.1	136.2	121.5	-7.5
2001	124.3	125.3	137.0	119.2	134.0	121.3	-1.1
2002	137.3	124.5	134.2	119.3	131.8	121.2	12.8
2003	138.9	123.7	131.4	119.4	129.6	121.1	15.2
2004	126.0	122.8	128.6	119.5	127.4	120.9	3.1
2005	121.0	122.0	125.8	119.6	125.2	120.8	-1.0
2006	123.0	121.2	123.0	119.7	123.0	120.6	1.8
2007	119.8	120.3	120.3	119.8	120.8	120.5	-0.5
2008	119.5	119.5	117.5	119.9	118.6	120.3	0.0
2009	114.7	118.7	114.7	120.0	116.4	120.2	-4.0
2010	120.0	117.8	111.9	120.1	114.1	120.0	2.2
2011	114.7	117.0	109.1	120.2	111.9	119.9	-2.3
2012	119.1	116.2	106.3	120.3	109.7	119.8	2.9

Slopes and series data are expressed in ppb CO
Qmin99: the lower limit of the 99 % confidence interval of Q (α= 0.1)
Qmax99 the upper limit of the 99 % confidence interval of Q (α= 0.1)
Qmin95: the lower limit of the 95 % confidence interval of Q (α= 0.05)
Qmax95: the upper limit of the 95 % confidence interval of Q (α= 0.05)
Bmin99: estimate of the constant Bmin99 for 99% confidence level of linear trend
Bmax99: estimate of the constant Bmax99 for 99% confidence level of linear trend
Bmin95: estimate of the constant Bmin95 for 95% confidence level of linear trend
Bmax95: estimate of the constant Bmax95 for 95% confidence level of linear trend
Residual: Difference between data and Sen's estimate

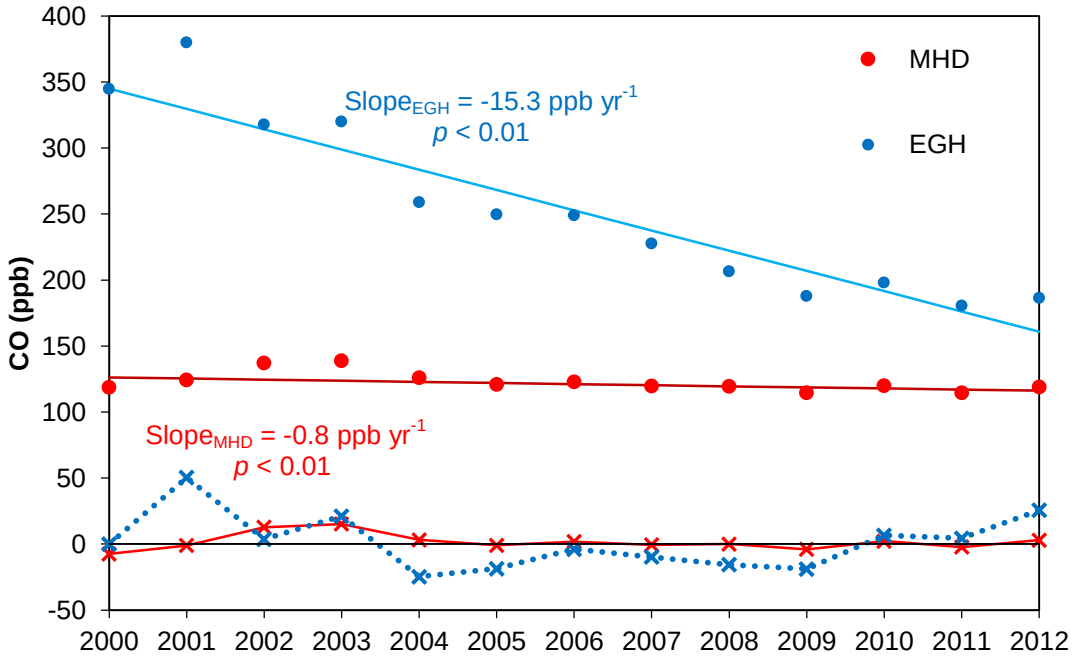

Figure 5.15. Linear trends calculated using annual averages with Sen's estimate at EGH and MHD during 2000-2012.

5.7. Summary

CO varies on time scales ranging from minutes to inter-annual and seasonal cycles. Daily means recorded during 2000-2012 for CO exhibited significant a decline. Peak values post-2010 were much closer to the minimum values recorded. The CO diurnal cycle revealed that concentrations were strongly influenced by PBL height and by changes in the traffic patterns (higher during weekdays than at weekends and therefore larger emissions during weekdays than in weekends). The seasonal cycle was mostly driven by changes in meteorological conditions (PBL height). The largest concentrations were recorded during winter when the emissions from domestic heating are the highest. A statistically significant declining trend in AV_s of -16.4 ppb CO yr^{-1} was observed at EGH, which has been influenced by the decline in CO emissions in the UK during 1990-2011.

The largest concentrations of CO were measured in air masses from the E and NE sectors, which is related to the transport of CO emissions from the London region and Heathrow airport. By contrast, the lowest concentrations were observed for air masses from the S and SW (background) sectors. The statistical analysis of annual averages of CO exhibited a declining trend during 2000-2012 of 15.3 ppb CO yr^{-1}.

Such decline is in good agreement with observations made at North Kensington and Marylebone Road in the London area (Bigi and Harrison, 2010; von Schneidemesser et al., 2010). The rate of change of CO recorded at EGH is lower by about 2-4 times than that reported for CO emissions in the UK during 2000-2011. The increase in CO levels observed during 2009 may be related to the cold weather experienced in 2010 and to the consequent increase in CO emissions (NAEI, 2013).

The decline in CO observed during 2000-2012 at EGH suggests a significant and progressive improvement in air quality in the UK, which is consistent with emission inventories. The cause of the decline is almost certainly the strict controls on vehicle emissions introduced by the UK legislation to manage the air quality.

6. ANALYSIS AND INTERPRETATION OF AMBIENT DATA FOR CH_4 RECORDED AT THE EGH SITE DURING 2000 TO 2012

Long-term records of precise and accurate ambient CH_4 measurements can help to reveal important features of its evolution such as long-term trends, interannual variations, seasonal cycles, and short-term variations like daily and weekly cycles, and pollution episodes. CH_4 is measured continuously at different monitoring stations around the world and by different cooperative networks. Figure A2 shows some monitoring stations around the globe that record CH_4 as part of the NOAA/ESRL/GMD. Table 6.1 summarises studies concerning CH_4 at different locations, from Antarctica to the Arctic Ocean, including equatorial and mid-southern and -northern latitudes.

CH_4 increased from a global average of 722 ± 25 ppb in 1750 to 1803 ± 2 ppb in 2011 (IPCC, 2013; NOAA/ESRL, 2014). During the period since systematic measurements began the CH_4 growth rate has not been constant. For example, Wahlen (1993) reported an increasing trend of 1% yr^{-1} from 1978 to 1993, due to anthropogenic activities such as rice production, ruminants and biomass burning. He also assessed the distribution of CH_4 in the boundary layer and represented latitudinal variations from 1984 to 1987. Therein, seasonal and interannual variations are observed at both hemispheres through the period, but they are more marked in the northern hemisphere especially from 30° to 90°N.

Dlugokencky et al. (2011) reported the evolution of atmospheric CH_4 from analyses of weekly samples of the NOAA cooperative network. They observed a sustained increase of atmospheric CH_4 from 1985 to 1997, and a steady state from 1998 to 2006. They also calculated the CH_4 seasonal cycle, which is attributed to seasonal variations in abundance of OH radicals in the atmosphere, changes in the PBL height, and changes in emissions from the most important sources (Dlugokencky et al., 2011). Most recently, the IPCC reports a global average growth rate of atmospheric CH_4 of 0.5 ppb yr^{-1} from 1999 to 2006 to 6 ppb yr^{-1} from 2007 to 2011 (IPCC, 2013). Changes in CH_4 growth rates are determined by the balance between surface emissions and its loss via oxidation by the hydroxyl radical in the atmosphere (Rigby et al., 2008a).

Table 6.1. Summary of previous studies of atmospheric CH_4 at different monitoring stations.

Reference	Sampling site	Type of site	Coordenates	Period studied	Type of analysis
Saito et al., 2013	NOAA[a]/NIES[b]	Aircraft measurements	Both hemispheres	2001 - 2007	Horizontal and vertical transport at different heights
Khalil et al., 2007	NOAA[a]/CMDL[c]	Background	Both hemispheres	1981 - 2004	Interannual variations, seasonal cycle, long-term trend, OH trends
Fiore et al., 2006	NOAA[a]	Background	Both hemispheres	1990 - 2004	Long-term trend, emission estimates
Dentener et al., 2005	NOAA[a]/CMDL[c]	Background	Both hemispheres	1990 - 2010	Long-term trend, emissions modelling
Kirschke et al., 2013	NOAA[a]/AGAGE[d]/UCI[e]/ CSIRO[f]	Background, continental	Both hemispheres	1980 - 2010	Long-term trend, inventories verification
Kai et al., 2011	UCI[e]	Background	Both hemispheres	1980 - 2004	Long-term trend, spatial variations, inventories verification, isotopic analyses
Rigby et al., 2008a	AGAGE[d]/CSIRO[f]	Background	Both hemispheres	1997 - 2007	Seasonal cycle, long-term trend, OH annomalies
Patra et al., 2009	WDCGG[g]	Background	Both hemispheres	1990 - 2001	Seasonal cycle, long-term trend, global distribution modelling
Dlugokencky et al., 2011	NOAA[a]	Background	Both hemispheres	1983 - 2010	Seasonal cycle, spatial variations
Manning et al., 2011	NOAA[a]/ESRL[h]/GMD[i]	Background, continental, rural	Both hemispheres	2001 - 2010	Seasonal cycle, spatial variations
Wahlen, 1993	NOAA[a]/CMDL[c]	Background	Both hemispheres	1984 - 1987	Seasonal cycle, spatial variations, inventories verification
Pedersen et al., 2005	Ny-Ålesund, Norway	Background	78.90 °N, 11.88 °E	1998 - 2003	Seasonal cycle, long-term trend
Simpson et al., 2006	UCI[e]	Background	70°N-47°S	1996 - 2006	Long-term trend, spatial variations

Table 6.1. (Continuation) Summary of previous studies of atmospheric CH_4 at different monitoring stations.

Reference	Sampling site	Type of site	Coordenates	Period studied	Type of analysis
Derwent et al., 2006	Mace Head, Ireland	Background	53.33 °N, 9.90° W	1990 - 2030	Seasonal cycle, long-term trend modelling
Lowry et al., 2001	EGH, UK	Semi-rural, sub-urban	51.43 °N, 0.55°W	1996 - 1999	Diurnal cycle, seasonal cycle, inventories verification
Thompson et al., 2009	Ochsenkopf, Germany	Background	50.03°N, 11.48°E	2006 - 2008	Diurnal cycle, seasonal cycle, sectorial analysis
Sanchez et al., 2013	Valladolid, Spain	Rural	41.81° N, 4.93° W	2010 - 2012	Diurnal cycle, seasonal cycle, sectorial analysis
Nguyen et al., 2010	Seoul, Korea	Urban, urban background	37.56° N, 126.97° E	1996 - 2006	Diurnal cycle, seasonal cycle, long-term trend

Superscripts correspond to the abreviations of the full name of cooperative networks.

[a]National Oceanic and Atmospheric Administration

[b]National Institute for Environmental Studies

[c]Climate Monitoring and Diagnostics Laboratory

[d]Advanced Global Atmospheric Gases Experiment

[e]University of California, Irvine Network

[f]Commonwealth Scientific and Industrial Research Organisation

[g]World Data Centre for Greenhouse Gases

[h]Earth System Research Laboratory

The observational networks now provide enough data to quantify global annual average burdens and to constrain global emission rates (with knowledge of loss rates), but they are not sufficiently accurate to estimate regional scale emissions and how they are changing with time. Therefore, more continuous measurements of atmospheric CH_4 are required to improve the quality and accuracy of regional emissions and global trends.

At the EGH site, Lowry et al. (2001) used continuous measurements of atmospheric CH_4 from 1996 to 1999 to study daily cycles and seasonal variations together with isotopic measurements. They also verified the accuracy of official UK emission inventories from isotopic observations. CH_4 data from continuous measurements combined with other tools such as air mass back trajectory analysis and modelling can help to understand CH_4 emissions and furthermore, also can be used to locate sources. Fisher (2006) also used continuous and isotopic measurements of CH_4 to evaluate CH_4 local sources adjacent to the EGH site to verify data in the UK NAEI.

Continuous, high-frequency and high-precision, in-situ measurements of atmospheric CH_4 have been made at the EGH site, in Surrey, UK from 2000 to 2012 as discussed in Section 2.3. CH_4 data at EGH data go back to late 1995, but in this thesis analysis has used data recorded from 2000 onwards, when meteorological data were also recorded. CH_4 data were analysed on 30-min, daily, weekly, monthly, seasonal and yearly time scales. CH_4 data recorded at EGH are compared with data from MHD station to test whether they fit the global observed trend.

6.1. Aims

The aims of this chapter are:

1. To interpret on hourly, daily, weekly, monthly, seasonal and long-term scales data for CH4 recorded at the EGH during 2000-2012.
2. To evaluate local sources of CH4 by comparing spatial variations in data recorded at EGH with data recorded at MHD during 2000-2012.

6.2. Continuous observations of CH_4 at EGH from 2000 to 2012

Figure 6.1(a) shows 30-min measurements of atmospheric CH_4 at EGH during 2000-2012. During the recorded period, CH_4 measurements ranged from 1,783 ppb CH_4 (June 2004) to 4,950 ppb CH_4 (April 2004). 30-min measurements were

classified in 4 categories to depict the histogram of 13-years records and are showed in Figure 6.2(b). The largest frequency was observed for CH_4 records between 1,783 and 2,000 ppb CH_4 (70.1%). Frequency decreased inversely as concentrations increased, a frequency of 27.4% was seen for records between 2,001 and 2,500 ppb CH_4, 2.0% for 2,501-3,000 ppb CH_4, and <1% for >3,000 ppb CH_4, respectively.

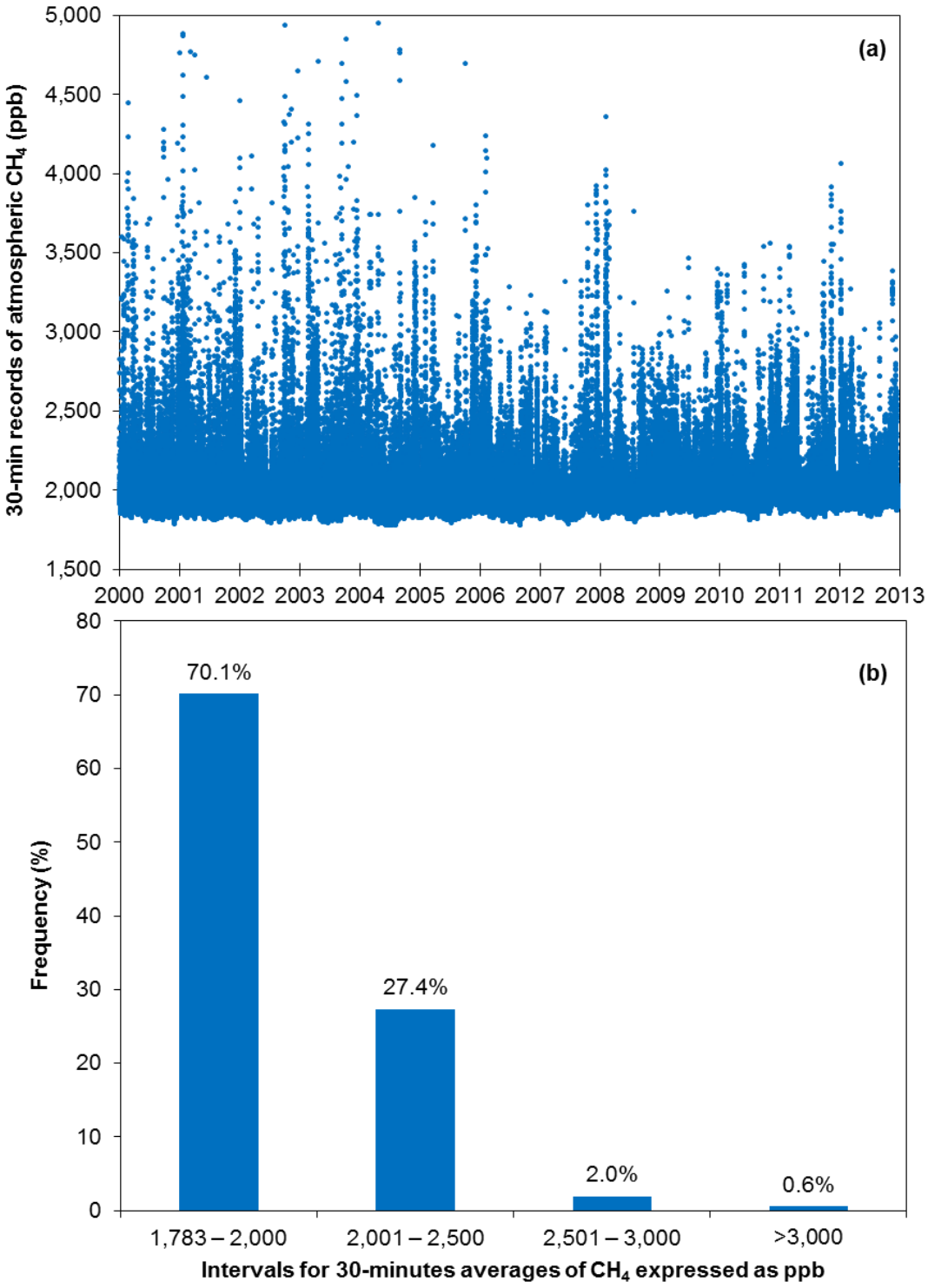

Figure 6.1(a). 30-min CH_4 values (averages since 2010); **(b).** histogram for 30-min values of CH_4 at the EGH site from January 2000 to December 2012.

Figure 6.1(a) shows some typical features of a CH_4 data set. The seasonal cycle with low CH_4 concentrations during summer and high in winter and pollution episodes during winter and summer. The largest CH_4 concentrations were observed mainly in winter, though their frequency decreased as the period progressed.

6.3. Analysis of CH_4 records on daily and weekly time-scales

CH_4 daily averages at the EGH site were calculated from 30-min values during 2000 to 2012. Averages were calculated only if data capture was >75%. Figure 6.2(a) shows CH_4 daily averages at EGH. CH_4 daily averages ranged between 1,813 ppb CH_4 (June 2004) and 3,067 ppb CH_4 (January 2002). The highest concentrations of CH_4 were observed during winter each year, which contrasts with low concentrations of CH_4 recorded during summer. CH_4 concentrations in spring and autumn are observed between the highest and the lowest averages and are considered as transition between the peak and trough of the CH_4 seasonal cycle.

CH_4 daily averages were classified into 5 categories to depict the histogram of daily averages. Figure 6.2(b) shows the histogram for daily averages of CH_4 calculated from 30-min values from 2000 to 2012. Similarly to that observed in the 30-min values plot, large CH_4 concentrations are observed in winter, which decreased as the period progressed. The CH_4 lowest daily-averaged concentrations were recorded in summer. The frequency of lowest CH_4 daily averages increased over the period.

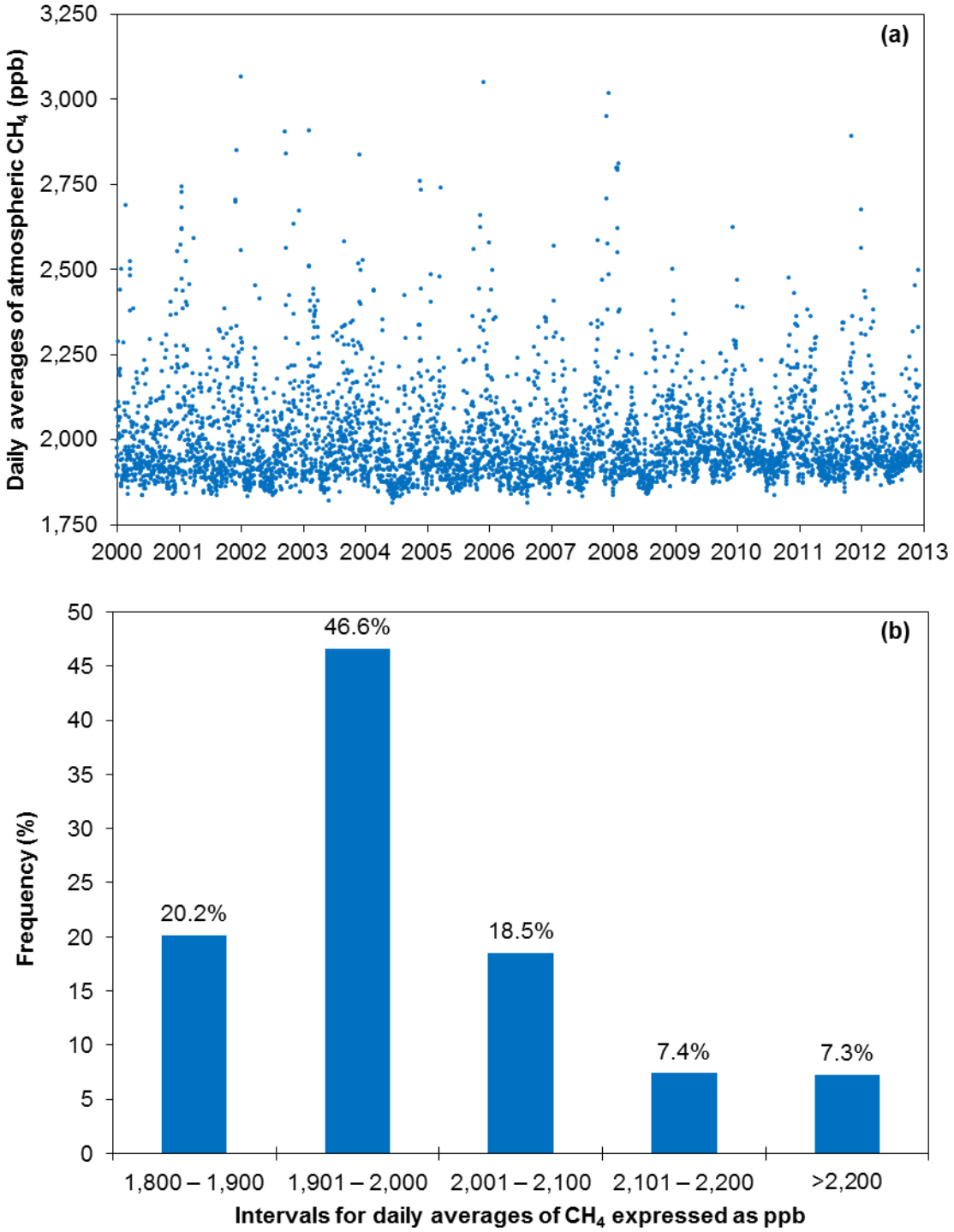

Figure 6.2(a). CH_4 daily averages calculated from 30-min values; **(b).** histogram for daily averages of CH_4 recorded at EGH from 2000 to 2012.

6.3.1. CH_4 diurnal and weekly cycles at the EGH site

Diurnal variations for CH_4 were calculated by averaging values for 30-minute intervals over 13-years of measurements of 24-hour periods in order to remove the impacts of long-term trends (Zhang et al., 2013). Figure 6.3 shows the averaged

CH_4 daily cycle at EGH from 2000 to 2012. No significant differences (p>0.05) were observed between daily averages and median values and therefore averages can be used to analyse daily variations. CH_4 hourly averages ranged from 1,926.1 to 2,071.3 ppb CH_4. The cycle maxima was observed by 05:00, and the minima by 14:00. An average daily amplitude (AV_d) of 145.3 ppb CH_4 was found.

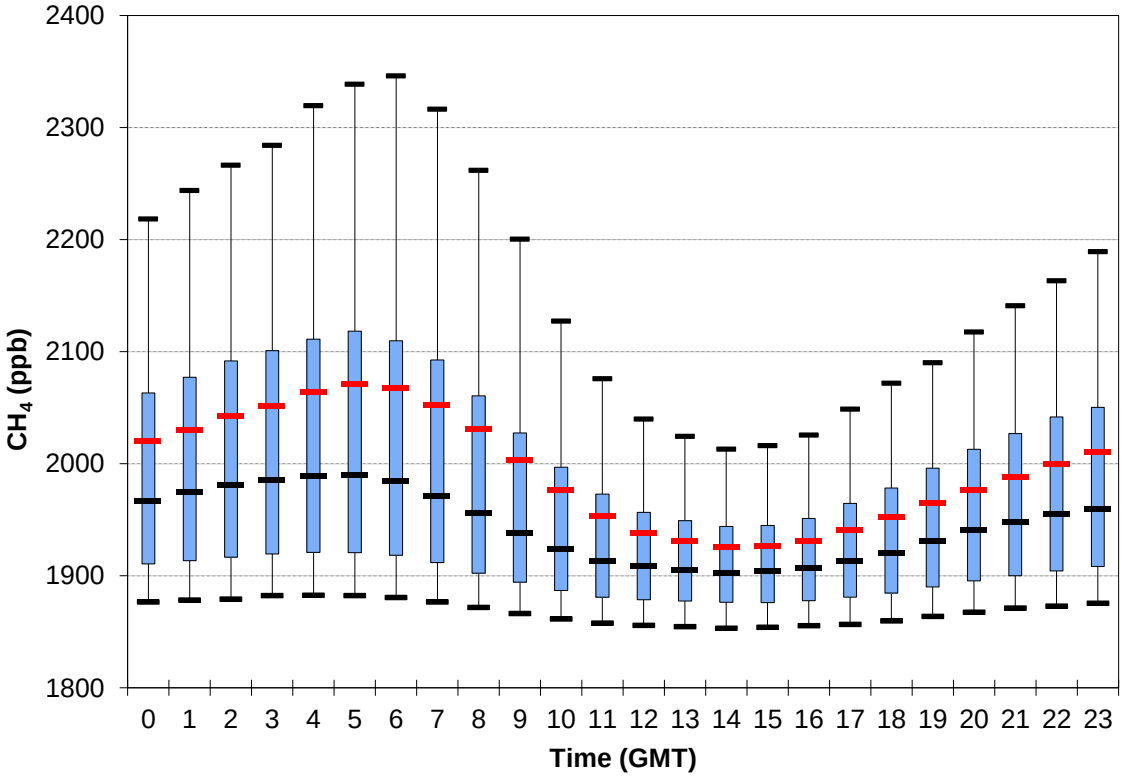

Figure 6.3. Averaged daily cycle for CH_4 records at the EGH site from 2000 to 2012. Black and red lines represent the median and average respectively. Vertical bars (whiskers) correspond to the 10^{th} and 90^{th} percentiles.

The CH_4 averages and medians show an increase from 17:00 to 05:00. Larger differences between the average and median were observed from 03:00 to 08:00, mostly during nighttime, which coincides with the maxima of the cycle. By contrast, differences remained almost constant between 11:00 and 16:00, during cycle's trough.

At EGH, the maximum concentrations of CH_4 are observed during the radiative cooling period, when PBL height is the lowest. Peaks of CH_4 concentrations during nighttime are due to the low PBL. By contrast, minimum CH_4 concentrations were observed when convective processes are enhanced and, to a lesser extent, loss via reaction with OH radicals, whose abundance depends strongly on solar radiation and temperature (Sanchez et al., 2013). Differences in the AV_d can be caused by changes in emissions from sub-urban areas, variation in the dispersion rates

caused and differences in the boundary layer evolution (Haszpra and Barcza , 2010; Zhang et al., 2013).

Studies carried out at Seoul (Korea), Valladolid (Spain) and Hegyhátsál (Hungary) show similar CH_4 daily cycles to those at EGH (Table 6.1). In good agreement with the CH_4 daily cycle reported here, Haszpra et al. (2008), Nguyen et al. (2010) and Sanchez et al. (2013) observed the maximas of the CH_4 diurnal cycle during night-time and the minimas during early afternoon. The AV_d of 145.3 ppb CH_4 calculated at EGH is 4 times larger than the AV_d of 35 ppb reported by Haszpra et al. (2008) for a rural station in Hungary. Differences in AV_d are due to the advection of north easterly, easterly and south easterly air masses passing over the Greater London area that can transport elevated CH_4 in air from the continent and emissions from local sources to the EGH site.

Nguyen et al. (2010) observed AV_d from ~200 to ~250 ppb CH_4 at an urban background site and at an urban road side station, respectively, during 2000-2006. These AV_d are 1.3 to 1.7 times larger than the AV_d calculated at EGH. The largest AV_d observed by Nguyen et al. (2010) are due to larger CH_4 atmospheric concentrations caused by higher emissions nearby the stations, as those are located in an urban environment and surrounded by urban CH_4 sources. Sources within 4km of the EGH site have greatly reduced since the study of Lowry et al. (2001).

Normalised daily cycles for CH_4 data recorded at EGH from 2000 to 2012 were calculated by season (Figure 6.3). These can be further separated by day of week to highlight changes in anthropogenic activities related to the working week (Figure 6.4). CH_4 cycles do not show variation of frequency between seasons. No significant differences were found among AV_d for weekdays and weekends (p>0.05) for all seasons. However, the average AV_d of weekly cycles varied seasonally, thus in winter it was 117.5 ppb CH_4, 169.5 ppb CH_4 in spring, 160.8 ppb CH_4 in summer and 169.2 ppb CH_4 in autumn.

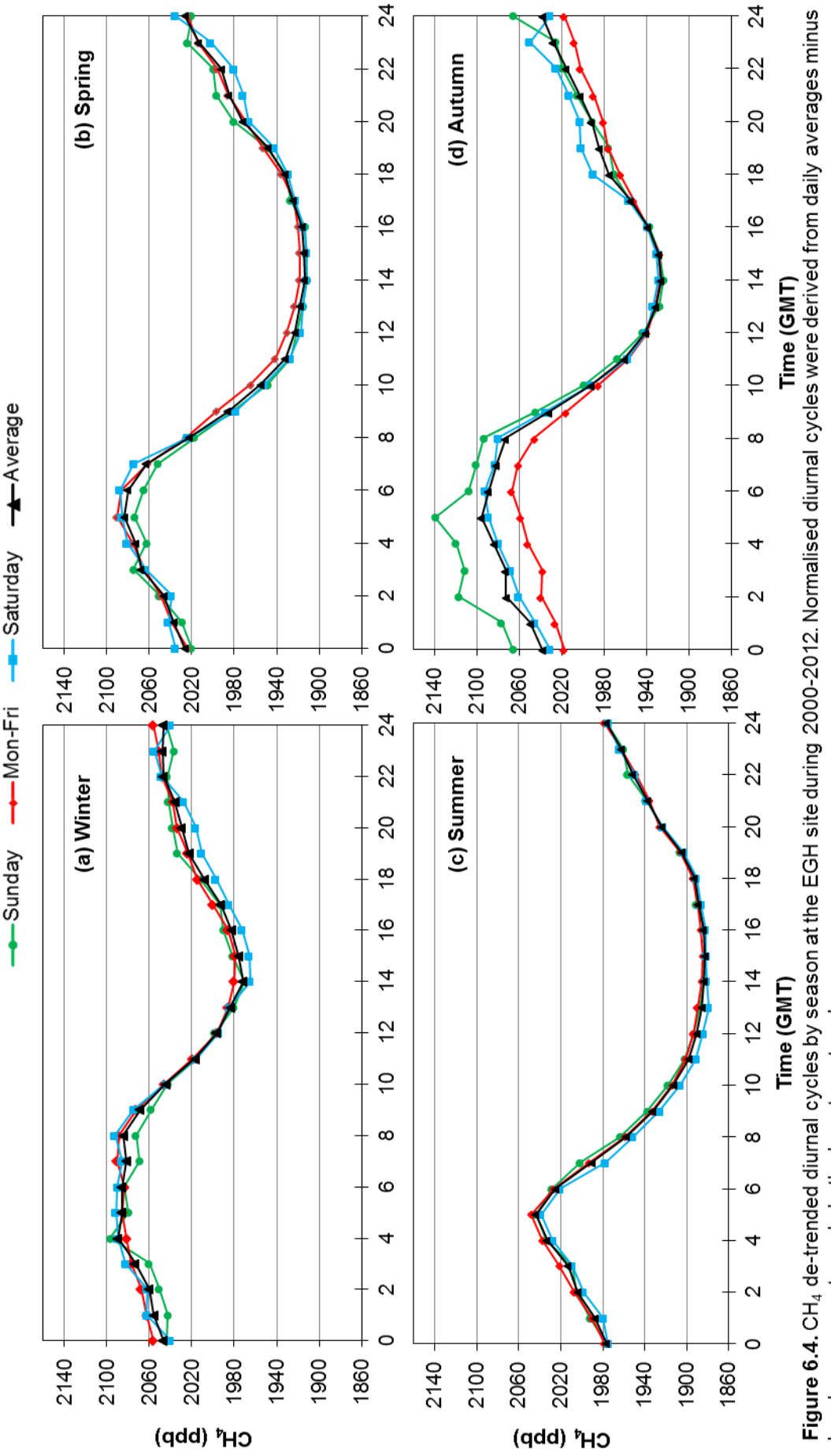

Figure 6.4. CH_4 de-trended diurnal cycles by season at the EGH site during 2000-2012. Normalised diurnal cycles were derived from daily averages minus hourly averages to exclude the long-term trend.

The largest CH_4 concentrations in weekly cycles are observed in autumn and winter (~2,100 ppb CH_4). These concentrations can be ascribed to the low heights of the averaged daily PBL (~300 m; PORG, 1997), and contrasts with the largest heights of PBL during summer when the lowest CH_4 concentrations were observed ~1,880 ppb. The lowest CH_4 concentrations observed in summer coincide with the maximum loss of CH_4 via oxidation with OH radicals (Sanchez et al., 2013). This finding agrees well with previous studies carried out by Fisher (2006), who observed larger CH_4 concentrations and larger AV_d in winter than in summer at EGH. In winter, large AV_d are associated to poor dispersion under low inversion levels and, to a lesser extent, increases in local and global sources, and reduced sink activity.

6.3.2. CH_4 diurnal and weekly cycles at the EGH site on wind direction basis

To separate the effect of season and meteorology on CH_4 diurnal cycles, averaged CH_4 week-long records were calculated as function of wind direction and season. Figure 6.5 shows CH_4 week-long records calculated from 30-min values from 2000 to 2012 by season and wind direction. CH_4 weekly cycles show distinctive features: in winter, large variability is observed for all sectors except S and SW, which are the clean sectors, including the background sector. Variability was larger during Friday night and contrasted with conditions observed from Sunday to Tuesday, which could be due to larger emissions from automobiles. From Figure 6.5, it is apparent that cycles in spring and autumn correspond to transition periods in meteorological conditions to stable PBL during winter to larger convective processes in summer.

CH_4 show less variability and smaller AV_d in spring and autumn than in summer and winter. However, CH_4 cycles vary more in autumn than in spring. In spring for example, E, SE and NE show similar AV_d during weekdays, and decrease at weekends. By contrast, in autumn the same sectors show larger variations during weekdays and weekends, possibly related to increased combustion of fossil fuels (heating). CH_4 summer cycles show larger AV_d for sub-urban sectors (NE, E and SE) and small AV_d for backgrounds sectors (semi-rural). For the NE sector, the peaks on Monday and Tuesday produce AV_ds around ~10% larger than AV_ds during the rest of week.

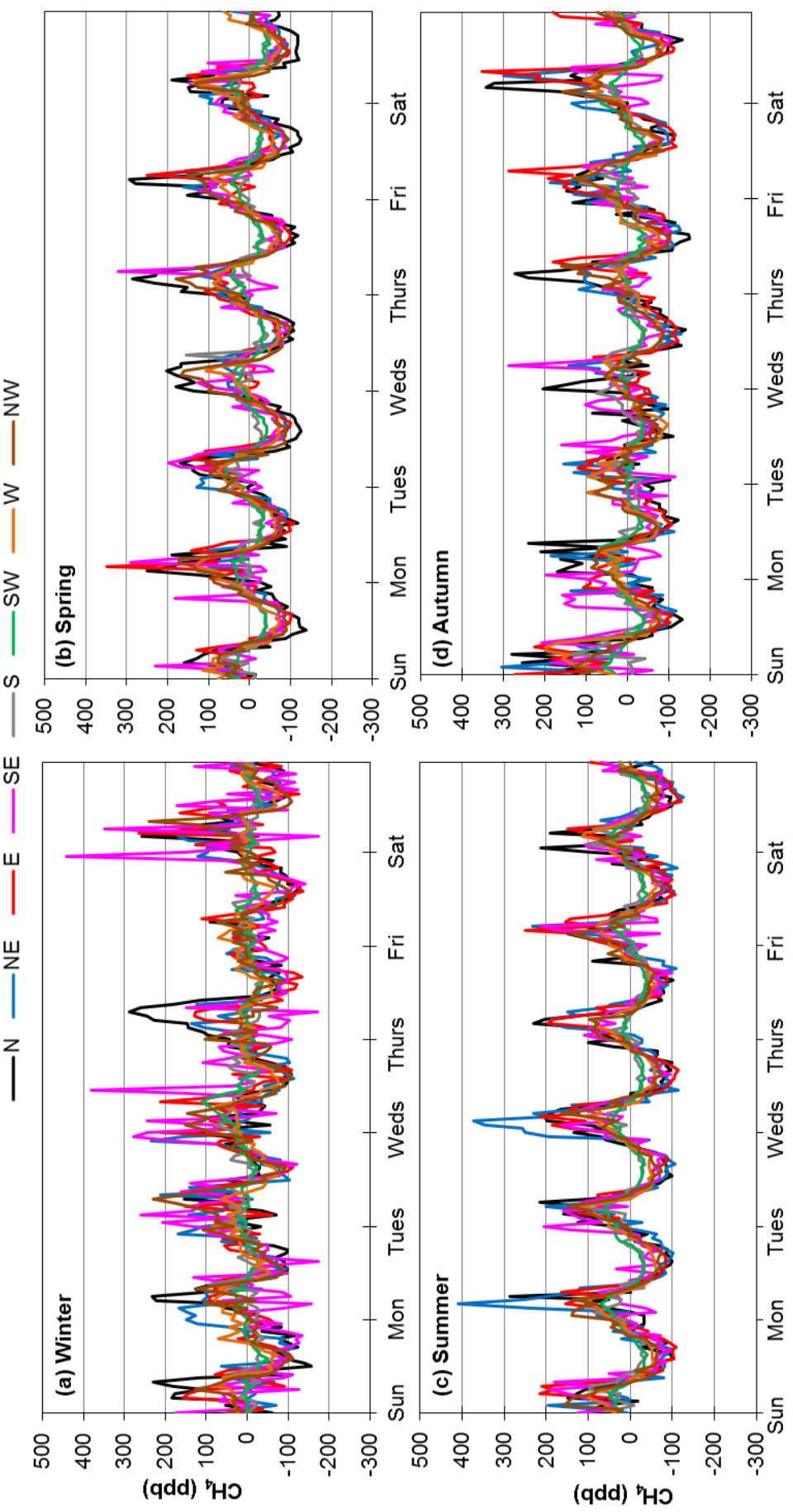

Figure 6.5. CH_4 de-trended week-long cycles by wind sector at the EGH site during 2000-2012. Normalised week-long cycles were derived from hourly averages min weekly averages to exclude the long-term trend.

These peaks are associated with air masses arriving at EGH that passed over important urban areas that can transport CH_4 from local sources and to increased vehicle traffic on M25 motorway and air traffic from Heathrow at the start of the working week. Similar to other seasons, in summer SW and S sectors show low variation in AV_d compared to sub-urban sectors (Staines, Egham). It can be observed that important contributions to the CH_4 daily cycle are due to anthropogenic emissions, mostly combustion processes.

6.4. STL CH_4 seasonal cycles at the EGH site

The seasonal cycle of CH_4 at EGH was computed by filtering monthly averages using the STL technique developed by Cleveland et al. (1990). The averaged yearly cycle of CH_4 was calculated by averaging each month during the 13-year data set. AV_s for CH_4 were calculated as the difference between the peak and trough for a-seasonal cycle, within one-cycle without considering calendar years. Figure 6.6(a) shows CH_4 STL seasonal cycles at EGH from 2000 to 2012.

The seasonal cycle of CH_4 shows the highest concentrations during winter and lowest in summer. Shoulders in the seasonal cycle are observed before and after the winter peak except for 2011. These anomalies were largest in 2003, 2004, and from 2007 to 2009. Interestingly, CH_4 winter values show fewer perturbations during recent years. By contrast, summer values do not show anomalies in any year. Troughs are constant in magnitude, except for 2003 and 2004 when lower summer concentrations were recorded.

Figure 6.6(b) shows the averaged yearly cycle of CH_4 with the largest concentrations in winter, then concentrations decrease gradually during spring to summer. The largest concentration of CH_4 is observed in December, after it decreased in January and increased again, though slightly, in February. The lowest concentrations were observed in summer, June and July, and then a smooth increase is seen during autumn. At EGH, high concentrations of CH_4 during winter are ascribed to the low PBL height which traps CH_4 emissions close to the earth's surface, and increased fossil fuel use for heating.

Large CH_4 winter concentrations are due, mostly, to meteorological conditions which are the main force driving them since biological activity is reduced during winter due to low temperatures. Previous studies have showed that CH_4 build-up in winter is

due to a decrease in the PBL height (PORG, 1997), which is strongly coupled with daytime period and, to a lesser extent, to low UV radiation which reduces OH radical production. By contrast, low summer CH_4 concentrations are due to strong vertical mixing and to high oxidation rates due to higher atmospheric concentrations of OH radicals (Fisher, 2006; Wahlen, 1993).

Figure 6.6(c) shows AV_s of seasonal cycles of CH_4 at EGH during 2000-2012. AV_s ranged from 169.1 ppb CH_4 to 90.9 ppb CH_4 in 2003 and 2012, respectively. The higher AV_s from 2002 to 2004 seem to be related to the intense heat wave experienced in 2003, which could have led to low microbial activity due to dry conditions, and higher rates of production of OH due to the intense sunlight (Piao et al., 2008; Haszpra et al., 2008). AV_s decreased from 2007 to 2012. Despite the variations observed, no trend was detected in AV_s (p>0.05) at EGH.

Manning et al. (2011) modelled the seasonal cycles for atmospheric CH_4 at different latitudes using data from the NOAA/ESRL/GMD programme. They observed seasonal cycles with higher concentrations in winter, whilst lower concentrations were seen in early autumn at northern latitudes. Features such as shoulders during winter, transition phases in spring and autumn and lowest values in summer were also observed at north latitudes. The seasonal cycles of CH_4 at EGH are in good agreement with those observed at other monitoring stations in the northern hemisphere. Pedersen et al. (2005) observed larger amplitudes in CH_4 seasonal cycles at the Ny-Alesund research station than those seen at EGH. At Ny-Ålesund, CH_4 winter peaks were ascribed to cyclonic activity and strong winds in the Arctic region. Air mass transport to Ny-Ålesund carries important CH_4 contributions from regions as far as western Russia and Siberia, where important sources of CH_4 such as gas-fields and natural wetlands are located.

The seasonal cycle of CH_4 at EGH contrasts with that observed from continuous measurements made at 163 m above ground level at Ochsenkopf, Germany durin 200-2008, where double maximum in April and November have been reported and the minimum in August (Thomson et al., 2009). Thomson et al. (2009) ascribed that variation to combined influences of the variability of the main sink in the troposphere (oxidation via OH) and natural emissions, i.e. wetlands. The averaged seasonal cycle at EGH is 3.8 times larger than that observed at Ochsenkopf (34.2 ppb CH_4).

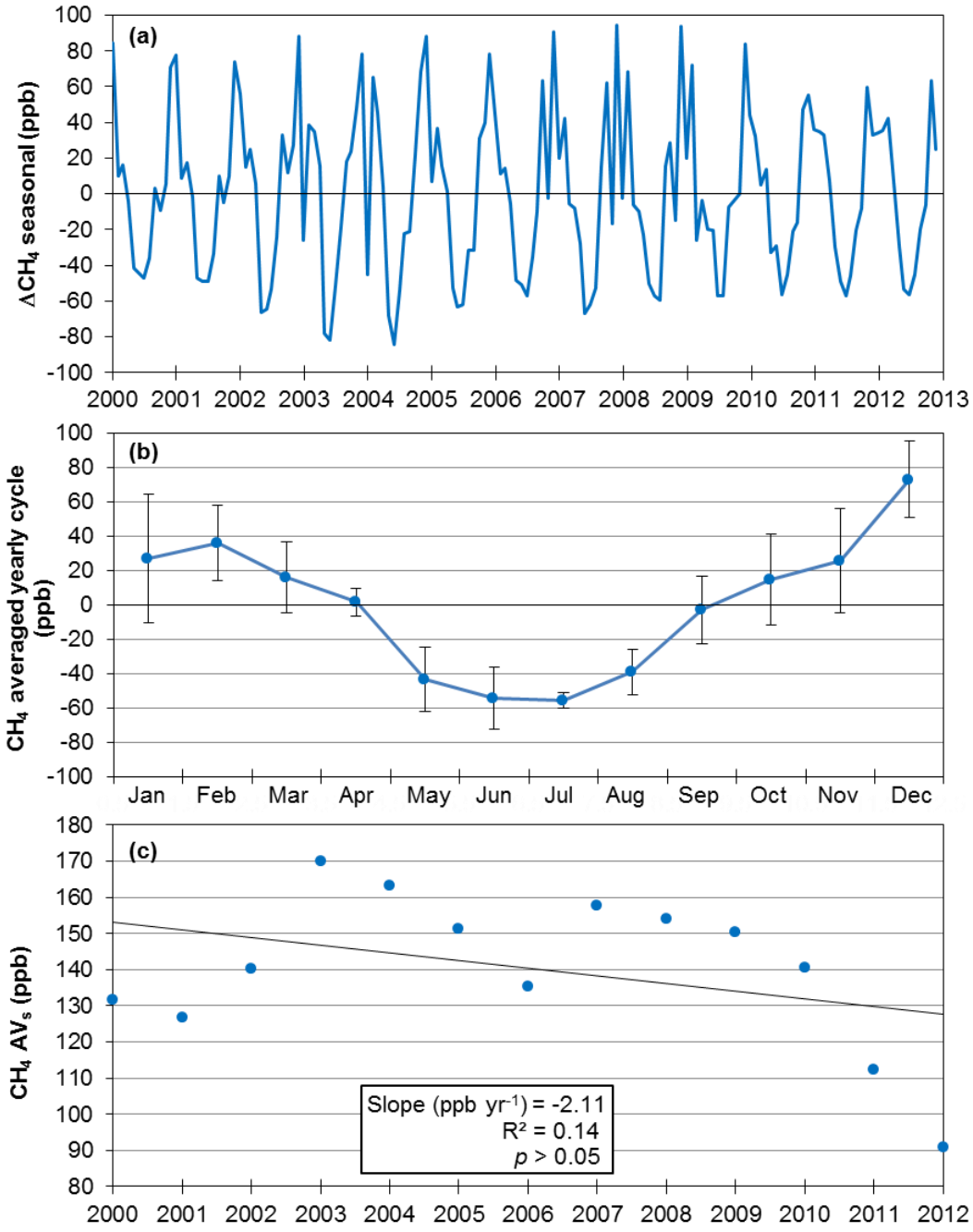

Figure 6.6(a). De-trended seasonal cycles of CH_4 at EGH during 2000-2012 calculated using the STL technique; **(b).** yearly averaged cycle of atmospheric CH_4 calculated from filtered values with STL, error bars represent 1SD; **(c).** long-term trend in seasonal amplitudes of CH_4 (AV_s). AV_s is defined as the difference in ppb CH_4 from peak-to-trough within one seasonal cycle.

6.4.1. Influence of the PBL height on CH_4 yearly cycle

The averaged yearly cycle of CH_4 from 13-years of measurements was used to investigate the relationship with the PBL depth at EGH. Figure 6.7 shows the linear regression between PBL depth and CH_4 at EGH. Averaged heights of the PBL for the UK were obtained from PORG (1997). A strong anti-correlation (R^2=0.90) was

found between PBL and CH_4 concentrations, with a slope of -0.13 significant at $p<0.01$.

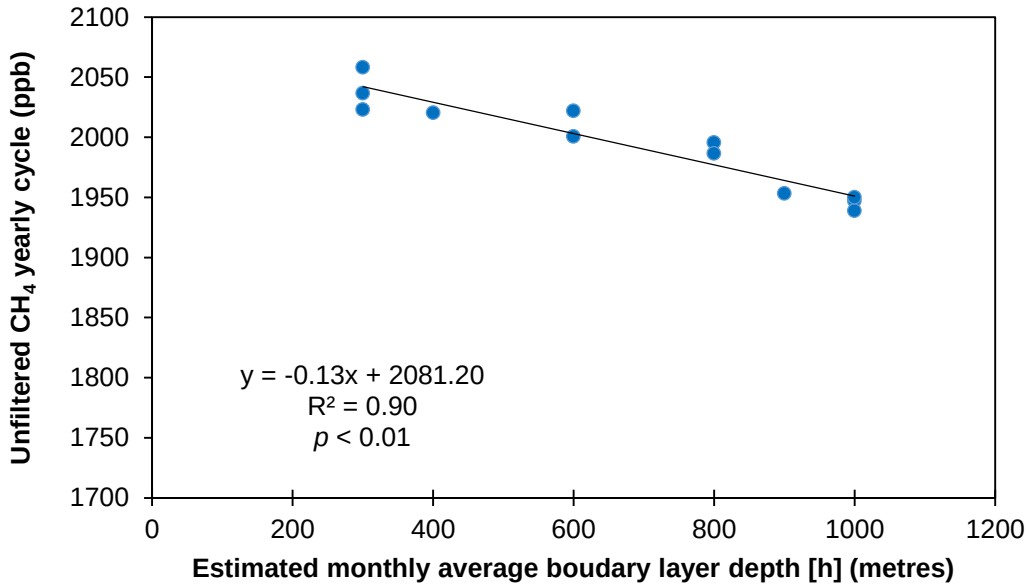

Figure 6.7. Relationship between PBL depth and CH_4 at EGH averaged by month of year from 2000 to 2012.

Concentrations of CH_4 were higher in winter, from December to February when the PBL is the lowest. High winter averages of CH_4 are caused by poor dispersion due to the shallow PBL. Such conditions are promoted by the Earth cooling during winter (negative surface flux), which leads to air surface layer stratification and inhibits turbulent conditions that could disperse CH_4 emissions. By contrast, during summer when mixing is strong CH_4 concentrations were the lowest.

6.5. Long-term trends of CH_4 at the EGH site during 2000-2012

6.5.1. CH_4 monthly averages and filtered trend computed with STL

CH_4 long-term trends at EGH were computed using monthly averages of both unfiltered and STL filtered data. Monthly averages were calculated from daily averages and required a minimum of 75% data capture to be considered valid. During 13-years of measurements, 156 monthly averages were calculated from daily averages, which represent 100% coverage. Monthly standard deviations were calculated from daily averages. Figure 6.8(a) shows unfiltered monthly averages and 1SD from 2000 to 2012. CH_4 monthly averages ranged from 1,868.4 to 2,164.6 ppb CH_4 in June 2004 and January 2001, respectively, whilst standard deviations

ranged from 28.8 ppb CH_4 in December 2011 to 331.6 ppb CH_4 in February 2008. As shown in Figure 6.8(a) CH_4 remained almost steady at EGH within the recorded period. Variations observed correspond to annual cycles of CH_4. Concentrations of CH_4 decrease in summer and increase in winter, and likewise smallest SDs were observed in summer and the largest in winter.

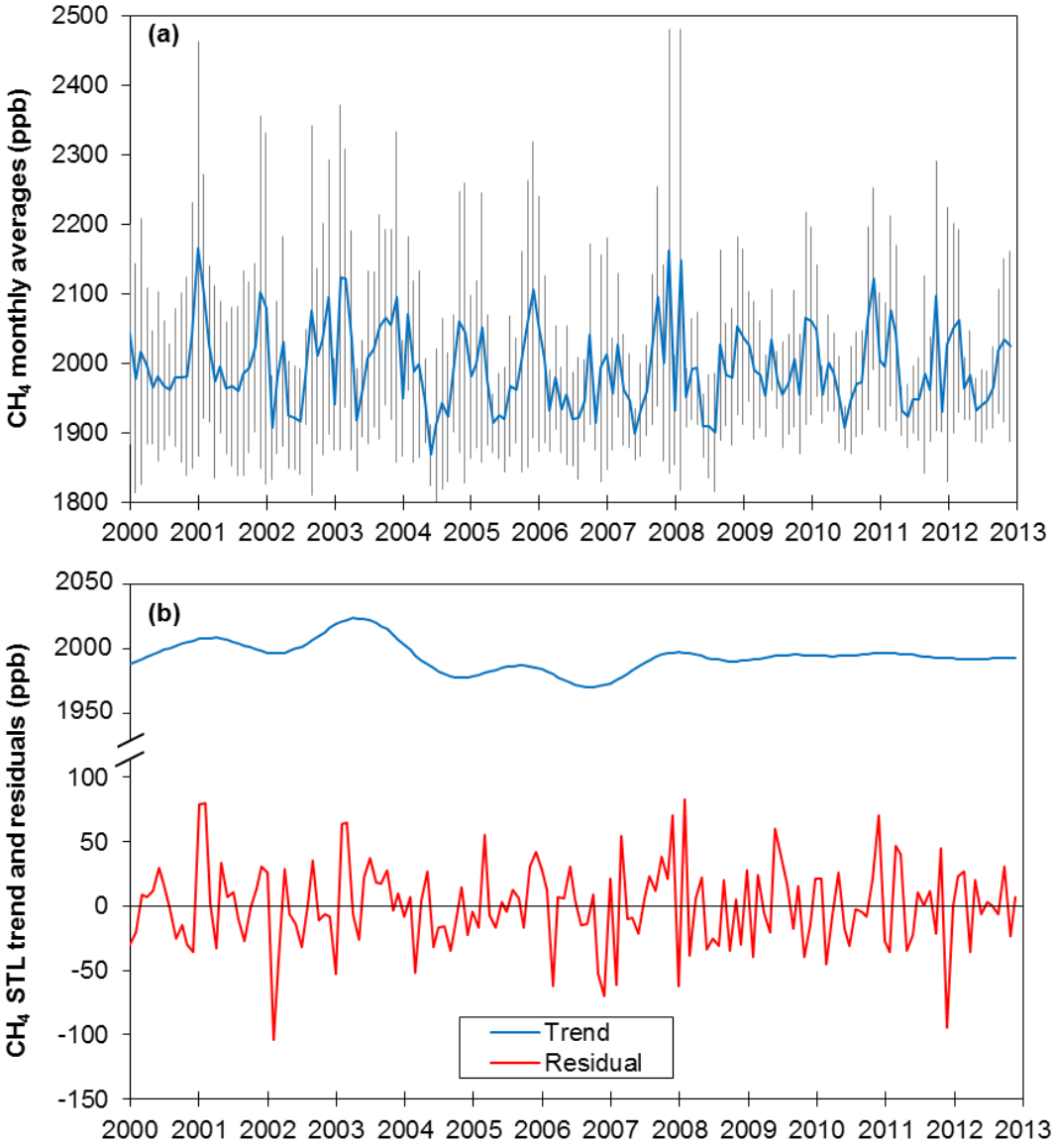

Figure 6.8(a). Unfiltered monthly averages of CH_4 ± 1SD calculated from daily averages; **(b).** STL filtered CH_4 long-term trend and residuals observed at EGH during 2000-2012. The residuals represent the remaining CH_4 beyond the trend and seasonal components as defined by Cleveland et al. (1990).

The secular trend and residuals of CH_4 at EGH were computed by filtering monthly averages with the STL technique, and are shown in Figure 6.8(b). The CH_4 secular trend has remained almost steady at EGH during the period. Interestingly, more variability in CH_4 concentrations were observed in the first half of the studied period,

from 2000 to 2007. The highest concentrations of CH_4 were recorded in winter 2004 and then, decreased through annual cycles up to summer 2006, when the lowest concentrations was recorded. Since this time there have been no large variations in the secular trend. Residuals showed large variability during the studied period. They did not follow a defined pattern, although were larger in winter than in other other seasons. Large negative residuals were observed mostly in winter each year and then, positive residuals from spring onwards. By contrast, positive residuals were smaller and frequently observed during summer.

The CH_4 steady state observed at EGH, seems to follow the Khalil et al.'s (2007) interpretation of constant emissions, and is in good agreement also with findings of constant averaged atmospheric CH_4 concentrations until 2007, based on data from the NOAA global cooperative air sampling network (Duglokencky et al., 2011). Spahni et al. (2011) reported that atmospheric CH_4 concentrations remained roughly stable during the late 1990s to 2006, which agrees well with results found in this work. Rigby et al. (2008a) and Dlugokencky et al. (2009) reported that CH_4 concentrations started to rise from 2007 onwards. This rise was also observed at EGH but only for 2007. The trend observed here is opposite to that reported by the IPCC of 0.5 to 6 ppb yr^{-1} from 1999 to 2006 (IPCC, 2013). This might be due to decreases in local emissions as reported in the NAEI (2013), which could have compensated for the increase observed worldwide.

6.5.2. Long-term trends in CH_4 observed at EGH during 2000-2012

During the 19th century, atmospheric CH_4 increased dramatically until late 1990s when the growth rate decreased (Fiore et al., 2006), which Dlugokencky et al. (2003) interpreted as an approach to a steady state due to constant CH_4 emissions. Based on data from the NOAA global cooperative air sampling network, globally averaged CH_4 concentrations were relatively constant from 1999 to 2006 (Duglokencky et al., 2011). To test whether records of atmospheric CH_4 at EGH fit the global observed trend, CH_4 annual averages were calculated from monthly averages. The Mann-Kendall test and Sen's estimate were used to calculate CH_4 trends and magnitudes from unfiltered and STL filtered data (Table 6.2).

No minimum significant differences (p>0.05) were observed between unfiltered and filtered STL data. Figure 6.9 shows the Mann-Kendall test and Sen's estimate for unfiltered annual averages of CH_4 at EGH from 2000 to 2012. Although an overall

declining trend of 0.27 ppb CH_4 yr^{-1} is apparent is not significant at a level of p=0.05. When data are split, different trends are observed during the studied period: an increasing trend from 2000 to 2003 of 6.2 ppb CH_4 yr^{-1} (p=0.11), a declining trend from 2003 to 2006 at a decline rate of 13.4 ppb CH_4 yr^{-1} (p=0.94) and a steady state from 2006 to 2012, slope = 2.5 ppb CH_4 yr^{-1} (p=0.06). None of these trend were significant at a level of p=0.05.

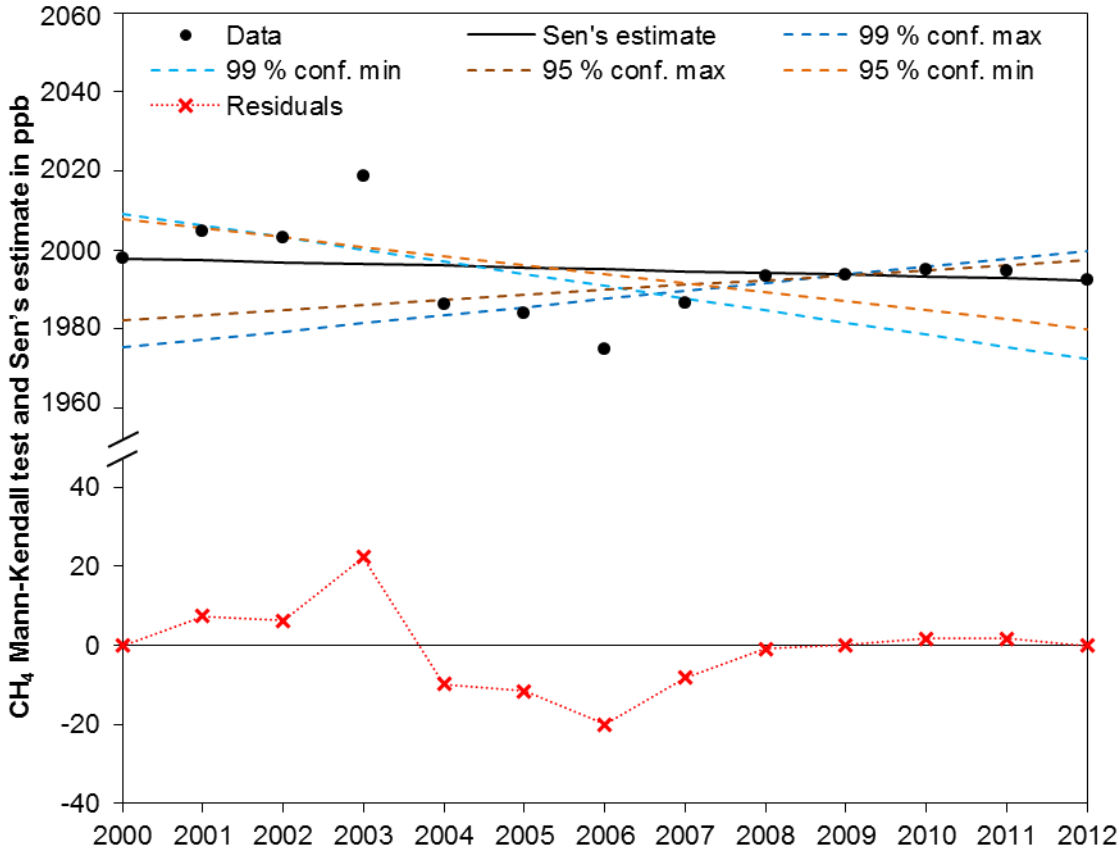

Figure 6.9. CH_4 annual averages and long-term trend at EGH during 2000-2012 calculated with the Mann-Kendall test and Sen's estimate.

Table 6.3 shows a comparison of trends calculated with the Mann-Kendall test and Sen's estimate and least squares linear regressions using Excel and SigmaPlot software. For unfiltered CH_4 annual averages, least squares methods coincided, calculating a slope of -1.22 ppb CH_4 yr^{-1} whereas Sen's estimate calculated -0.27 ppb CH_4 yr^{-1}. Similarly, the first data of the series was roughly the same in the least squares at 2001.8 ppb CH_4 and 2001.2 ppb CH_4, respectively, whilst the Sen's estimate showed a difference of ~3.4 ppb with the other tests.

Table 6.2. Comparison between Mann-Kendall and Sen's estimate tests for unfiltered and STL filtered data of CH_4 at EGH during 2000-2012.

CH_4 data	Test Z	Significance	Q[a]	Qmin99	Qmax99	Qmin95	Qmax95	B[b]	Bmin99	Bmax99	Bmin95	Bmax95
Unfiltered	-0.43		-0.3	-5.0	4.1	-3.9	2.1	1997.1	2026.2	1959.3	2025.1	1977.9
STL filtered	-0.67		-0.5	-3.1	2.0	-2.3	1.3	1997.9	2009.3	1975.4	2007.8	1982.4

Slopes and series data are expressed in ppb CH_4

°Test Z is performed when n≥10. The absolute value of Z is compared to the standard normal cumulative distribution to define if there is a trend or not at the selected level α of significance. A positive (negative) value of Z indicates an upward (downward) trend.

[a]True slope of linear trend

[b]First data of the series

The following symbols are used for the four tested significance levels α with which the Mann-Kendall trend shows that the null hypothesis of no trend should be rejected:

*** if trend at a = 0.001 level of significance

** if trend at a = 0.01 level of significance

* if trend at a = 0.05 level of significance

+ if trend at a = 0.1 level of significance (no symbol if a is greater than 0.1).

Qmin99: the lower limit of the 99 % confidence interval of Q (α= 0.1)

Qmax99 the upper limit of the 99 % confidence interval of Q (α= 0.1)

Qmin95: the lower limit of the 95 % confidence interval of Q (α= 0.05)

Qmax95: the upper limit of the 95 % confidence interval of Q (α= 0.05)

Bmin99: estimate of the constant Bmin99 for 99% confidence level of linear trend

Bmax99: estimate of the constant Bmax99 for 99% confidence level of linear trend

Bmin95: estimate of the constant Bmin95 for 95% confidence level of linear trend

Bmax95: estimate of the constant Bmax95 for 95% confidence level of linear trend

Table 6.3. Comparison between trends of CH_4 calculated at EGH from 2000 to 2012 using Mann-Kendall and Sen's tests and Excel and SigmaPlot least squares linear regression.

Year	Unfiltered annual averages	STL annual averages	Unfiltered Sen's estimate	STL Sen's estimate	Unfiltered least squares Excel	STL least squares Excel	Unfiltered least squares SigmaPlot	STL least squares SigmaPlot
2000	1991.1	1997.8	1997.1	1997.9	2001.8	2000.0	2001.2	2004.4
2001	2021.2	2004.8	1996.8	1997.4	2000.6	1999.1	2000.0	2003.4
2002	1996.5	2003.2	1996.5	1997.0	1999.3	1998.1	1998.8	2002.4
2003	2033.3	2018.9	1996.3	1996.5	1998.1	1997.2	1997.6	2001.5
2004	1974.0	1986.3	1996.0	1996.1	1996.9	1996.2	1996.3	2000.5
2005	1988.3	1984.0	1995.7	1995.6	1995.7	1995.2	1995.1	1999.6
2006	1966.5	1975.1	1995.5	1995.1	1994.5	1994.3	1993.9	1998.6
2007	1997.9	1986.5	1995.2	1994.7	1993.2	1993.3	1992.7	1997.6
2008	1981.8	1993.3	1994.9	1994.2	1992.0	1992.4	1991.5	1996.7
2009	1996.1	1993.8	1994.7	1993.8	1990.8	1991.4	1990.2	1995.7
2010	1998.5	1994.9	1994.4	1993.3	1989.6	1990.4	1989.0	1994.8
2011	1987.2	1994.6	1994.1	1992.8	1988.4	1989.5	1987.8	1993.8
2012	1995.5	1992.4	1993.9	1992.4	1987.1	1988.5	1986.6	1992.8
Slope (ppb CH_4 yr^{-1})	N.A.	N.A.	-0.27	-0.45	-1.22	-0.96	-1.22	-0.96
Change in CH_4 ppb	4.4	-5.4	-3.2	-5.5	-14.6	-11.5	-14.6	-11.5
% change (13-years)	0.2	-0.3	-0.2	-0.3	-0.7	-0.6	-0.7	-0.6
Significance (*p*)	N.A.	N.A.	>0.05	>0.05	>0.05	>0.05	>0.05	>0.05

Annual averages and data series expressed in ppb CH4.
N.A.: *Not applicable.*

Trends of STL filtered data show smaller differences among the three tests than for unfiltered data. Sen's estimate calculated a slope of -0.45 ppb yr^{-1} from STL data, which is ~51% of the slope calculated by least squares methods -0.96 ppb yr^{-1}. First values of the series were also different, but differences were larger. They were 2.1 and 4.5 ppb CH_4 between Sen's estimate and least squares method of Excel and SigmaPlot, respectively. Differences in magnitude of trends are explained as the least squares linear regression models how the average concentration changes linearly with time; whereas Sen's estimate models how the median (50th percentile) concentration changes linearly with time (Salmi et al., 2002). The slope of the Sen's estimate is significantly different from zero when Mann-Kendall is significantly different from zero (and vice versa). The *p* values found are not significant ($p>0.05$), which agrees with the variations in the trend observed graphically.

Results obtained in the present study are in good agreement with CH_4 trends observed during the last decades. Khalil et al. (2007) studied CH_4 atmospheric trends during 1980 to 2004 at six monitoring stations of the NOAA global monitoring network. They observed annual variations in global atmospheric CH_4 concentrations between -3 to 5 ppb CH_4 yr^{-1}. Spahni et al. (2011) observed steady atmospheric CH_4 concentrations from 1990s to 2006. The changes observed at EGH were also observed in other monitoring stations across the globe. Kai et al. (2011) reported an increase of atmospheric CH_4 from 2002 to 2003 of 12 ppb CH_4, declines in atmospheric CH_4 were observed during 2004 (11 ppb CH_4) and 2005 (6 ppb CH_4) in the Northern Hemisphere.

On the other hand, Rigby et al. (2008a) and Dlugokencky et al. (2009) measured near-constant CH_4 concentrations during 2000s until 2006, and in 2007 detected an increment. Such an increase was also recorded at EGH between 2006-2007 followed by a steady state, as shown in Figure 6.9. The decline observed, relative to past decades and steady state during recent years has been ascribed, mostly, to reduction in the microbial sources at the Northern hemisphere and decline in emissions of CH_4 from industrial processes (NAEI, 2013). Microbial sources are important in terms of CH_4 emissions, as the agricultural sector contributes the largest emissions in the northern hemisphere (Garg et al., 2006). Methane emissions from waste disposal are also important contributors as fugitive emissions from landfills coupled with leakages from the urban gas distribution network can produce peaks of concentrations during short-time scales. Thus, at a suburban monitoring station such as EGH where concentrations are usually well above those

at background stations at the same latitude, trends are mostly driven by changes in local source emissions and, to a lesser extent, by the growth rate in the northern hemisphere (Lowry et al., 2001).

6.5.3. Wind sector analysis of long-term trends of CH_4 at EGH during 2000-2012

Annual averages of CH_4 by wind sector at EGH were calculated from unfiltered monthly averages in order to assess the variability recorded. Figure 6.10 shows annual averages for the 8 wind sectors and calm (<0.1 m/s). Trends calculated ranged from -2.9 ppb CH_4 yr^{-1} for E sector to 6.2 ppb CH_4 yr^{-1} for N sector, whilst significances (*p*) ranged from 0.01 to >0.1 (Table 6.4). Data show that significant trends with confidence $p<0.1$ existed for four wind sectors: N, S, SW and W. All the significant trends were positive, with slopes from 3.3 to 6.2 ppb CH_4 yr^{-1}. Interestingly, SW and W show the same increase of 4.3 ppb CH_4 yr^{-1} but at different level of confidence, 0.05 and 0.01, respectively.

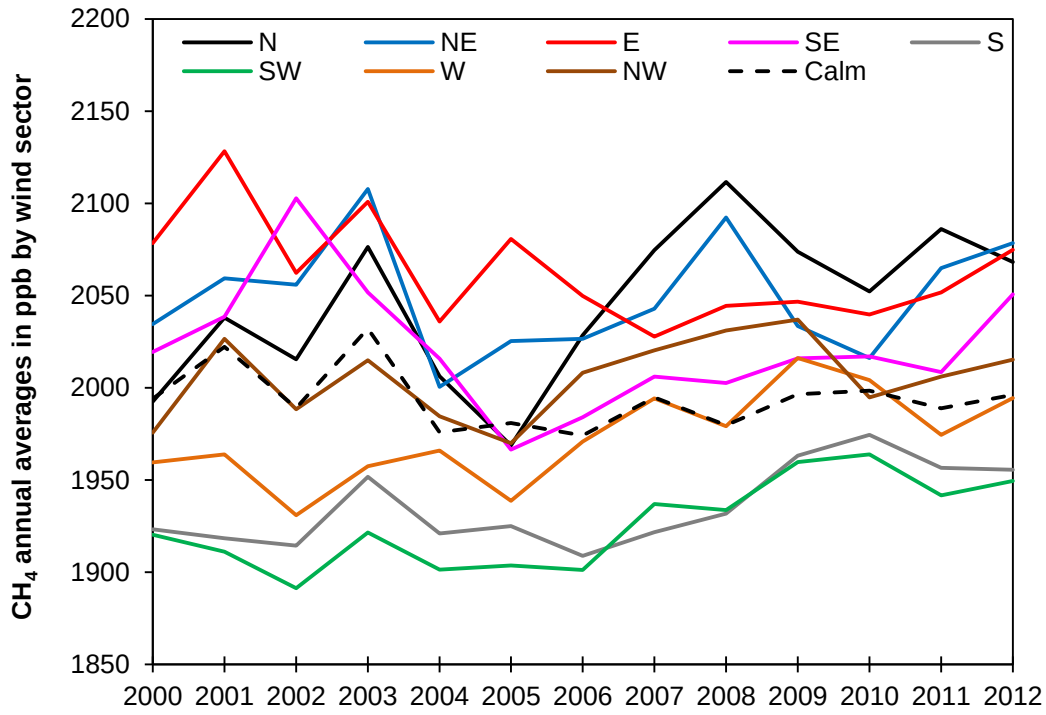

Figure 6.10. CH_4 trends observed by wind sector at EGH during 2000-2012. Long-term trends were calculated using the Mann-Kendall and Sen's tests from unfiltered annual averages.

Table 6.4. CH_4 Mann-Kendall test and Sen's estimates for wind sectors at EGH during 2000-2012.

Wind sector	Test Z	Significance	Q[a]	Qmin99	Qmax99	Qmin95	Qmax95	B[b]	Bmin99	Bmax99	Bmin95	Bmax95
N	1.65	+	6.2	-3.6	15.2	-0.5	11.7	2003.1	2087.2	1945.4	2057.0	1968.1
NE	0.31		1.3	-6.6	10.9	-3.6	7.7	2034.5	2082.6	1966.4	2063.1	1986.7
E	-1.28		-2.9	-10.2	4.0	-8.5	2.1	2072.5	2131.5	2025.8	2123.2	2036.9
SE	-0.43		-1.0	-10.5	10.2	-5.9	7.0	2019.6	2083.2	1928.8	2049.9	1957.0
S	2.14	*	3.3	-1.4	8.8	0.3	7.0	1915.0	1932.1	1884.2	1923.3	1893.1
SW	2.38	*	4.3	-1.9	9.1	1.9	7.8	1899.5	1927.2	1873.0	1918.3	1875.7
W	2.75	**	4.3	0.6	9.8	1.4	8.4	1945.3	1967.1	1912.0	1962.5	1920.6
NW	1.16		2.4	-3.5	9.3	-2.0	6.8	1985.9	2030.1	1953.5	2020.8	1972.5
Calm	0		0.0	-4.6	3.7	-3.4	2.6	1994.1	2026.8	1962.5	2018.4	1972.8

Slopes and series data are expressed in ppb CH_4

°Test Z is performed when n≥10. The absolute value of Z is compared to the standard normal cumulative distribution to define if there is a trend or not at the selected level α of significance. A positive (negative) value of Z indicates an upward (downward) trend.

[a]Slope calculated by the Sen's estimate

[b]First data of the series

The following symbols are used for the four tested significance levels α with which the Mann-Kendall trend shows that the null hypothesis of no trend should be rejected:

*** if trend at α = 0.001 level of significance

** if trend at α = 0.01 level of significance

* if trend at α = 0.05 level of significance

+ if trend at α = 0.1 level of significance (no symbol if α is greater than 0.1).

Qmin99: the lower limit of the 99 % confidence interval of Q (α= 0.1)

Qmax99 the upper limit of the 99 % confidence interval of Q (α= 0.1)

Qmin95: the lower limit of the 95 % confidence interval of Q (α= 0.05)

Qmax95: the upper limit of the 95 % confidence interval of Q (α= 0.05)

Bmin99: estimate of the constant Bmin99 for 99% confidence level of linear trend

Bmax99: estimate of the constant Bmax99 for 99% confidence level of linear trend

Bmin95: estimate of the constant Bmin95 for 95% confidence level of linear trend

Bmax95: estimate of the constant Bmax95 for 95% confidence level of linear trend

By contrast, trends with significance at p>0.1 were observed for NE, E, SE, NW and Calm. Among them, positive and negative slopes were seen from -2.9 to 2.4 ppb CH_4 yr^{-1}. The calm sector did not show increase or decrease since a slope of 0.0 ppb CH_4 yr^{-1} was observed, it was the only sector that showed this behaviour. Notably, decreases were observed for sectors that comprise Greater London except for NE, where an increase was observed. By contrast, for background and clean sectors increases were detected.

6.6. Comparison of CH_4 recorded at EGH and MHD

6.6.1. CH_4 monthly averages comparison

Comparison of CH_4 records at EGH with those at MHD can provide new insights into the main factors driving concentration changes at the EGH site and, at certain level, some ideas of possible local sources. Figure 6.11 compares CH_4 monthly averages with averages calculated from flask measurements at MHD during 2000-2012. Data show consistently higher overall and background CH_4 concentrations at EGH than at MHD during the period. Overall, similar patterns were observed: high concentrations in winter, low concentrations in summer and variability.

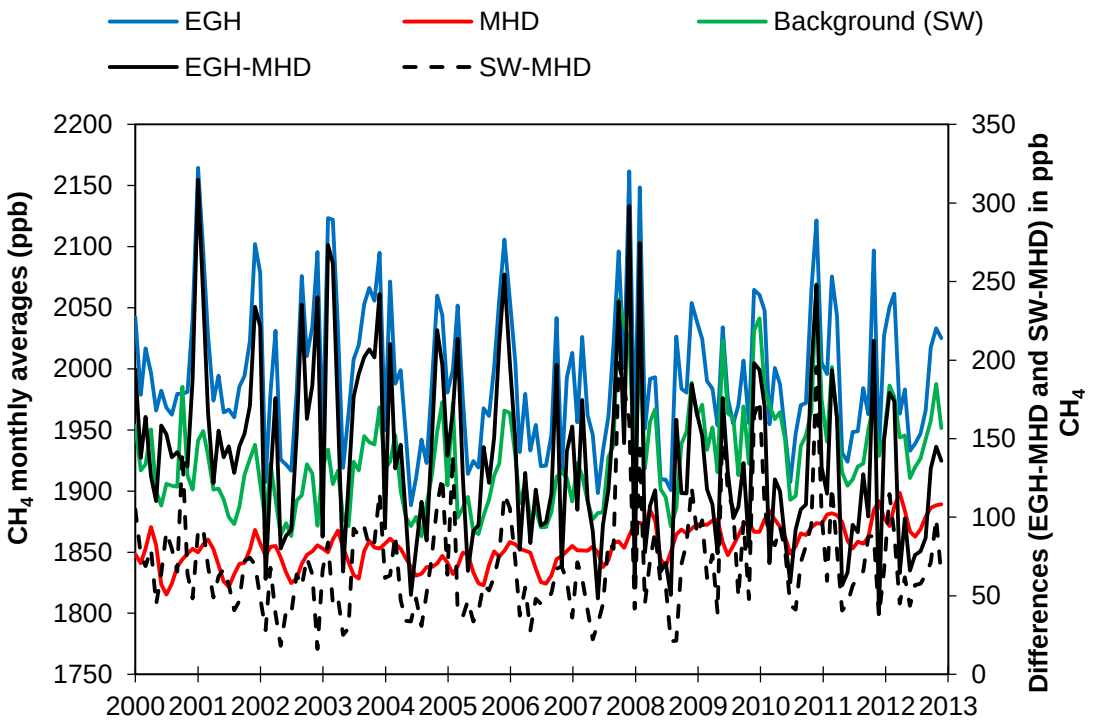

Figure 6.11. Comparison of CH_4 overall monthly averages at EGH and monthly averages for flasks measurements at MHD and differences between averages during 2000-2012.

Differences in concentrations were calculated by subtracting flask averages from MHD to overall averages from EGH. The differences between overall and flasks averages show a sharp decline along the period (slope = -0.01, p>0.05), however no significant difference (95% of confidence) was observed to be considered as a trend. Linear correlation was observed for SW and flask measurements at a level of confidence of 99% (Figure 6.12) whereas it was poor (<95%) for overall and flask averages. It demonstrates effectively that SW air flow to EGH closely represent Atlantic background levels of CH_4.

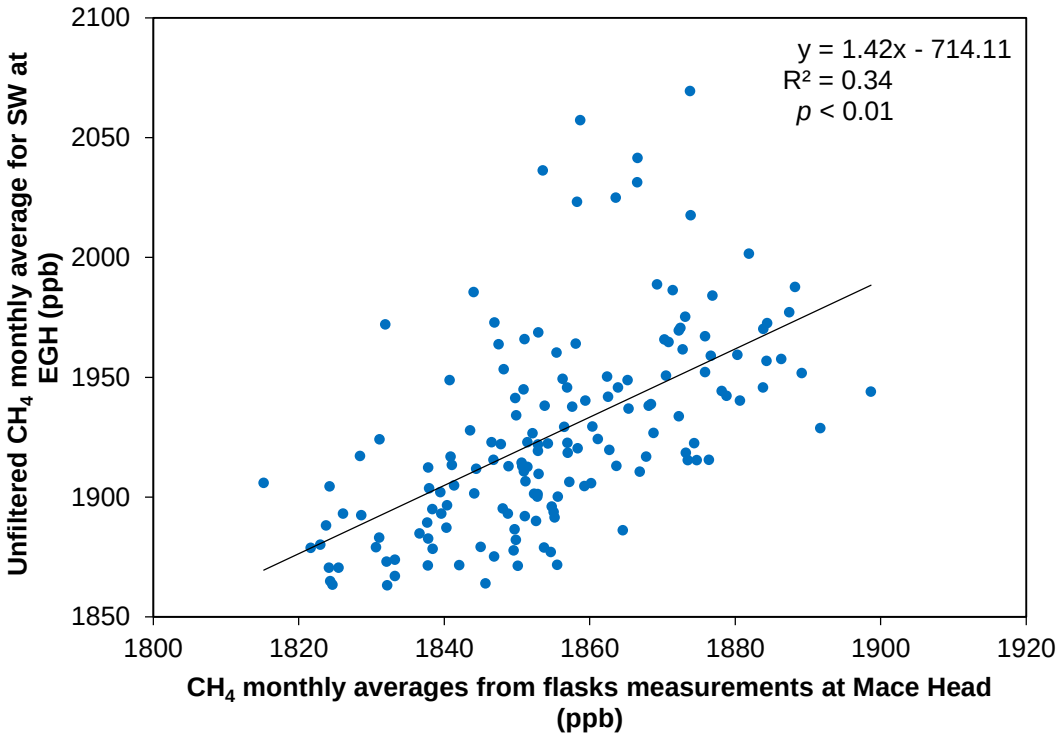

Figure 6.12. Linear correlation observed between unfiltered monthly averages of CH_4 for SW sector at EGH and flask monthly averages at MHD during 2000-2012. The correlation is significant for n=156 at level of 99% of confidence.

Notably, the differences were larger in winter and decreased during summer for both analyses. Larger differences in winter are possibly due to meteorological conditions which can keep close to the ground CH_4 emissions from local sources, which are stronger at EGH than at MHD. The PBL which shows the lowest height in winter coupled with poor dispersion may explain these differences with a much windier MHD site (PORG, 1997). It can be clearly appreciated by comparing both differences, which show minor variations contributions in the SW sector that at the overall data.

Larger differences during summer were observed from overall and flasks measurements. At EGH, the better mixing during summer can promote dispersion together with the maximum height of the PBL can lead to the observed concentrations. Surprisingly, the smallest difference was not observed in summer but in autumn 2002. It was caused by a high prevalence of SW air masses which led to similar concentrations being recorded both at MHD and EGH.

6.6.2. CH_4 seasonal cycles comparison

The CH_4 MHD flask time-series for 2000-2012 was decomposed using the STL technique to filter the seasonal component. Figure 6.13(a) shows the comparison of seasonal cycles at EGH and MHD during the period. Overall, the plot shows good agreement between both records. At EGH, variations in the annual cycle were observed during 2002-2005 and 2007-2009, which contrasted with the smooth cycles at MHD during the period. Larger shoulders in winter were seen at EGH, while at MHD were smaller in magnitude, some coincided with the ones observed at EGH and contrast with cycles from 2010 to 2012.

Derwent et al. (2006) used 40-minutes observations of CH_4 at MDH to model trends in baseline air masses from 1990 to 2030. They observed interannual variations spanning periods of ~4-years in the data set. Such variations were detected during the entire period and no pattern seemed to be present. They observed that models cannot simulate accurately interannual variations due to changing environmental factors such as El Niño in 1998 which lead to a large increase in biomass burning.

Conversely, Manning et al. (2011) studied latitudinal distributions of atmospheric CH_4 in the marine boundary layer from 2001 to 2010 using data from the Carbon Cycle Cooperative Global Air-Sampling Network. Their representation shows distinctive marked interannual CH_4 variations during the period modelled at mid-northern latitudes, which are in good agreement with the observations made at EGH and MHD. The interannual variations are ascribed to the different and changing meteorological conditions as seen by Derwent et al. (2006). Changes in wind speed and wind direction at EGH and MHD the sites year-to-year can lead to larger/lower seasonal AV_s (Khalil et al., 2007).

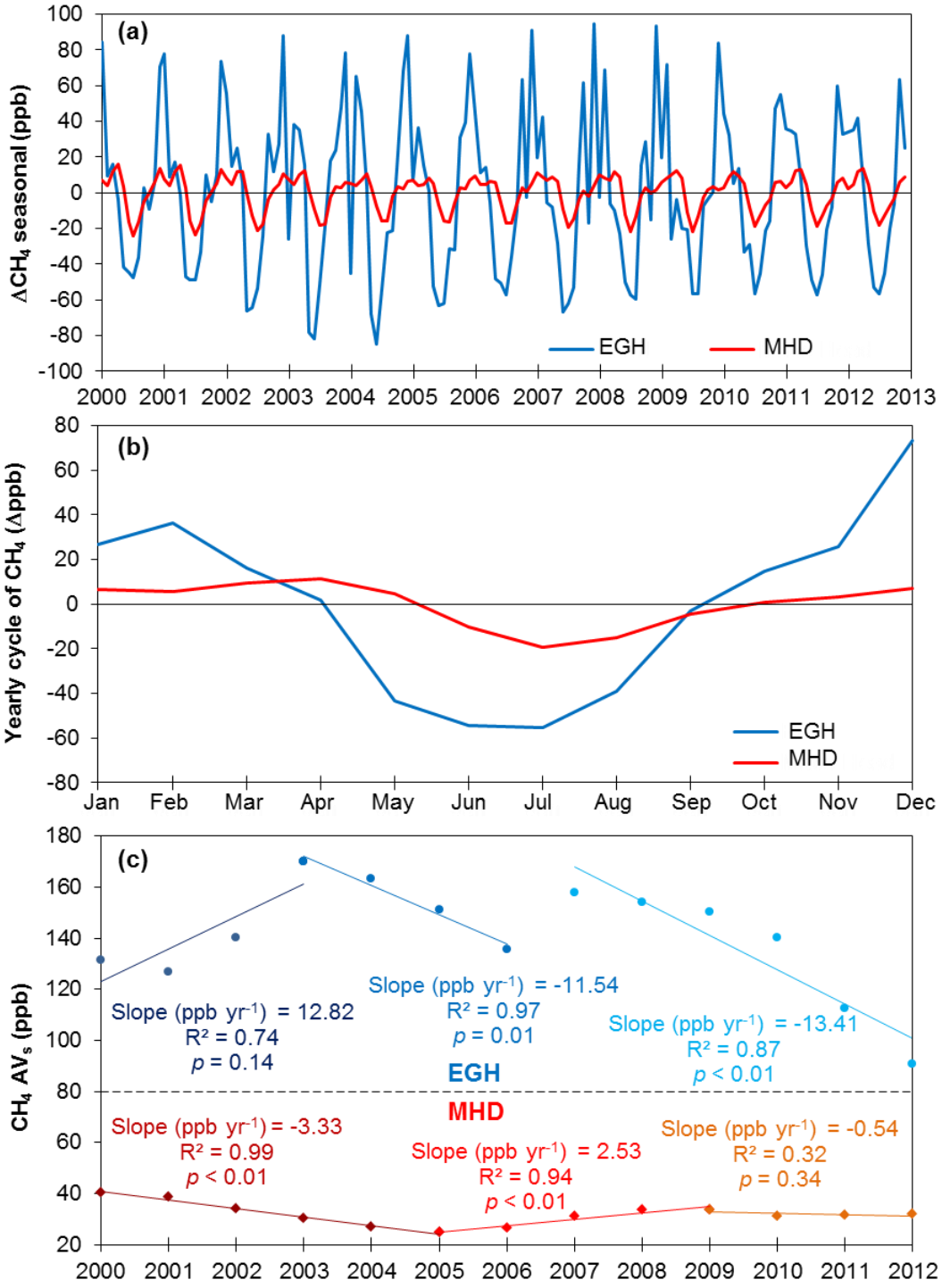

Figure 6.13(a). STL seasonal cycles; **(b).** yearly cycle averaged calculated from 13-years of measurements; **(c).** seasonal amplitudes peak-to-trough of each seasonal cycle and trends at EGH and MHD from 2000 to 2012.

The STL yearly averaged cycles at EGH and MHD have been calculated by averaging calendar months during 13-years of measurements and are shown in Figure 6.13(b). Although the cycles show the same shape, the timing of highest concentration differs by four months between the two sites. It is observed on average in December at EGH, while it occurs at MHD in April. Interestingly, a sharp decline is observed during winter, January at EGH and February at MHD, due to

changes in meteorological conditions. Concentrations increase after such decline the following month. Concentrations decline smoothly after February to July, when the trough of the cycles is observed. After the trough in summer, CH_4 concentrations increase during autumn before reaching the maximum in winter.

The yearly cycle of CH_4 in the Northern Hemisphere has been studied previously by Derwent et al. (2006) at MHD (Ireland), Thompson et al. (2009) at Ochsenkopf (Germany), Nguyen et al. (2010) in South Korea and Sanchez et al. (2013) at the Spanish upper plateau. In general terms, the cycles are consistent with the findings reported in the present project. Derwent et al. (2006) observed the same behaviour with the maxima of the cycle in April and minima in July for averaged data from 1990 to 2003 at MHD. Such findings confirm that no substantial changes have occurred at MHD as the cycle reported here is based on observations from 2000 to 2012. Sanchez et al. (2013) findings are in good agreement with data from EGH. They observed the peak of the cycle in December followed by smooth decline with a small-halt in March and the trough in July.

Nguyen et al. (2010) identified at an urban road site in Seoul, Korea the peak of the seasonal cycle in winter and trough in summer, which is consistent with data at EGH. By contrast, at an urban background site, they observed the peak in July and the trough in winter. They suggested that the enhancement of CH_4 during summer is probably due to non-traffic sources, which become important in areas where temperature increases substantially in summer. Sanchez et al. (2013) reported that the major factors controlling CH_4 concentrations are prevailing meteorological conditions, atmospheric transport and changes in sources and sinks. To a lesser extent, the effects of wet conditions anaerobic processes, soil types and land uses can increase CH_4 uptake during summer. At EGH, the yearly cycle of the PBL and the contrasting conditions of photochemistry from winter to summer are the main factors driving CH_4 concentrations.

AV_s at both sites were calculated from peak-to-trough of each cycle, without considering calendar cycles and are plotted in Figure 6.13(c). The results show three different trends in AV_s at both sites. At EGH statistical significant decreasing trends (p<0.05) were observed from 2003-2006 (decline) and 2007-2012 (decline), while at MHD trends were significant from 2000-2005 (decline) and 2005-2009 (increase). The trends in AV_s result from interannual variations which span ~4-years

in average. The interannual variations are ascribed to changes in meteorological conditions as described above.

6.6.3. Long-term trends of CH_4 at EGH and MHD

The long-term trends for CH_4 at EGH and MHD were calculated from annual averages. The Mann-Kendall test and Sen's estimate were used to compute the trends and their residuals, and are plotted in Figure 6.14. Table 6.5 and Table 6.6 summarise slope and significance the results of the Mann-Kendall analysis. The trends contrasted in magnitude and were not statistically significant (p>0.05); EGH a decline of 0.27 ppb CH_4 yr^{-1} was observed, whereas at MHD an increase of 2.85 ppb CH_4 yr^{-1}. As discussed above, at EGH annual averages showed increases and decreases during the period, while at MHD fewer variations were observed (Figure 6.14). It can be corroborated if residuals are analysed in an absolute magnitude, as out of 13 values, eight (62%) were larger at EGH than at MHD. Those residuals were especially larger in years when meteorological conditions vary drastically from one year to another, for example in 2003 when a heat wave affected the northern hemisphere, and specifically Europe.

CH_4 long-term trend at MHD was studied previously by Derwent et al. (2006) and Rigby et al. (2008a). Steady concentrations were reported for the period 2000-2006, while a sudden increase was observed from 2007 onwards. Rigby et al. (2008a) attributed this increase, which was also observed at several monitoring stations in both hemispheres, to increments in the boreal and tropical emissions. They explained that these can be affected by several factors such as temperature, water table level and rainfall. They also suggested that probably the most important factor was the high annual average temperature at Siberia. On the other hand, Derwent et al. (2006) projected long-term trends from 2000 to 2030 using various scenarios. Although some the projections therein showed positive trends, the magnitudes were overestimated by few ppb beyond the growth rate observed during 2007-2012. Thus, the closest scenario to the real increase projected a growth rate of 10.8 ppb CH_4 yr^{-1}, which is 7.9 ppb CH_4 yr^{-1} larger than current observations. It was computed by forcing the climate for pre-industrial conditions.

Table 6.5. Mann-Kendall test and Sen's estimate for CH_4 records at Mace Head during 2000-2012.

Test Z	Significance	Q[a]	Qmin99	Qmax99	Qmin95	Qmax95	B[b]	Bmin99	Bmax99	Bmin95	Bmax95
3.2	**	2.8	1.0	5.3	2.0	4.4	1840.1	1845.5	1820.0	1843.0	1827.1

Slopes and series data are expressed in ppb CH_4
°Test Z is performed when n≥10. The absolute value of Z is compared to the standard normal cumulative distribution to define if there is a trend or not at the selected level α of significance. A positive (negative) value of Z indicates an upward (downward) trend.
[a]True slope of linear trend
[b]First data of the series
The following symbols are used for the four tested significance levels α with which the Mann-Kendall trend shows that the null hypothesis of no trend should be rejected:
*** if trend at a = 0.001 level of significance
** if trend at a = 0.01 level of significance
* if trend at a = 0.05 level of significance
+ if trend at a = 0.1 level of significance (no symbol if a is greater than 0.1).
Qmin99: the lower limit of the 99 % confidence interval of Q (α= 0.1)
Qmax99 the upper limit of the 99 % confidence interval of Q (α= 0.1)
Qmin95: the lower limit of the 95 % confidence interval of Q (α= 0.05)
Qmax95: the upper limit of the 95 % confidence interval of Q (α= 0.05)
Bmin99: estimate of the constant Bmin99 for 99% confidence level of linear trend
Bmax99: estimate of the constant Bmax99 for 99% confidence level of linear trend
Bmin95: estimate of the constant Bmin95 for 95% confidence level of linear trend
Bmax95: estimate of the constant Bmax95 for 95% confidence level of linear trend

Table 6.6. Mann-Kendall test and Sen's estimate for the long-term trend of CH_4 records at Mace Head during 2000-2012.

Year	Data	Sen's estimate	99 % conf. min	99 % conf. max	95 % conf. min	95 % conf. max	Residual
2000	1843.0	1840.1	1845.5	1820.0	1843.0	1827.1	2.9
2001	1845.0	1842.9	1846.5	1825.2	1845.0	1831.5	2.1
2002	1845.0	1845.8	1847.5	1830.5	1847.0	1835.9	-0.8
2003	1850.3	1848.6	1848.5	1835.8	1849.0	1840.3	1.7
2004	1844.8	1851.5	1849.5	1841.0	1851.0	1844.8	-6.7
2005	1839.9	1854.3	1850.4	1846.3	1853.0	1849.2	-14.5
2006	1844.0	1857.2	1851.4	1851.6	1855.1	1853.6	-13.2
2007	1852.4	1860.0	1852.4	1856.8	1857.1	1858.0	-7.6
2008	1865.1	1862.9	1853.4	1862.1	1859.1	1862.4	2.2
2009	1867.4	1865.7	1854.4	1867.4	1861.1	1866.9	1.6
2010	1867.9	1868.6	1855.4	1872.6	1863.1	1871.3	-0.7
2011	1871.4	1871.4	1856.3	1877.9	1865.1	1875.7	0.0
2012	1880.1	1874.3	1857.3	1883.1	1867.1	1880.1	5.8

Slopes and series data are expressed in ppb CH_4
Qmin99: the lower limit of the 99 % confidence interval of Q (α= 0.1)
Qmax99 the upper limit of the 99 % confidence interval of Q (α= 0.1)
Qmin95: the lower limit of the 95 % confidence interval of Q (α= 0.05)
Qmax95: the upper limit of the 95 % confidence interval of Q (α= 0.05)
Bmin99: estimate of the constant Bmin99 for 99% confidence level of linear trend
Bmax99: estimate of the constant Bmax99 for 99% confidence level of linear trend
Bmin95: estimate of the constant Bmin95 for 95% confidence level of linear trend
Bmax95: estimate of the constant Bmax95 for 95% confidence level of linear trend

By contrast, at EGH an increase in CH4 concentrations was observed in 2007 but concentrations remained steady from 2008 to 2012 (Figure 6.14). It is interesting that EGH does not show the increase observed globally, which means that CH_4 at EGH is dominantly affected by changes in local emissions. It agrees with the fact that CH_4 concentrations at EGH are so much higher than background levels. Another possible explanation is that decrements in CH_4 local emissions as reported by the NAEI (2013) may balance the global increment observed, which would maintain the steady levels observed.

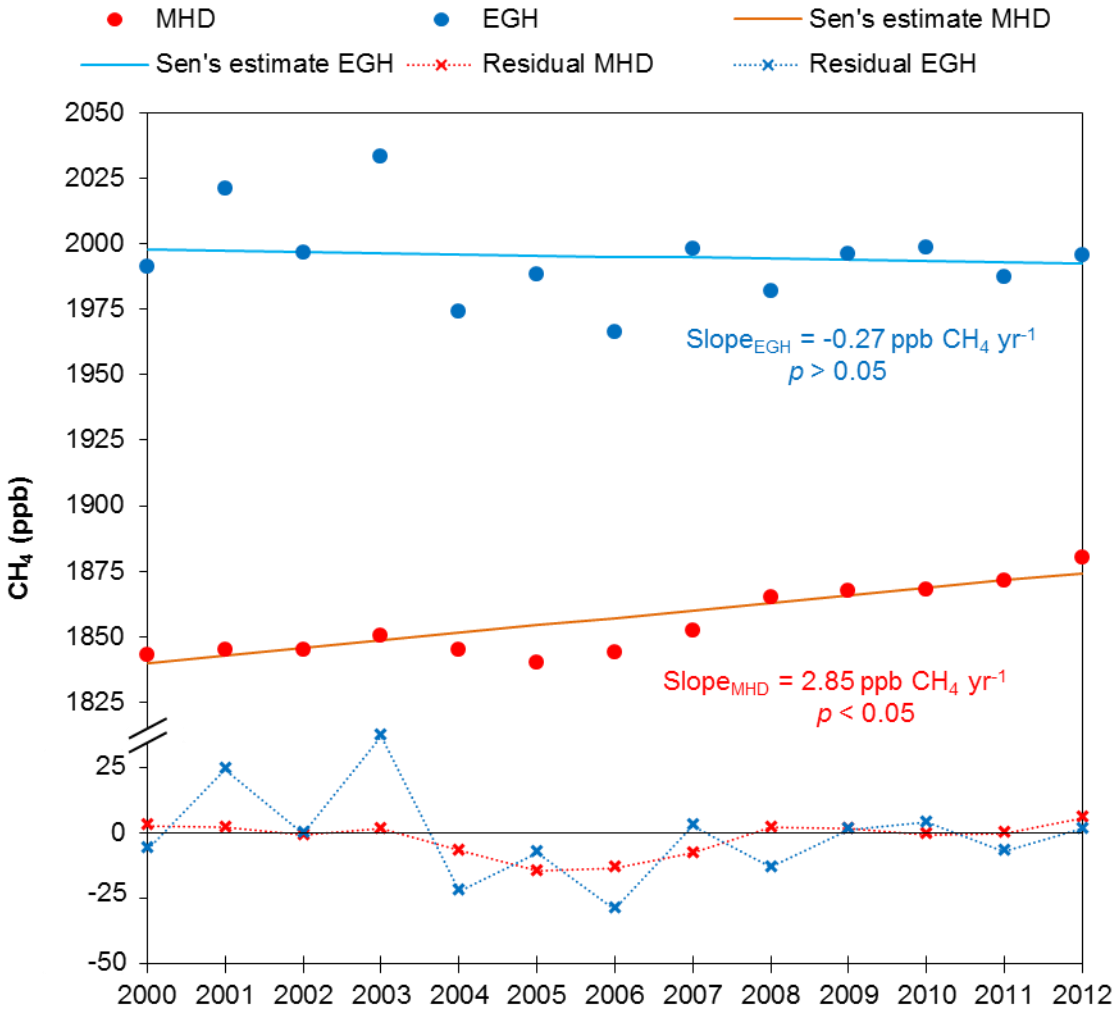

Figure 6.14. Long-term trends for CH_4 at EGH and MHD during 2000-2012 calculated from annual averages. Trends were computed with the Mann-Kendall test and Sen's estimate.

6.7. Summary

Atmospheric CH_4 measured at EGH during 2000-2012 ranged on time scales from inter-annual to annual cycles. The diurnal cycle of CH_4 showed variations related to atmospheric transport and length of daylight. AV_d were not influenced by anthropogenic emissions and were similar during weekdays and weekends. Seasonal cycles of CH_4 were driven by variations in the PBL height. Annual cycles showed maxima in winter and minima in late summer. The largest seasonal AV_s observed was 169.9 ppb CH_4 in 2003, whereas the smallest AV_s was 90.8 ppb CH_4 in 2012. A declining trend in AV_s of 2.1 ppb CH_4 yr^{-1} not statistical significant (p>0.05) was observed during 2000-2012 due to a decline in CH_4 emissions in the UK during 2000-2012 and to the global increase of the background levels of CH_4 since 2007.

The highest concentrations of CH_4 were recorded in air masses from E and NE sectors, which are related to transport of CH_4 from anthropogenic sources in the London region and near EGH. By contrast, the lowest concentrations were recorded in air masses from S and SW sectors. A not significant declining trend (p>0.05) of 0.27 ppb CH_4 yr^{-1} was observed at EGH during 2000-2012. When data were split, an increasing trend from 2000-2003, a declining trend from 2003-2006 and a steady state from 2006-2012 were observed. None of these trend were significant (p>0.05). The increase of CH_4 levels recorded in 2007 at EGH is in good agreement with observations made at other monitoring stations, which has been ascribed to an increase of CH_4 emissions in the Northern Hemisphere during 2006-2007 (Rigby et al., 2008a). The long-term trend of atmospheric CH_4 calculated at EGH contrasts with the decline in CH_4 emissions reported in the UK NAEI during 2000-2012.

7. COMBINED ANALYSIS AND INTERPRETATION OF CO_2, CO AND CH_4 RECORDS AT THE EGH SITE

The location of the EGH monitoring station is ideal to study carbon gas emissions because of its proximity to the M25 motorway, Heathrow airport and the Greater London area. The EGH site is a semi-rural monitoring station for the background sector and sub-urban station for the other sectors. With a population of 8.17 million inhabitants (ONS, 2012), the area within the M25 motorway encompasses the 32 London boroughs and is a major source of anthropogenic carbon gases (NAEI, 2013). London is the most populated city of the European Union, therefore the emissions of the area are significant at local and regional scale.

The combined analysis, interpretation and comparison of CO_2, CO and CH_4 atmospheric records at the EGH site can provide new insights about the inter-relationship and some of the most important processes and sources involved in carbon gas emission near EGH. Furthermore, comparison with official data from the UK National Emission Inventory permits evaluation of the success of air quality policies implementation.

7.1. The role of meteorology on atmospheric carbon gases recorded at the EGH site

Air mass back trajectories analysis is an important tool to understand the transport of air pollutants and atmospheric composition (Fleming et al., 2012). Wind speed and direction can be used to identify different local emissions sources (Carslaw and Beevers, 2013). At EGH, measured CO_2, CO and CH_4 depend strongly on meteorological conditions and on air mass origins. Air masses passing over large conurbations and air pollutant sources can transport emissions to sub-urban and rural areas. High wind speeds of air masses generally can result in lower concentrations as they generate turbulent conditions, which increase dilution (Grant et al., 2010). However, during certain conditions high wind speeds can increase concentrations close to the ground, e.g. under high wind speeds buoyant chimney plumes from tall stacks may be dragged down. By contrast, low wind speeds can reduce the dispersion of air pollutants. Table 7.1 summarises some important CO_2, CO and CH_4 local sources and the distance at which they are located from EGH.

Table 7.1. Relevant local CO_2, CO and CH_4 sources nearby the EGH site.

Wind sector	Source	Site	Distance (km)
N	Residential	Egham Hill residential area	0.4
	Automobiles	Car parking on campus	0.1
	Gas pipeline	Along A30 motorway	0.2
NE	Automobile	A30 roundabout	0.75
	Aircraft	Heathrow airport	7
E	Automobiles	M25 motorway	1.5
	Domestic	Egham residential area	0.3 - 1.5
	Domestic	Staines residential area	3
SE	Automobiles	M25 and M3 motorways junction	3.2
S	Residential	Virginia Water residential area	2.2
SW	Residential	Virginia Water residential area	2.7
W	Residential	On campus	0.2
	Residential	Englefield Green residential area	0.9
	Automobiles	A30 and A328 road junction	0.7
NW	Boiler house	On campus	0.02
	Residential	Englefield Green residential area	1

Previous reports have shown the importance of analysing wind occurrence at monitoring sites. Meng et al. (2009) observed that in summer at the Chinese Northern Plain, southwesterly air masses transported CO emissions from regions where biomass burning is intense, which increased the CO concentrations recorded at the background station. The CO transported increased the monthly averages up to levels observed in winter. Hossain and Easa (2012) reported that during winter months lower wind speeds and temperature developed stronger inversions than in summer at Dhaka city in Bangladesh, which led to larger CO averages in winter than in summer. Thus, to perform a proper interpretation of CO observations, wind speed and direction must be considered and its variation of occurrence depending on the season.

7.1.1. Cluster analysis of CO_2 local sources and regional sources

To identify local sources nearby the EGH site, bivariate plots were constructed using the data set recorded from 2000 to 2012. Figure 7.1(a) shows the bivariate polar plot of CO_2 average concentrations at EGH during 2000-2012. Variations in CO_2 concentrations are observed dependant upon wind direction and wind speed. High CO_2 concentrations are observed at low wind speeds, and are clearly noticeble for the NE, E and SE wind sectors. By contrast, at high wind speed CO_2 concentrations decreased considerably. The lowest concentrations are observed for the background (SW) and W wind sectors, where few local sources of CO_2 are located (Table 7.1). This is expected as the SW sector at EGH is considered as

semi-rural. Interestingly, moderate CO_2 concentrations are also observed to the north-west which can be ascribed to CO_2 domestic emissions from the residential area of Englefield green.

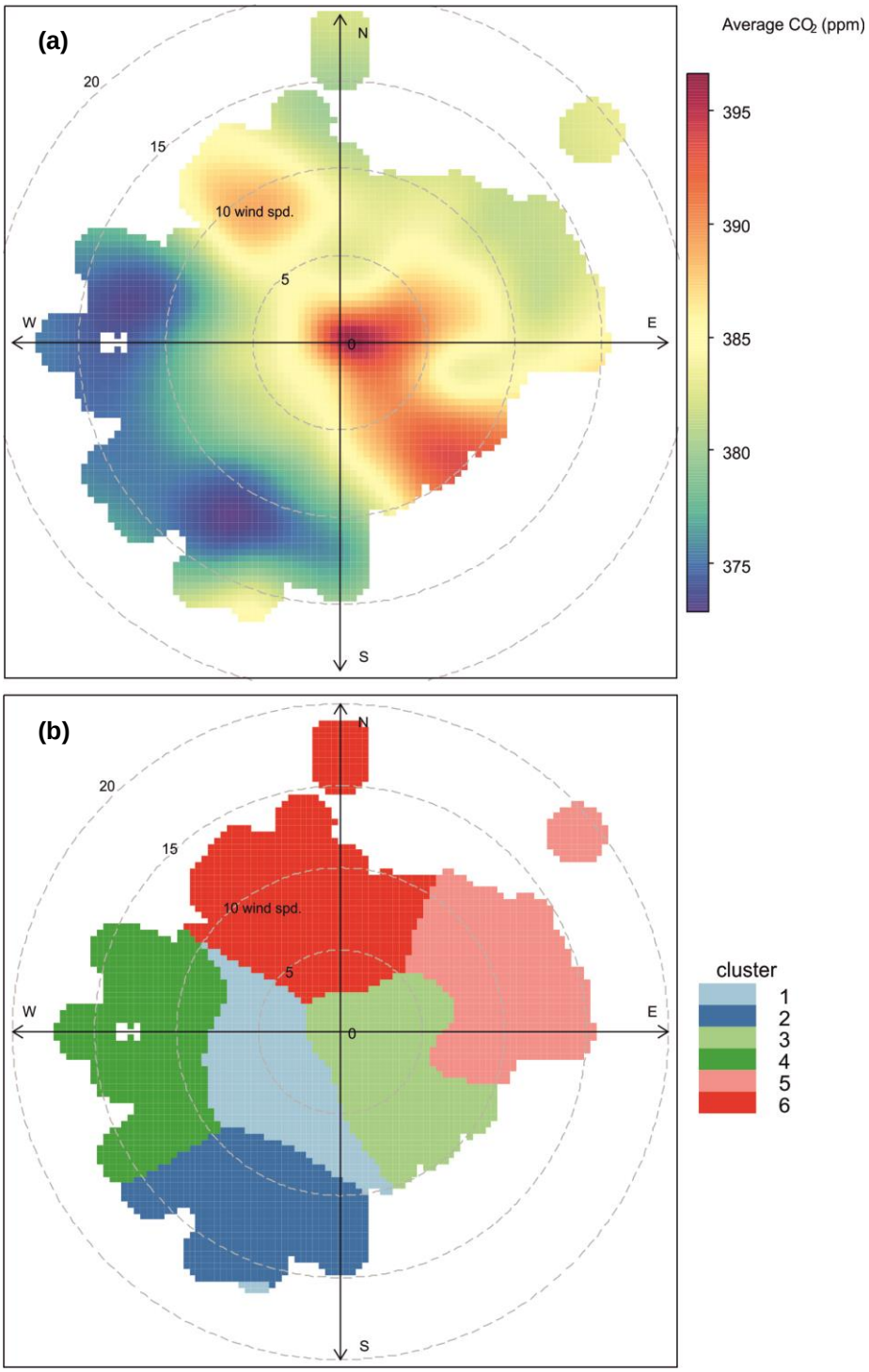

Figure 7.1(a). Bivariate polar plot of CO_2 atmospheric concentrations (The radial scale shows wind speed in m s^{-1}, which increases from the centre of the plot radially out-wards, the colour scale shows CO_2 concentrations in ppm); **(b).** Identification of 6 clusters for CO_2 concentrations measured at the EGH site from 2000 to 2012.

Cluster analysis was performed for the CO_2 surface shown in Figure 7.1(a) from 2 to 10 clusters as reported by Carslaw and Beevers (2013) (Figure E1). They represented in a bivariate polar plot NO_x concentrations recorded at London Heathrow airport during 2000-2010 and observed that seven clusters are required before the high concentration region (low wind speeds) was separately. Figure 7.1(b) shows six clusters for CO_2 concentrations recorded at EGH during 2000-2012. Cluster 1 comprises CO_2 emissions on campus and from the residential areas in Englefield Green located in the background (SW) and S sectors. Clusters 2 and 4 comprise the forest areas of Great Wood and Windsor Great Park located SW and W of EGH, respectively. It can be noticed that scarce CO_2 source areas lead to lowest concentrations recorded at the site, which coincides with the background sector. Cluster 3 comprises the largest CO_2 concentrations recorded for the SE and E sectors. Such high CO_2 concentrations are ascribed to the advection of air masses passing over the junction of the M25 and M3 motorways, two of the busiest motorways in the UK, and to CO_2 emissions from the Egham residential areas.

Relatively low CO_2 concentrations arriving in air masses from the NE sector are captured in cluster 5. Such emissions can be ascribed to the residential area of Egham and to automobiles especially during rush hour, when high loading of vehicles is observed before the A30 roundabout, which leads to the junction with the M25 motorway. Cluster 6 represents the N sector, which contains a large part of Englefield Green and where high concentrations of CO_2 are observed at relatively high wind speeds (>5 m s^{-1}) that can transport emissions from the residential area.

7.1.2. Cluster analysis of CO local sources and regional sources

Figure 7.2(a) shows the bivariate polar plot of CO average concentrations at EGH during 2000-2012. Relatively low CO concentrations are observed almost in all sectors except for N and NE. The largest CO concentrations (>400 ppb CO) were recorded during the prevalence of high northerly and northeasterly wind speeds. Although such data represent less than 1% data capture, they can be related to CO emissions probably from Heathrow airport. In the E sector, concentrations ranged from about 300 to 375 ppb CO, and are associated to CO emissions from the residential area of Egham and from the M25 motorway. Interestingly, high CO concentrations ~400 ppb CO are observed on the E at low wind speeds (<2 m s^{-1}), which can be ascribed to emissions from boilers on campus, and in the vicinity, mostly from heating systems in the Egham area. Similarly, high CO concentrations

are observed at large wind speeds for easterly air masses and are ascribed to automobile emissions.

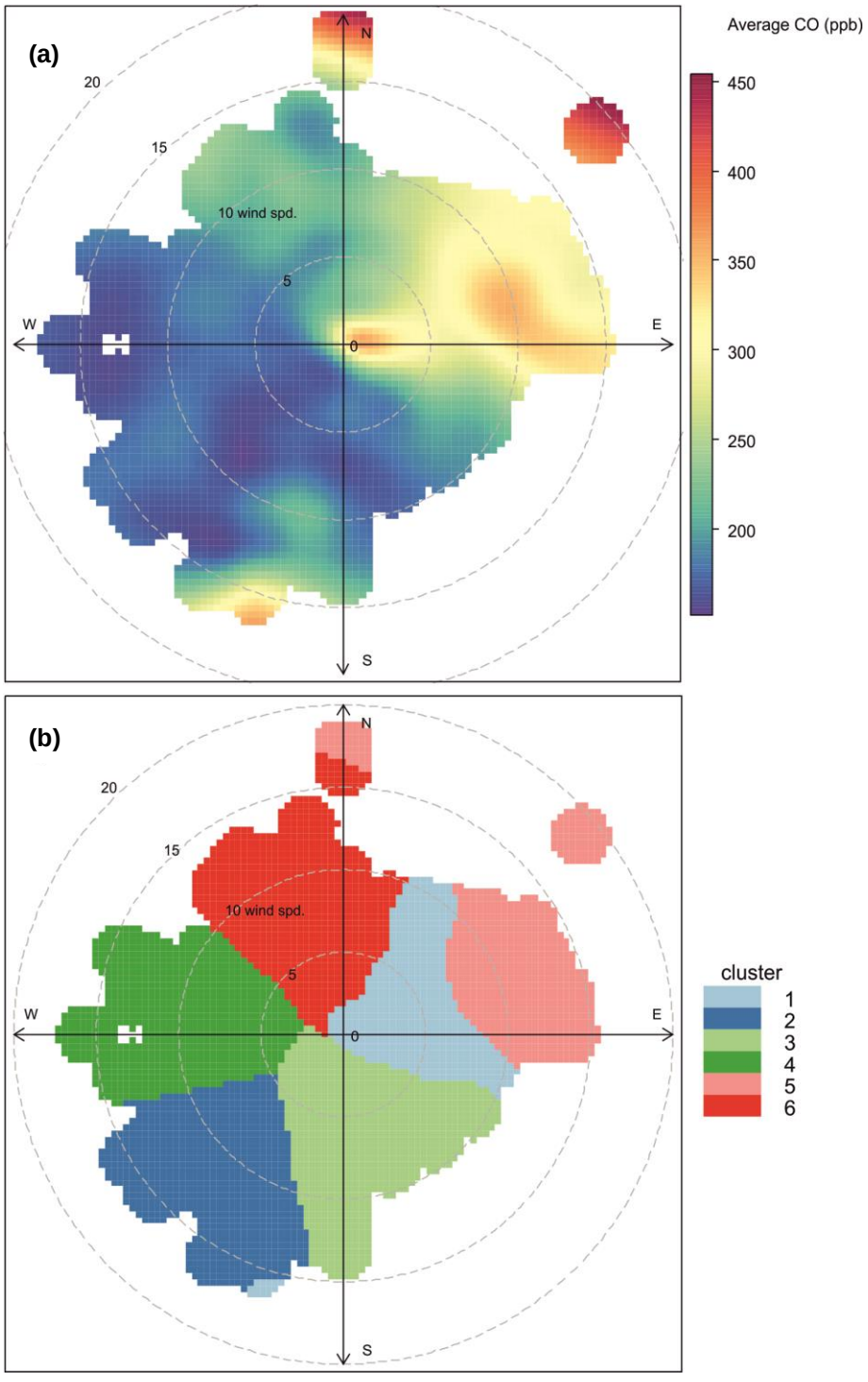

Figure 7.2(a). Bivariate polar plot of CO atmospheric concentrations (The radial scale shows wind speed in m s^{-1}, which increases from the centre of the plot radially out-wards, the colour scale shows CO concentrations in ppb); **(b).** Identification of 6 clusters for CO concentrations measured at the EGH site from 2000 to 2012.

Very low CO concentrations (<200 ppb CO) are observed in southerly, southwesterly and westerly air masses. Those CO concentrations are in good

agreement with the presence of few CO sources on such sectors and with the presence of large forest areas (Great Wood and Great Windsor Park). Interestingly, CO concentrations higher than 300 ppb are observed in southerly air masses at high wind speeds (>12.5 m s^{-1}). That could be related to the transport of emissions from residential areas at Virginia Water, which can emit CO especially during winter when the domestic heating use is enhanced. Moderate concentrations of 200-250 ppb CO are observed for wind speed >5 m s^{-1} to the N and NW of EGH. Emissions from the residential area in Englefield Green and automobiles can contribute to the larger CO concentrations observed than for the background sector.

Figure 7.2(b) shows the cluster analysis for the CO surface shown in Figure 7.1(a) at EGH during 2000-2012. Cluster analysis was performed from 2 to 10 clusters (Figure E2). Similarly to CO_2 records, 6 clusters are required to capture the features observed in the bivariate polar plot for CO_2 at EGH. Cluster 1 comprises CO emissions on campus, and from the west area of the Egham conurbation, and possible from automobiles on the A30 road. Clusters 2 and 4 capture the lowest CO concentrations recorded, which are ascribed to few sources located SW and W of EGH. Cluster 3 captures low concentrations arriving in southerly air masses.

Interestingly, cluster 5 comprises the CO emissions possibly ascribed to aircraft at Heathrow airport and automobiles on the M25 motorway, with the largest CO concentrations recorded during high wind speeds in the N and NE sectors. Cluster 6 represents the CO emissions from the residential area in Englefield Green to the N of EGH and from automobiles on the A320 road.

7.1.3. Cluster analysis of CH_4 local sources and regional sources

Figure 7.3(a) shows the bivariate polar plot of CH_4 concentrations for EGH during 2000-2012. The lowest CH_4 concentrations (<1900 ppb CH_4) are observed for wind speeds greater than 5 m s^{-1} in the SW (background) and W sectors. Low CH_4 concentrations are also observed in the N sector when wind speed ranged between 10 and 15 m s^{-1}. By contrast, the highest CH_4 concentrations (>2500 ppb CH_4) are recorded for wind speeds lower than 2 m s^{-1} in all sectors, but for the E below 5 m s^{-1}. Moderate CH_4 concentrations (~1900 ppb CH_4) are observed in the E sector for wind speeds greater than 5 m s^{-1}, and at large wind speeds for the S sector. CH_4 concentrations about 2000 ppb are observed for the NE sector at wind speeds larger than 15 m s^{-1}.

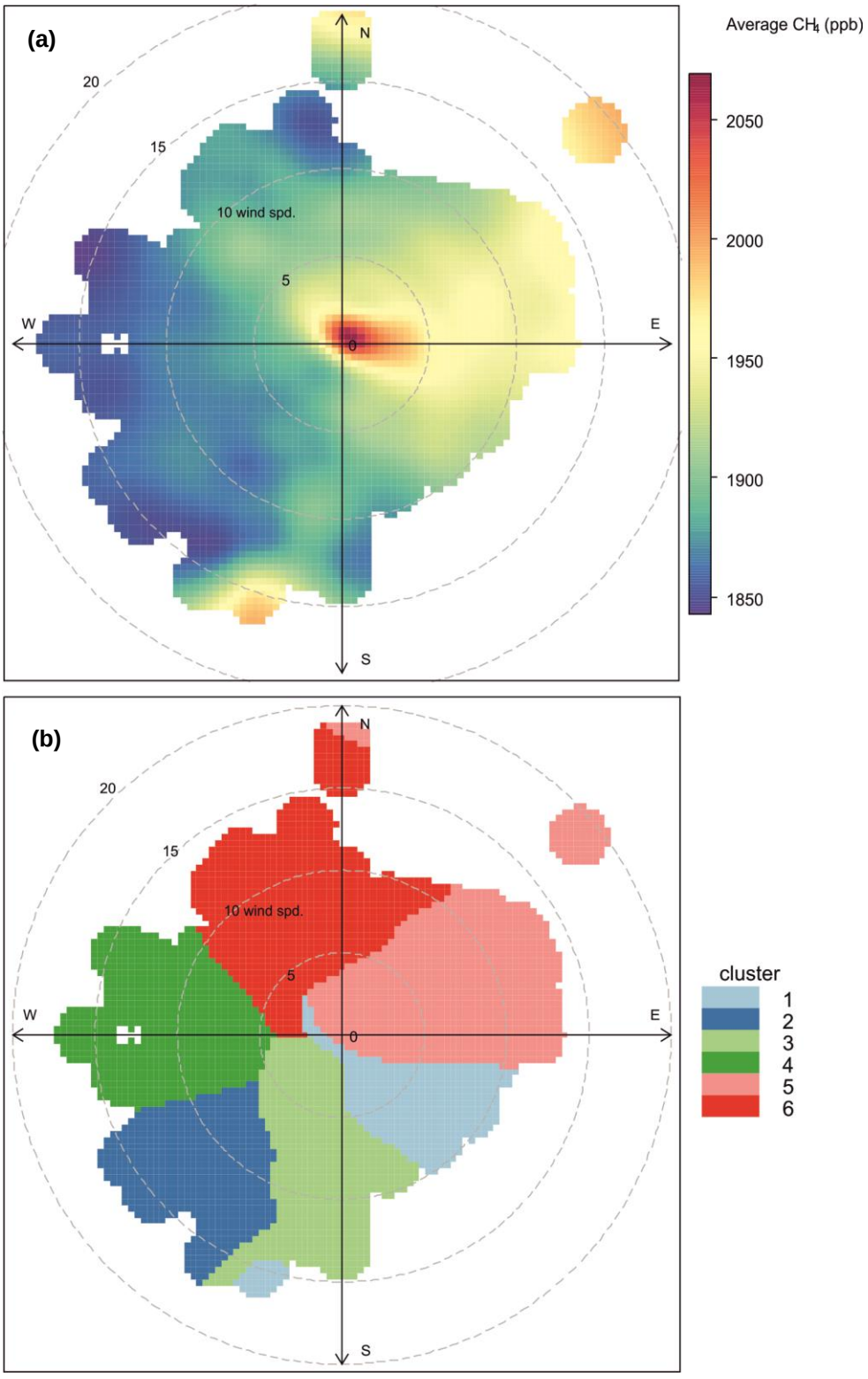

Figure 7.3(a). Bivariate polar plot of CH_4 concentrations (The radial scale shows wind speed in m s^{-1}, which increases from the centre of the plot radially out-wards, the colour scale shows CH_4 concentrations in ppb); **(b).** Identification of 6 clusters for CH_4 concentrations measured at the EGH site from 2000 to 2012.

Cluster analysis from 2 to 10 clusters (Figure E3) was applied to the surface shown in Figure 7.3(a). Similar to CO_2 and CO, it was observed that 6 clusters are required

to depict the features observed in Figure 7.3(a) as shown in Figure 7.3(b). Cluster 1 depicts low CH_4 concentrations that arrive in southeasterly air masses. Clusters 2 and 4 capture the lowest CH_4 concentrations recorded at the EGH site, which are ascribed to air masses passing over the large forest areas of Great Wood and the Great Windsor Park. Interestingly, clusters 3 and 6 comprise also low CH_4 concentrations for the S and N sectors, where sources are scarce and the residential area of Englefield Green is located. Cluster 6 comprises emissions from combustion sources mostly houses in Englefield Green and automobiles on the A30 motorway. Finally, cluster 5 depicts CH_4 emissions mostly from urban Egham and from the gas storage facility on the road to Staines (E to NE sector).

7.2. Pollution episodes

Atmospheric levels of CO_2, CO and CH_4 vary day-to-day causing short-term variations. Pollution episodes occur when air pollutant concentrations are particularly high. These high concentrations are generated for two reasons:

1. Increased pollutant emissions
2. Changes in atmospheric conditions that allow air pollutants to concentrate and be transported from other areas

In the UK, air pollution episodes can be classified into three types: a) winter smog, b) summer smog and c) long-range transport (Netcen, 2003; LAQN, 2014). Winter smogs occur during cold, calm and foggy weather; these conditions trap pollutants emitted by combustion sources such as motor vehicles, domestic heating and other sources close to the ground, which allows their build up over time (Worthy, 1994). Urban areas, particularly those close to the major roads are usually worst affected.

By contrast, summer smogs occur during hot, calm and sunny weather. The chemical reactions in mixtures of air pollutants emitted from road vehicles, fuel burning and solvent usage are accelerated by the sunlight and high temperatures. The pollutants that cause summer episodes can often travel long distances, sometimes even from other parts of Europe (Netcen, 2003).

The third type of pollution episode is caused by long-range transport of pollutants from Europe, or occasionally from North Africa. These episodes occur during summer, either in isolation or in combination with summer smog. Conversely, short-range transport can result in elevated concentrations of primary pollutants close to

major emissions sources such as power stations or large industrial plants (Netcen, 2003; Defra, 2006).

At the EGH site, air pollution episodes vary widely in terms of duration and timing. Four pollution episodes have been selected for assessment and interpretation. Pollution episodes were selected by comparing dates and concentrations recorded at EGH with pollution episodes published by Netcen (2003) and Defra (2011).

7.2.1. Summer smog episode in 2003

2003 was a record-breaking year in the UK and Europe (Met Office, 2014). It was the sunniest and the second driest year in England since 1766. At the EGH site, records show that the highest temperature, 38.1°, was recorded on August 10 at 15:30 GMT, which is close to the highest temperature, 38.5°, ever recorded in the UK, the same day at Faversham, Kent (Met Office, 2014). 2003 was the hottest year over many parts of Europe and the third warmest year since records began in 1861. These weather conditions caused high photochemical production of ozone, which is not studied in this thesis, over large areas of UK and Europe (Netcen, 2003). The most important episode occurred from 1 to 15 August, when many monitoring stations not only in England but also in Wales recorded high ozone concentrations up to for 10 consecutive days, which is an unusually long period for an ozone episode. Air mass back trajectory analyses show that air masses from continental Europe influenced importantly the concentrations recorded in the UK (Figure 7.4).

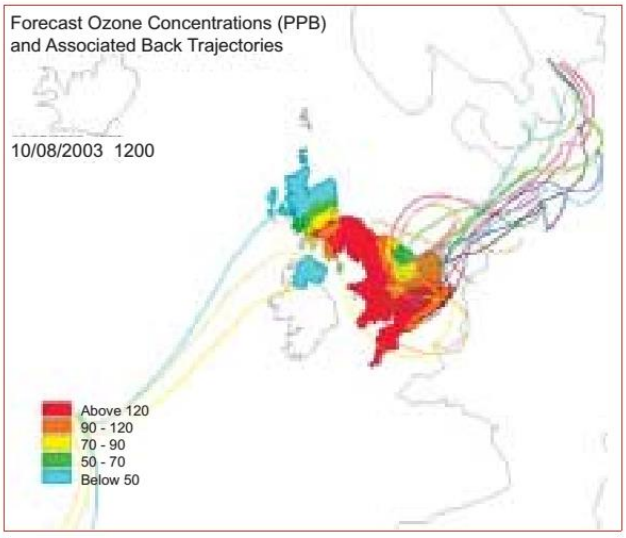

Figure 7.4. Air mass back trajectories and meteorological analysis showing transport of air from Continental Europe to different parts of the UK during the August 2003 summer smog. *Source: Netcen, 2003.*

A calendar plot for CO_2, CO and CH_4 records at the EGH site from 1 July to 31 August 2003 has been constructed to identify changes of concentrations recorded caused by the extreme weather conditions. Figure 7.5(a) shows two clear periods of combined increases in CO_2, CO and CH_4 concentrations, from 11 to 18 July (first period, E1) and, one longer, from 2 to 14 August (second period E2), which is the episode observed all over the UK and reported previously by Defra (Netcen, 2003). During E1, CO_2, CO and CH_4 increased clearly simultaneously as shown in Figure 7.6(a). Figure 7.6(b) shows wind direction and wind speed during the occurrence of E1. A trough is observed before the combined increase on 11 July for all pollutants, which corresponds with air masses arriving from SE. Then, the increase continues until 16 July when the greatest averages during E1 were recorded for all air pollutants (403.6 ppm CO_2, 388.9 ppb CO and 2,305.3 ppb CH_4, daily averages). Those greatest daily averages were recorded when air masses arrived from NW-N and the daily wind speed average was 0.1 m s^{-1}.

Figure 7.6 suggests that the combined increase of air pollutants could be due to emissions from the same sources because only during E1, their combined increase shows exactly the same behaviour and duration. Furthermore, the concentrations recorded during E1 suggest a combination of long-range transport from continental Europe at moderate wind speed (3-5 m s^{-1}) added to by emissions from the London conurbation. The potential local sources for such emissions are a boiler located ~20 metres NW from the air inlet and automobiles and on campus the A30 motorway, which tends to have high loads of traffic during summer due to visitors going to Windsor Great Park and Virginia Water. Also, emissions are potentially produced at the residential area of Englefield Green, which is situated NW-W of the EGH site. As shown in Figure 7.1-3, cluster analyses indicates strong sources of air pollutants in the same direction, and polar plots shows large concentrations of them during low wind speeds similar to those observed during E1.

Two peaks of CO_2, CO and CH_4 were recorded at the EGH during E2. Larger CO_2 concentrations during E2 than in E1 were observed, while the peaks of CO and CH_4 concentrations were similar to those in E1. E2 at EGH coincides with the occurrence of the pollution episode of high ozone levels recorded all over the UK, reported previously by Defra (Netcen, 2003) from 1 to 15 August 2003. At EGH, combined increases in CO_2, CO and CH_4 were seen from 2 and 7 August 2003. Interestingly, from 2 to 4 August the peak is very similar for all air pollutants but the trough after it

does not coincide, while for the second peak air pollutants show the same trough after the highest concentrations on 14 August.

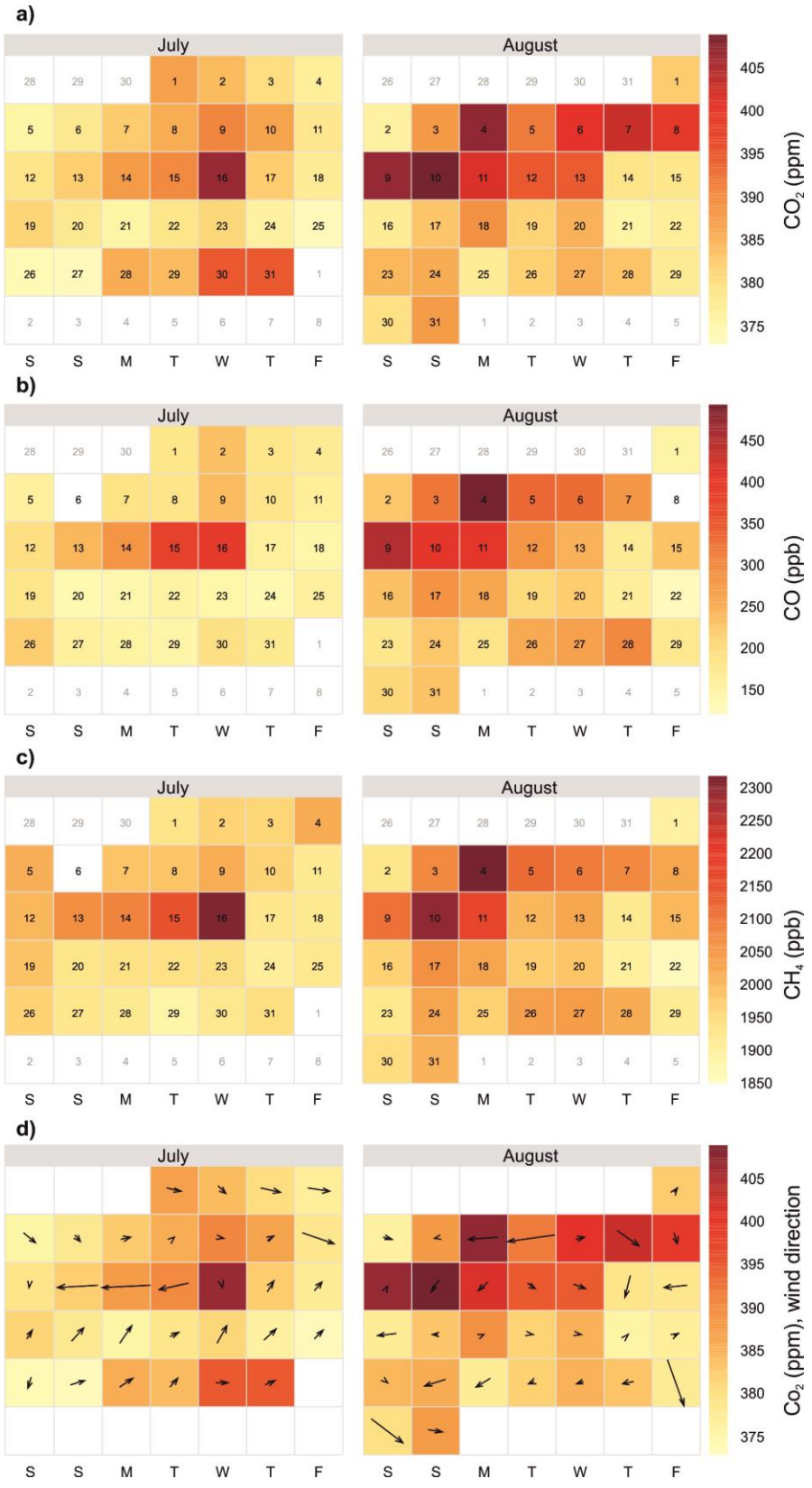

Figure 7.5(a). Calendar plot for CO_2; **(b).** CO; **(c).** CH_4; **(d).** CO_2 and wind direction and scaled speed records at the EGH site during July and August 2003. Colour scale shows daily averages. For the scaled wind speed annotation means the longer the arrow, the higher the wind speed but not scaled.

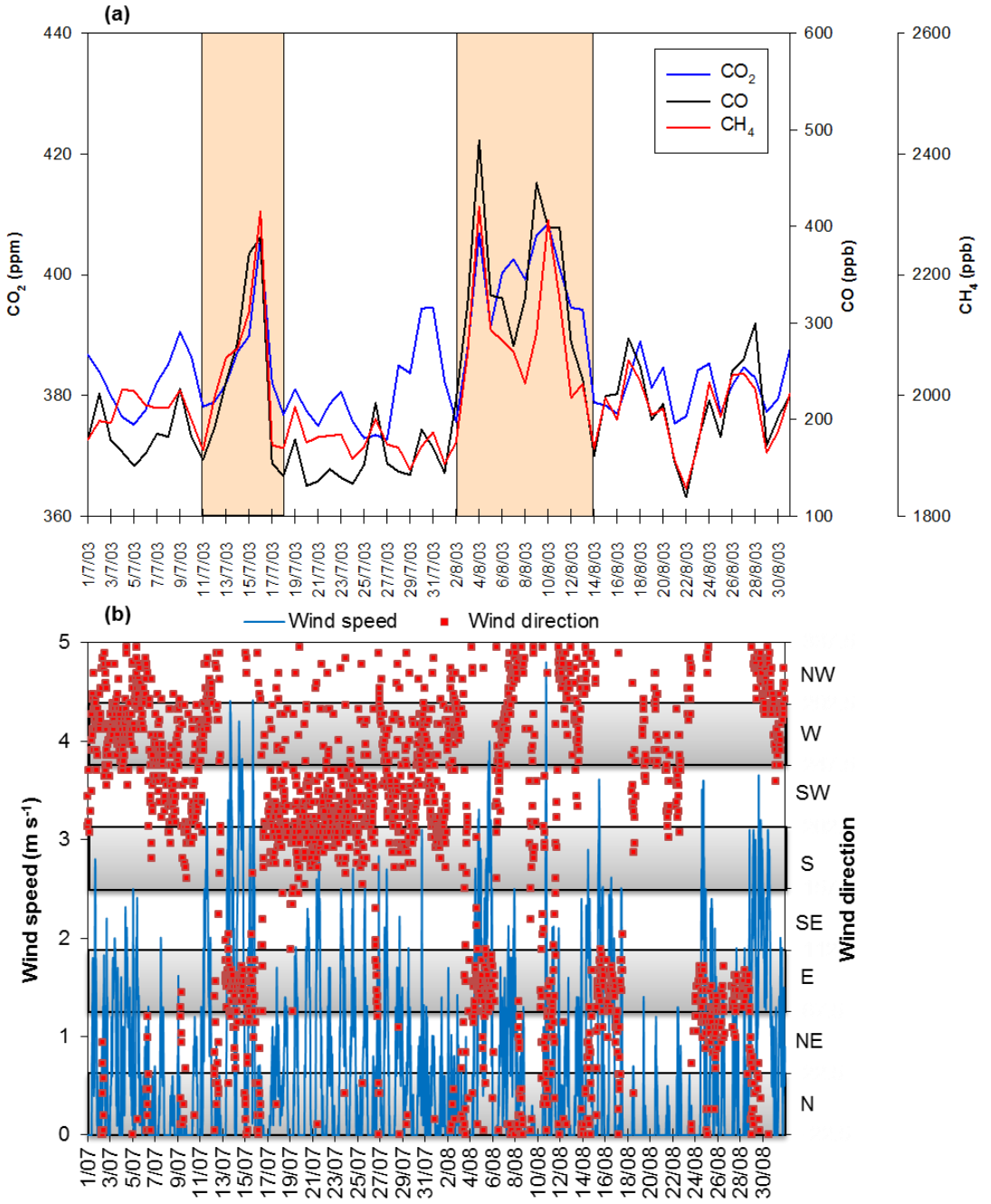

Figure 7.6(a). 30-min values of CO_2, CO and CH_4 measured; **(b).** wind speed and wind direction recorded at EGH from 1 July to 31 August 2003.

During E2, the largest concentrations for CO_2 were recorded in the second peak (408.4 ppm CO_2), while for CO and CH_4 were recorded in the first peak (489.0 ppb CO and 2,312.3 ppb CH_4). Coincidently, during both peaks air masses arrived from NE-E, wind speeds were larger during the first one though. Table 7.2 and Figure 7.6 show that the largest concentrations were associated with low wind speeds and variable wind direction though and that when air masses arrived from the clean sectors (SW, W) concentrations decreased, despite the low wind speed (except 9

August). Concentrations during peak 2 decreased with air masses arriving from NE, E and wind speeds greater than 1 m s^{-1}.

Like during E1, peaks were probably produced by local sources and air pollutants transported to EGH site by slow air masses moving locally. Similarly to E1, local sources on NE, E sector comprise automobiles emissions from the A30 motorway and houses within Egham Hill are and West of Egham. Slightly farer are located the Egham by-pass which receives high loads of traffic, especially during rush hours and the M25-A30 junction.

Table 7.2. Summary of daily averages of all air pollutants, predominant wind direction and wind speed average recorded at the EGH site during E1 and E2 in 2003.

	Date	Daily average			Wind direction	Wind speed daily average
		CO_2 (ppm)	CO (ppb)	CH_4 (ppb)	(Predominant)	(m s^{-1})
Episode1 (E1)	11/07/2003	378.2	158.6	1910.1	SE	1.6
	12/07/2003	378.9	191.7	1996.8	NE	0.1
	13/07/2003	382.0	239.3	2062.9	E	1.8
	14/07/2003	387.2	279.5	2078.0	E	2.2
	15/07/2003	389.9	371.9	2138.7	SE,E	1.4
	16/07/2003	406.3	388.9	2305.3	NW,N	0.1
	17/07/2003	382.2	155.2	1918.2	SW	0.5
	18/07/2003	376.9	141.8	1912.8	SW	0.6
Episode 2 (E2)	01/08/2003	382.4	144.9	1887.3	SW	0.2
	02/08/2003	375.7	220.8	1923.0	W	0.4
	03/08/2003	387.7	319.4	2071.3	E	0.1
	04/08/2003	406.9	489.0	2312.3	NE,E	1.4
	05/08/2003	391.5	328.9	2109.6	NE,E	2.2
	06/08/2003	400.3	326.0	2090.9	W	0.4
	07/08/2003	402.6	276.5	2072.7	NW,N	1.2
	08/08/2003	399.3	325.6	2020.5	NW,N	0.5
	09/08/2003	406.5	445.2	2103.5	SW	0.0
	10/08/2003	408.4	399.2	2290.6	NE	0.7
	11/08/2003	401.2	399.0	2160.5	NE	0.6
	12/08/2003	394.6	279.7	1996.4	NW	0.4
	13/08/2003	394.3	242.4	2019.4	NW	0.6
	14/08/2003	378.9	162.4	1912.2	NE	1.0
	15/08/2003	378.3	224.7	1996.0	NE,E	1.1

7.2.2. Winter smog episode January 2012

During winter time pollution episodes occur due to: the breakdown of the surface inversion which lead to higher concentrations of pollutants at the upper levels being mixed downwards (Worthy et al., 1994), and long-range transport associated with high wind speeds and air mass moving from or passing over large conurbations and industrial areas (Grant et al., 2010). From 14-18 January 2012, high levels of PM_{10} and $PM_{2.5}$ were measured at several stations of the LAQN in the Greater London area, which are not studied in this thesis, close to busy roads due to settled cold

weather (Figure 7.7). Well west of London in the area of Reading, only moderate levels of PM_{10} and $PM_{2.5}$ were recorded. Similarly, moderate levels of PM_{10} and $PM_{2.5}$ were measured in the eastern half of England. In order to assess the influence of settled, cold weather observed also at the EGH site, a calendar plot for CO_2, CO and CH_4 was constructed and is shown in Figure 7.8.

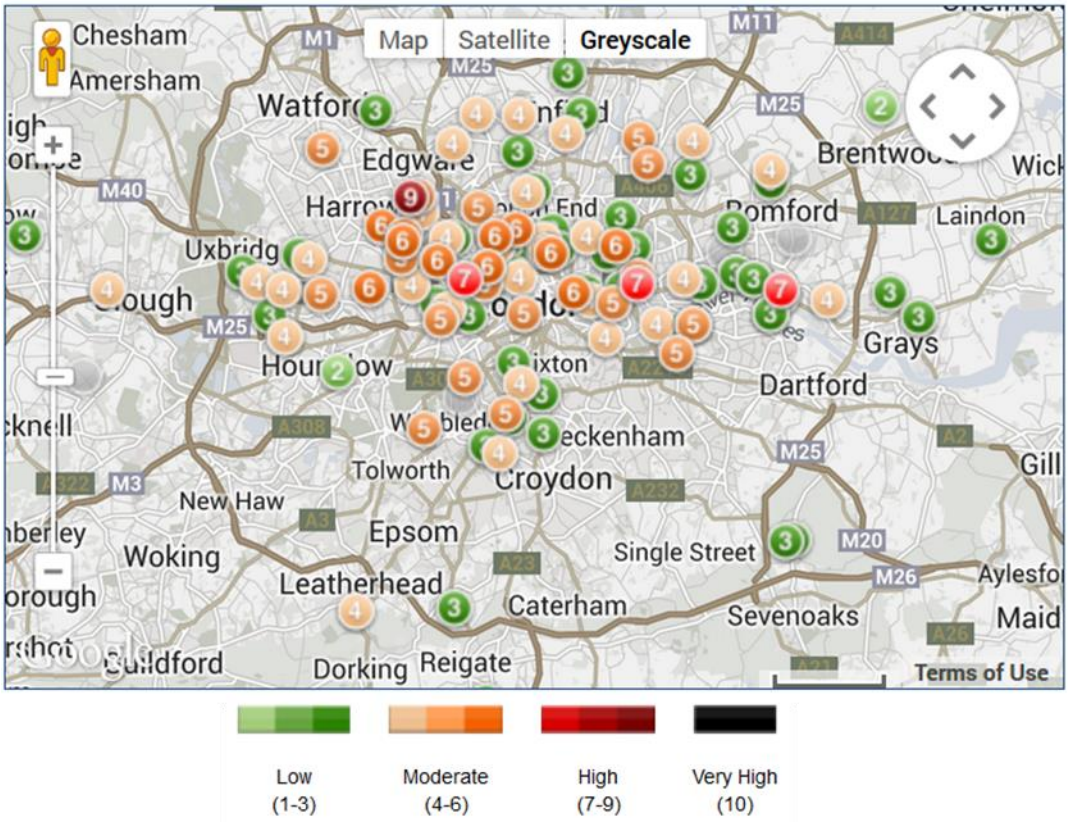

Figure 7.7. Peak readings of PM_{10} $PM_{2.5}$ and NO_2 recorded in Southeast England during the winter smog in January 2012. *Source: Available at http://www.londonair.org.uk/london/asp/publicepisodes.asp?species=All&region=0&site=&postcode=&la_id=&level=All&bulletindate=03%2F05%2F2014&MapType=Google&zoom=9&lat=51.4750&lon=-0.119824&VenueCode=&bulletin=peakvalues&episodeID=PM10midJanuary 2012*

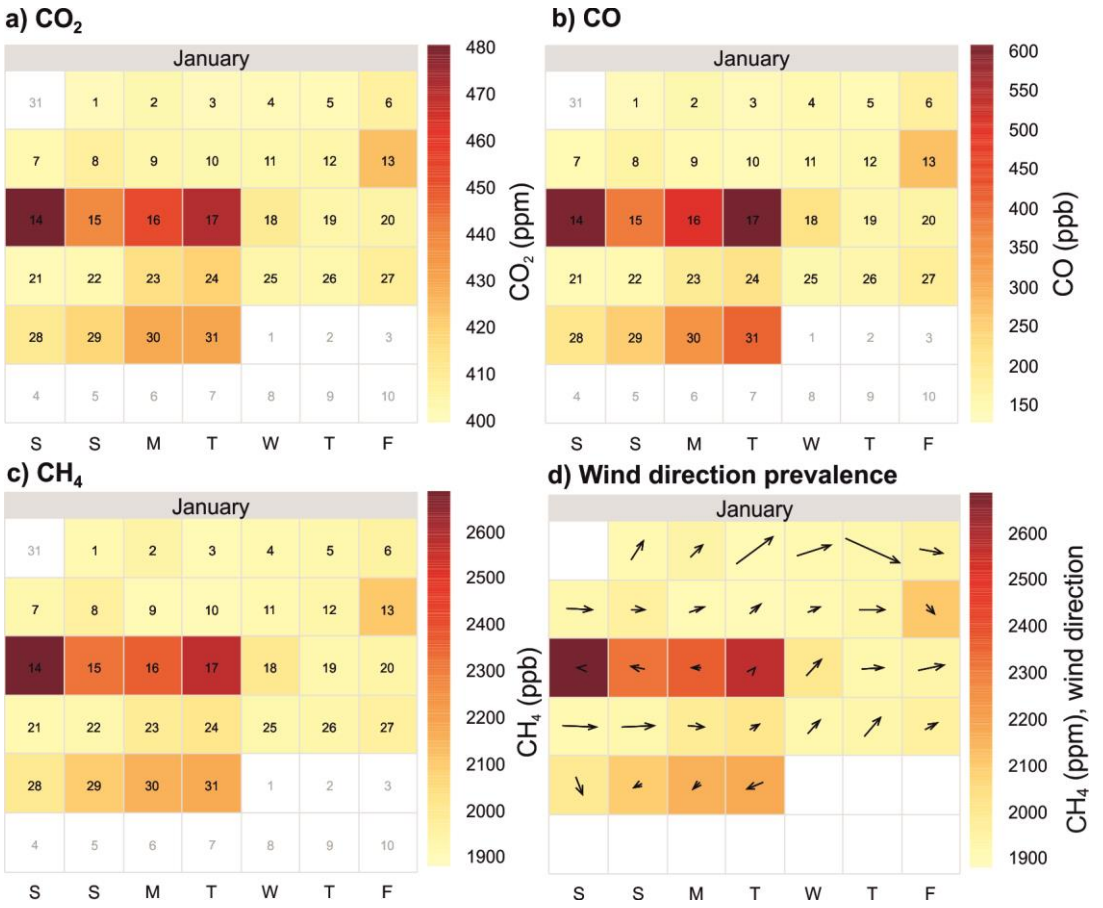

Figure 7.8(a). Calendar plot for CO_2, **(b).** CO, **(c)** CH_4; **(d).** CH_4 and wind direction and scaled speed records at the EGH site during January 2012. Colour scale shows daily averages. For the scaled wind speed annotation means the longer the arrow, the higher the wind speed but not scaled.

Figure 7.8 shows large concentrations of CO_2, CO and CH_4 and low wind speeds from 13 to 17 January 2012 at EGH. Figure 7.9 shows the combined increase of CO_2, CO and CH_4 during low speed wind prevalence. Table 7.3 summarises daily averages of CO_2, CO and CH_4 and wind speed and the predominant wind direction at EGH. The peak of air pollutants begins on January 12, when a combined increase is observed, then on 14 January the highest values of CO_2 and CH_4 during the episode were recorded. Interestingly, those high daily averages were recorded when air masses arrived from E and wind speed was ~2.6 m s^{-1}. Easterly air masses passing over residential areas of Egham and Ashford, and M25 motorway could have transported to the EGH site CO_2 and CH_4 emissions from combustion sources such as automobiles and domestic heating, enhanced during the episode due to cold weather.

By contrast, although the largest CO daily average was recorded on January 17, it was similar to the daily average recorded on January 14, with a difference of 6.5

ppb CO and air masses arriving from SW. Air mass back trajectory analyses show that during the pollution episode air masses moved slowly over southeast England.

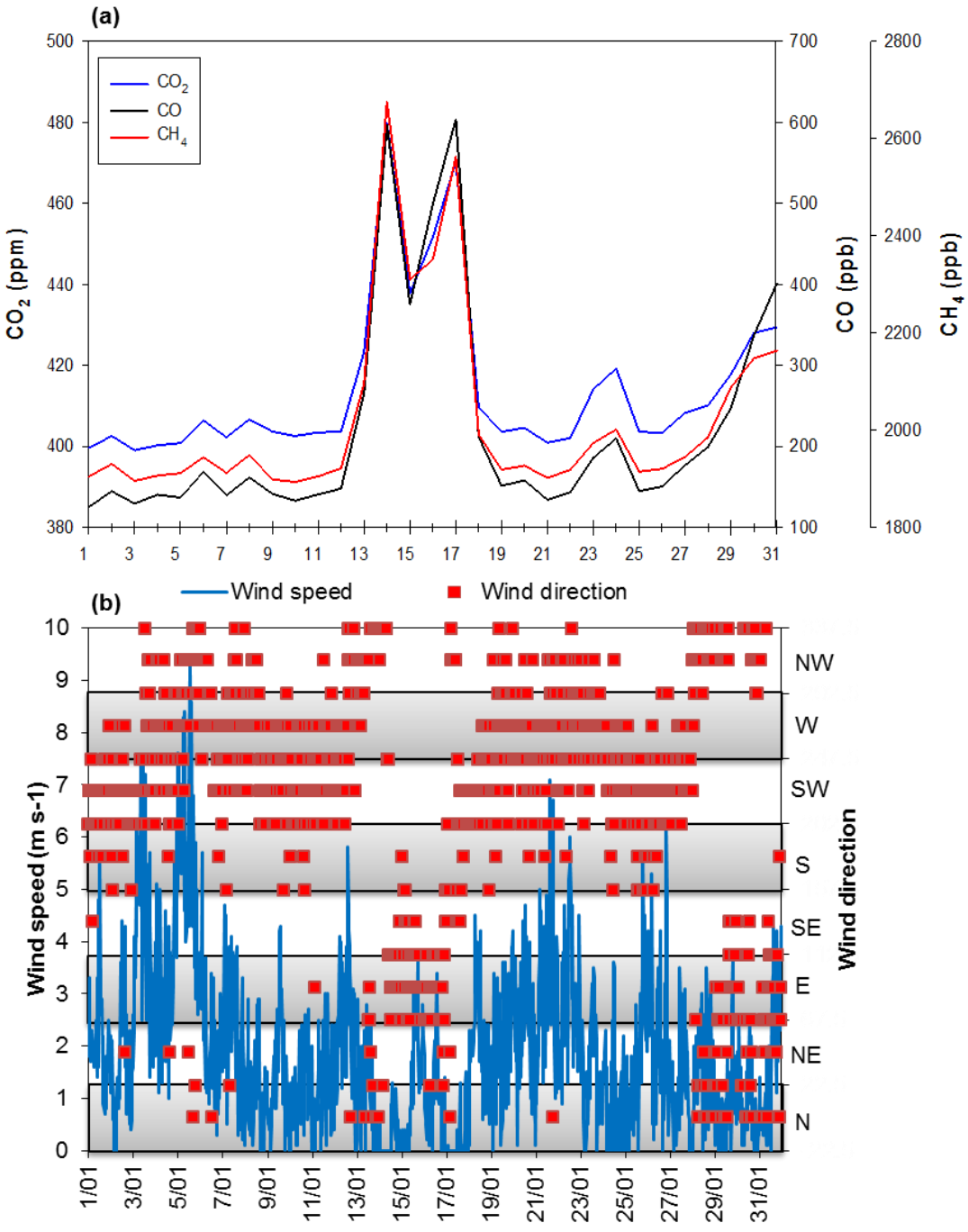

Figure 7.9(a). 30-min values of CO_2, CO and CH_4; **(b).** wind speed and wind direction measured at EGH from 1 to 31 January 2012.

Wind speeds during the episode were over 1.1 m s^{-1}, which may indicate that high concentrations recorded during the episode were transported from sources beyond the RHUL campus to the EGH site. Emission sources in the W-SW wind sectors are combustion sources and are located mostly on campus, which may be responsible

for the increase observed. Among the sources are a boiler flue 20 metres WNW from the air inlet and a local road within the campus. The peak of CO_2, CO and CH_4 recorded at EGH during the pollution episode is similar in time duration to that reported in the LAQN web site (2012). It highlights the importance of monitoring air pollutants during pollution events in order to assess not only in Central London but also on the city periphery to evaluate the effects of such weather conditions on the build-up of air pollutants.

Table 7.3. Summary of daily averages of all air pollutants, predominant wind direction and wind speed average recorded at the EGH site during the pollution episode in January 2012.

Date	Daily average			Wind direction	Wind speed daily average
	CO_2 (ppm)	CO (ppb)	CH_4 (ppb)	(Predominant)	(m s^{-1})
12/01/2012	403.6	147.9	1921.9	W	2.4
13/01/2012	423.4	265.2	2096.5	NW	1.1
14/01/2012	479.7	597.1	2675.4	E	0.2
15/01/2012	437.8	375.7	2310.7	E,SE	1.2
16/01/2012	451.6	499.1	2351.1	E	0.9
17/01/2012	470.3	603.6	2562.3	SW	0.2
18/01/2012	409.7	211.6	1990.5	SW	2.0
19/01/2012	403.6	151.5	1919.0	W	2.0
20/01/2012	404.6	158.3	1927.3	W, SW	2.4
21/01/2012	400.9	134.0	1902.0	W	3.2

7.2.3. Long-range transport episode in April 2003

High levels of ozone and PM_{10} were recorded at many monitoring stations of the LAQN, from 12 to 23 April 2003. The pollution episode was named as the Easter Weekend Smog and was associated with seasonally unusual warm and sunny weather, and long-range transport of air masses from Scandinavia and Central Europe (Netcen, 2003). Figure 7.10 and 7.11 show a combined increase in atmospheric CO_2, CO and CH_4 levels from the 11th to 25th of April at the EGH site. Table 7 summarises CO_2, CO and CH_4 daily averages, predominant wind direction and wind speed daily averages. CO_2, CO and CH_4 increase begins on the 11th, when air masses arrived from SE and wind speed daily average was 0.2 m s^{-1}. CO_2, CO and CH_4 levels continued increasing up to the 15th, when the greatest daily averages of CO_2 and CH_4 were recorded and wind speed daily average was 0.6 m s^{-1}, and air masses arrived from E sector. Greatest CO concentrations during the episode were recorded the following day, 16th, but interestingly the wind speed daily average increased to 2.4 m s^{-1}, whereas the predominant wind direction was NE.

HYSPLIT air mass back trajectory analyses show that from 11-16 April, the increase observed at EGH is ascribed to air masses passing over large residential areas of

Greater London, and that when wind speed decreased the highest concentrations were recorded (Figure 7.12). The high levels of CO_2, CO and CH_4 were caused by local sources, building up under poor dispersion conditions (Worthy et al., 1994; Ohara, 2011), and substantial import of CO_2, CO and CH_4 from residential areas of Egham, Staines and Ashford. Similar highly-elevated levels of other pollutants were measured across SE England and evidence of plume grounding from industrial sources in the East Thames corridor was associated with the increment (Netcen, 2003; LAQN, 2014).

At EGH, CO_2, CO and CH_4 atmospheric levels started to decrease from the 17th April onwards. This decrease is probably associated with the advection of north-easterly air masses and large wind speeds. Table 7.4 shows that during the Easter episode, the lowest concentrations of CO_2, CO and CH_4 recorded at EGH coincided with the largest wind speed daily average, 8.4 m s^{-1}. Air masses with less air pollutant loading may have diluted the build-up of CO_2, CO and CH_4 and at the same time, high wind speeds could have enhanced the mixing of polluted and non-polluted air masses and air pollutant dispersion. Data show that CO_2, CO and CH_4 daily averages at EGH increased again during 23-25 April, however that increase is not studied in this thesis.

Table 7.4. Summary CO_2, CO and CH_4 daily averages, predominant wind direction and wind speed average recorded at the EGH site during the Easter Weekend Smog in April 2003.

Date	Daily average			Wind direction	Wind speed daily average
	CO_2 (ppm)	CO (ppb)	CH_4 (ppb)	(Predominant)	(m s^{-1})
11/04/2003	396.0	441.9	2121.7	SE	0.2
12/04/2003	405.5	612.7	2329.0	SE	1.5
13/04/2003	388.9	376.7	2141.1	SE	3.2
14/04/2003	394.7	556.9	2215.0	E	2.8
15/04/2003	412.4	658.7	2407.6	E	0.6
16/04/2003	411.0	668.8	2301.4	NE	2.4
17/04/2003	396.2	473.0	2103.0	NE	4.8
18/04/2003	382.6	318.5	2010.4	NE	6.5
19/04/2003	380.1	282.1	1974.4	NE	8.4
20/04/2003	383.6	415.1	2104.4	E,NE	6.6
21/04/2003	383.3	314.1	2026.8	SE	1.9
22/04/2003	385.8	379.4	2023.0	NW	0.6
23/04/2003	400.6	520.4	2252.5	E	3.2

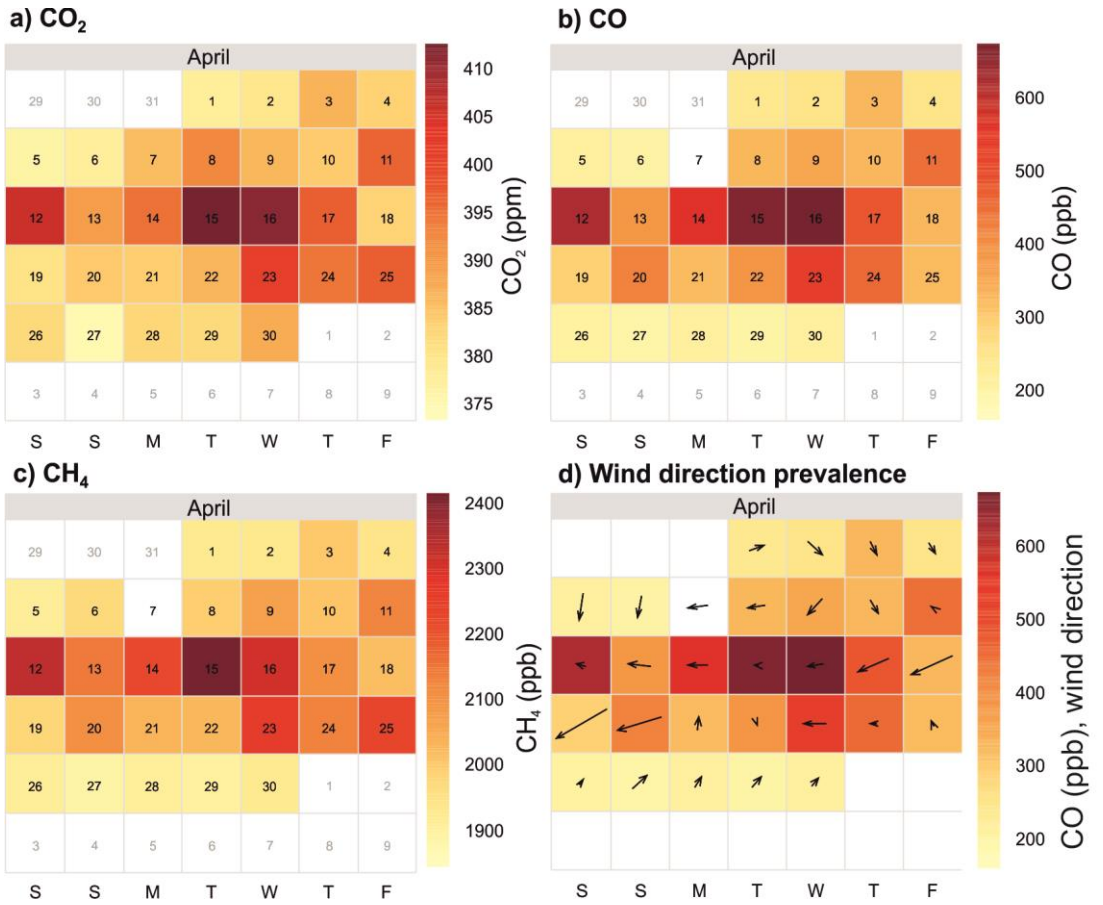

Figure 7.10(a). Calendar plot for CO_2; **(b).** CO; **(c);** CH_4; **(d).** CO and wind direction and scaled speed records at the EGH site during April 2003. Colour scale shows daily averages. For the scaled wind speed annotation means the longer the arrow, the higher the wind speed.

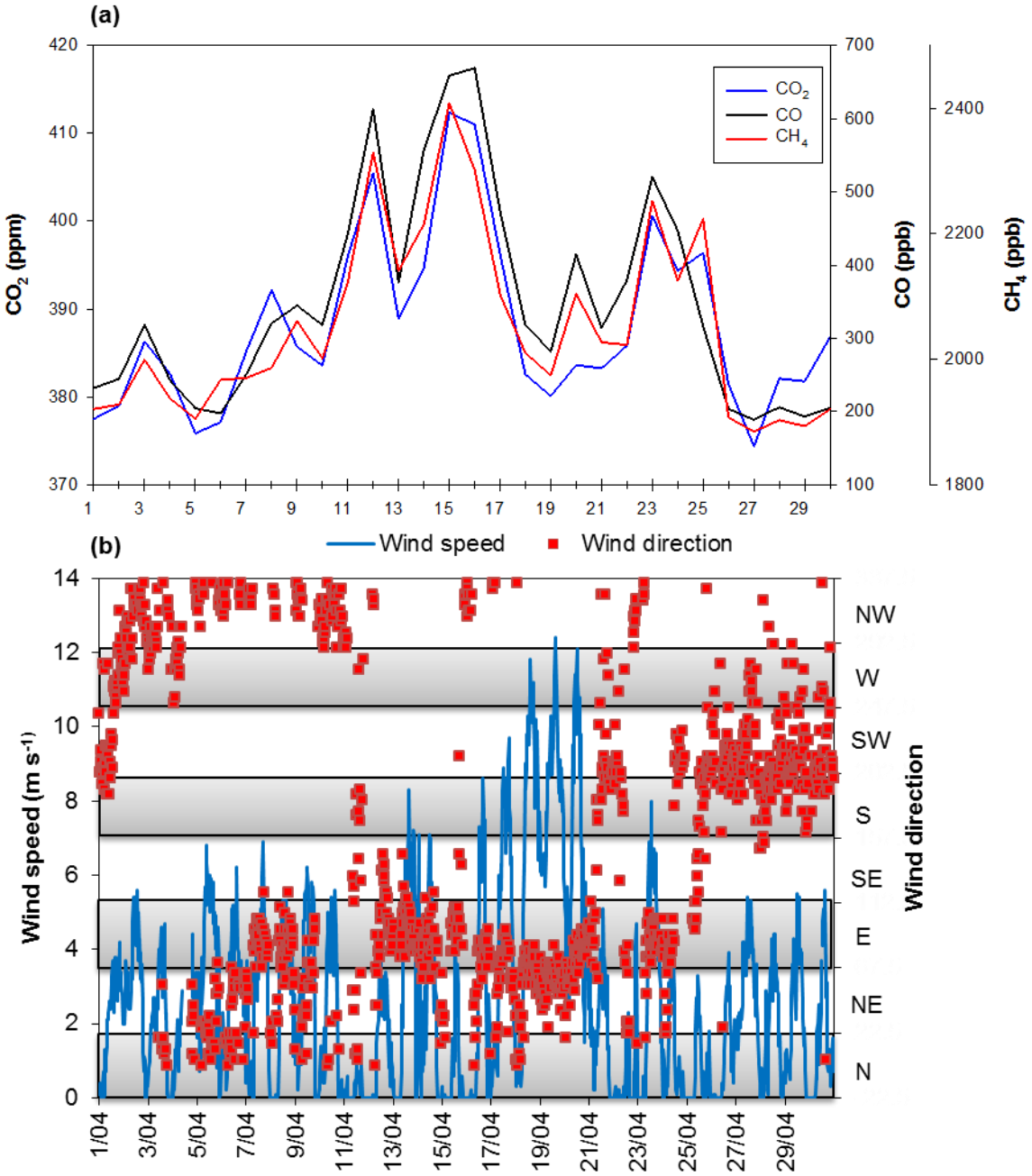

Figure 7.11(a). 30-min values of CO_2, CO and CH_4; **(b).** wind speed and wind direction measured at EGH from 11 to 23 April 2003.

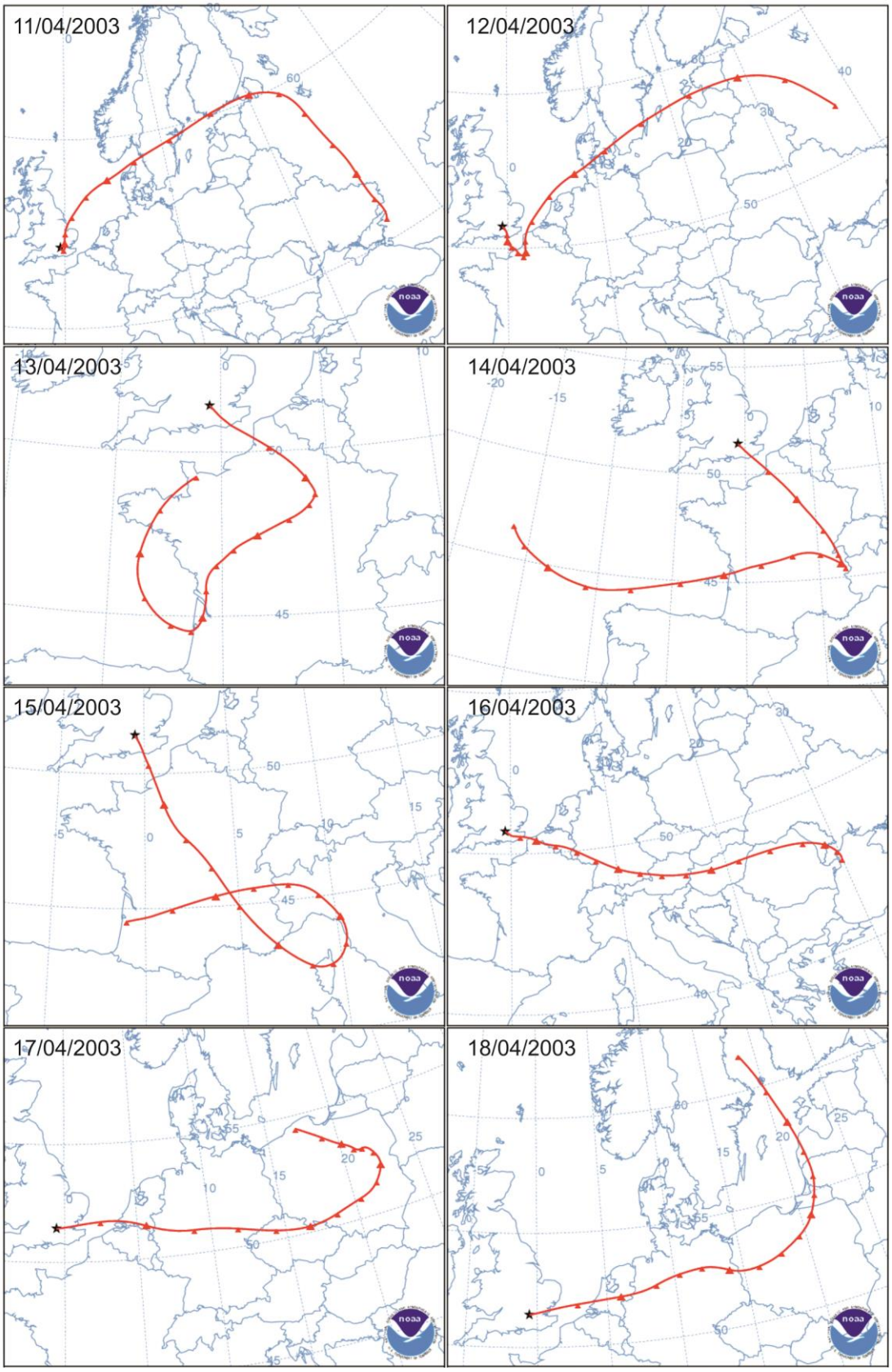

Figure 7.12. 96-hour air mass back trajectories arriving at EGH during the Easter Weekend Smog in April 2003 arriving at 12:00 of each day and at a height of 500 m above ground level.

7.3. Assessment of background conditions for CO_2, CO and CH_4 at EGH

Air pollutant concentrations are influenced by emissions from local sources and sinks under low wind speed conditions, particularly at night when they can be trapped under a shallow stable boundary layer (Derwent et al., 2002). Air pollutant levels are also affected by pollution episodes and increases in uptake by vegetation (Netcen, 2003; Barichivich et al., 2013). The concentration of air pollutants in the atmosphere is governed by the atmospheric motion. During low wind speed conditions pollutants will remain close to the ground and emitting sources and in strong wind speed conditions they will be dispersed and transported from their sources to different regions and sometimes even different latitudes (Morimoto et al., 2003) as layers at high altitudes in the troposphere. Therefore, in order to better assess the contribution to the CO_2, CO and CH_4 build-up close to EGH, the baseline for those carbon gases has to be calculated and then compared with records at MHD.

EGH CO_2, CO and CH_4 records include both frequent background input of SSW-SW Atlantic air, and episodic easterly polluted air masses. By identifying both components in detail it can be demonstrated whether the long-term trends observed are dominated by a changes of global or local sources. EGH receives maritime background air surprisingly frequently. Prevailing SSW-SW air masses move up the English Channel, and make landfall over Hampshire at altitude, then descend as they pass over largely wooded land close to Egham. The prevailing wind at Egham is SSW (Chapter 3). Winds are very variable in all seasons though SSW winds are common in summer (June-September), and also in spring (March-June). In both these quarters the Atlantic air dominates. In contrast, in Autumn (October-December) the dominant air masses often have strong local source inputs.

Background conditions at EGH were established to remove air masses not representative of atmospheric background conditions (Bousquet et al., 1996). At the EGH site background conditions for CH_4 correspond to wind direction of 203° to 247.5° (southwesterly) at wind speeds higher than 4 m s^{-1} (Lowry et al., 2001). CO_2, CO and CH_4 records were categorised as the overall data set, records for wind speeds >4 m s^{-1} for southwesterly air masses. Filtered records for wind speeds >4 m s^{-1} are compared with the CO_2, CO and CH_4 records at MHD.

7.3.1. CO_2 background conditions at EGH

Similarly to MHD, CO_2 background conditions at EGH correspond to air masses arriving from the SW sector 203° - 247.5° and for wind speeds greater than 4 m s^{-1} (Bousquet et al., 1996; Lowry et al., 2001). The overall data set at EGH was filtered considering this assumption to obtain the CO_2 data that represent background concentrations. Figure 7.13 shows the comparison of CO_2 records at the EGH site for the background sector (SW 203° - 247.5°) for the entire dataset with records at wind speeds >4 m s^{-1} (Derwent et al., 2002). For the background sector (SW), 25.0% (52,065 data points) of overall records were filtered. Data capture for CO_2 background concentrations is 1.38% (2,885 data points) of the overall data set.

Differences between EGH filtered monthly averages for background conditions (>4 m s^{-1}) and flask monthly averages at MHD were calculated by subtracting MHD monthly averages from EGH monthly averages. Figure 7.14 shows CO_2 monthly averages from flasks measurements at MHD and monthly averages at EGH from filtered background conditions for records at wind speeds >4 m s^{-1}. Differences ranged from -7.8 ppm CO_2 in April 2000 to 22.7 ppm CO_2 in October 2007. Such differences represent absolute variations of 2% and 6.0% relative to MHD averages, respectively, for the same months.

Statistical analyses carried out showed no significant difference (p>0.05) between CO_2 EGH background monthly averages and MHD flask monthly averages. This confirms that filtered EGH CO_2 data represent good background conditions and are in good agreement with CO_2 observations at MHD. It also suggests that the impact of CO_2 local emissions on the background sector is not significant to the calculated monthly averages. Uglietti et al. (2008) observed that long-term transport has a small influence on CO_2 records at the Jungfraujoch monitoring station in Switzerland. By contrast, they reported that local and regional CO_2 emissions and the biosphere strongly influence CO_2 measurements. That is in good agreement with observations at EGH, where the influence of CO_2 local emissions and the biosphere is observed at low wind speeds, even for the background sector and, that during the prevalence of background air masses (southwesterly) at wind speeds larger than >4 m s^{-1} CO_2 levels do not differ statistically to those recorded at MHD.

Zhou et al. (2003) determined the background conditions for CO_2 records at Mount Waliguan monitoring station (China) by removing hourly averages with standard

deviations >1ppm, retaining two consecutive hourly averages where the difference was <0.5 ppm and removing data associated with trajectories passing over the urban sector. They also removed CO_2 hourly averages during calm conditions and when the wind speed was >10 m s^{-1} or vertical wind speed >± 1m s^{-1}. The CO_2 filtered dataset at Waliguan station accounted for 70% of the overall dataset, which contrasts significantly with the filtered EGH dataset which accounted for 1.38% of the overall dataset. This is explained by the location of Waliguan station, which is surrounded primarily by a natural environment of sparse vegetation and desert, whereas EGH station is surrounded by large areas of forests and important urban areas, and its proximity to the most loaded motorway (M25) in the UK.

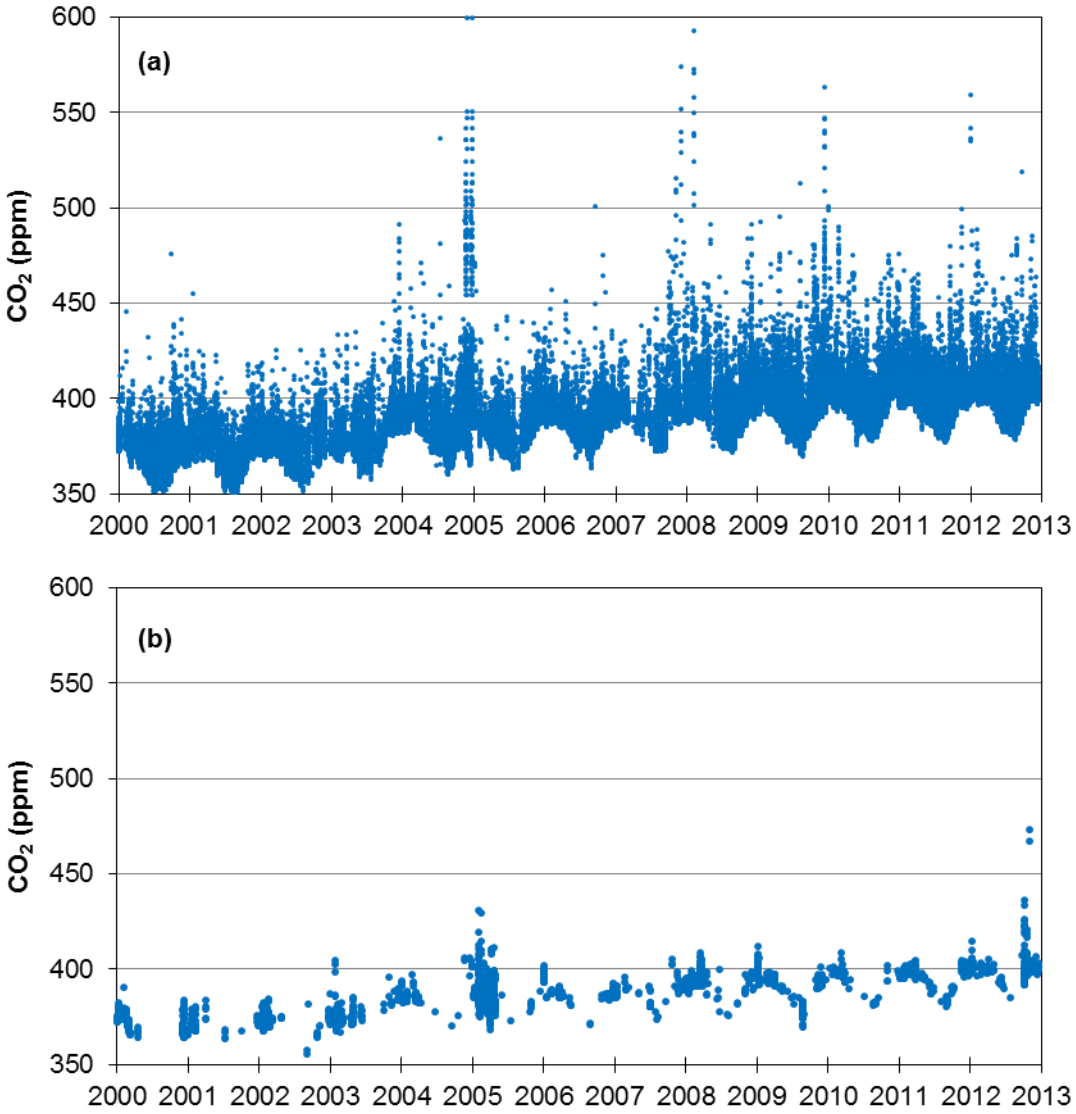

Figure 7.13(a). Comparison of CO_2 records at the EGH site for the background sector (SW 203° - 247.5°) for the entire dataset; **(b).** records at wind speeds >4 m s^{-1} during 2000-2012.

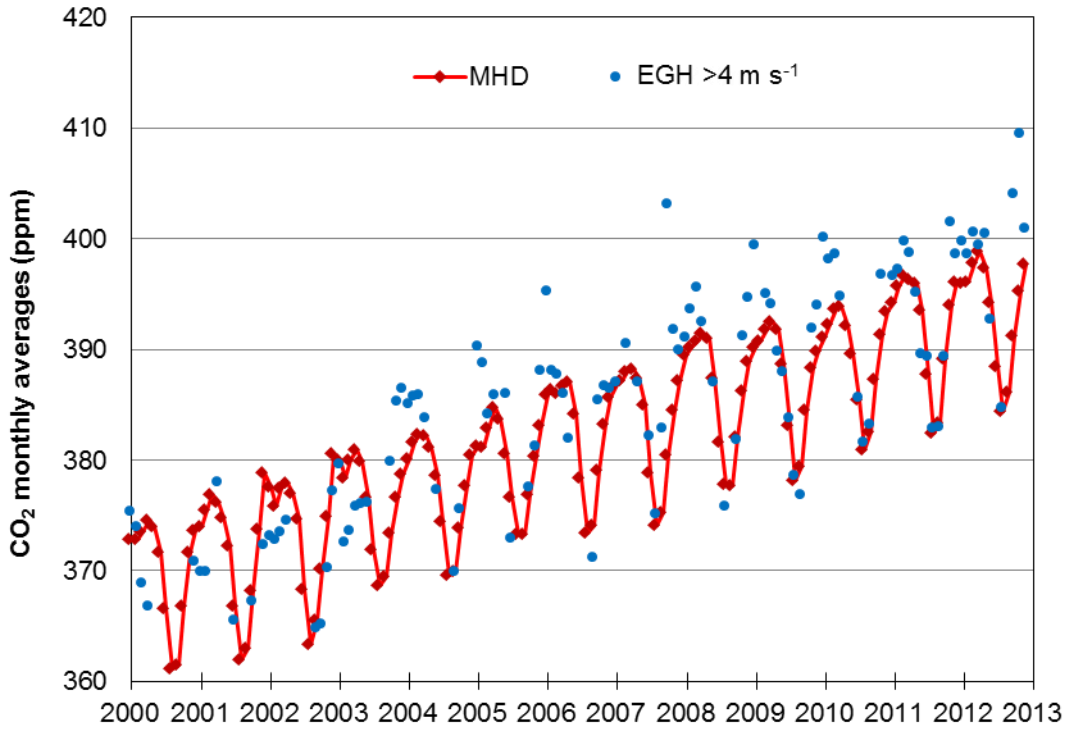

Figure 7.14. CO_2 monthly averages from flask measurements at MHD and monthly averages at EGH from filtered background conditions for records at wind speed >4 m s^{-1}.

7.3.2. CO background conditions at EGH

CO background levels at EGH were filtered from overall records to remove data that are not representative of background conditions. Lowry et al. (2001) reported that at EGH, background conditions correspond to air masses between 203° - 247.5° at winds speeds >4 m s^{-1}. CO records were filtered considering the criteria of wind speeds >4 m s^{-1} to assess the variations in data capture and CO concentrations during the sampled period after filtering the records (Bousquet et al., 1996). Figure 7.15 shows the comparison of CO records at the EGH site for the background sector (SW 203° - 247.5°) for the entire dataset with records for wind speeds >4 m s^{-1}. CO overall records for the background sector correspond to data capture of 25.0% (49,631 data points) of the total data captured (195,831 data points) during 2000-2012 at EGH. Background records after filtering the background overall records for wind speeds >4 m s^{-1} are 1.3% (2,571 data points).

CO monthly averages for background conditions (wind speeds >4 m s-1) at EGH were compared with CO monthly averages from flasks measurements at MHD to the assess variability of CO levels during the sampled period. Figure 7.16 shows CO monthly averages from flasks measurements at MHD and monthly averages at EGH from filtered background conditions for records at wind speeds >4 m s^{-1}.

Differences between EGH and MHD monthly averages were calculated by subtracting MHD monthly averages from the EGH monthly averages. Differences ranged from -31.5 ppb CO in December 2004 to 135.9 ppb CO in July 2001. Such differences represent absolute variations of 24.6% (December 2004) for CO levels higher at EGH, however for July 2001, a difference of 156% for CO higher concentrations at MHD was calculated.

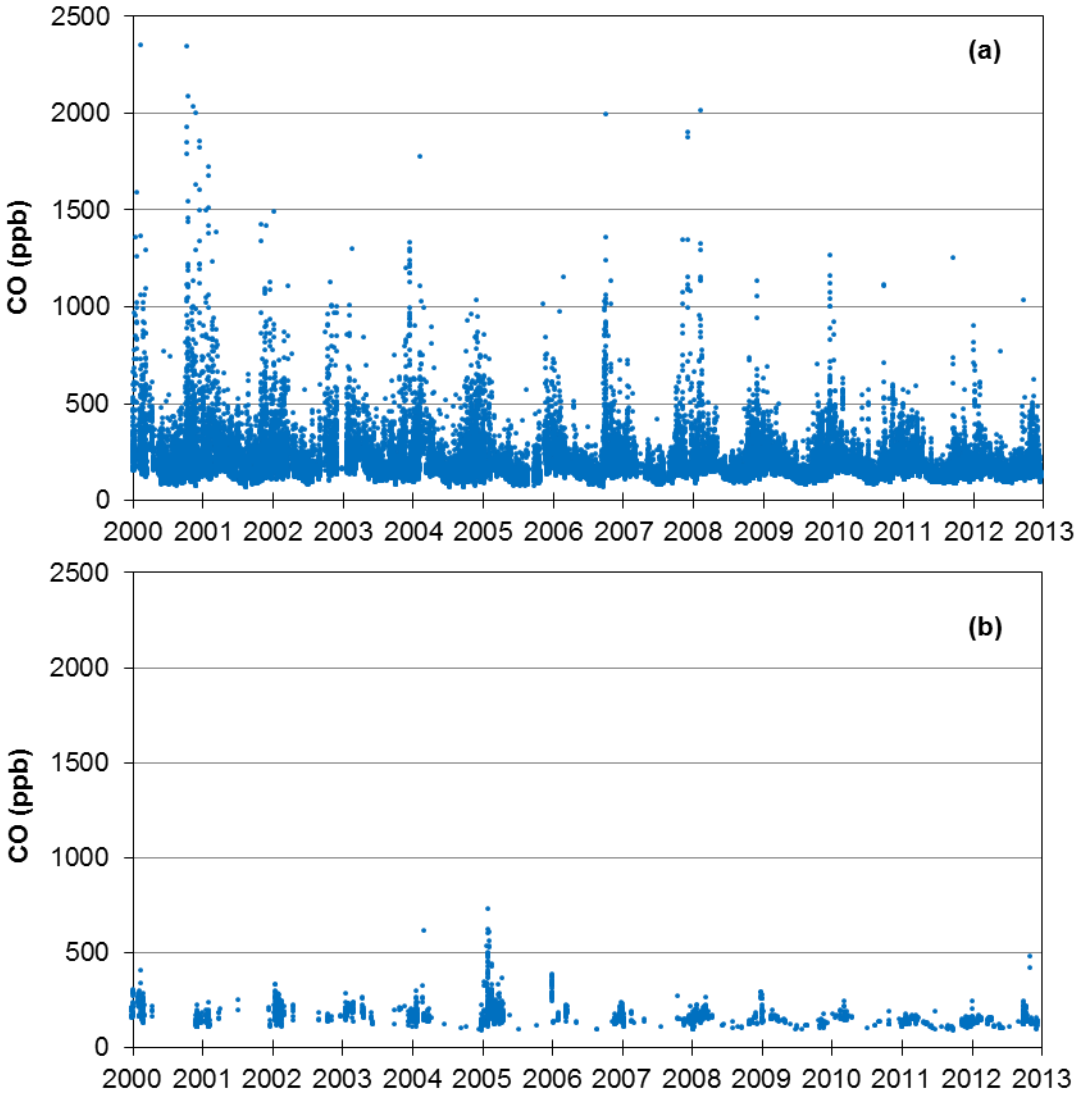

Figure 7.15(a). Comparison of CO records at the EGH site for the background sector (SW 203° - 247.5°) for the entire dataset; **(b).** records at wind speeds >4 m s^{-1} during 2000-2012.

Statistical analyses showed significant difference (p>0.05) between EGH CO background monthly averages and MHD flasks measurements. Such difference might be due to addition of CO from local sources even during background conditions. Xu et al. (2011) observed at the Wuqing station in the North China Plain the lowest CO concentrations (<1 ppm CO) during the prevalence of air masses

from the background sector. The CO concentrations were similar for records at wind speed >4 m s^{-1} even when the air masses passed over sub-urban regions. By contrast, they observed high CO concentrations when wind speeds were <2 m s^{-1}. At the EGH site, higher CO monthly averages than at MHD were calculated even for background conditions. This suggests an important contribution of local source emissions to explain the differences. Xu et al. (2011) also observed high CO concentrations over the urban areas based on satellite observations compared to the peripheries. This is in good agreement with the CO records for the sub-urban sectors at EGH which showed higher CO concentrations than the background and clean sectors.

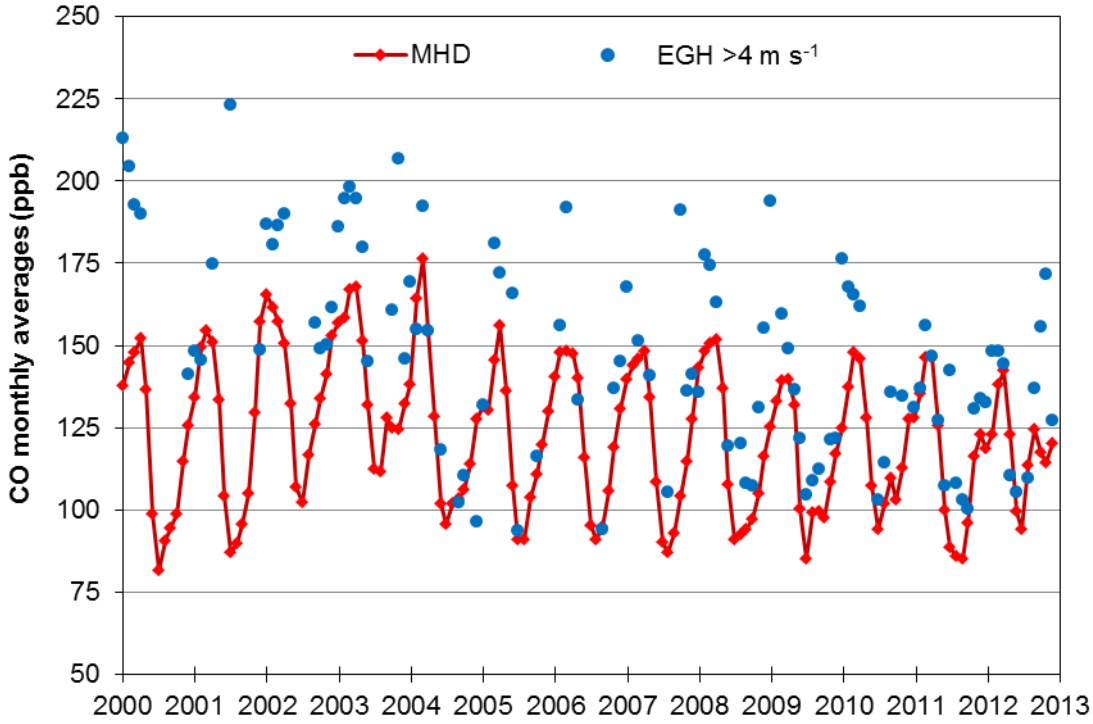

Figure 7.16. CO monthly averages from flasks measurements at MHD and monthly averages at EGH from filtered background conditions for records at wind speeds >4 m s^{-1}. As local CO emissions have reduced over time the EGH CO is now closer to the MHD concentrations.

Zellweger et al. (2009) carried out CO measurements at the Jungfraujoch station in Switzerland during 1996-2007. They discriminated CO records during background conditions and during pollution events. They also observed that even at this background station, CO concentrations can be greatly affected by the development of pollution events which increase background concentrations by up to 400%. At EGH, the background monthly averages calculated are relatively higher than monthly averages at MHD during winter. This could be explained by shallower

boundary layers which trap CO emissions close to the ground and that during low wind speeds are not dispersed. CO monthly averages for background conditions are closer to MHD monthly averages with differences <5% during summer, which suggests that CO emissions are diluted by the advection of clean air masses.

7.3.3. CH_4 background conditions at EGH

Similar to the CO_2 and CO records, CH_4 background concentrations at the EGH were calculated by filtering the overall data set for wind direction between 203° – 247.5° and wind speeds >4 m s^{-1}. Figure 7.17 shows the comparison of CH_4 records at the EGH site for the background sector (SW 203° - 247.5°) for the entire dataset with records at wind speeds >4 m s^{-1}. CH_4 records for the background sector (SW) at EGH represent 25% (50,791 data points) of the overall data (202,799 data points) during 2000-2012. Filtered data for background conditions (wind speeds >4 m s^{-1}) are 1.3% (2,640 data points).

To assess differences between EGH CH_4 background concentrations and MHD CH_4 levels, monthly averages from flasks measurements at MHD are compared with monthly averages at EGH from filtered records (wind speeds >4 m s^{-1}). Differences were calculated by subtracting CH_4 monthly averages from the EGH monthly averages (Figure 7.18). Differences ranged from -32.4 ppb CH_4 June 2003 to 93.0 ppb CH_4 in December 2012. Such differences represent absolute variations between 1.8% higher and 4.9% lower CH_4 concentrations at MHD than at EGH.

Minimum significant difference (p<0.05) was found between CH_4 flasks measurements at MHD and background monthly averages at EGH. Lowry et al. (2001) reported that the excess of CH_4 recorded at EGH is due to local emissions nearby the monitoring station. Such differences increase during winter and are ascribed to higher emissions from increased use of natural gas and incomplete combustion due to enhanced domestic heating use and to shallower PBL, which trap emissions close to the ground. Differences between monthly averages at EGH and MHD decrease during summer months due to the prevalence of enhanced mixing which decreases the ambient CH_4 concentrations recorded.

Sanchez et al. (2013) studied CH_4 records at a rural site on the Spanish Plateau from June 2010 to May 2012. They discriminated between air masses not representative of background conditions and air masses containing CH_4 loading

from local sources, and observed that local sources yielded an increment about 40.8 ppb CH_4 compared with background concentrations. At the EGH site, great influences of CH_4 local sources were observed even for the background sector even during background conditions, which is in good agreement with the observations of Lowry et al. (2001). Such contributions explain the differences observed with records at MHD and denote the importance of evaluating CH_4 sources close to EGH.

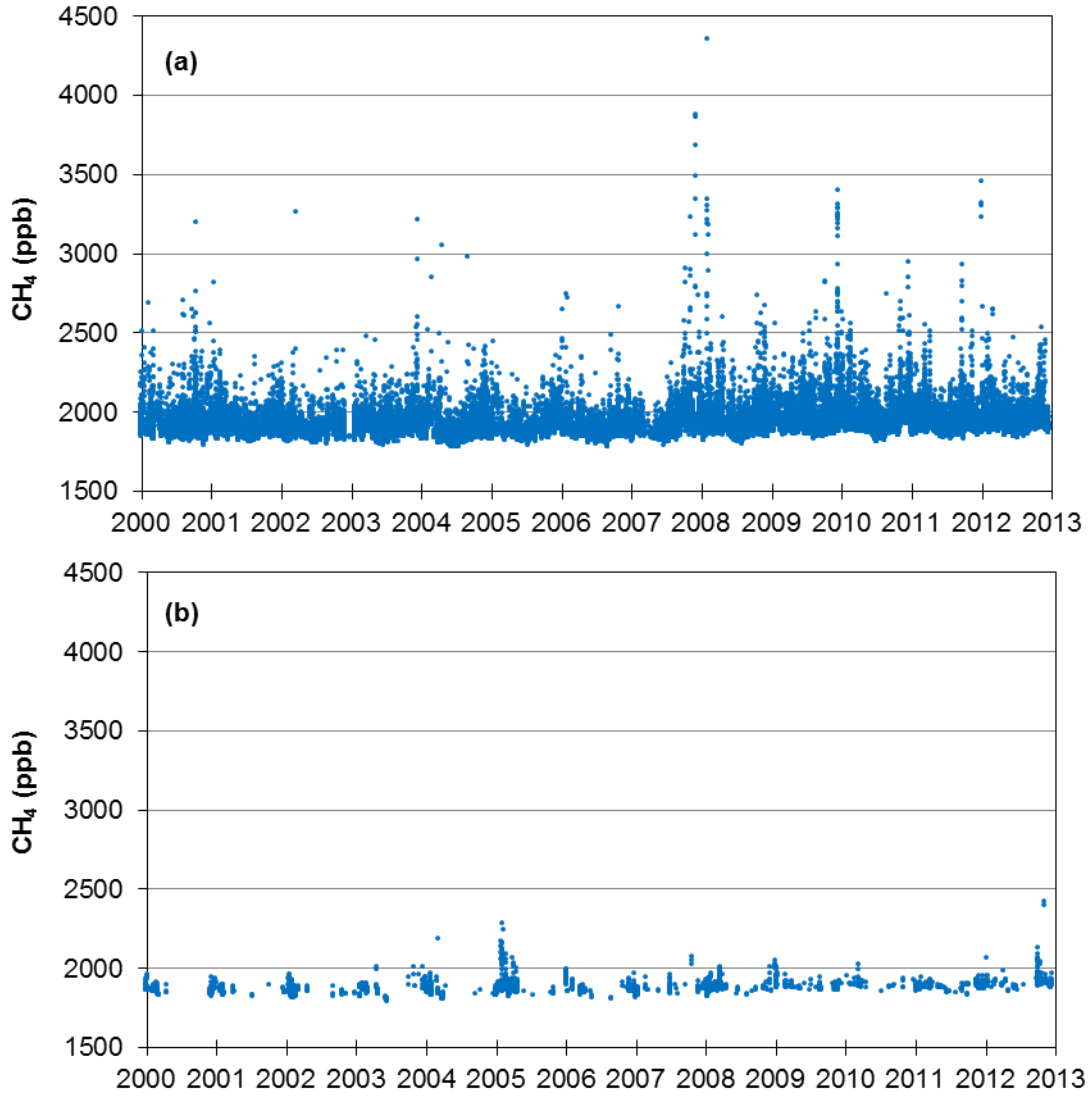

Figure 7.17(a). Comparison of CH_4 records at the EGH site for the background sector (SW 203° - 247.5°) for the entire dataset; **(b).** records at wind speeds >4 m s^{-1} during 2000-2012.

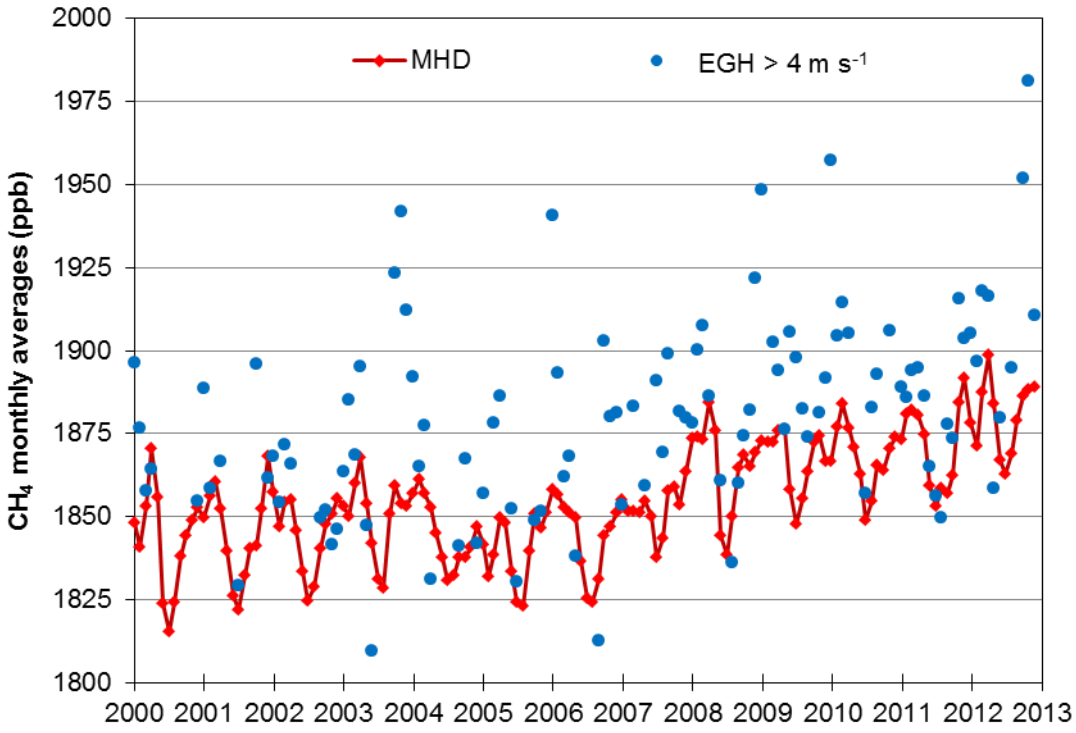

Figure 7.18. CH_4 monthly averages from flasks measurements at MHD and monthly averages at EGH from filtered background conditions for records at wind speeds >4 m s^{-1} during 2000-2012.

7.4. Comparison of long-term trends between background records at EGH and MHD and with the UK Greenhouse Gas Inventory and National Emissions Inventory

7.4.1. CO_2 long-term trends from background records at EGH and MHD and comparison with the UK Greenhouse Gas Inventory

The long-term trend for CO_2 background records at EGH was compared with the CO_2 long-term trend at MHD during 2000-2012. At EGH, CO_2 background annual averages were calculated from background monthly averages. Annual averages for CO_2 records at MHD were calculated from monthly averages of flask measurements. Figure 7.19 shows the CO_2 long-term trends calculated with the Mann-Kendall test and Sen's estimate and residuals at EGH and MHD during 2000-2012. A significant growth rate (p<0.001) of 2.30 ppm CO_2 yr^{-1} was calculated for background records at EGH, whereas a growth rate of 1.97 ppm CO_2 yr^{-1} (p<0.001) was calculated at MHD. Annual residuals at EGH ranged from -14.0 ppm CO_2 in 2005 to 15.6 ppm CO_2 in 2000, whilst at MHD residuals ranged from -14.5 ppm in 2005 to 5.8 ppm in 2012. Interestingly, the lowest annual residuals coincided in 2005 but the largest residual at EGH was in 2002 and in 2011 at MHD.

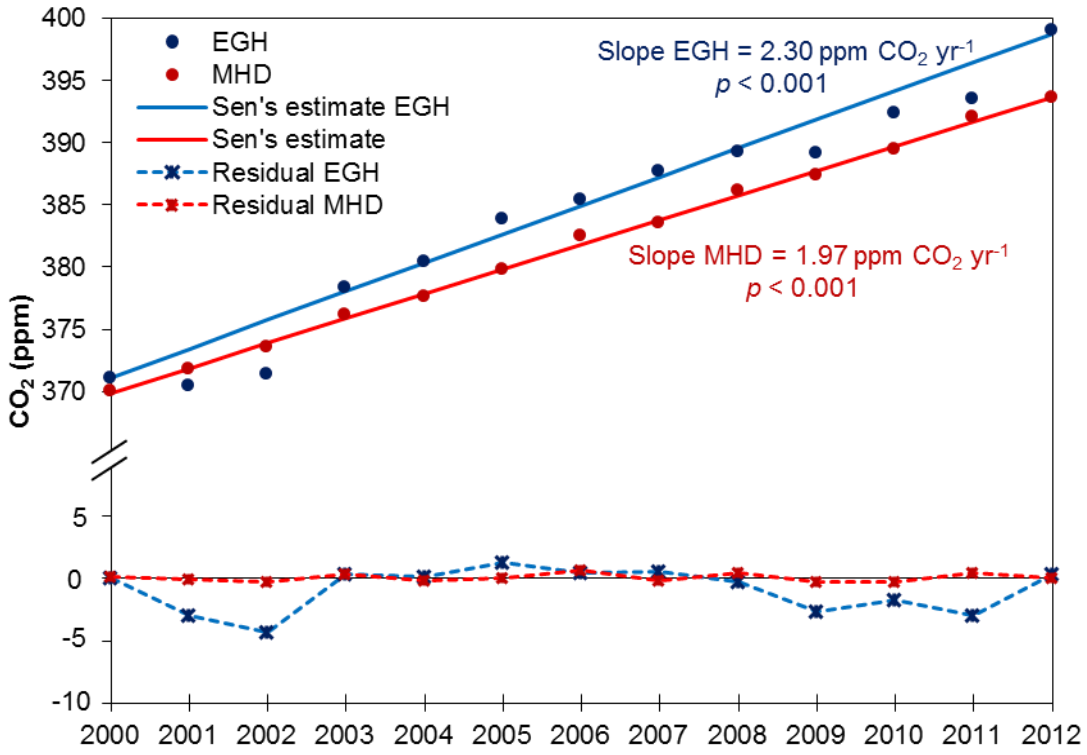

Figure 7.19. CO_2 long-term trends calculated from annual averages during background conditions at EGH (SW, wind speed >4 m s^{-1}) and from flasks measurements at MHD. Upward trends were calculated with the Mann-Kendall test and Sen's estimate.

No significant differences (p>0.05) were found between annual averages at EGH and MHD during 2000-2012. The CO_2 growth rates observed at EGH during 2000-2012 (2.30 ppm CO_2 yr^{-1}) and at MHD (1.97 ppm CO_2 yr^{-1}) are in good agreement with the growth rates observed at MLO monitoring station, which ranged between 1.56 ppm CO_2 yr^{-1} in 2004 to 2.66 ppm CO_2 yr^{-1} in 2012 (Tans and Keeling, 2014). The CO_2 growth rate at EGH is 0.43 ppm yr^{-1} larger than the global average growth rate during 2000-2003 (1.87 ppm CO_2 yr^{-1}) and 0.23 ppm CO_2 yr^{-1} larger than the global average growth rate (2.07 ppm CO_2 yr^{-1}) during 2004-2012 (NOAA/ESRL, 2014).

The UK GGI (2014) reports a total decrease of 15.9% in CO_2 emissions from 2000 to 2012 with emissions from the transport and energy sectors declining by 32.2% and 5.0%, respectively. By contrast, CO_2 ambient concentrations at EGH recorded during the 2000-2012 show a total increase of 7.5%. This increase is in good agreement with CO_2 observations carried out worldwide (Table 4.1), which show that CO_2 concentrations increase year to year in the atmosphere (Aulagnier et al., 2010; Ramonet et al., 2010; Manning et al., 2011; Zhang and Zhou, 2013). Interestingly, despite the decrease in CO_2 emissions reported by the UK GGI

(2014), records at EGH show the appearance of new local CO_2 sources as discussed in section 7.1.1 and that global atmospheric circulation dominates the CO_2 long-term trends (Tans and Keeling, 2014).

7.4.2. CO long-term trends from background records at EGH and MHD and comparison with the UK NAEI

Long-term trends for background CO at EGH were compared with the long-term trend at MHD to examine changes in ambient CO concentrations. Background CO annual averages at EGH during 2000-2012 were calculated from data filtered under background conditions. Annual CO averages at MHD were calculated from flasks measurements during 2000-2012. Figure 7.20 shows the CO long-term trends calculated at EGH during background conditions and from flasks measurements at MHD with the Mann-Kendall test and Sen's estimate. At EGH, a CO decline rate (p<0.01) of 4.09 ppb CO yr^{-1} was calculated, which much more that the CO decline rate at MHD (p<0.05) of 0.83 ppb CO yr^{-1}. Annual CO residuals ranged between -18.57 to 19.10 ppb CO at EGH, and -7.48 to 15.24 ppb CO at MHD. The lowest CO residual at EGH was observed in 2004 whereas at MHD it was in 2000. Interestingly, the largest residuals coincided in 2003.

Statistical analyses were carried out to test difference in the decline CO rate at EGH and MHD. Minimum significant difference was observed (p<0.001) for annual CO averages at EGH and MHD. CO decline rates at EGH and MHD were compared with records at MLO to test if they fit the observed global trend. The CO decline rates observed at EGH and MHD are within the CO decline rate observed at the MLO station, which ranged between -11.93 ppb CO in 2008 to 9.01 ppb CO in 2007. Significant differences (p<0.001) were observed between CO annual averages at EGH and MLO and also for records at MHD and MLO. The decline rate at EGH is 5 times larger than at MLO where it is 0.80 ppb CO. The decline rate at MLO is in good agreement with that observed at MHD (0.83 ppb CO).

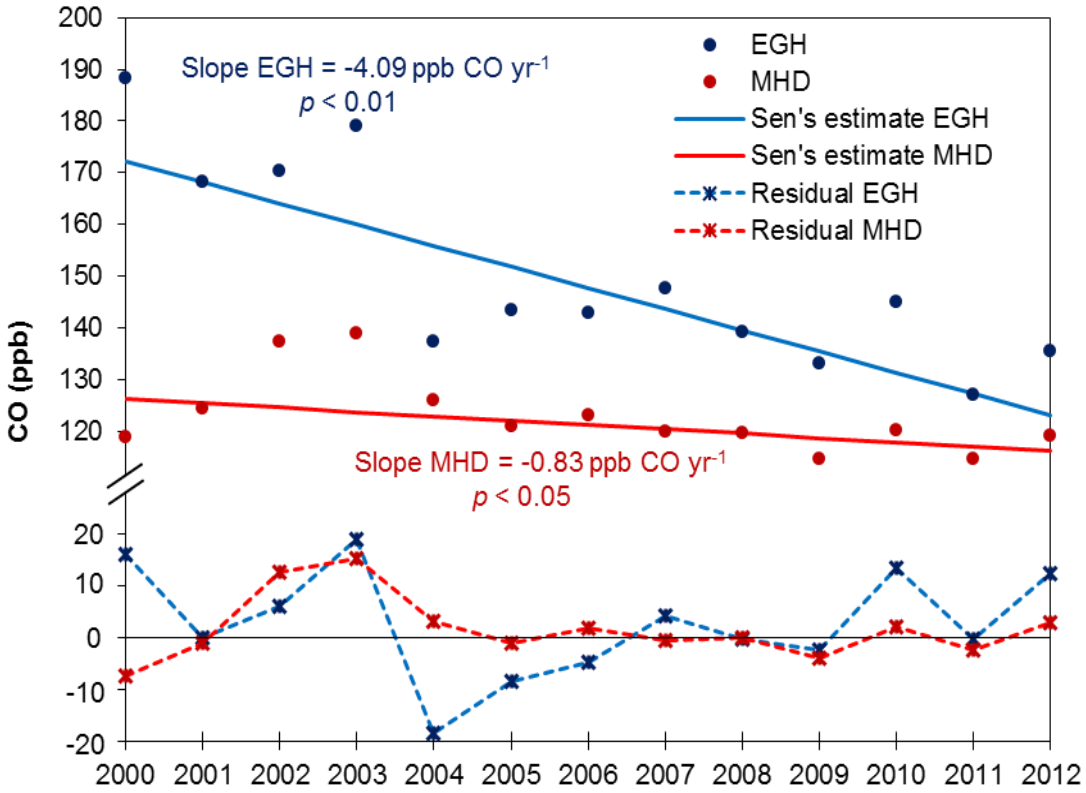

Figure 7.20. CO long-term trends calculated from annual averages during background conditions at EGH and from flask measurements at MHD. Decline trends were calculated with the Mann-Kendall test and Sen's estimate.

CO emissions in the UK have decreased linearly (p<0.001) since 2000 at a rate of 271 kt CO yr^{-1} (NAEI, 2013), this is reflected in background CO, which also decreases linearly during 2000-2012. Figure 7.21 shows the annual averages pf CO/CO_2 ratios expressed in ppb during 2000-2012 at EGH. A significant correlation in the decline ratio was found (p<0.05). The change in ratio is dominated by the large percentage decline in CO. The sustained decline in CO observed during 2000-2012 suggests a significant and progressive underlying improvement in air quality in the UK. This decline of CO concentrations at EGH (-4.78% yr^{-1}) is consistent with emission inventories as shown above. The cause of the decline is almost certainly the strict controls on vehicle emissions introduced by the EU and UK legislation to manage the air quality (Lowry et al., in preparation 2014).

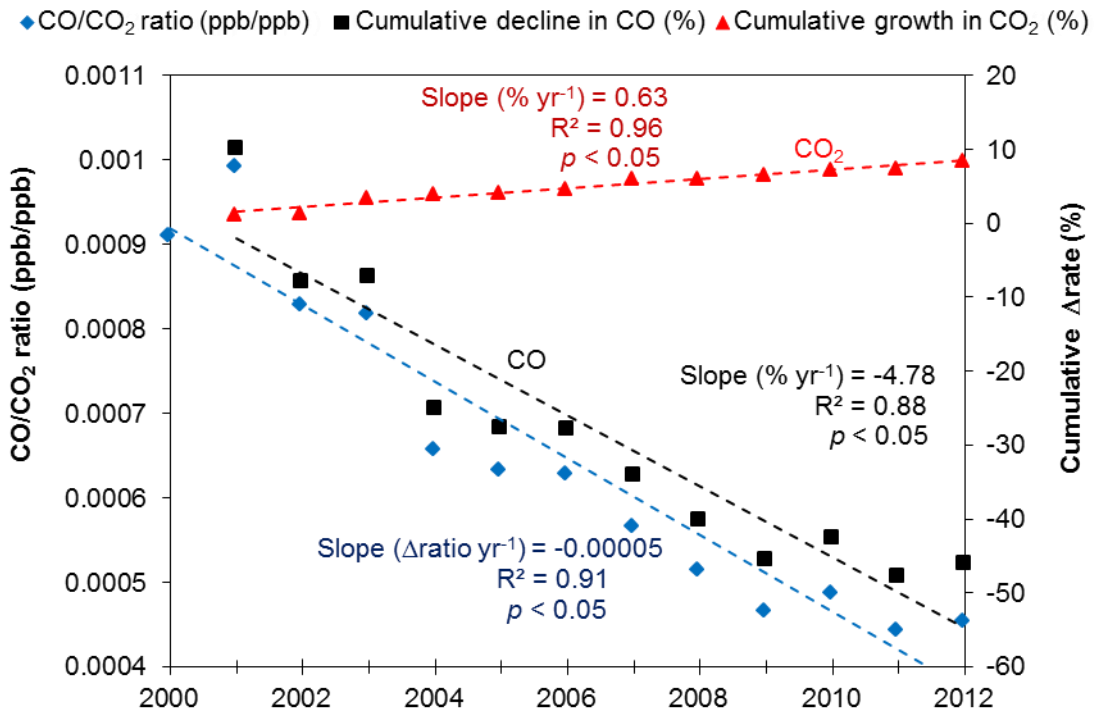

Figure 7.21. Ratios of CO/CO_2 annual averages at EGH during 2000-2012.

7.4.3. CH_4 long-term trends from background records at EGH and MHD and comparison with the UK NAEI

Long-term trend in annual averages of background CH_4 from 2000-2012 was compared with the long-term trend at MHD calculated from CH_4 flasks measurements. Figure 7.22 shows the CH_4 long-term trends at EGH and MHD calculated with the Mann-Kendall test and Sen's estimate. A significant growth rate (p<0.01) of 3.51 ppb yr^{-1} was calculated at EGH during 2000-2012, whereas at MHD the growth rate was 2.85 ppb yr^{-1} (p<0.05). Annual residuals at EGH ranged from -13.98 ppb CH_4 to 18.09 ppb CH_4, whilst at MHD ranged from -14.48 ppb CH_4 to 5.79 ppb CH_4. Interestingly, the CH_4 lowest residuals coincided in 2005, and the largest residuals were observed at EGH in 2003 and in 2012 for MHD.

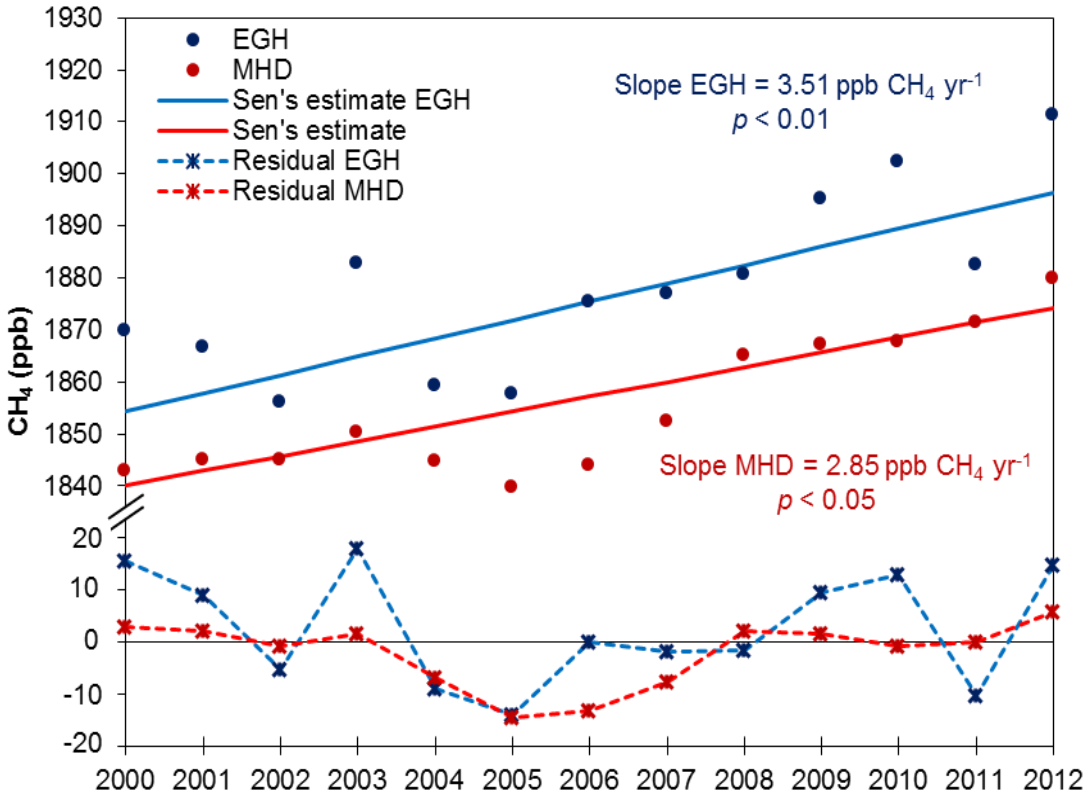

Figure 7.22. CH_4 long-term trends calculated from annual averages during background conditions at EGH and from flasks measurements at MHD. Upward trends were calculated with the Mann-Kendall test and Sen's estimate.

Statistical analyses were carried out to test differences between CH_4 growth rates at EGH and MHD. Minimum significant difference (p<0.001) was observed for CH_4 background annual averages at EGH and MHD. CH_4 growth rates at EGH and MHD are compared with CH_4 records at the MLO monitoring station (which are close to CH_4 global averages) to test if they fit the global increasing trend of atmospheric CH_4 (NOAA/ESRL, 2014). At MLO, the CH_4 long-term trend during 2000-2012 was calculated from flasks measurements. A significant CH_4 growth rate of 3.07 ppb CH_4 yr^{-1} was observed at MLO. At MLO, such trend is 1.07 times larger than at MHD, whereas it is 0.87 times of the trend observed at EGH. The statistical differences observed between growth rates at MHD and MLO, and MLO and EGH are due to contrasting environments surrounding the sampling station. At EGH the largest CH_4 growth rate may be explained by increases in emissions from local sources as discussed in section 7.1.3. The UK GGI (2014) reports a decline in CH_4 emissions of 35.2% during 2000-2012, which contrasts with the increase in CH_4 ambient concentrations recorded at EGH, even for background data, which increased 2.2%. The increase at EGH follows the CH_4 global atmospheric trend but at a higher rate. This is due to the increase of local CH_4 sources as shown in section 7.1.3.

7.5. Summary

The combined interpretation of bivariate polar plots and cluster analysis for carbon gas data recorded at EGH during 2000-2012 showed that the most important sources are located to the NE, E and SE of EGH. High concentrations of CO_2 were recorded when air masses arrived from the SE sector at wind speeds <2 m s^{-1} and >7.5 m s^{-1}. The highest concentrations of CO were observed when air masses arrived from the E sector at wind speed >8 m s^{-1}. Interestingly, the highest concentrations of CH_4 were recorded in air masses arriving at EGH from NE at wind speed <2 m s^{-1}. By contrast, the lowest concentrations of CO_2, CO and CH_4 were measured in air masses from SW and W sectors.

Records of ambient CO_2, CO and CH_4 at EGH show the occurrence of summer, winter and long-range transport pollution episodes during 2000-2012, which have been also observed at other monitoring stations in SE England (LAQN, 2014). During summer 2003, two pollution episodes were recorded at EGH from 11-18 July and 1-18 August. Such pollution episodes were ascribed to the transport of air pollutants emitted in the London region to EGH during hot and calm weather (low wind speed).

A winter pollution episode was observed at EGH from 12-21 January 2012. The combined increase in concentrations of CO_2, CO and CH_4 recorded was attributed to low wind speeds and calm weather. Air mass back trajectories analyses show the transport of emissions in air masses passing over the London region and then arriving at EGH, which explains the increase in levels of carbon gas observed. A long-range transport episode was observed in SE England from 12-13 April 2003. At central London, several stations of the LAQN recorded high concentrations of ozone and PM_{10}. Records at EGH show a combined increase of CO_2, CO and CH_4 concentrations during the occurrence of the episode. The elevated concentrations of air pollutants observed in in SE England were ascribed to transport of emissions from the east region of Europe and London region which was confirmed with air mass back trajectories analysis.

8. CONCLUSIONS AND FUTURE WORK

The world has developed drastically during the last 60 years. Nowadays, there are more than 10 times the number of cars than in 1950s, the number of people living in urban areas has increased by a factor of four, which has triggered the energy demand by a factor of five (Fenger, 2009). Such development has brought environmental problems as the atmospheric increase of levels of air pollutants and GHGs (IPCC, 2013).

GHGs and air pollutants are emitted from anthropogenic activities related to productions of fuels, domestic and industrial combustion, transportation, waste disposal, industrial processes and agriculture. Concern about human health has motivated the implementation of air quality policies worldwide to decrease air pollutants emissions. On the other hand, the unprecedented changes in the weather system since 1950s have motivated governments and scientific community not only to study and interpret the observed changes but also to issue policies to mitigate GHGs emissions.

In the UK, since the establishment of the Air Quality Strategy in 1997 and the Climate Change Act in 2008, the emissions of air pollutants and GHGs have decreased notably (NAEI, 2013; GGI, 2014). The UK NAEI reports that emissions of CO declined by 77% during 1990-2011. On the other hand, the UK GGI reports that emissions of CO_2 and CH_4 decline by 20% and 51%, respectively during 1990-2012. The decline in CO emissions was dominated by the reduction in emissions from the road transport sector due to the implementation of three-way catalysts in automobiles. The decline in CO_2 emissions was driven by reduction in emissions from the energy industry related to the change from coal and oil towards use of gas. Also the shift from conventional steam stations (36.0% efficiency) burning coal and oil towards use of CCGT (47.7% efficiency) and the slight increase in electricity generated from non-fossil fuel have contributed to mitigate CO_2 emissions. CH_4 decline has been driven by reduction in emissions from coal mining activity, improvements to the gas network distribution, decline in emissions from the waste sector due to the implementation of CH_4 recovery systems at landfill sites and decline in emissions from agriculture as consequence of decreasing livestock numbers.

In this thesis the objective was to study and interpret inter-annual and seasonal variations, quantify long-term trends and understand the origins of concentrations of CO_2, CO and CH_4 at the EGH site during 2000-2012. Additionally, data recorded at EGH was aimed to compare with data at MHD background station to predict changes in response to measures to control CO_2, CO and CH_4 emissions (Lowry et al., in preparation 2014; Hernandez-Paniagua et al., submitted 2014a).

8.1. Interpretation of CO_2 records

Continuous high-precision and high-frequency CO_2 data recorded at EGH were used to estimate CO_2 growth rate from 2000 to 2012. CO_2 concentrations varied on time scales ranging from minutes to inter-annual and annual cycles. The greatest concentrations were recorded for winds from the E and SE sectors, representing CO_2 transported from anthropogenic sources in the London region and continental Europe. The lowest concentrations were observed for the S and SW sectors, where air travels from the Atlantic Ocean over a maximum of 100-150 km of semi-rural England.

The diurnal cycle of CO_2 varied with patterns of atmospheric transport and heating use, and biologically with length of daylight. Week-long cycles were strongly influenced by anthropogenic emissions during weekdays when fossil fuel burning and combustion processes are higher than at weekends. Seasonal cycles were driven by temporal variations in human behaviour, atmospheric transport and in photosynthesis. Annual cycles exhibited maxima and minima in winter and late summer, respectively. The smallest seasonal amplitude of CO_2 observed was 17.0 ppm in 2003 and the largest was 27.1 ppm in 2008. This underlies an increasing trend in seasonal amplitudes observed at other northern hemisphere locations.

An annual averaged growth rate of 2.45 ppm yr^{-1} (p<0.05) of CO_2 was calculated at EGH during 2000-2012. The growth rate observed at EGH was presumably due to local and regional increases in CO_2 emissions from fossil fuel combustion. The faster rate of increase at EGH compared to the global upward trend is not consistent with the decreasing trend in CO_2 emissions reported in the UK NAEI, probably due to the continuing increases in traffic on the motorways west of London. More continuous long-term measurements of CO_2, particularly in regions of high emissions, are required to better understand the growth rate.

8.2. Interpretation of CO records

Continuous high-precision and high-frequency CO data recorded at EGH were used to estimate CO decline rate from 2000 to 2012. Variations on time scales ranging from minutes to inter-annual and seasonal cycles were observed for the CO data set recorded. Daily means recorded during 2000-2012 for CO exhibited significant decline. The very high concentrations of the early 2000s were less frequent. Peak values post-2010 were much closer to the minimum values recorded. Wind sector analysis showed that the CO largest concentrations were measured in air masses from the E and NE sectors, which is related to the transport of CO emissions from the London region and Heathrow airport. By contrast, the lowest concentrations were observed for air masses from the S and SW (background) sectors, which is explained by the existence of few CO sources lying on such sectors.

The analysis of the CO diurnal cycle revealed that concentrations were strongly influenced by PBL height which changed with length of daylight and by changes in the traffic patterns (higher during weekdays than at weekends and therefore larger emissions during weekdays than in weekends). Seasonal daily cycles of CO at EGH typically comprise two peaks and troughs. The morning-peak shifts season-to-season whereas the afternoon trough is always recorded by 14:00 GMT. Larger AV_d were observed during winter due reduced vertical mixing and poor dispersion than AV_d during summer when the convective processes in the atmosphere are enhanced and the rate of OH production peaks.

The seasonal cycle was driven by changes in meteorological conditions, PBL height and, to a lesser extent, changes in anthropogenic emissions. The largest concentrations were recorded during winter when the emissions from domestic heating are the highest. The largest seasonal AV observed at EGH was 399.7 ppb CO in 2001 and the lowest was 115.6 ppb CO in 2012. A statistically significant declining trend in AV_s of -16.4 ppb CO yr^{-1} was observed at EGH. Such trend is influenced by the decline in CO emissions in the UK during 1990-2011.

The statistical analysis of annual averages of CO exhibited a declining trend during 2000-2012. The non-parametric Mann-Kendall test showed a decline rate of 15.3 ppb CO yr^{-1}, which is a change of 3.6% CO yr^{-1}. Such decline is in good agreement with the decline trends of CO observed at the monitoring sites of North Kensington and Marylebone Road in the London area (Bigi and Harrison, 2010; von Schneidemesser et al., 2010). However the rate of change at EGH is lower by 3.4

times than that observed at Marylebone. The rate of change of CO recorded at EGH is lower by about 2-4 times than that reported for CO emissions in the UK during 2000-2011. However, it was lower by 5.6 times during 2009, which may be related to the cold weather experienced in 2010 and consequent increase in CO emissions (NAEI, 2013). Overall, the decline in CO for all sectors is clear and consistent with sustained reduction in emissions. The largest decline rate was observed for E sector and during calm conditions. By contrast, smaller declines were observed in the SW and S, background sectors, which show a consistent drop throughout the study period.

The sustained decline in CO observed during 2000-2012 suggests a significant and progressive underlying improvement in air quality in the UK, which is consistent with emission inventories. The cause of the decline is almost certainly the strict controls on vehicle emissions introduced by the UK legislation to manage the air quality.

8.3. Interpretation of CH_4 records

Atmospheric CH_4 was measured at high-precision and high frequency at EGH to estimate the decline rate during 2000-2012. 30-min values of CH_4 showed no clear trend with large variability. CH_4 ranged on time scales from inter-annual to annual cycles. The highest concentrations were recorded in air masses moving from E and NE sectors, which are related to CH_4 transported from anthropogenic sources in the London region and near EGH. The S and SW sectors showed the lowest concentrations, when air masses moved from the Atlantic Ocean and passed over a large wood area before arriving at EGH.

The diurnal cycle of CH_4 showed variations related to atmospheric transport and length of daylight. Anthropogenic emissions influenced weakly week-long cycles and similar AV_d were observed during weekdays and weekends. Seasonal cycles were driven by variations in meteorology and specifically in the PBL height. Annual cycles showed maxima in winter and minima in late summer. The largest seasonal AV observed was 169.9 ppb CH_4 in 2003, whereas the smallest AV was 90.8 ppb CH_4 in 2012. A not statistical significant declining trend in AV_s of 2.1 ppb CH_4 yr^{-1} was observed during 2000-2012. Such variation in the seasonal AV might be related to the decline in CH_4 emissions in the UK during 2000-2012 and to the global increase of the background levels of CH_4 since 2007.

CH_4 annual averages showed a not significant (p>0.05) declining trend of 0.27 ppb CH_4 yr^{-1} at EGH during 2000-2012. When data were split, an increasing trend at a rate of 6.2 ppb CH_4 yr^{-1} from 2000-2003, from 2003-2006 a declining trend at rate of 13.4 ppb CH_4 yr^{-1} and a steady state from 2006-2012 (slope= 2.5 ppb CH_4 yr^{-1}) were observed. None of these trend were significant at a level of p=0.05. The increase of CH_4 concentrations observed in 2007 at EGH is in good agreement with observations made at other monitoring stations in the NH (AGAGE/NOAA/ESRL), which has been ascribed to an increase of CH_4 emissions in the NH during 2006-2007 (Rigby et al., 2008a). The long-term trend of ambient CH_4 observed at EGH contrasts with the declining trend of CH_4 emissions of 1.9% yr^{-1} reported in the UK NAEI during 2000-2012.

8.4. Analysis of summer, winter and long-range pollution episodes of CO_2, CO and CH_4

The location of the EGH monitoring station is ideal to measure CO_2, CO and CH_4 because its proximity to the London region, M25 motorway and Heathrow airport. EGH is a semi-rural monitoring station for the SW sector and sub-urban for the others. Analysis and interpretation of records during background conditions (SW, wind speed >4 m s^{-1}) can provide new insights about the important processes and sources involved in carbon emissions near EGH. Records of CO_2, CO and CH_4 in air masses from NE, E and NE sectors, can help to interpret changes in response to measures to control their emissions. On the other hand, during the occurrence of pollution episodes records of carbon gas at EGH can help to interpret the origin of the concentrations measured.

Wind sector analysis of CO_2 at EGH during 2000-2012 showed that the highest concentrations were recorded during the occurrence of air masses from NE and E sectors at low wind speeds (<2.5 m s^{-1}), which correspond to the location of the Greater London area, M25 motorway, the junction of M3 and M25 motorways and Heathrow airport. Similarly high concentrations were observed in air masses from SE sector at wind speed <2.5 m s^{-1}, when speed ranged between 2.5 and 6 m s^{-1} concentrations decreased slightly and then increased when wind speed was >6 m s^{-1}. By contrast, the lowest concentrations were recorded with air mass origin SW and W when wind speed was >10 m s^{-1}. Such concentrations were ascribed to air passes passing over large wood areas before arrived at EGH (Great Windsor Park and Great Wood area). Moderate concentrations were recorded when air masses

arrived from NW sector when air speed ranged between 7 and 12 m s^{-1}. Those concentrations could be associated to emission from the residential area in Englefield Green.

The wind sector analysis of CO records at EGH during 2000-2012 suggested large CO emissions on the E, NE and N sectors. The highest concentrations were recorded when air masses arrived from N and NE sectors, when wind speed was >15 m s^{-1}, although data capture for such sectors represent <1% of the overall data points recorded. Such high concentrations were ascribed to exhaust gas from aircraft at Heathrow airport and to residential emissions in the Old Windsor area. By contrast, the lowest concentrations were recorded when wind speed was >1 m s^{-1} and air masses arrived from S, SW and W sectors, which passed over large wood areas before arrived at EGH.

The largest concentrations of CH_4 at EGH during 2000-2012 were measured when wind speed was <2 m s^{-1} from N, NE and E wind sectors, which were ascribed to emissions from urban Egham and from the gas storage facility on the road to Staines. Moderate concentrations were recorded in air masses from the E sector at wind speeds >5 m s^{-1} which were attributed to emissions from the London region and when wind speed was >15 m s^{-1} from S which were ascribed to emissions from the Virginia Water urban area and M3 and M25 motorways junction. Finally, similar to CO_2 and CO the lowest concentrations of CH_4 were measured when air masses arrived from SW and W sector at wind speed >5 m s^{-1}.

Cluster analysis for the bivariate polar plots of CO_2, CO and CH_4 was performed to identify the most likely sources of the carbon gas. Six clusters were required to represent the features observed in the polar plots. The highest concentrations of CO_2, CO and CH_4 were recorded when air masses arrived from the NE, E and SE sectors. This was due to transport of emissions from the London region to EGH and hotspots near EGH such as Heathrow airport, M25 motorway and urban Egham. CO_2, CO and CH_4 are possible produced by common sources as cluster analysis and bivariate polar plots showed similarities for the largest concentrations recorded for same wind direction and wind speeds.

In this thesis summer, winter and long-range transport pollution episodes were studied to interpret the origin of high concentrations recorded at EGH. The summer smog in 2003 reported by the LAQN from 1 to 15 of August 2003 was also observed

in records of CO_2, CO and CH_4 at EGH. A combined increase of carbon gas was clearly observed from 2 to 14 of August 2003 (summer episode). Meteorological records showed that when the highest concentrations during the episode were recorded, air masses at wind speeds between 1.5 to 3 m s^{-1} arrived from E sector at EGH. Such concentrations were ascribed to emissions transported from the London region under hot and calm weather.

High levels of PM_{10}, $PM_{2.5}$ and NO_x (winter episode) were recorded at several monitoring stations of the AURN in the Greater London area from 14 to 18 January 2012. High concentrations of CO_2, CO and CH_4 were also measured at EGH during the episode. A combined increase of carbon gas was observed from January 12 2012. The highest concentrations were recorded on January 14 when wind speed daily average was 0.2 m s^{-1} and air masses arrived from E sector at EGH. High concentrations were observed on January 16 and 17 when wind speed daily average was 0.9 and 0.2 m s^{-1}, respectively. Such high levels of CO_2, CO and CH_4 were attributed to emissions from the London region and urban Egham transported to EGH during cold and calm weather.

A long-range transport episode was observed in Southeast England from 12 to 23 April 2003 (Eastern weekend smog). Monitoring stations of the LAQN in the Greater London area recorded high levels of ozone and PM_{10}. During the episode high concentrations of CO_2, CO and CH_4 were measured at EGH. The highest concentrations of carbon gas were recorded on April 15 and 16 when air masses arrived at EGH from E sector and wind speed daily average was 0.6 and 2.4 m s^{-1}, respectively. Similar to winter and summer pollution episodes, the highest concentrations observed were ascribed to emissions from the Greater London area transported to EGH.

8.5. Interpretation and comparison of background measurements at EGH and MHD

Background conditions at EGH were defined as measurements of CO_2, CO and CH_4 in air masses arriving from SW sector at wind speed >4 m s^{-1}. Data captured of background carbon gas was 1.3% of the overall data set. Linear correlation between EGH and MHD data for CO_2, CO and CH_4 showed R^2>0.8 with statistically significance at p<0.05. This confirmed that under background conditions records at EGH are close to Atlantic background levels.

Long-term trends at EGH were calculated from background annual averages of CO_2, CO and CH_4 during 2000-2012. The long-term trend of CO_2 at EGH of 2.30 ppm CO_2 yr^{-1} was 1.16 times larger than that observed at MHD (1.97 ppm CO_2 yr^{-1}). Such trend is in good agreement with increasing trends of CO_2 calculated from measurements around the world by different cooperative networks (NOAA/ESRL, AGAGE). Interestingly, the background trend observed at EGH contrasted with the declining trend in CO_2 emissions in the UK. This might be due to the arising of new local CO_2 sources near EGH, region not representative of the trend in CO_2 emissions in the rest of UK.

The long-term trend of background CO calculated at EGH during 2000-2012 was in good agreement with the global declining trend observed at other monitoring stations around the world (NOAA/ESRL, AGAGE). Such trend is about 5.1 times larger than those observed at MHD and MLO monitoring stations. It is also in good agreement with the declining trend in CO emissions reported in the UK NAEI during 2000-2011. The sustained decline in CO has been ascribed to the success of strict controls on vehicle emissions introduced by the EU and UK legislation.

The long-term trend of CH_4 records at EGH during 2000-2012 showed statistical significance at a level of $p<0.05$. An increasing trend of 3.51 ppb CH_4 yr^{-1} was calculated, which was 1.23 times larger than that observed at MHD (2.85 ppb CH_4 yr^{-1}) also statistically significant at $p<0.05$. The background trend of CH_4 data at EGH was 1.14 times larger than that observed at MLO of 3.07 ppb CH_4 yr^{-1}. The long-term at MHD contrasted with the declining trend in CH_4 emissions reported by the UK NAEI during 2000-2012. This reveals that background measurements at EGH well represent the global increase of background CH_4 observed also at monitoring stations around the world (NOAA/ESRL, AGAGE).

8.6. Future work

High-frequency and high-precision measurements of carbon gas are particularly useful at a monitoring station that is semi-rural and sub-urban like EGH. The analysis and interpretation of data recorded on hourly, daily, weekly and annual time scales can help to understand the origins of concentrations recorded. Therefore, continuing with the measurements is recommended to better understand long-term trends and the response of carbon gas to measures to control their emissions.

Diurnal variations of carbon gas are ascribed to the hourly evolution of the PBL height, which changes from season-to-season. At EGH, one limitation to better interpret diurnal variations observed of carbon gas was the lack of data of measurements of the PBL height during different seasons as data recorded in the proximities of EGH (Heathrow airport) to measure the PBL height are restricted and not available for public. It is suggested to implement a precise and low-cost method to measure the evolution of the PBL height at EGH at different hours of the day and season. One proposed method to calculate the diurnal and seasonal variation of the PBL height is the launch of a helium filled balloon adapted with a theta-sonde (different commercial models available). Then, with data of temperature, wind speed, wind direction and relative humidity recorded mathematical analysis can be applied to calculate the PBL height. However, the location of EGH close to Heathrow airport may be a limitation to obtain the authorization from the Civil Aviation Authority to perform the described measurements.

Another possible option is the use of a sodar system. Such system provides measurements of vertical wind velocity, which in combination with mathematical analysis allows the calculation of the PBL. An advantage of the sodar system use is the precision of the measurements and consequently the uncertainty in average vertical velocities (<0.05 m s^{-1}). Therefore the use of a sodar system is also proposed to calculate the diurnal evolution of the PBL height at EGH.

The long-term trend of CO records calculated at EGH is in good agreement with the declining trend in CO emissions reported in the UK NAEI. By contrast, the long-term trends of CO_2 and CH_4 contrast with data reported in the UK GGI. Therefore, comparison with other monitoring stations at remote sites in the UK is recommended to ratify the long-term trends calculated at EGH. Ideally, the monitoring stations should be located where the impact of local emissions does not obscure the long-term trend component and can be used to verify data reported in the UK NAEI and GGI. Additionally, comparison of EGH data with those recorded at remote and sub-urban monitoring stations around the world could help, firstly, to ratify the increase in background levels of carbon gas observed at EGH and MHD and, secondly, to evaluate the impact of local emissions from urban areas on the long-term trend component as observed at EGH.

REFERENCES

Adame, J.A., Hernández-Ceballos, M.A., Bolívar, J.P., De la Morena, B. (2012). Assessment of an air pollution event in the southwestern Iberian peninsula. *Atmospheric Environment,* 55, 245-256.

An, X., Sun, Z., Lin, W., Jin, M., Li, N. (2013). Emission inventory evaluation using observations of regional atmospheric background stations of China. *Journal of Environmental Sciences (China),* 25(3), 537-546.

Anderson, H.R., Bremner, S.A., Atkinson, R.W., Harrison, R.M., Walters, S. (2001). Particulate matter and daily mortality and hospital admissions in the west midlands conurbation of the United Kingdom: Associations with fine and coarse particles, black smoke and sulphate. *Occupational and Environmental Medicine,* 58(8), 504-510.

Antonovsky, M.Ya., Buchstaber, V.M. (1991). An exploratory analysis of long-term trends in atmospheric CO_2 concentrations. *Tellus, Series B*, 43B(2), 171–187.

Aulagnier, C., Rayner, P., Ciais, P., Vautard, R., Rivier, L., Ramonet, M. (2010). Is the recent build-up of atmospheric CO_2 over Europe reproduced by models. Part 2: An overview with the atmospheric mesoscale transport model CHIMERE. *Tellus, Series B: Chemical and Physical Meteorology,* 62(1), 14-25.

Azmi, S.Z., Latif, M.T., Ismail, A.S., Juneng, L. and Jemain, A.A. (2010). Trend and status of air quality at three different monitoring stations in the Klang Valley, Malaysia. *Air Quality, Atmosphere and Health,* 3(1), 53-64.

Bakwin, P.S., Tans, P.P., Novelli, P.C. (1994). Carbon monoxide budget in the northern hemisphere. *Geophysical Research Letters,* 21(6), 433-436.

Barichivich, J., Briffa, K. R., Osborn, T. J., Melvin, T.M., Caesar, J. (2012). Thermal growing season and timing of biospheric carbon uptake across the northern hemisphere. *Global Biogeochemical Cycles,* 26(4), GB4015.

Barichivich, J., Briffa, K.R., Myneni, R.B., Osborn, T.J., Melvin, T.M., Ciais, P., Piao, S., Tucker, C. (2013). Large-scale variations in the vegetation growing season and annual cycle of atmospheric CO_2 at high northern latitudes from 1950 to 2011. *Global Change Biology,* 19(10), 3167-3183.

Bigi, A., Harrison, R.M. (2010). Analysis of the air pollution climate at a central urban background site. *Atmospheric Environment*, 44, 2004-2012.

Bigi, A., Ghermandi, G., Harrison, R.M. (2012). Analysis of the air pollution climate at a background site in the Po valley. *Journal of Environmental Monitoring,* 14(2), 552-563.

Bousquet, P., Gaudry, A., Ciais, P., Kazan, V., Monfray, P., Simmonds, P., Jennings, S., O'Connor, T. (1996). Atmospheric CO_2 concentration variations recorded at Mace Head, Ireland, from 1992 to 1994. *Physics and Chemistry of The Earth*, 21(5-6), 477-481.

Brasseur, G.P., Orlando, J.J., Tyndall, G.S. (eds) (1999). Atmospheric Chemistry and Global Change. Oxford University Press. New York, US.

Carslaw, D.C., Ropkins, K. (2012). openair - An R package for air quality data analysis. *Environmental Modelling & Software*, 27-28, 52-61.

Carslaw, D.C., Beevers, S.D. (2013). Characterising and understanding emission sources using bivariate polar plots and k-means clustering. *Environmental Modelling and Software,* 40, 325-329.

Carslaw, D.C. (2014). The openair manual — open-source tools for analysing air pollution data. Manual for version 1.0, King's College London.

Chase, T. N., Pielke, R. A., Kittel, T. G. F., Nemani, R., Running, S.W. (1996). Sensitivity of a general circulation model to global changes in leaf area index. *Journal of Geophysical Research D,* 101(D3), 7393-7408.

Chevalier, A., Gheusi, F., Attié, J.L., Delmas, R., Zbinden, R., Athier, G., Counsin, J.M. (2008). Carbon monoxide observations from ground stations in France and Europe and long-term trends in the free troposphere. *Atmospheric Chemistry and Physics Discussions*, 8, 3313-3356.

Ciais, P., Sabine, C., Govindasamy, B., Bopp, L., Brovkin, V., Canadell, J., Chhabra, A., DeFries, R., Galloway, J., Heimann, M., Jones, C., Le Quéré, C., Myneni, R., Piao, S., Thornton, P. (2013). Chapter 6: Carbon and Other Biogeochemical Cycles, in: Climate Change 2013 The Physical Science Basis, edited by: Stocker, T., Qin, D., and Platner, G.-K., Cambridge University Press, Cambridge.

Climate Change Act. (2008). *Available at: http://www.legislation.gov.uk/ukpga/2008/27/pdfs/ukpga_20080027_en.pdf*

Cleveland, W.S., Freeny, A.E., Graedel, T.E. (1983). The seasonal component of atmospheric CO_2: Information from new approaches to the decomposition of seasonal time series (Mauna Loa, Hawaii, South Pole). *Journal of Geophysical Research,* 88(C15), 10934-10946.

Cleveland, R.B., Cleveland, W.S., McRae, J., Terpenning, I. (1990). STL: a seasonal-trend decomposition procedure based on loess. *Journal of Official Statistics*, 6(1), 3-33.

Cofala, J., Amann, M., Klimont, Z., Kupiainen, K., Höglund-Isaksson, L. (2007). Scenarios of global anthropogenic emissions of air pollutants and methane until 2030. *Atmospheric Environment*, 41, 8486–8499.

Defra, 2006. Air Pollution Forecasting: OZONE POLLUTION EPISODE REPORT (JUNE-JULY 2006). *Available at: http://uk-air.defra.gov.uk/assets/documents/reports/cat12/0701241100_ APF_episode_JunJul06_FINAL_low.pdf*

Defra, 2007. The Air Quality Strategy for England, Scotland, Wales and Northern Ireland. *Available at: https://www.gov.uk/government/uploads/system/uploads/attachment_data/file/250801/7169_i.pdf and https://www.gov.uk/government/*

uploads/system/uploads/attachment_data/file/69337/pb12670-air-quality-strategy-vol2-070712.pdf

Defra, 2011. High pollution episode warning: First “summer-smog” of 2011. *Available at: https://www.gov.uk/government/news/high-pollution-episode-warning-first-summer-smog-of-2011*

Department of Energy and Climate Change (DECC) (2012). Local Authority CO_2 emissions estimates 2010 Statistical Summary and UK Maps. *Available at: http://www.decc.gov.uk/en/content/cms/statistics/climate_stats/gg_emissions/laco2/laco2.aspx).*

Department of Energy and Climate Change (DECC) (2012). Local Authority CO_2 emissions estimates 2012 Statistical Summary and UK Maps. *Available at:*https://www.gov.uk/government/uploads/system/uploads/attachment_data/file/322819/20140624_Statistical_release_Local_Authority_CO2_emissions.pdf

Department of Energy and Climate Change (DEC) (2012). *Web site: https://www.gov.uk/government/organisations/department-of-energy-climate-change*

Dentener, F., Stevenson, D., Cofala, J., Mechler, R., Amann, M., Bergamaschi, P., Raes, F., Derwent, R. (2005). The impact of air pollutant and methane emission controls on tropospheric ozone and radiative forcing: CTM calculations for the period 1990-2030. *Atmospheric Chemistry and Physics,* 5(7), 1731-1755.

Derwent, R.G., Simmonds, P.G., Seuring, S., Dimmer, C. (1998a). Observation and interpretation of the seasonal cycles in the surface concentrations of ozone and carbon monoxide at Mace Head, Ireland from 1990 to 1994. *Atmospheric Environment*, 32(2), 145-157.

Derwent, R.G., Simmonds, P.G., O'Doherty, S., Ciais, P., Ryall, D.B. (1998b). European source strengths and northern hemisphere baseline concentrations of radiatively active trace gases at Mace Head Ireland. *Atmospheric Environment*, 32(21), 3703-3715.

Derwent, R.G., Ryall, D.B., Manning, A., Simmonds, P.G., O'Doherty, S., Biraud, S. (2002). Continuous observations of carbon dioxide at Mace Head, Ireland from 1995 to 1999 and its net European ecosystem exchange. *Atmospheric Environment*, 36, 2799-2807.

Derwent, R.G., Simmonds, P.G., O'Doherty, S., Stevenson, D.S., Collins, W.J., Sanderson, M.G., Johnson, C.E., Dentener, F., Cofala, J., Mechler, R., Amann, M. (2006). External influences on Europe's air quality: Baseline methane, carbon monoxide and ozone from 1990 to 2030 at Mace Head, Ireland. *Atmospheric Environment,* 40(5), 844-855.

Dettinger, M.D., Ghil, M. (1998). Seasonal and interannual variations of atmospheric CO_2 and climate. *Tellus, Series B: Chemical and Physical Meteorology*, 50(1), 1-24.

Dlugokencky, E.J., Houweling, S., Bruhwiler, L., Masarie, K A., Lang, P.M., Miller, J.B., Tans, P.P. (2003). Atmospheric methane levels off: Temporary pause or a new steady-state?. *Geophysical Research Letters,* 30(19), ASC5-1-ASC5-4.

Dlugokencky, E.J., Bruhwiler, L., White, J.W.C., Emmons, L.K., Novelli, P.C., Montzka, S.A., Gatti, L.V. (2009). Observational constraints on recent increases in the atmospheric CH_4 burden. *Geophysical Research Letters*, 36(18).

Dlugokencky, E.J., Nisbet, E.G., Fisher, R., Lowry, D. (2011). Global atmospheric methane: budget, changes and dangers. *Philosophical Transactions of the Royal Society A: Mathematical, Physical and Engineering Sciences,* 369(1943), 2058-2072.

Dlugokencky, E.J., Lang, P.M., Crotwell, A.M., Masarie, K.A., Crotwell, M.J. (2014). Atmospheric methane dry air mole fractions from the NOAA ESRL carbon cycle cooperative global air sampling network, 1983-2013, Version: 2014-06-24, Path: ftp://aftp.cmdl.noaa.gov/data/trace_gases/ch4/flask/surface/.

Fenger, J. (2009). Air pollution in the last 50 years - from local to global. *Atmospheric Environment*, 43(1), 13-22.

Finlayson-Pitts, B.J., Pitts, J.N. (2000). Chemistry of the Upper and Lower Atmosphere, Theory, Experiments, and Applications. Academic Press. ISBN: 978-0-12-257060-5.

Fiore, A.M., Horowitz, L.W., Dlugokencky, E.J., West, J.J. (2006). Impact of meteorology and emissions on methane trends, 1990-2004. *Geophysical Research Letters,* 33(12).

Fisher, R.E. (2006). Development and applications of continuous-flow gas chromatography isotope ratio mass spectrometry for atmospheric methane and carbon studies. Ph.D. Thesis. Royal Holloway University of London. UK.

Fisher, R., Lowry, D., Wilkin, O., Sriskantharajah, S., Nisbet, E.G. (2006). High-precision, automated stable isotope analysis of atmospheric methane and carbon dioxide using continuous-flow isotope-ratio mass spectrometry. *Rapid Communications in Mass Spectrometry,* 20(2), 200-208.

Fleming, Z.L., Monks, P.S., Manning, A.J. (2012). Review: Untangling the influence of air-mass history in interpreting observed atmospheric composition. *Atmospheric Research,* 104-105, 1-39.

Garg, A., Shukla, P.R., Kapshe, M. (2006). The sectoral trends of multigas emissions inventory of India. *Atmospheric Environment*, 40, 4608–4620.

Gifford, F.A. (1982). Horizontal diffusion in the atmosphere: A lagrangian-dynamical theory. *Atmospheric Environment - Part A General Topics,* 16(3), 505-512.

Granier, C., Müller, J.-., Madronich, S., Brasseur, G.P. (1996). Possible causes for the 1990-1993 decrease in the global tropospheric CO abundances: A three-dimensional sensitivity study. *Atmospheric Environment,* 30(10-11), 1673-1682.

Grant, A., Stanley, K.F., Henshaw, S.J., Shallcross, D.E., O'Doherty, S. (2010). High-frequency urban measurements of molecular hydrogen and carbon monoxide in the United Kingdom. *Atmospheric Chemistry and Physics*, 10(10), 4715-4724.

Graven, H.D., Guilderson, T.P., Keeling, R.F. (2012). Observations of radiocarbon in CO_2 at La Jolla, California, USA 1992-2007: Analysis of the long-term trend. *Journal of Geophysical Research D: Atmospheres,* 117(2).

Harrison, R.M. (2001). Pollution: Causes, effects and control. 4th ed. The Royal Society of Chemistry. Birmingham, UK.

Haszpra, L., Barcza, Z., Hidy, D., Szilagyi, I., Dlugokencky, E., Tans, R. (2008). Trends and temporal variations of major greenhouse gases at a rural site in Central Europe. *Atmospheric Environment*, 42, 8707-8716.

Haszpra, L., Barcza, Z. (2010). Climate variability as reflected in a regional atmospheric CO_2 record. *Tellus, Series B: Chemical and Physical Meteorology*, 62(5), 417-426.

Helfter, C., Famulari, D., Phillips, G.J., Barlow, J.F., Wood, C.R., Grimmond, C.S.B., Nemitz, E. (2011). Controls of carbon dioxide concentrations and fluxes above Central London. *Atmospheric Chemistry and Physics,* 11(5), 1913-1928.

Hewitt, C.N., Jackson, A. (2003). Handbook of Atmospheric Science Principles and Aplications. Blackwell Publishing.

Higuchi, K., Trivett, N.B.A., Daggupaty, S.M. (1987). A preliminary climatology of trajectories related to atmospheric CO_2 measurements at Alert and Mould Bay. *Atmospheric Environment*, 21(9), 1915-1926.

Hobbs, P.V. (2000). Introduction to Atmospheric Chemistry. Cambridge University Press. New York, US.

Hossain, K.M.A., Easa, S.M. (2012). Pollutant dispersion characteristics in Dhaka City, Bangladesh. *Asia-Pacific Journal of Atmospheric Sciences* 48(1), 35-41.

Hunt, J.C.R., Kaimal, J.C., Gaynor, J. E. (1988). Eddy structure in the convective boundary layer - New measurements and new concepts. *Q.J.R. Meteorol. Soc*.,114, 827-858.

IPCC. (1996), *Climate Change 1995: A report of the Intergovernmental Panel on Climate Change*, Second Assessment Report of the Intergovernmental Panel on Climate Change, IPCC. The "Full Report", consisting of "The IPCC Second Assessment Synthesis of Scientific-Technical Information Relevant to Interpreting Article 2 of the UN Framework Convention on Climate Change" and the Summaries for Policymakers of the three Working Groups.

IPCC. (2001), Watson, R. T.; and the Core Writing Team, ed., *Climate Change 2001: Synthesis Report*, Contribution of Working Groups I, II, and III to the Third Assessment Report of the Intergovernmental Panel on Climate Change, Cambridge University Press, ISBN 0-521-80770-0.

IPCC. (2007), Core Writing Team; Pachauri, R.K; and Reisinger, A., ed., *Climate Change 2007: Synthesis Report*, Contribution of Working Groups I, II and III to the Fourth Assessment Report of the Intergovernmental Panel on Climate Change, IPCC, ISBN 92-9169-122-4.

IPCC, 2013: Climate Change 2013: The Physical Science Basis. Contribution of Working Group I to the Fifth Assessment Report of the Intergovernmental Panel on Climate Change [Stocker, T.F., D. Qin, G.-K. Plattner, M. Tignor, S.K. Allen, J. Boschung, A. Nauels, Y. Xia, V. Bex and P.M. Midgley (eds.)]. Cambridge University Press, Cambridge, United Kingdom and New York, NY, USA, 1535 pp.Jacobson, M.Z. (2002). Atmospheric Pollution: History, science, and Regulation. Cambridge University Press, New York.

Jin, F., Kim, J., Kim, K. (2010). Estimation of potential source region in Northeast Asia through continuous in-situ measurement of atmospheric CO_2 at Gosan, Jeju Island, Korea. Terrestrial, *Atmospheric and Oceanic Sciences*, 21(2), 313-323.

Johnson, D.E., Seidl, A.F., Phetteplace, H. (2001). Livestock system greenhouse gases: Effects of practices and policies on emissions and economic returns. Final report to US-EPA. Washington, D.C.

Johnston, H., Kinnison, D. (1998). Methane photooxidation in the atmosphere: Contrast between two methods of analysis. *Journal of Geophysical Research D: Atmospheres,* 103(D17), 21967-21984.

Kai, F.M., Tyler, S.C., Randerson, J.T., Blake, D.R. (2011). Reduced methane growth rate explained by decreased Northern Hemisphere microbial sources. *Nature,* 476(7359), 194-197.

Kanawade, V.P., Benson, D.R., Lee, S.-H. (2012). Statistical analysis of 4-year observations of aerosol sizes in a semi-rural continental environment. *Atmospheric Environment,* 59, 30-38.

Keeling, C.D., Bacastow, R.B., Bainbridge, A.E., Ekdahl, C.A., Guenther, P.R., Waterman, L.S.. (1976). Atmospheric carbon dioxide variations at Mauna Loa Observatory, Hawaii. *Tellus,* 28, 538-551.

Keeling, C.D., Bacastow, R.B., Carter, A.F., Piper, S.C., Whorf, T.P., Heineman, M., Mook, W. G., Roeloffzen, H. (1989). A three-dimensional model of atmospheric CO_2 transport based on observed winds: 1. Analysis of observational data. 165-236. In: *Aspects of climate variability in the Pacific and the western Americas* (ed. D. H. Peterson). Monograph No. 55 (December 1989). American Geophysical Union, Washington, DC.

Keeling, C.D., Piper, S.C., Whorf, T.P., Keeling, R.F. (2011). Evolution of natural and anthropogenic fluxes of atmospheric CO_2 from 1957 to 2003. *Tellus, Series B: Chemical and Physical Meteorology*, 63(1), 1-22.

Khalil, M.A.K., Butenhoff, C.L., Rasmussen, R.A. (2007). Atmospheric methane: Trends and cycles of sources and sinks. *Environmental Science and Technology,* 41(7), 2131-2137.

Kim, K.H., Shon, Z.H. (2011). Nationwide shift in CO concentration levels in urban areas of Korea after 2000. *Journal of Hazardous Materials,* 188(1-3), 235-246.

Kirschke, S., Bousquet, P., Ciais, P., Saunois, M., Canadell, J.G., Dlugokencky, E.J., Zeng, G. (2013). Three decades of global methane sources and sinks. *Nature Geoscience,* 6(10), 813-823.

Kotthaus, S., Grimmond, C.S.B. (2012). Identification of micro-scale anthropogenic CO_2, heat and moisture sources - processing eddy covariance fluxes for a dense urban environment. *Atmospheric Environment,* 57, 301-316.

Kuebler, J., Van Den Bergh, H., Russell, A.G. (2001). Long-term trends of primary and secondary pollutant concentrations in Switzerland and their response to emission controls and economic changes. *Atmospheric Environment*, 35(8), 1351-1363.

Larson, V.E., Volkmer, H. (2008). An idealized model of the one-dimensional carbon dioxide rectifier effect. *Tellus, Series B,* 60(4), 525-536.

Law, K.S. (1999). Theoretical studies of carbon monoxide distributions, budgets and trends. *Chemosphere - Global Change Science,* 1(1-3), 19-31.

Le Quéré, C. (2013). Global carbon budget 2013. *Earth Syst. Sci. Data Discuss*., 6, 689-760.

Levy II, H. (1972). Photochemistry of the lower troposphere. *Planetary and Space Science*, 20(6), 919-935.

Levy II, H. (1973a). Photochemistry of minor constituents in the troposphere. *Planetary and Space Science*, 21(4), 575-591.

Levy II, H. (1973b). Tropospheric budgets for methane, carbon monoxide, and related species. *Journal of Geophysical Research*, 78(24), 5325-5332.

Li, L., Liu, Y. (2011). Space-borne and ground observations of the characteristics of CO pollution in Beijing, 2000-2010. *Atmospheric Environment,* 45(14), 2367-2372.

Lin, Y. C., Lan, Y. Y., Tsuang, B. -J., Engling, G. (2008). Long-term spatial distributions and trends of ambient CO concentrations in the central Taiwan basin. *Atmospheric Environment*, 42(18), 4320-4331.

Lintner, B.R., Buermann, W., Koven, C.D., Fung, I.Y. (2006). Seasonal circulation and Mauna Loa CO_2 variability. *Journal of Geophysical Research D*, 111(13).

London Air Quality Network (LAQN). (2014). Environmental Research Group, King's College London. *Web site: http://www.londonair.org.uk/LondonAir/Default.aspx*

Lowry, D., O'Brien, P., Nisbet, E.G., Rata, N.D. (1998). $\delta^{13}C$ of atmospheric methane: An integrated technique for constraining emission sources in urban and background air, in *Isotope Techniques in the Study of Environmental Change*. Proceedings of IAEA Symposium, Vienna, April 1997, 57-67.

Lowry, D., Holmes, C.W., Rata, N.D., O'Brien, P., Nisbet, E. (2001). London methane emissions: Use of diurnal changes in concentration and delta C-13 to identify urban sources and verify inventories. *Journal of Geophysical Research*. 106, D7, 7427-7448.

Manning, A.C., Nisbet, E.G., Keeling, R.F., Liss, P.S. (2011). Greenhouse gases in the Earth system: Setting the agenda to 2030. *Philosophical Transactions of the Royal Society A: Mathematical, Physical and Engineering Sciences,* 369(1943), 1885-1890.

Makarova, M.V., Poberovskii, A.V., Osipov, S.I. (2011). Time variations of the total CO content in the atmosphere near St. Petersburg. *Izvestiya - Atmospheric and Ocean Physics,* 47(6), 739-746.

Meghea, I., Mihai, M., Lacatusu, I., Apostol, T. (2012). Time series model applied to environmental monitoring data analyses. *Journal of Environmental Protection and Ecology,* 13(2), 426-434.

Meng, Z.Y., Xu, X.B., Yan, P., Ding, G.A., Tang, J., Lin, W.L., Xu, X.D., Wang, S.F. (2009). Characteristics of trace gaseous pollutants at a regional background station in Northern China. *Atmospheric Chemistry and Physics,* 9(3), 927-936.

Messager, C., Schmidt, M., Ramonet, M., Bousquet, P., Simmonds, P., Manning, A. Ciais, P. (2008). Ten years of CO_2, CH_4, CO and N_2O fluxes over Western Europe inferred from atmospheric measurements at Mace Head, Ireland. *Atmospheric Chemistry and Physics Discussions*, 8(1), 1191-1237.

Met Office. (2014). Hot spell - August 2003. *Available at: http://www.metoffice.gov.uk/ climate/uk/interesting/aug03maxtemps.html*

Monks, P.S., Granier, C., Fuzzi, S., Stohl, A., Williams, M.L., Akimoto, H., von Glasow, R. (2009). Atmospheric composition change - global and regional air quality. *Atmospheric Environment,* 43(33), 5268-5350.

Monni, S., Syri, S. (2011). Weekly greenhouse gas emissions of municipalities: Methods and comparisons. *Energy Policy,* 39(9), 4755-4765.

Morimoto, S., Nakazawa, T., Aoki, S., Hashida, G., Yamanouchi, T. (2003). Concentration variations of atmospheric CO_2 observed at Syowa Station, Antarctica from 1984 to 2000. *Tellus, series B: Chemical and Physical Meteorology*, 55(2), 170-177.

Nakazawa, T., Miyashita, K., Aoki, S., Tanaka, M. (1991a). Temporal and spatial variations of upper tropospheric and lower stratospheric carbon dioxide. *Tellus, Series B*, 43B(2), 106-117.

Nakazawa, T., Aoki, S., Murayama, S., Fukabori, M., Yamanouchi, T., Murayama, H., Shiobara, M., Hashida, S., Kawaguchi, S., Tanaka, M. (1991b). The concentration of atmospheric carbon dioxide at the Japanese Antarctic Station, Syowa. *Tellus, Series B*, 43B(2), 126-135.

National Environmental Technology Centre (Netcen). (2003). UK Air Pollution. *Available at: http://uk-air.defra.gov.uk/assets/documents/reports/cat05/0408161000_ Defra_AQ_Brochure _2004_s.pdf*

Navascués, B., Rus, C. (1991). Carbon dioxide observations at Izaña baseline station, Tenerife (Canary Islands): 1984–1988. *Tellus, Series B*, 43B(2), 118–125.

Neue, H.U., Wassmann, R., Kludze, H.K., Wang, B., Lantin, R.S. (1997). Factors and processes controlling methane emissions from rice fields. *Nutrient Cycling in Agroecosystems,* 49(1-3), 111-117.

Nguyen, H., Kim, K., Ma, C., Cho, S., Sohn, J. (2010). A dramatic shift in CO and CH_4 levels at urban locations in Korea after the implementation of the natural gas vehicle supply (NGVS) program. *Environmental Research,* 110(4), 396-409.

Novelli, P.C., Masarie, K.A., Tans, P.P., Lang, P.M. (1994). Recent changes in atmospheric carbon monoxide. *Science,* 263(5153), 1587-1590.

Novelli, P.C., Masarie, K.A., Lang, P.M. (1998). Distributions and recent changes of carbon monoxide in the lower troposphere. *Journal of Geophysical Research D*, 103(D15), 19015-19033.

O'Shea, S.J., Allen, G., Fleming, Z.L., Bauguitte, S.J.-B., Percival, C.J., Gallagher, M.W., Lee, J., Helfter, C., Nemitz, E. (2014). Area fluxes of carbon dioxide, methane, and carbon monoxide derived from airborne measurements around Greater London: A case study during summer 2012. *Journal of Geophysical Research D: Atmospheres,* 119(8), 4940-4952.

Office for National Statistics (ONS) – Census Information Scheme. 2011 Census first results: London boroughs' populations by age by sex. (2012). Accessed on 6 May 2014. *Available at: http://data.london.gov.uk/datastorefiles/documents/2011-census-first-results.pdf*

Ohara, T. (2011). Long-Range Transport and Deposition of Air Pollution. *Module in Earth Systems and Environmental Sciences*, *Encyclopedia of Environmental Health,* 515–519.

Patra, P.K., Takigawa, M., Ishijima, K., Choi, B. -., Cunnold, D., Dlugokencky, E.J., Fraser, P., Gomez-Pelaez, A.J., Goo, T.Y., Kim, J.S., Krummel, P., Langenfelds, R., Meinhardst, F., Mukai, H., O'Doherty, S., Prinn, R.G., Simmonds, P., Steele, P., Tohjima, Y., Tsuboi, K., Uhse, K., Weiss, R., Worth, D., Nakazawa, T. (2009). Growth rate, seasonal, synoptic, diurnal variations and budget of methane in the lower atmosphere. *Journal of the Meteorological Society of Japan,* 87(4), 635-663.

Pedersen, I.-., Holmén, K., Hermansen, O. (2005). Atmospheric methane at Zeppelin station in Ny-Ålesund: Presentation and analysis of in situ measurements. *Journal of Environmental Monitoring,* 7(5), 488-492.

Petit, J.R., Jouzel, J., Raynaud, D., Barkov, N.I., Barnola, J.M., Basile, I., Bender, M., Chapellaz, J., Davis, M., Delaygue, G., Delmotte, M., Kotlyakov, V.M.,

Legrand, M., Lipenkov, V.Y., Lorius, C., Pepin, L., Ritz, C., Saltzman, E., Stievenard, M. (1999). Climate and atmospheric history of the past 420,000 years from the Vostok ice core, Antarctica. *Nature*, 399, 429-436.

Piao, S., Ciais, P., Friedlingstein, P., Peylin, P., Reichstein, M., Luyssaert, Luyssaert S., Margolis, H., Fang, J., Barr, A., Chen, A., Grelle, A., Hollinger, D. Y., Laurila, T., Lindroth, A., Richardson, A. D., Vesala, T. (2008). Net carbon dioxide losses of Northern ecosystems in response to autumn warming. *Nature,* 451(7174), 49-52.

PORG, 1997. Ozone in the United Kingdom. Fourth Report of the UK Photochemical Oxidants Review Group, Department of the Environment, Transport and the Regions, London. Published by Institute of Terrestrial Ecology, Bush Estate, Penicuik, Midlothian, EH26 0QB, UK. ISBN: 0-870393-30-9.

Ramanathan, V., Feng, Y. (2009). Air pollution, greenhouse gases and climate change: Global and regional perspectives. *Atmospheric Environment*, 43(1), 37-50.

Ramonet, M., Ciais, P., Aalto, T., Aulagnier, C., Chevallier, F., Cipriano, D., Necki, J.N. (2010). A recent build-up of atmospheric CO_2 over Europe. Part 1: Observed signals and possible explanations. *Tellus, Series B: Chemical and Physical Meteorology,* 62(1), 1-13.

Randerson, J.T., Thompson, M.V., Conway, T.J., Fung, I.Y., Field, C.B. (1997). The contribution of terrestrial sources and sinks to trends in the seasonal cycle of atmospheric carbon dioxide. *Global Biogeochemical Cycles,* 11(4), 535-560.

Randerson, J.T., Field, C.B., Fung, I.Y., Tans, P.P. (1999). Increases in early season ecosystem uptake explain recent changes in the seasonal cycle of atmospheric CO_2 at high northern latitudes. *Geophysical Research Letters*, 26(17), 2765-2768.

Rigby, M., Prinn, R.G., Fraser, P.J., Simmonds, P.G., Langenfelds, R.L., Huang, J. Cunnold, D.M., Steele, L.P., Krummel, P.B., Weiss, R.F., O'Doherty, S., Salameh, P.K., Wag, H.J., Harth, C.M., Müjle, J. and Porter L.W. (2008a). Renewed growth of atmospheric methane. *Geophysical Research Letters*, 35(22).

Rigby, M., Toumi, R., Fisher, R., Lowry, D., Nisbet, E.G. (2008b). First continuous measurements of CO_2 mixing ratio in central London using a compact diffusion probe. *Atmospheric Environment,* 42(39), 8943-8953.

Saito, R., Patra, P.K., Sweeney, C., Machida, T., Krol, M., Houweling, S., Bousquet, P., Agusti-Panared, A., Belikov, D., Bergmann, D., Bian, H., Cameron-Smith, P., Chipperfield, M.P., Fortems-Cheiney, A., Fraser, A., Gatti, L.V., Gloor, E., Hess, P., Kawa, S.R., Law, R.M., Locatelli, R., Loh, Z., Maksyutov, S., Meng, L., Miller, J.B., Palmer, P.I., Prinn, R.G., Rigby, M., Wilson, C. (2013). TransCom model simulations of methane: Comparison of vertical profiles with aircraft measurements. *Journal of Geophysical Research D: Atmospheres,* 118(9), 3891-3904.

Salmi, T., Määttä, A., Anttila, P., Ruoho-Airola, T., Amnell, T. (2002). Detecting trends of anual values of atmospheric pollutants by the Mann-Kendall test and Sen's slope estimates – the Excel template application MAKESENS. *Publications on Air Quality Report code FMI-AQ-31*, (31), 1-35. Helsinki, Finland.

Sánchez, M.L., García, M.A., Pérez, I.A., Pardo, N. (2013). CH_4 continuous measurements in the upper Spanish plateau. *Environmental Monitoring and Assessment*, 1-12, doi:10.1007/s10661-013-3583-7.

von Schneidemesser, E., Monks, P.S. and Plass-Duelmer, C. (2010). Global comparison of VOC and CO observations in urban areas. *Atmospheric Environment, 44*(39), 5053-5064.

Schwela, D. (2000). Air pollution and health in urban areas. *Reviews on Environmental Health,* 15(1-2), 13-42.

Seinfeld, J.H., Pandis, N.S. (2006), Atmospheric Chemistry and Physics: From Air Pollution to Climate Change, 2nd ed, Wiley, New Jersey.

Simmonds, P.G., Seuring, S., Nickless, G., Derwent, R.G. (1997). Segregation and interpretation of ozone and carbon monoxide measurements by air mass origin at the TOR Station Mace head, Ireland from 1987–1995. *Journal of Atmospheric Chemistry*, 28, 45–59.

Simpson, I.J., Rowland, F.S., Meinardi, S., Blake, D.R. (2006). Influence of biomass burning during recent fluctuations in the slow growth of global tropospheric methane. *Geophysical Research Letters,* 33(22).

Spahni, R., Wania, R., Neef, L., Van Weele, M., Pison, I., Bousquet, P., Van Velthoven, P. (2011). Constraining global methane emissions and uptake by ecosystems. *Biogeosciences*, 8(6), 1643-1665.

Tans, D., Keeling, R. (2014). *NOAA/ESRL web site. (www.esrl.noaa.gov/ gmd/ccgg/trends/)*

Thompson, R.L., Manning, A.C., Gloor, E., Schultz, U., Seifert, T., Ḧansel, F., Jordan, M.H. (2009). In-situ measurements of oxygen, carbon monoxide and greenhouse gases from Ochsenkopf Tall tower in Germany. *Atmospheric Measurement Techniques,* 2(2), 573-591.

Thoning, K.W., Tans, P.P. (1989). Atmospheric carbon dioxide at Mauna Loa observatory 2. analysis of the NOAA GMCC data, 1974-1985. *Journal of Geophysical Research*, 94(D6), 8549-8565.

Trivett, N.B.A., Worthy, D.E.J., Brice, K.A. (1989). Surface measurements of carbon dioxide and methane at alert during an arctic haze event in April, 1986. *Journal of Atmospheric Chemistry,* 9(1-3), 383-397.

Uglietti, C., Leuenberger, M., Valentino, F. (2008) Comparison between real time and flask measurements of atmospheric O_2 and CO_2 performed at the High Altitude Research Station Jungfraujoch, Switzerland. *Science of The Total Environment*, 391(2-3), 196-202.

UK Greenhouse Gas Inventory (UK GGI), 1990 to 2011. (2013). Annual Report for Submission under the Framework Convention on Climate Change. Available at https://www.gov.uk/government/publications/uk-greenhouse-gas-inventory

UK Greenhouse Gas Inventory (UK GGI), 1990 to 2012. (2014). Annual Report for Submission under the Framework Convention on Climate Change. Available at https://www.gov.uk/government/publications/uk-greenhouse-gas-inventory

UK National Atmospheric Emissions Inventory, NAEI (2013). Air quality pollutant inventories for England, Scotland, Wales and Northern Ireland: 1990 – 2011. A report of the National Atmospheric Emissions Inventory. Available at: http://naei.defra.gov.uk/.

UK National Atmospheric Emissions Inventory, NAEI (2014). Air quality pollutant inventories for England, Scotland, Wales and Northern Ireland: 1990 – 2012. A report of the National Atmospheric Emissions Inventory. Available at: http://naei.defra.gov.uk/.

Valentino, F.L., Leuenberger, M., Uglietti, C. and Sturm, P. (2008). Measurements and trend analysis of O_2, CO_2 and $\delta^{13}C$ of CO_2 from the high altitude research station Junfgraujoch, Switzerland - A comparison with the observations from the remote site Puy de Dôme, France. *Science of the Total Environment,* 391(2-3), 203-210.

Varon, J., Marik, P.E. (1997) Carbon monoxide poisoning. Int. J. Emerg. Intens. Care Med. 1(2).

Vogt, R., Christen, A., Rotach, M.W., Roth, M., Satyanarayana, A.N.V. (2006). Temporal dynamics of CO_2 fluxes and profiles over a central European city. *Theoretical and Applied Climatology,* 84(1-3), 117-126.

Waibel, A.E., Fischer, H., Wienhold, F.G., Siegmund, P.C., Lee, B., Ström, J., Lelieveld, J., Crutzen, P.J. (1999). Highly elevated carbon monoxide concentrations in the upper troposphere and lowermost stratosphere at northern midlatitudes during the STREAM II summer campaign in 1994. Chemosphere - Global Change Science, 1(1-3), 233-248.

Wahlen, M. (1993). The Global Methane Cycle. *Annual Review of Earth and Planetary Sciences*, 21, 407-426.

Weber, E. (1982). Air pollution. *Assessment Methodology and Modelling*, Plenum, New York.

World Health Organization (2014) (WHO). Wold Health Statistics 2012. *Available at: http://apps.who.int/iris/bitstream/10665/112738/1/9789240692671_eng.pdf?ua=1*

Worthy, D.E.J., Trivett, N.B.A., Hopper, J.F., Bottenheim, J.W., Levin, I. (1994). Analysis of long-range transport events at Alert, Northwest Territories, during the Polar Sunrise Experiment. *Journal of Geophysical Research,* 99(D12), 25,329-25,344.

Xie, B., Hunt, J.C.R., Carruthers, D.J., Fung, J.C.H., Barlow, J. F. (2013). Structure of the planetary boundary layer over Southeast England: Modeling and measurements. *Journal of Geophysical Research D: Atmospheres,* 118(14), 7799-7818.

Xu, W.Y., Zhao, C.S., Ran, L., Deng, Z.Z., Liu, P.F., Ma, N., Lin, W.L., Xu, X.B., Yan, P., He, X., Yu, J., Liang, W.D., Chen, L.L. (2011). Characteristics of pollutants and their correlation to meteorological conditions at a suburban site in the North China Plain. *Atmospheric Chemistry and Physics,* 11(9), 4353-4369.

Yurganov, L.N., Grechko, E.I., Dzhola, A.V. (1999). Zvenigorod carbon monoxide total column time series: 27-yr of measurements. *Chemosphere - Global Change Science,* 1(1-3), 127-136.

Yver, C., Schmidt, M., Bousquet, P., Ramonet, M. (2011a). Measurements of molecular hydrogen and carbon monoxide on the Trainou Tall Tower. *Tellus, Series B: Chemical and Physical Meteorology,* 63(1), 52-63.

Zander, R., Demoulin, P., Ehhalt, D.H., Schmidt, U., Rinsland, C.P. (1989). Secular increase of the total vertical column abundance of carbon monoxide above central Europe since 1950. *Journal of Geophysical Research, 94*(D8), 11,021-11,028.

Zellweger, C., Hüglin, C., Klausen, J., Steinbacher, M., Vollmer, M., Buchmann, B. (2009). Inter-comparison of four different carbon monoxide measurement techniques and evaluation of the long-term carbon monoxide time series of Jungfraujoch. *Atmospheric Chemistry and Physics,* 9(11), 3491-3503.

Zhang, R., Wang, M. and Ren, L. (2001). Long-term trends of carbon monoxide inferred using a two-dimensional model. *Chemosphere: Global Change Science,* 3, 123–132.

Zhang, F., Zhou, L., Conway, T. J., Tans, P. P., Wang, Y. (2013). Short-term variations of atmospheric CO_2 and dominant causes in summer and winter: Analysis of 14-year continuous observational data at Waliguan, China. *Atmospheric Environment,* 77, 140-148.

Zhang, F., Zhou, L.X. (2013). Implications for CO_2 emissions and sinks changes in western China during 1995-2008 from atmospheric CO_2 at Waliguan. *Tellus, Series B: Chemical and Physical Meteorology,* 65(1), doi: 10.3402/tellusb.v65i0.19576.

Zhou, L., Tang, J., Wen, Y., Li, J., Yan, P. and Zhang, X. (2003). The impact of local winds and long-range transport on the continuous carbon dioxide record at mount waliguan, china. *Tellus, Series B: Chemical and Physical Meteorology, 55*(2), 145-158.

Zimnoch M., Godlowska J., Necki J.M., Rozanski, K. (2010). Assessing surface fluxes of CO_2 and CH_4 in urban environment: A reconnaissance study in Krakow, Southern Poland. *Tellus Series B-Chemical and Physical Meteorology*, 62(5), 573-580.

Abbreviation	Description
APs	Air pollutants
AQ	Air quality
CCGT	Combined cycle gas turbine
CFCs	Chlorofluorocarbons
CH_3O_2	Methyldioxy radical
CH_4	Methane
CO	Carbon monoxide
CO_2	Carbon dioxide
COHb	Carboxyhemoglobin
CRDS	Cavity ringdown spectrometer
Defra	Department for Environment, Food & Rural Affairs
EGH	Egham
ESRL	Earth System Research Laboratory
GGI	Greenhouse Gas Inventory
GGLES	Greenhouse Gas Laboratory of the Earth Sciences Department
GHGs	Greenhouse Gases
GMD	Global monitoring Division
H_2	Hydrogen
H_2O	Water
H_2O_2	Hydrogen peroxide
HO_2	Hydroperoxyl radical
HO_x	Hydrogen oxide radicals
IPCC	Intergovernmental Panel on Climate Change
ITCZ	Inter-Tropical Convergence Zone
LULUCF	Land use and land change and forestry
LWR	Longwave Radiation
MHD	Mace Head
MLO	Mauna Loa

Abbreviation	Description
N_2O	Nitrous oxide
NAEI	National Emissions Inventory
NIR	National Inventory Report
NMVOC	Non-Methane Volatile Organic Compounds
NO_2	Nitrogen dioxide
NO_3	Nitrate
NOAA	National Oceanic and Atmospheric Administration
NO_x	Mono-nitrogen oxides
O_3	Ozone
OH	Hydroxyl radical
Pb	Plumbum
PBL	Planetary boundary layer
PM	Particulate matter
RHUL	Royal Holloway University of London
SD	Standard deviation
SO_2	Sulphur dioxide
STL	Seasonal-Trend Decomposition
Tg	Teragram
UK	United Kingdom
UNFCCC	United Nations Framework Convention on Climate Chamge
US	United States
UVB	Ultraviolet B
UVC	Ultraviolet C
VOC	Volatile organic compounds
WHO	World Health Organization
WMO	World Meteorological Organization
Yr	Year

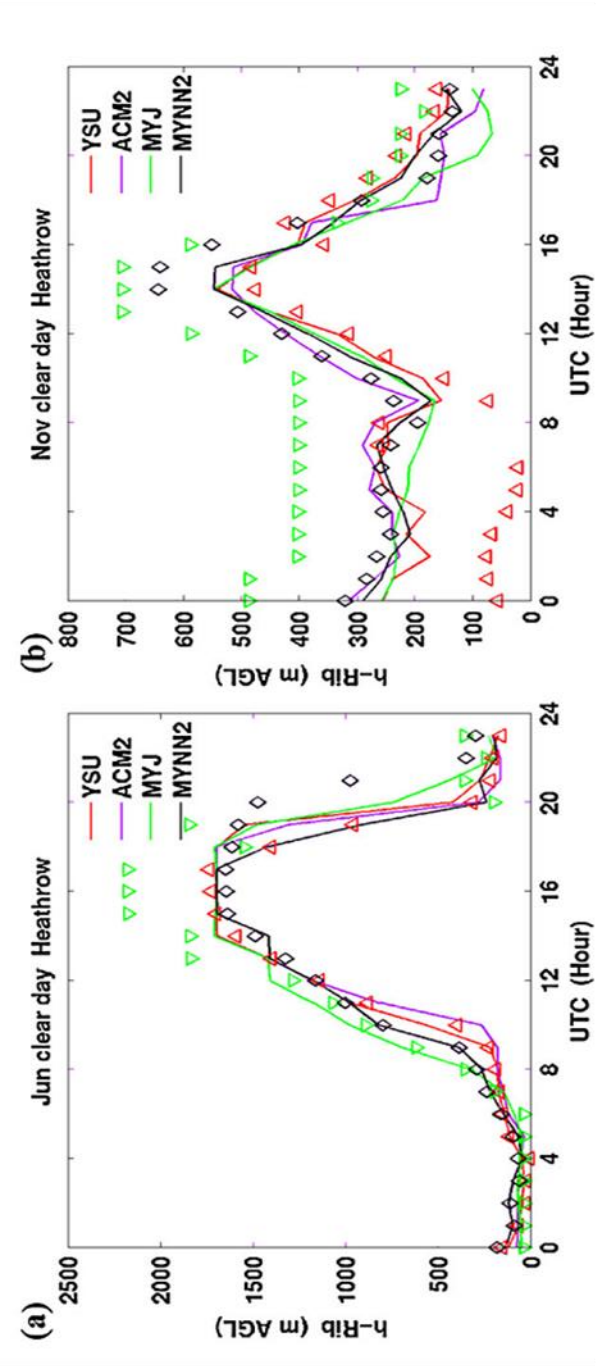

Figure A1(a). PBL height on clear days of 2 June; **(b)** on 12 November 2007 at Heathrow airport. Symbols represent predictions by the Yonsei University (YSU), Asymmetric Convective Model version 2 (ACM2), Mellor-Yamada-Janic (MYJ) and Mellor-Yamada-Nakanishi-Niino (MYNN2) PBL schemes. Solid lines represent predictions of PBL height by the bulk Richardson number method. *Source: Xie et al., 2013.*

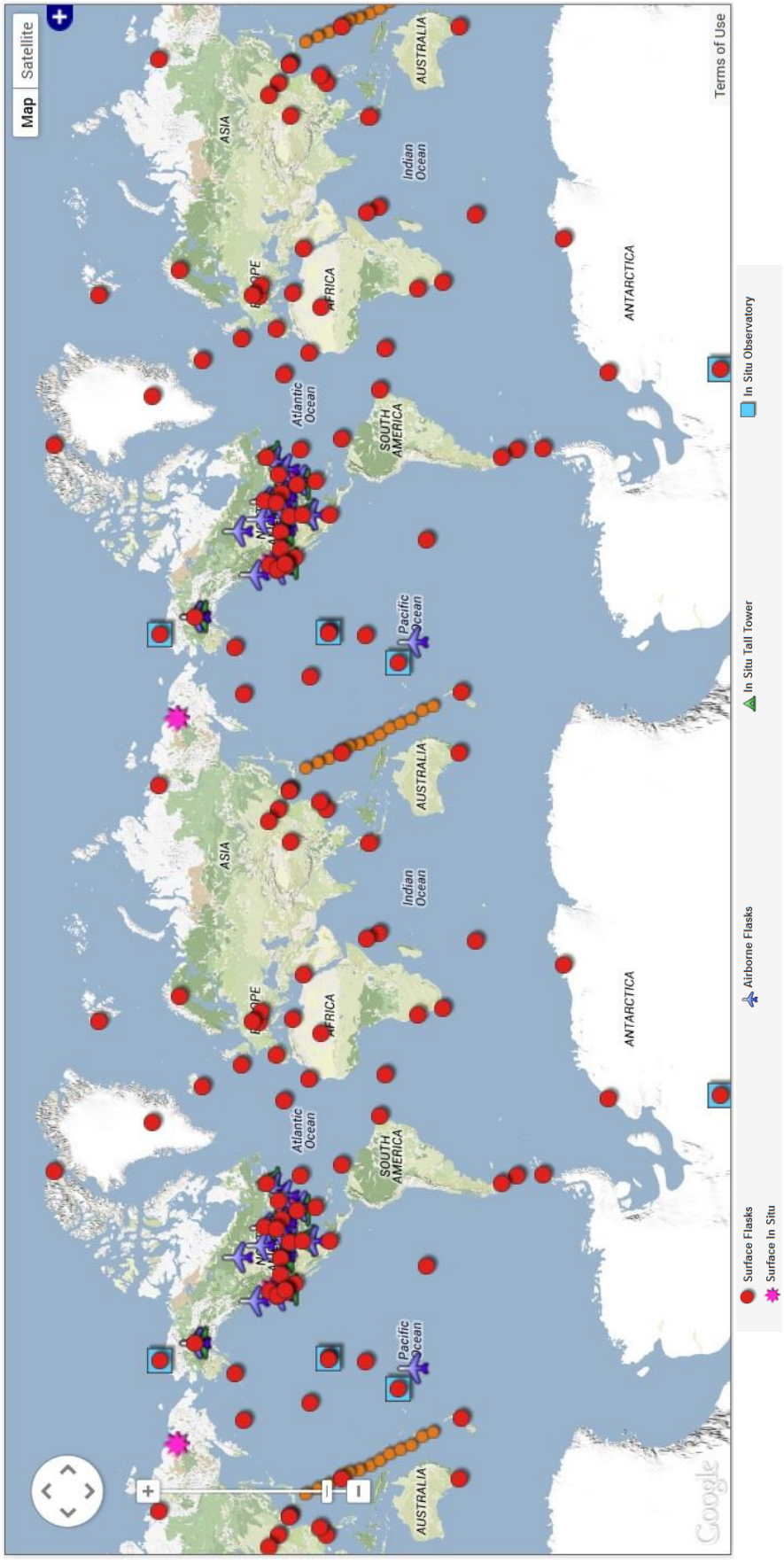

Figure A2. Active sites of the Greenhouse Gas Reference Network (GGRN) for atmospheric CO_2 monitoring. The Reference Network is part of NOAA's Earth System Research Laboratory (ESRL) in Boulder, Colorado.

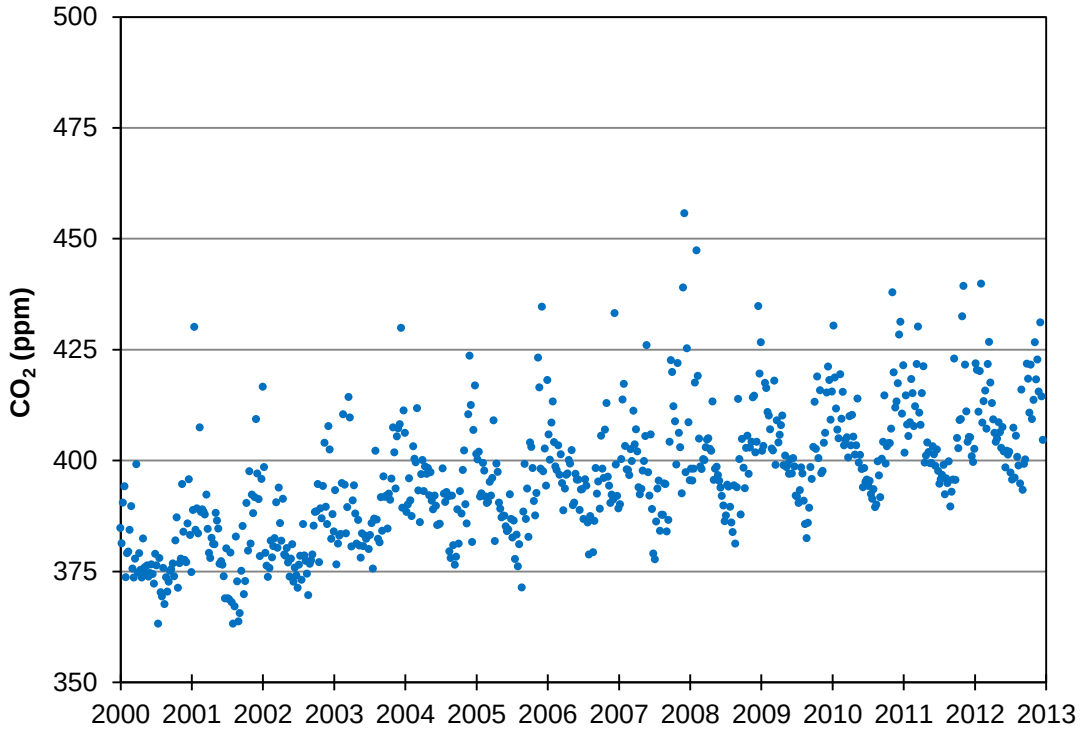

Figure B1. CO_2 weekly averages at the EGH site calculated from daily averages during 2000-2012.

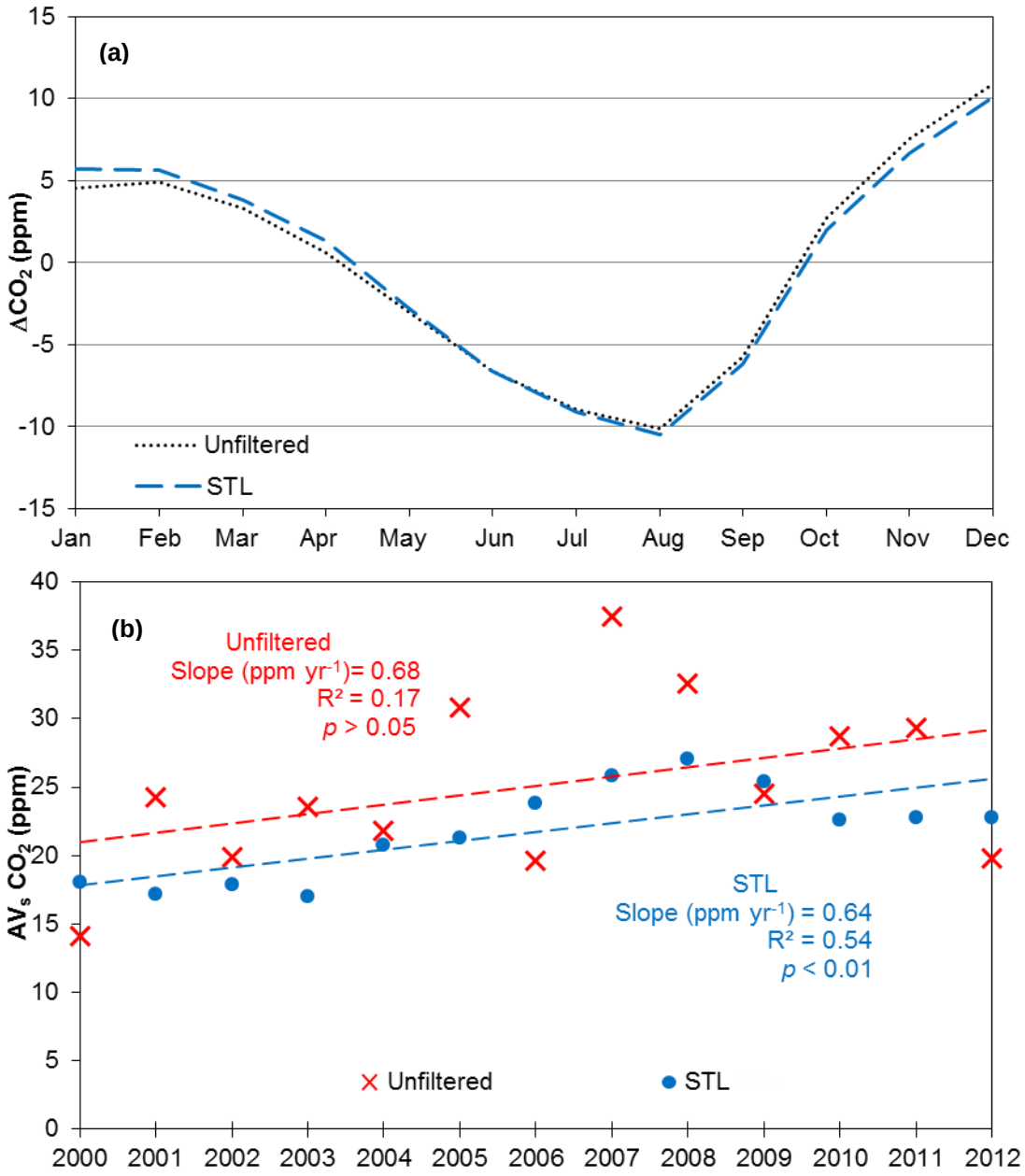

Figure B2. Comparison of averaged yearly cycles from STL filtered and unfiltered data at EGH during 2000-2012.

Table B1. Hourly averages of the CO_2 average diurnal cycle and 1SD by season at EGH during 2000-2012.

Time/Season	Winter	Spring	Summer	Autumn
00:00	403.6 ± 24.1	401.3 ± 17.6	395.3 ± 14.4	400.2 ± 21.9
01:00	402.9 ± 24.0	402.2 ± 18.4	397.3 ± 15.5	400.6 ± 22.3
02:00	402.1 ± 23.5	402.8 ± 19.1	399.0 ± 16.7	400.7 ± 21.9
03:00	402.0 ± 23.4	403.6 ± 19.7	400.9 ± 17.9	400.9 ± 22.1
04:00	401.8 ± 23.5	404.8 ± 21.0	402.9 ± 19.4	401.7 ± 23.0
05:00	402.2 ± 23.6	406.1 ± 22.3	403.2 ± 20.4	403.4 ± 24.5
06:00	403.3 ± 23.7	406.6 ± 23.6	399.3 ± 19.7	405.7 ± 26.6
07:00	405.8 ± 25.9	404.8 ± 24.2	392.9 ± 17.2	406.5 ± 28.7
08:00	407.5 ± 27.4	400.8 ± 22.2	387.2 ± 15.0	403.7 ± 28.7
09:00	407.6 ± 28.8	396.1 ± 19.3	383.0 ± 14.3	398.3 ± 26.6
10:00	404.9 ± 27.3	392.4 ± 16.2	380.4 ± 13.3	393.1 ± 23.8
11:00	402.2 ± 25.4	389.8 ± 14.1	378.9 ± 12.6	389.5 ± 20.7
12:00	400.0 ± 22.4	388.3 ± 12.8	377.9 ± 12.3	387.2 ± 18.0
13:00	398.4 ± 21.0	387.3 ± 12.4	377.3 ± 12.2	386.1 ± 16.5
14:00	397.4 ± 19.2	386.9 ± 12.3	376.9 ± 12.1	385.8 ± 16.1
15:00	397.9 ± 19.0	387.1 ± 12.7	376.9 ± 11.9	386.5 ± 16.3
16:00	399.6 ± 18.6	387.6 ± 12.8	377.2 ± 11.9	388.7 ± 17.4
17:00	401.9 ± 19.0	388.4 ± 12.5	377.8 ± 12.5	392.0 ± 19.1
18:00	403.7 ± 20.3	390.4 ± 13.4	378.9 ± 12.7	395.0 ± 19.5
19:00	404.8 ± 21.7	393.2 ± 13.8	381.2 ± 12.2	397.3 ± 20.5
20:00	405.3 ± 23.2	396.0 ± 13.9	384.9 ± 12.3	398.7 ± 21.5
21:00	405.4 ± 23.8	398.0 ± 14.7	388.3 ± 12.7	399.4 ± 21.4
22:00	405.3 ± 24.5	399.4 ± 15.6	391.2 ± 13.5	399.9 ± 21.4
23:00	404.9 ± 25.1	400.4 ± 16.4	393.3 ± 13.9	400.3 ± 22.2

Table B2. Hourly averages of the CO_2 diurnal cycle on Sunday and 1SD by season at EGH during 2000-2012.

	Time/Season	Winter	Spring	Summer	Autumn
Sunday	**00:00**	402.0 ± 21.9	400.5 ± 15.8	395.2 ± 14.6	401.2 ± 20.6
	01:00	401.1 ± 22.0	401.9 ± 16.6	396.9 ± 15.4	402.8 ± 22.4
	02:00	400.6 ± 21.5	402.3 ± 16.4	399.0 ± 17.0	403.0 ± 23.2
	03:00	400.5 ± 22.3	402.8 ± 16.9	400.6 ± 17.9	403.5 ± 23.9
	04:00	401.0 ± 23.5	404.1 ± 18.0	402.2 ± 18.8	404.1 ± 25.2
	05:00	401.2 ± 22.4	404.9 ± 19.1	402.5 ± 20.1	405.2 ± 26.4
	06:00	401.9 ± 22.9	404.5 ± 20.0	398.4 ± 20.0	406.3 ± 28.9
	07:00	402.9 ± 24.5	402.5 ± 19.9	391.8 ± 18.4	405.8 ± 31.0
	08:00	404.0 ± 27.0	398.2 ± 17.6	386.0 ± 16.3	402.1 ± 30.2
	09:00	403.7 ± 28.8	393.3 ± 15.8	381.6 ± 15.2	396.2 ± 26.0
	10:00	402.0 ± 28.0	389.7 ± 14.2	378.5 ± 14.8	390.8 ± 21.5
	11:00	399.3 ± 25.3	387.3 ± 13.3	376.6 ± 14.3	387.6 ± 19.3
	12:00	397.2 ± 23.0	386.3 ± 12.5	375.4 ± 14.2	384.8 ± 15.8
	13:00	395.7 ± 21.9	385.2 ± 12.6	374.6 ± 13.3	383.3 ± 14.6
	14:00	394.7 ± 21.7	384.8 ± 13.2	374.1 ± 12.7	383.0 ± 14.8
	15:00	395.1 ± 22.1	384.8 ± 12.4	374.1 ± 12.6	383.3 ± 14.9
	16:00	396.2 ± 18.9	385.2 ± 12.2	374.5 ± 12.6	385.2 ± 15.9
	17:00	398.2 ± 18.3	386.6 ± 12.9	375.1 ± 12.9	388.4 ± 17.5
	18:00	400.1 ± 19.0	389.1 ± 14.7	376.3 ± 13.0	391.5 ± 18.2
	19:00	402.2 ± 21.9	392.0 ± 14.4	378.8 ± 12.9	394.1 ± 20.2
	20:00	403.1 ± 25.2	394.7 ± 13.5	383.1 ± 12.6	395.8 ± 21.3
	21:00	403.6 ± 25.0	397.0 ± 13.8	386.9 ± 13.1	396.9 ± 22.9
	22:00	403.5 ± 23.6	398.8 ± 14.5	390.4 ± 14.7	398.5 ± 24.4
	23:00	402.4 ± 22.3	399.9 ± 15.0	392.9 ± 15.5	398.4 ± 25.3

**Averages are expressed in ppm CO_2*

***Hour corresponds to GMT*

Table B3. Hourly averages of the CO_2 diurnal cycle on weekdays and 1SD by season at EGH during 2000-2012.

	Time/Season	Winter	Spring	Summer	Autumn
Weekdays	**00:00**	403.9 ± 1.6	401.3 ± 2.4	395.2 ± 0.7	399.8 ± 1.5
	01:00	403.0 ± 1.7	402.1 ± 2.6	397.3 ± 0.7	400.0 ± 1.0
	02:00	402.3 ± 1.3	402.8 ± 2.6	398.9 ± 1.3	400.0 ± 1.0
	03:00	402.2 ± 1.5	403.5 ± 2.1	400.8 ± 1.6	400.9 ± 0.9
	04:00	401.7 ± 1.4	404.7 ± 1.8	402.9 ± 1.9	402.7 ± 0.6
	05:00	402.2 ± 1.4	406.1 ± 2.4	403.2 ± 2.1	405.4 ± 0.7
	06:00	403.5 ± 1.3	406.8 ± 2.1	399.5 ± 1.7	406.6 ± 0.9
	07:00	406.4 ± 1.3	405.2 ± 3.0	393.3 ± 1.4	404.2 ± 1.0
	08:00	408.3 ± 1.6	401.5 ± 2.7	387.7 ± 0.8	398.9 ± 1.5
	09:00	408.6 ± 2.3	396.9 ± 3.8	383.5 ± 0.7	393.8 ± 1.9
	10:00	405.8 ± 1.6	393.3 ± 3.4	381.1 ± 0.6	390.2 ± 1.9
	11:00	403.2 ± 1.7	390.7 ± 4.1	379.8 ± 0.7	388.1 ± 1.9
	12:00	400.9 ± 1.1	389.1 ± 3.5	378.8 ± 0.8	387.0 ± 1.4
	13:00	399.3 ± 1.1	388.1 ± 3.4	378.2 ± 0.7	386.8 ± 1.1
	14:00	398.4 ± 0.8	387.6 ± 2.2	377.8 ± 0.6	387.6 ± 1.1
	15:00	399.0 ± 0.6	387.9 ± 2.1	377.9 ± 0.8	389.9 ± 1.1
	16:00	400.8 ± 0.6	388.3 ± 1.2	378.2 ± 0.7	393.3 ± 1.2
	17:00	403.3 ± 0.7	389.0 ± 0.9	378.8 ± 0.7	396.2 ± 1.5
	18:00	405.2 ± 0.8	390.8 ± 0.9	379.8 ± 0.6	398.4 ± 1.4
	19:00	405.9 ± 0.5	393.8 ± 0.6	381.9 ± 0.4	399.4 ± 1.3
	20:00	406.3 ± 0.8	396.6 ± 1.5	385.5 ± 0.4	400.1 ± 1.1
	21:00	406.3 ± 1.1	398.6 ± 1.1	388.7 ± 0.2	400.3 ± 1.3
	22:00	406.0 ± 1.3	399.8 ± 1.5	391.4 ± 0.3	400.7 ± 1.5
	23:00	405.7 ± 1.1	400.7 ± 1.5	393.4 ± 0.7	400.1 ± 1.5

**Averages are expressed in ppm CO_2*

***Hour corresponds to GMT*

Table B4. Hourly averages of the CO_2 diurnal cycle on Saturday and 1SD by season at EGH during 2000-2012.

	Time/Season	Winter	Spring	Summer	Autumn
Saturday	**00:00**	403.4 ± 24.4	401.8 ± 18.8	395.8 ± 14.4	401.8 20.7
	01:00	403.8 ± 25.0	402.8 ± 19.9	398.0 ± 14.9	402.2 ± 21.3
	02:00	402.7 ± 24.0	403.3 ± 20.9	400.0 ± 16.3	402.0 ± 21.2
	03:00	403.1 ± 24.9	404.9 ± 22.7	401.4 ± 16.8	402.7 ± 23.8
	04:00	403.5 ± 26.9	405.9 ± 24.0	403.4 ± 18.5	403.1 ± 24.6
	05:00	403.4 ± 26.3	407.3 ± 25.5	403.7 ± 19.8	405.1 ± 25.7
	06:00	404.0 ± 26.2	407.4 ± 28.1	399.1 ± 19.1	406.6 ± 27.6
	07:00	405.8 ± 27.0	405.3 ± 27.8	392.0 ± 15.3	406.5 ± 31.0
	08:00	407.2 ± 28.5	400.0 ± 23.3	386.4 ± 13.5	403.1 ± 29.6
	09:00	406.6 ± 29.4	394.5 ± 19.9	381.7 ± 12.8	398.0 ± 26.8
	10:00	403.4 ± 27.1	390.6 ± 16.1	378.7 ± 12.0	392.0 ± 21.7
	11:00	400.1 ± 25.1	387.9 ± 13.9	377.1 ± 12.1	387.6 ± 17.0
	12:00	397.8 ± 22.1	386.3 ± 12.8	376.0 ± 12.0	385.3 ± 15.6
	13:00	396.3 ± 20.4	385.8 ± 12.7	375.3 ± 12.3	384.4 ± 14.7
	14:00	395.4 ± 19.2	385.3 ± 12.5	375.1 ± 12.7	383.8 ± 14.7
	15:00	394.8 ± 18.2	385.4 ± 12.6	374.8 ± 12.4	384.5 ± 16.3
	16:00	396.5 ± 18.0	386.1 ± 12.7	374.9 ± 12.1	386.4 ± 17.6
	17:00	398.6 ± 16.8	387.3 ± 13.9	375.4 ± 12.1	389.2 ± 17.1
	18:00	400.2 ± 17.0	389.4 ± 14.2	376.8 ± 11.9	392.8 ± 16.8
	19:00	401.5 ± 17.9	391.3 ± 13.0	379.7 ± 12.1	395.5 ± 17.0
	20:00	402.2 ± 19.3	394.1 ± 11.9	383.5 ± 12.3	398.0 ± 18.4
	21:00	402.6 ± 20.0	396.1 ± 12.6	387.6 ± 12.8	398.7 ± 18.7
	22:00	403.2 ± 20.7	398.1 ± 13.5	390.8 ± 13.3	399.6 ± 19.4
	23:00	403.5 ± 22.7	399.6 ± 14.9	393.0 ± 13.6	400.5 ± 20.0

**Averages are expressed in ppm CO_2*

***Hour corresponds to GMT*

Table B5. Monthly averages of CO_2 and 1SD calculated at EGH during 2000-2012.

Month/Year	2000	2001	2002	2003	2004	2005	2006
Jan	385.7 ± 9.7	394.3 ± 24.7	391.2 ± 18.3	382.6 ± 8.0	391.3 ± 6.2	397.5 ± 11.3	405.6 ± 16.7
Feb	382.9 ± 10.9	390.9 ± 14.7	377.3 ± 5.1	395.5 ± 16.9	403.7 ± 11.0	391.5 ± 12.1	399.3 ± 8.8
Mar	379.8 ± 12.2	389.2 ± 9.8	384.3 ± 8.7	397.6 ± 16.7	395.6 ± 8.7	396.1 ± 13.1	394.8 ± 6.3
Apr	377.3 ± 8.5	380.4 ± 4.7	386.5 ± 9.8	388.8 ± 10.1	396.5 ± 8.3	393.4 ± 8.4	399.5 ± 6.4
May	375.4 ± 4.4	384.2 ± 7.3	377.2 ± 4.7	380.8 ± 4.9	393.0 ± 6.3	386.9 ± 4.1	394.0 ± 5.1
Jun	375.4 ± 6.8	375.6 ± 6.1	376.6 ± 5.8	382.7 ± 4.9	386.1 ± 3.3	386.9 ± 8.8	391.9 ± 8.4
Jul	372.1 ± 8.9	373.4 ± 7.8	374.2 ± 6.2	386.7 ± 11.4	393.0 ± 7.4	382.0 ± 6.3	389.2 ± 8.7
Aug	371.7 ± 5.0	370.0 ± 10.2	377.6 ± 9.3	385.3 ± 8.0	384.7 ± 10.3	385.0 ± 9.1	386.0 ± 7.2
Sep	373.0 ± 6.8	372.3 ± 13.5	381.9 ± 12.5	389.0 ± 8.7	381.9 ± 13.2	391.0 ± 10.8	393.6 ± 8.2
Oct	379.3 ± 10.1	378.6 ± 10.1	386.6 ± 11.0	396.1 ± 12.2	393.8 ± 10.6	396.7 ± 11.0	405.1 ± 15.8
Nov	383.5 ± 15.4	390.0 ± 13.4	392.5 ± 17.6	403.8 ± 15.0	400.2 ± 21.8	406.4 ± 23.2	393.6 ± 5.7
Dec	384.7 ± 11.9	394.0 ± 21.8	394.1 ± 14.6	404.4 ± 22.3	403.4 ± 25.3	412.8 ± 25.6	402.4 ± 19.8
Annual average	378.4 ± 5.0	382.7 ± 8.8	383.3 ± 6.9	391.1 ± 8.2	393.6 ± 7.0	393.8 ± 8.9	396.2 ± 6.2

**Averages are expressed in ppm CO_2*

*** Annual standard deviation was calculated from monthly averages*

Table B5. (Continuation) Monthly averages of CO_2 and 1SD calculated at EGH during 2000-2012.

Month/Year	2007	2008	2009	2010	2011	2012
Jan	404.9 ± 15.7	399.2 ± 9.8	412.9 ± 15.7	415.8 ± 15.6	410.6 ± 9.7	414.8 ± 20.2
Feb	398.9 ± 6.5	419.4 ± 31.5	408.2 ± 7.2	412.5 ± 10.9	411.3 ± 11.7	419.5 ± 17.9
Mar	404.9 ± 10.4	401.2 ± 5.6	406.5 ± 10.2	403.7 ± 4.1	417.4 ± 12.6	418.3 ± 12.7
Apr	396.7 ± 6.0	403.9 ± 5.3	406.1 ± 8.5	407.0 ± 7.5	410.3 ± 10.8	408.3 ± 6.6
May	406.0 ± 16.1	399.3 ± 8.4	399.2 ± 6.4	403.8 ± 7.6	401.5 ± 3.1	405.8 ± 5.4
Jun	395.1 ± 11.2	392.2 ± 6.0	398.7 ± 6.4	397.0 ± 4.0	401.1 ± 5.2	401.6 ± 5.5
Jul	385.8 ± 8.1	391.2 ± 7.2	392.4 ± 3.9	394.1 ± 3.9	396.7 ± 4.7	400.1 ± 7.3
Aug	389.3 ± 8.7	386.8 ± 10.7	390.3 ± 7.7	393.1 ± 6.1	396.1 ± 6.0	399.8 ± 8.3
Sep	395.2 ± 13.4	399.4 ± 11.7	393.3 ± 9.2	399.0 ± 9.2	399.8 ± 15.7	402.9 ± 14.0
Oct	413.3 ± 15.7	401.7 ± 9.8	407.9 ± 14.0	403.7 ± 9.1	403.8 ± 9.0	415.9 ± 15.3
Nov	404.9 ± 18.3	404.0 ± 12.7	404.0 ± 13.4	418.5 ± 20.2	425.4 ± 22.0	418.2 ± 15.1
Dec	423.3 ± 37.6	412.1 ± 13.0	414.9 ± 17.0	421.7 ± 13.4	403.7 ± 4.5	417.1 ± 18.9
Annual average	401.5 ± 10.3	400.9 ± 8.9	402.9 ± 8.0	405.8 ± 9.5	406.5 ± 8.8	410.2 ± 7.9

**Averages are expressed in ppm CO_2*

*** Annual standard deviation was calculated from monthly averages*

Table B6. Annual averages of CO_2 by wind sector and 1SD calculated at EGH during 2000-2012.

Year/Sector	N	NE	E	SE	S	SW	W	NW
2000	376.6 ± 14.6	375.7 ± 15.6	380.4 ± 15.4	376.1 ± 14.2	373.5 ± 10.3	374.0 ± 11.1	376.7 ± 13.3	376.9 ± 14.5
2001	384.0 ± 19.9	387.7 ± 18.0	388.9 ± 21.8	379.6 ± 16.8	373.8 ± 10.5	374.1 ± 11.0	378.5 ± 14.9	380.9 ± 17.7
2002	379.5 ± 15.8	386.3 ± 17.6	391.0 ± 18.6	384.0 ± 17.3	377.7 ± 10.5	376.1 ± 9.2	378.6 ± 11.9	379.7 ± 13.7
2003	391.4 ± 19.0	393.8 ± 18.8	395.9 ± 20.1	391.4 ± 18.4	384.3 ± 14.1	382.4 ± 12.2	386.1 ± 14.4	389.0 ± 15.4
2004	394.4 ± 17.0	393.9 ± 17.0	395.0 ± 19.5	395.9 ± 17.9	388.1 ± 18.2	390.9 ± 21.9	391.7 ± 16.0	393.5 ± 15.7
2005	387.6 ± 13.2	389.0 ± 14.3	396.0 ± 17.1	392.1 ± 13.0	388.3 ± 11.8	386.3 ± 11.7	388.8 ± 15.1	390.5 ± 16.9
2006	397.1 ± 19.7	398.2 ± 14.3	401.1 ± 15.7	394.9 ± 14.1	390.8 ± 9.7	390.5 ± 9.8	395.5 ± 15.8	396.6 ± 18.8
2007	400.2 ± 24.8	405.4 ± 30.0	405.8 ± 23.7	412.2 ± 43.5	392.3 ± 14.0	394.5 ± 17.7	401.8 ± 24.8	397.2 ± 19.3
2008	412.3 ± 29.5	408.0 ± 23.9	406.8 ± 23.7	401.0 ± 21.7	395.5 ± 14.2	396.4 ± 15.5	401.3 ± 18.2	402.6 ± 19.2
2009	405.1 ± 19.8	401.9 ± 17.1	406.0 ± 18.5	405.9 ± 18.0	401.1 ± 16.6	399.6 ± 16.4	406.2 ± 21.6	404.5 ± 19.1
2010	407.9 ± 19.4	406.8 ± 18.1	410.3 ± 20.8	408.0 ± 20.5	403.2 ± 16.4	401.8 ± 14.9	408.1 ± 21.2	405.2 ± 14.9
2011	412.1 ± 23.7	410.8 ± 20.2	418.1 ± 24.5	411.5 ± 20.9	403.7 ± 17.6	401.9 ± 12.8	404.9 ± 17.4	406.4 ± 16.5
2012	415.4 ± 26.2	415.2 ± 23.0	418.4 ± 23.4	414.8 ± 27.4	404.0 ± 15.6	404.1 ± 13.7	412.5 ± 21.2	411.6 ± 21.0

Averages are expressed in ppm CO_2

Annual standard deviation was calculated from montly averages

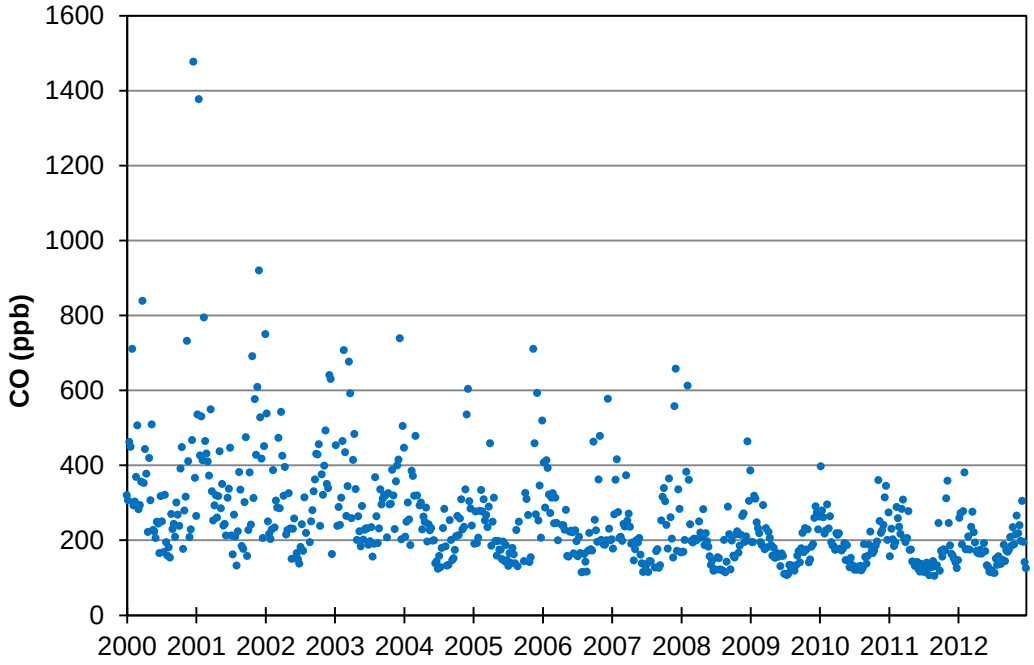

Figure C1. CO weekly averages at the EGH site calculated from daily averages during 2000-2012.

Table C1. Hourly averages of the CO average diurnal cycle and 1SD by season at EGH during 2000-2012.

Time/Season	Winter	Spring	Summer	Autumn
00:00	339.4 ± 323.5	269.6 ± 184.0	183.3 ± 109.3	255.5 ± 240.7
01:00	315.2 ± 295.9	254.8 ± 168.8	173.5 ± 98.9	238.9 ± 219.7
02:00	294.6 ± 261.4	243.8 ± 160.7	165.5 ± 94.1	226.3 ± 200.8
03:00	283.7 ± 251.3	235.4 ± 151.8	162.1 ± 91.5	213.6 ± 186.2
04:00	273.6 ± 239.2	232.3 ± 146.9	163.1 ± 96.2	205.1 ± 160.6
05:00	268.2 ± 228.3	238.7 ± 146.9	172.4 ± 107.4	209.8 ± 172.5
06:00	271.2 ± 220.7	257.3 ± 161.2	183.7 ± 119.5	230.1 ± 180.2
07:00	296.6 ± 245.4	286.3 ± 199.9	191.9 ± 129.5	266.2 ± 206.7
08:00	346.3 ± 311.1	303.9 ± 233.6	192.4 ± 129.7	300.6 ± 259.3
09:00	379.2 ± 345.5	286.0 ± 213.2	179.8 ± 117.4	286.7 ± 253.7
10:00	358.6 ± 326.3	258.0 ± 170.9	166.3 ± 98.9	252.8 ± 217.5
11:00	330.5 ± 292.0	234.7 ± 132.5	155.5 ± 77.5	223.7 ± 180.0
12:00	313.2 ± 271.2	225.8 ± 112.4	151.9 ± 73.9	206.8 ± 162.2
13:00	300.7 ± 253.4	218.6 ± 102.3	149.7 ± 73.0	198.0 ± 139.8
14:00	292.0 ± 241.1	215.2 ± 98.6	147.6 ± 65.2	195.7 ± 125.2
15:00	300.4 ± 245.3	218.8 ± 96.8	149.9 ± 69.9	208.6 ± 128.0
16:00	324.1 ± 246.3	228.0 ± 104.0	157.4 ± 73.6	239.5 ± 162.2
17:00	366.1 ± 278.3	242.0 ± 122.9	162.0 ± 79.7	276.5 ± 219.3
18:00	396.4 ± 324.2	261.8 ± 149.3	167.6 ± 84.4	303.5 ± 248.0
19:00	398.8 ± 330.8	279.4 ± 168.0	178.8 ± 96.9	307.7 ± 246.7
20:00	391.6 ± 327.2	294.7 ± 183.1	192.9 ± 109.9	304.2 ± 261.4
21:00	383.6 ± 339.3	295.5 ± 186.0	199.2 ± 111.5	293.3 ± 258.4
22:00	375.6 ± 344.0	292.7 ± 191.4	200.1 ± 119.3	285.5 ± 246.6
23:00	365.7 ± 344.3	281.9 ± 188.1	193.9 ± 119.1	275.0 ± 250.3

**Averages are expressed in ppb CO*

***Hour corresponds to GMT*

Table C2. Hourly averages of the CO diurnal cycle on Sunday and 1SD by season at EGH during 2000-2012.

	Time/Season	Winter	Spring	Summer	Autumn
Sunday	**00:00**	327.6 ± 336.1	257.5 ± 141.8	186.1 ± 87.8	280.9 ± 259.4
	01:00	306.2 ± 311.3	250.4 ± 138.4	177.8 ± 86.3	269.4 ± 244.8
	02:00	292.1 ± 294.5	237.6 ± 120.0	166.7 ± 77.3	264.8 ± 243.2
	03:00	281.0 ± 277.9	228.2 ± 112.9	166.0 ± 82.8	250.0 ± 241.7
	04:00	273.5 ± 263.0	225.1 ± 109.2	169.7 ± 95.5	232.2 ± 171.0
	05:00	265.3 ± 234.6	225.1 ± 112.6	174.7 ± 102.8	231.3 ± 174.5
	06:00	258.7 ± 214.1	230.7 ± 118.8	171.7 ± 95.3	227.7 ± 165.8
	07:00	255.7 ± 194.8	235.2 ± 135.3	168.2 ± 97.4	241.2 ± 192.1
	08:00	262.3 ± 199.9	238.4 ± 144.2	162.0 ± 86.4	241.4 ± 180.9
	09:00	276.9 ± 232.4	230.5 ± 124.4	158.5 ± 77.3	236.3 ± 184.4
	10:00	296.1 ± 294.4	221.6 ± 97.9	152.8 ± 68.3	222.6 ± 160.9
	11:00	290.7 ± 239.8	211.2 ± 86.5	147.4 ± 62.7	208.8 ± 150.5
	12:00	290.1 ± 250.5	212.8 ± 88.1	145.7 ± 61.7	198.3 ± 133.5
	13:00	281.4 ± 251.2	204.4 ± 71.1	144.3 ± 62.4	187.0 ± 106.0
	14:00	275.4 ± 263.3	202.5 ± 70.6	144.1 ± 61.4	180.5 ± 86.9
	15:00	277.7 ± 261.9	200.8 ± 61.0	146.2 ± 67.3	186.9 ± 98.5
	16:00	292.7 ± 246.9	206.6 ± 67.5	146.4 ± 61.1	204.9 ± 121.2
	17:00	315.4 ± 271.0	217.4 ± 83.3	153.9 ± 66.9	231.9 ± 173.8
	18:00	342.9 ± 349.3	237.0 ± 111.5	158.6 ± 69.5	248.6 ± 177.9
	19:00	359.4 ± 331.6	265.3 ± 141.8	172.4 ± 85.0	262.7 ± 173.8
	20:00	360.0 ± 315.1	289.8 ± 171.6	194.1 ± 108.3	267.0 ± 205.5
	21:00	355.6 ± 318.8	296.3 ± 180.3	205.6 ± 120.0	263.5 ± 183.7
	22:00	353.1 ± 334.5	302.4 ± 222.2	208.9 ± 137.9	262.4 ± 187.9
	23:00	325.9 ± 272.2	293.9 ± 222.8	197.1 ± 127.6	250.2 ± 170.8

**Averages are expressed in ppb CO*
***Hour corresponds to GMT*

Table C3. Hourly averages of the CO diurnal cycle on weekdays and 1SD by season at EGH during 2000-2012.

	Time/Season	Winter	Spring	Summer	Autumn
Weekdays	**00:00**	340.5 ± 19.5	269.7 ± 30.2	184.1 ± 4.9	247.5 ± 24.5
	01:00	313.9 ± 16.2	253.8 ± 34.3	172.1 ± 6.5	229.9 ± 20.0
	02:00	293.4 ± 11.6	242.7 ± 9.0	165.0 ± 7.0	215.3 ± 16.8
	03:00	281.6 ± 14.5	233.6 ± 18.1	160.9 ± 8.3	201.6 ± 13.5
	04:00	270.5 ± 14.2	229.4 ± 15.8	161.8 ± 8.8	194.7 ± 10.2
	05:00	267.2 ± 16.0	238.1 ± 18.6	172.7 ± 9.6	201.8 ± 7.1
	06:00	273.9 ± 15.2	261.6 ± 20.8	188.5 ± 12.3	230.3 ± 7.2
	07:00	308.2 ± 15.9	298.6 ± 34.7	200.8 ± 13.9	275.1 ± 11.7
	08:00	373.1 ± 26.7	324.3 ± 63.5	202.0 ± 9.8	320.4 ± 19.0
	09:00	412.6 ± 23.0	304.2 ± 47.2	186.5 ± 7.2	300.6 ± 18.3
	10:00	379.5 ± 24.4	269.7 ± 43.5	170.2 ± 7.1	260.0 ± 19.6
	11:00	343.8 ± 23.0	241.9 ± 50.2	158.1 ± 5.6	226.7 ± 15.9
	12:00	321.5 ± 18.3	230.7 ± 43.3	154.0 ± 3.9	209.2 ± 12.4
	13:00	307.1 ± 12.6	222.8 ± 24.2	152.2 ± 2.8	199.8 ± 10.3
	14:00	298.5 ± 11.7	219.9 ± 32.6	149.2 ± 3.2	198.1 ± 8.3
	15:00	309.7 ± 7.3	225.1 ± 32.5	151.7 ± 4.4	213.3 ± 12.8
	16:00	338.3 ± 5.9	235.5 ± 18.9	161.6 ± 5.4	248.8 ± 14.5
	17:00	387.7 ± 8.7	250.5 ± 31.0	165.7 ± 8.0	288.7 ± 18.7
	18:00	419.4 ± 10.9	271.7 ± 33.9	170.4 ± 6.3	316.2 ± 24.5
	19:00	415.3 ± 8.3	286.8 ± 45.0	181.0 ± 6.7	317.3 ± 24.5
	20:00	406.2 ± 10.2	300.2 ± 21.6	193.9 ± 7.5	309.7 ± 26.1
	21:00	395.1 ± 12.2	300.6 ± 13.4	198.4 ± 6.3	298.4 ± 29.0
	22:00	383.5 ± 12.4	295.7 ± 19.6	198.7 ± 5.5	289.0 ± 32.2
	23:00	374.2 ± 14.4	282.7 ± 23.7	193.1 ± 4.6	277.2 ± 26.7

**Averages are expressed in ppb CO*
***Hour corresponds to GMT*

Table C4. Hourly averages of the CO diurnal cycle on Saturday and 1SD by season at EGH during 2000-2012.

	Time/Season	Winter	Spring	Summer	Autumn
Saturday	**00:00**	345.2 ± 325.3	281.0 ± 185.9	177.4 ± 86.9	270.0 ± 213.1
	01:00	330.9 ± 308.8	264.5 ± 173.6	176.8 ± 100.1	252.6 ± 186.1
	02:00	303.2 ± 263.8	256.1 ± 181.7	168.1 ± 92.8	241.9 ± 182.9
	03:00	297.2 ± 268.8	252.3 ± 192.0	165.0 ± 86.8	236.8 ± 200.5
	04:00	289.0 ± 251.5	254.6 ± 205.9	164.1 ± 87.1	229.8 ± 203.7
	05:00	276.5 ± 232.0	255.1 ± 200.9	169.4 ± 90.8	227.9 ± 188.3
	06:00	270.7 ± 211.0	262.9 ± 204.9	171.3 ± 90.3	231.6 ± 181.8
	07:00	280.8 ± 219.6	275.9 ± 239.8	169.6 ± 93.8	246.1 ± 200.3
	08:00	299.9 ± 233.7	266.6 ± 216.0	172.8 ± 108.2	258.9 ± 205.9
	09:00	320.6 ± 252.1	249.2 ± 167.5	165.5 ± 103.9	267.1 ± 256.7
	10:00	321.4 ± 240.6	234.8 ± 126.5	159.0 ± 94.0	247.8 ± 205.3
	11:00	306.8 ± 240.0	221.4 ± 100.1	149.6 ± 70.7	224.0 ± 156.4
	12:00	295.8 ± 238.5	213.3 ± 87.2	147.0 ± 73.1	203.5 ± 123.1
	13:00	288.7 ± 237.6	211.3 ± 91.1	142.0 ± 60.2	199.9 ± 122.6
	14:00	276.6 ± 229.4	203.6 ± 80.5	142.2 ± 58.0	199.0 ± 127.8
	15:00	276.8 ± 231.1	204.3 ± 82.2	144.1 ± 59.7	205.8 ± 125.1
	16:00	286.5 ± 230.9	210.3 ± 82.3	146.0 ± 63.2	225.9 ± 168.7
	17:00	310.8 ± 249.0	221.2 ± 94.9	150.8 ± 64.0	256.9 ± 226.1
	18:00	335.8 ± 272.1	234.4 ± 101.2	161.6 ± 79.0	291.0 ± 240.1
	19:00	356.0 ± 301.6	255.3 ± 121.3	173.4 ± 90.1	301.0 ± 231.4
	20:00	350.5 ± 293.6	271.1 ± 153.2	186.2 ± 95.8	311.6 ± 244.3
	21:00	354.1 ± 324.8	268.3 ± 130.8	197.3 ± 103.9	295.7 ± 219.5
	22:00	358.4 ± 345.0	267.3 ± 136.7	198.8 ± 103.4	289.1 ± 211.0
	23:00	363.0 ± 359.1	265.8 ± 150.3	194.4 ± 96.9	286.4 ± 224.4

**Averages are expressed in ppb CO*

***Hour corresponds to GMT*

Table C5. Monthly averages of CO and 1SD calculated at EGH during 2000-2012.

Month/Year	2000	2001	2002	2003	2004	2005	2006
Jan	463.4 ± 359.4	649.9 ± 612.5	399.3 ± 306.0	305.7 ± 174.1	273.1 ± 179.4	215.6 ± 127.4	389.3 ± 226.8
Feb	365.2 ± 321.4	524.8 ± 451.9	260.4 ± 139.9	478.0 ± 301.8	309.2 ± 195.1	304.3 ± 197.1	325.6 ± 170.5
Mar	413.7 ± 333.0	425.4 ± 283.9	389.5 ± 247.0	449.7 ± 278.2	380.6 ± 236.3	288.0 ± 133.7	273.5 ± 119.4
Apr	379.9 ± 240.2	283.7 ± 118.3	324.2 ± 216.4	353.6 ± 210.3	247.8 ± 111.7	249.8 ± 126.5	239.4 ± 86.7
May	293.7 ± 170.1	333.3 ± 173.1	227.4 ± 113.8	235.9 ± 119.2	225.1 ± 77.8	177.6 ± 55.5	207.7 ± 89.6
Jun	236.2 ± 152.0	276.1 ± 159.8	192.5 ± 98.3	221.0 ± 85.2	166.8 ± 67.1	166.6 ± 63.8	207.6 ± 73.0
Jul	229.0 ± 153.0	269.4 ± 157.4	199.4 ± 111.5	188.9 ± 80.7	163.8 ± 77.2	147.5 ± 63.9	184.3 ± 82.5
Aug	199.9 ± 106.5	266.5 ± 230.4	229.7 ± 126.7	252.7 ± 120.4	185.3 ± 96.5	173.0 ± 102.5	135.6 ± 45.0
Sep	236.6 ± 147.6	263.8 ± 231.4	313.2 ± 177.6	316.8 ± 187.9	187.8 ± 96.8	145.8 ± 56.4	175.9 ± 83.4
Oct	307.2 ± 262.8	250.2 ± 194.4	395.9 ± 241.0	291.9 ± 183.0	229.5 ± 142.6	247.7 ± 153.4	280.5 ± 204.1
Nov	421.7 ± 532.3	508.2 ± 459.2	382.6 ± 268.3	312.0 ± 234.1	303.4 ± 224.0	509.8 ± 360.2	284.8 ± 211.6
Dec	591.9 ± 598.9	507.4 ± 519.3	500.2 ± 286.6	433.5 ± 361.4	434.3 ± 273.8	370.0 ± 284.6	284.8 ± 204.9
Annual average	344.9 ± 116.5	379.9 ± 136.9	317.9 ± 97.4	320.0 ± 93.2	258.9 ± 85.5	249.6 ± 107.5	249.1 ± 71.1

**Averages expressed in ppb CO*

***Annual standard deviation was clculated from monthly averages*

Table C5. (Continuation) Monthly averages of CO and 1SD calculated at EGH during 2000-2012.

Month/Year	2007	2008	2009	2010	2011	2012
Jan	218.7 ± 78.8	195.4 ± 101.8	278.7 ± 140.0	292.4 ± 142.1	216.6 ± 86.8	222.9 149.1
Feb	305.2 ± 200.4	406.2 ± 307.1	249.3 ± 81.9	242.1 ± 93.5	229.2 ± 106.6	234.9 121.0
Mar	254.2 ± 116.2	196.0 ± 43.5	216.5 ± 85.8	203.5 ± 69.0	258.0 ± 89.6	229.0 90.2
Apr	236.2 ± 73.5	213.1 ± 58.1	206.3 ± 62.5	205.7 ± 52.1	207.8 ± 76.7	173.7 38.8
May	176.5 ± 44.8	223.2 ± 70.5	164.2 ± 37.9	169.9 ± 38.4	146.6 ± 26.3	174.7 44.8
Jun	166.1 ± 71.8	154.8 ± 36.4	154.6 ± 39.2	154.0 ± 43.3	127.8 ± 25.2	127.0 29.8
Jul	126.8 ± 55.8	137.5 ± 41.1	113.2 ± 24.8	123.9 ± 39.9	126.0 ± 30.5	124.6 29.3
Aug	143.4 ± 39.9	134.7 ± 59.5	126.6 ± 27.5	127.2 ± 27.2	124.5 ± 29.5	143.6 28.5
Sep	150.9 ± 61.0	186.2 ± 100.6	145.8 ± 50.1	166.9 ± 68.0	144.2 ± 76.1	166.4 51.6
Oct	300.0 ± 151.2	169.8 ± 81.1	191.8 ± 93.2	178.8 ± 64.0	161.6 ± 69.9	198.0 79.4
Nov	258.5 ± 168.1	198.8 ± 79.1	171.4 ± 81.2	246.3 ± 159.7	268.4 ± 158.2	226.7 120.2
Dec	396.9 ± 392.3	262.9 ± 137.1	237.1 ± 134.8	266.4 ± 103.0	156.6 ± 37.0	216.9 140.4
Annual average	227.8 ± 80.5	206.6 ± 72.6	188.0 ± 51.1	198.1 ± 54.4	180.6 ± 52.6	186.5 40.5

**Averages expressed in ppb CO*

***Annual standard deviation was clculated from monthly averages*

Table C6. Annual averages of CO by wind sector and 1SD calculated at EGH during 2000-2012.

Year/Sector	N	NE	E	SE	S	SW	W	NW
2000	372.8 ± 306.4	391.4 ± 332.9	624.4 ± 544.4	362.4 ± 330.6	236.5 ± 178.0	250.3 ± 196.0	281.9 ± 212.8	311.8 ± 239.5
2001	412.1 ± 368.4	481.2 ± 340.6	554.5 ± 415.5	358.4 ± 279.8	222.6 ± 149.5	241.3 ± 153.8	301.1 ± 256.6	358.0 ± 302.1
2002	307.9 ± 198.4	422.4 ± 233.4	494.2 ± 258.3	347.3 ± 243.6	223.4 ± 122.3	215.3 ± 115.4	239.3 ± 125.3	278.0 ± 158.2
2003	339.8 ± 232.1	417.1 ± 259.8	444.4 ± 247.9	364.4 ± 230.8	237.1 ± 157.7	216.1 ± 123.9	237.1 ± 151.7	292.2 ± 188.5
2004	270.6 ± 146.9	291.9 ± 160.6	316.2 ± 189.0	293.3 ± 180.6	192.2 ± 109.3	197.6 ± 116.7	226.5 ± 143.2	249.0 ± 144.6
2005	209.3 ± 102.7	247.1 ± 133.1	325.6 ± 164.6	244.4 ± 111.1	179.4 ± 103.8	170.9 ± 89.2	196.8 ± 110.5	232.2 ± 178.5
2006	273.5 ± 194.9	293.9 ± 156.8	298.9 ± 161.7	252.3 ± 116.8	196.6 ± 92.1	202.0 ± 117.9	245.1 ± 163.9	258.9 ± 183.1
2007	242.6 ± 190.0	294.5 ± 247.3	307.6 ± 177.3	348.4 ± 367.6	175.3 ± 89.0	184.9 ± 122.8	216.6 ± 153.7	221.2 ± 129.7
2008	292.9 ± 233.4	284.9 ± 196.9	288.0 ± 183.4	221.7 ± 139.0	176.1 ± 86.1	171.6 ± 93.1	186.8 ± 84.5	218.4 ± 126.7
2009	213.0 ± 100.8	209.2 ± 90.4	236.6 ± 109.8	214.9 ± 100.0	174.6 ± 85.6	159.3 ± 75.8	189.3 ± 97.2	204.6 ± 101.8
2010	215.8 ± 101.5	223.0 ± 105.9	246.0 ± 128.7	226.3 ± 121.8	184.3 ± 93.5	169.2 ± 76.8	191.9 ± 100.1	194.6 ± 77.5
2011	209.5 ± 99.7	227.6 ± 109.6	267.5 ± 133.4	218.9 ± 115.4	163.1 ± 76.2	149.5 ± 56.4	153.7 ± 61.0	180.6 ± 71.9
2012	223.0 ± 131.3	229.0 ± 119.6	245.8 ± 124.2	222.9 ± 142.4	158.6 ± 72.9	154.5 ± 58.0	178.5 ± 73.0	201.7 ± 100.4

**Averages are expressed in ppb CO*

***Annual standard deviation was calculated from monthly averages*

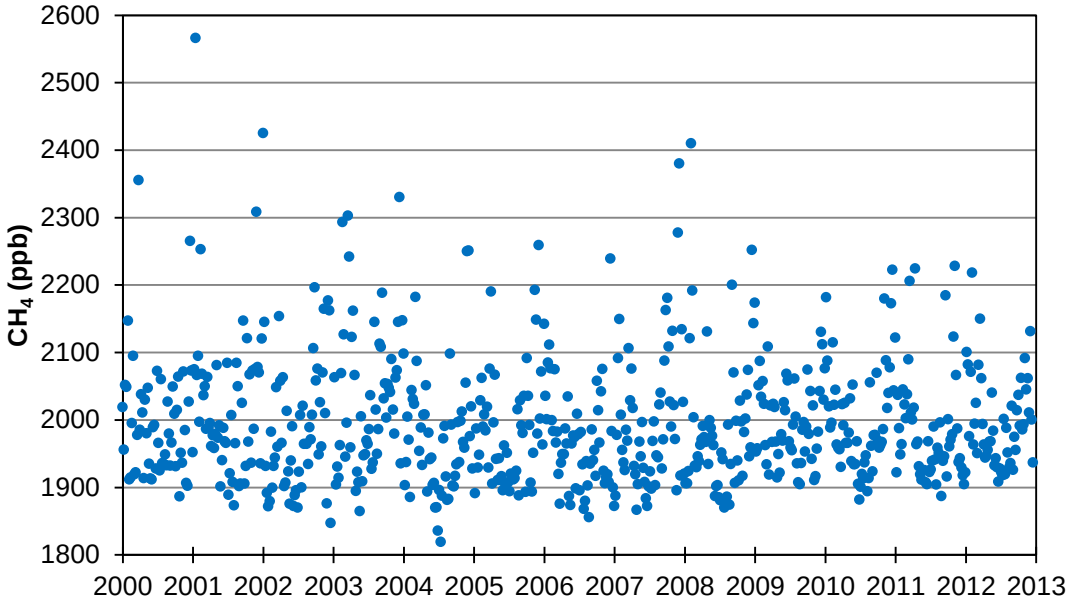

Figure D1. CH_4 weekly averages at the EGH site calculated from daily averages during 2000-2012.

Table D1. Hourly averages of the CH_4 average diurnal cycle and 1SD by season at EGH during 2000-2012.

Time/Season	Winter	Spring	Summer	Autumn
00:00	2052.2 ± 240.5	2025.0 ± 172.8	1977.6 ± 132.2	2026.7 ± 197.6
01:00	2059.5 ± 235.1	2038.1 ± 191.3	1988.9 ± 136.6	2036.3 ± 196.8
02:00	2064.4 ± 244.7	2047.6 ± 203.7	2005.6 ± 159.6	2053.9 ± 243.3
03:00	2075.5 ± 266.6	2065.5 ± 264.9	2017.4 ± 173.5	2053.5 ± 221.1
04:00	2085.0 ± 296.1	2074.5 ± 277.3	2035.4 ± 202.5	2066.0 ± 252.1
05:00	2085.3 ± 291.4	2087.4 ± 273.5	2046.2 ± 224.9	2074.8 ± 296.1
06:00	2084.4 ± 289.6	2083.6 ± 261.9	2025.5 ± 205.0	2077.0 ± 276.7
07:00	2086.5 ± 299.5	2062.0 ± 246.1	1991.8 ± 175.6	2070.3 ± 251.6
08:00	2086.9 ± 309.8	2023.9 ± 207.6	1958.4 ± 136.8	2057.8 ± 270.7
09:00	2070.5 ± 279.8	1992.0 ± 195.2	1932.5 ± 109.6	2023.0 ± 232.4
10:00	2045.0 ± 246.8	1960.2 ± 141.8	1913.2 ± 84.4	1988.9 ± 182.5
11:00	2018.2 ± 224.9	1937.3 ± 93.9	1899.9 ± 69.4	1959.5 ± 139.9
12:00	1996.3 ± 180.6	1927.2 ± 76.5	1892.5 ± 60.4	1940.6 ± 112.0
13:00	1985.1 ± 166.4	1921.0 ± 66.1	1888.2 ± 58.1	1931.8 ± 93.5
14:00	1976.8 ± 146.5	1916.4 ± 63.1	1885.0 ± 50.1	1927.1 ± 87.0
15:00	1977.8 ± 149.7	1916.7 ± 65.1	1883.9 ± 47.8	1928.8 ± 85.1
16:00	1984.5 ± 151.3	1918.2 ± 64.9	1885.6 ± 50.8	1939.3 ± 96.5
17:00	1997.0 ± 142.6	1924.3 ± 65.1	1889.2 ± 54.6	1953.6 ± 109.8
18:00	2012.0 ± 158.3	1934.0 ± 73.4	1893.7 ± 54.2	1969.6 ± 139.1
19:00	2023.2 ± 176.5	1951.0 ± 88.7	1905.6 ± 63.5	1980.2 ± 151.5
20:00	2031.9 ± 229.8	1970.2 ± 128.2	1925.1 ± 86.3	1985.9 ± 134.3
21:00	2037.0 ± 197.2	1985.5 ± 143.1	1936.3 ± 84.7	1996.0 ± 158.2
22:00	2047.6 ± 223.5	1994.7 ± 134.7	1949.5 ± 101.5	2008.3 ± 171.6
23:00	2049.6 ± 234.9	2013.6 ± 167.6	1962.9 ± 113.5	2016.9 ± 187.1

**Averages are expressed in ppb CH_4*

***Hour corresponds to GMT*

Table D2. Hourly averages of the CH_4 diurnal cycle on Sunday and 1SD by season at EGH during 2000-2012.

	Time/Season	Winter	Spring	Summer	Autumn
Sunday	**00:00**	2043.7 ± 240.3	2020.0 ± 153.2	1976.2 ± 132.6	2066.2 ± 262.5
	01:00	2042.3 ± 209.8	2029.4 ± 150.4	1992.3 ± 139.6	2076.9 ± 240.2
	02:00	2050.7 ± 222.2	2050.7 ± 206.4	2005.2 ± 152.9	2117.6 ± 363.0
	03:00	2060.0 ± 234.9	2074.7 ± 378.6	2008.9 ± 159.7	2112.0 ± 305.9
	04:00	2096.6 ± 374.9	2062.3 ± 194.6	2034.0 ± 197.8	2120.0 ± 310.0
	05:00	2079.6 ± 294.4	2073.6 ± 199.8	2043.6 ± 201.2	2139.7 ± 497.5
	06:00	2083.3 ± 322.3	2065.4 ± 207.3	2028.1 ± 189.6	2108.2 ± 326.4
	07:00	2068.9 ± 265.7	2052.1 ± 226.2	2001.5 ± 200.1	2100.8 ± 287.0
	08:00	2072.4 ± 300.6	2017.5 ± 174.5	1963.3 ± 149.9	2094.0 ± 316.4
	09:00	2058.4 ± 280.8	1981.9 ± 153.7	1937.8 ± 108.8	2044.8 ± 237.2
	10:00	2042.7 ± 264.2	1948.4 ± 113.9	1917.8 ± 92.0	1999.5 ± 175.1
	11:00	2015.3 ± 223.7	1926.8 ± 75.9	1902.0 ± 85.2	1968.4 ± 138.0
	12:00	1998.1 ± 206.0	1920.7 ± 58.9	1893.1 ± 72.0	1943.8 ± 113.3
	13:00	1980.3 ± 165.5	1914.8 ± 51.0	1888.0 ± 56.7	1928.1 ± 77.7
	14:00	1970.2 ± 167.1	1911.0 ± 46.0	1884.4 ± 46.2	1924.1 ± 77.8
	15:00	1981.8 ± 217.9	1912.4 ± 45.4	1881.7 ± 41.2	1928.5 ± 90.1
	16:00	1990.0 ± 228.9	1913.2 ± 46.5	1883.0 ± 40.9	1937.5 ± 97.2
	17:00	1993.3 ± 170.8	1927.1 ± 61.8	1891.0 ± 55.2	1955.8 ± 139.6
	18:00	2012.0 ± 175.8	1931.8 ± 59.1	1893.5 ± 53.6	1971.1 ± 142.1
	19:00	2033.4 ± 216.4	1949.1 ± 76.3	1906.1 ± 66.6	1976.0 ± 129.9
	20:00	2038.0 ± 223.3	1980.4 ± 229.8	1923.9 ± 76.3	1992.0 ± 164.5
	21:00	2042.2 ± 220.2	1996.7 ± 235.5	1939.2 ± 80.5	2006.0 ± 210.7
	22:00	2043.2 ± 214.9	1999.4 ± 131.4	1956.0 ± 142.8	2019.8 ± 211.6
	23:00	2036.6 ± 195.1	2024.5 ± 190.5	1960.4 ± 97.4	2025.9 ± 215.6

**Averages are expressed in ppb CH_4*

***Hour corresponds to GMT*

Table D3. Hourly averages of the CH_4 diurnal cycle on weekdays and 1SD by season at EGH during 2000-2012.

	Time/Season	Winter	Spring	Summer	Autumn
Weekdays	**00:00**	2056.2 ± 21.2	2023.9 ± 49.9	1978.4 ± 14.8	2026.6 ± 15.4
	01:00	2062.2 ± 17.9	2039.1 ± 17.2	1990.3 ± 13.8	2040.2 ± 11.6
	02:00	2067.7 ± 19.3	2049.0 ± 36.0	2007.4 ± 13.3	2038.8 ± 15.2
	03:00	2077.3 ± 22.4	2064.3 ± 33.8	2021.1 ± 13.7	2052.3 ± 13.8
	04:00	2081.7 ± 26.3	2075.9 ± 32.3	2037.5 ± 20.2	2059.2 ± 16.1
	05:00	2085.4 ± 27.6	2090.7 ± 38.9	2048.2 ± 22.2	2067.6 ± 14.0
	06:00	2083.5 ± 20.1	2086.7 ± 38.2	2026.2 ± 23.4	2061.5 ± 20.9
	07:00	2090.4 ± 20.3	2061.5 ± 43.6	1992.9 ± 16.7	2046.0 ± 19.6
	08:00	2088.5 ± 24.7	2025.4 ± 38.8	1958.8 ± 7.4	2016.2 ± 22.3
	09:00	2072.2 ± 30.6	1996.8 ± 58.9	1932.8 ± 7.9	1986.0 ± 21.8
	10:00	2045.7 ± 24.7	1964.3 ± 58.5	1913.6 ± 2.9	1958.1 ± 19.7
	11:00	2019.2 ± 22.8	1941.4 ± 65.2	1901.1 ± 3.2	1940.1 ± 16.9
	12:00	1996.2 ± 14.8	1930.3 ± 42.0	1893.9 ± 4.8	1932.0 ± 10.5
	13:00	1986.1 ± 9.6	1923.2 ± 20.2	1889.9 ± 2.9	1927.4 ± 9.3
	14:00	1980.4 ± 8.3	1918.3 ± 21.0	1885.8 ± 3.2	1928.4 ± 9.0
	15:00	1979.3 ± 8.9	1918.6 ± 21.1	1884.8 ± 4.4	1939.6 ± 9.3
	16:00	1985.7 ± 9.9	1919.9 ± 14.7	1886.7 ± 4.0	1952.4 ± 10.6
	17:00	2000.1 ± 9.4	1924.1 ± 12.5	1889.4 ± 4.6	1965.0 ± 10.3
	18:00	2014.9 ± 7.4	1935.3 ± 10.4	1894.2 ± 3.9	1976.7 ± 11.7
	19:00	2023.7 ± 6.8	1952.9 ± 11.5	1906.0 ± 4.2	1981.4 ± 11.9
	20:00	2033.7 ± 20.6	1969.0 ± 107.5	1925.8 ± 8.6	1990.6 ± 6.9
	21:00	2037.7 ± 14.1	1986.0 ± 21.2	1935.4 ± 7.4	2002.8 ± 10.4
	22:00	2048.1 ± 17.3	1996.5 ± 34.0	1948.4 ± 6.1	2008.5 ± 14.2
	23:00	2051.0 ± 20.0	2013.8 ± 56.1	1963.1 ± 11.0	2018.7 ± 16.5

**Averages are expressed in ppb CH_4*

***Hour corresponds to GMT*

Table D4. Hourly averages of the CH_4 diurnal cycle on Saturday and 1SD by season at EGH during 2000-2012.

	Time/Season	Winter	Spring	Summer	Autumn
Saturday	**00:00**	2040.0 ± 224.4	2035.5 ± 210.5	1974.9 ± 132.6	2031.5 ± 156.8
	01:00	2062.6 ± 250.9	2041.8 ± 212.3	1979.9 ± 119.0	2045.7 ± 213.5
	02:00	2062.1 ± 259.1	2039.3 ± 213.0	1998.6 ± 148.3	2061.0 ± 223.6
	03:00	2082.3 ± 299.2	2064.1 ± 259.5	2009.1 ± 152.1	2069.2 ± 226.8
	04:00	2089.7 ± 303.6	2080.9 ± 292.5	2027.6 ± 187.3	2080.6 ± 255.7
	05:00	2091.7 ± 327.3	2085.6 ± 267.2	2038.8 ± 198.6	2089.4 ± 267.9
	06:00	2090.2 ± 303.8	2087.4 ± 284.8	2020.7 ± 207.7	2093.0 ± 285.5
	07:00	2085.6 ± 282.4	2074.7 ± 286.5	1977.4 ± 135.7	2083.4 ± 264.1
	08:00	2092.4 ± 300.0	2024.1 ± 234.7	1951.6 ± 111.1	2080.4 ± 369.8
	09:00	2075.0 ± 284.8	1978.6 ± 181.5	1926.1 ± 94.6	2035.5 ± 233.9
	10:00	2044.1 ± 248.8	1951.7 ± 129.6	1906.3 ± 80.9	1992.9 ± 166.3
	11:00	2015.4 ± 236.5	1927.3 ± 79.1	1891.2 ± 59.6	1958.6 ± 113.5
	12:00	1995.1 ± 199.8	1917.4 ± 66.2	1884.5 ± 50.7	1941.1 ± 96.4
	13:00	1984.7 ± 190.7	1915.7 ± 67.2	1879.5 ± 46.0	1934.5 ± 86.3
	14:00	1964.9 ± 114.0	1912.0 ± 60.4	1881.5 ± 48.1	1929.0 ± 77.3
	15:00	1966.1 ± 137.6	1911.8 ± 57.8	1881.7 ± 50.5	1931.0 ± 80.6
	16:00	1972.4 ± 122.9	1914.4 ± 55.7	1882.4 ± 55.1	1939.6 ± 96.5
	17:00	1984.8 ± 122.2	1922.6 ± 68.4	1886.5 ± 56.8	1957.2 ± 105.0
	18:00	1997.5 ± 131.8	1929.2 ± 65.2	1891.1 ± 60.1	1991.2 ± 217.0
	19:00	2010.5 ± 145.6	1942.6 ± 83.7	1903.1 ± 62.7	2002.4 ± 227.6
	20:00	2016.5 ± 188.3	1966.3 ± 97.7	1922.9 ± 77.2	2003.3 ± 131.4
	21:00	2027.8 ± 206.1	1971.6 ± 102.5	1938.4 ± 88.9	2013.8 ± 174.1
	22:00	2048.6 ± 263.5	1980.6 ± 112.5	1949.4 ± 93.4	2025.5 ± 199.8
	23:00	2055.1 ± 266.7	2002.0 ± 144.5	1964.5 ± 139.0	2050.6 ± 257.2

**Averages are expressed in ppb CH_4*

***Hour corresponds to GMT*

Table D5. Monthly averages of CH_4 and 1SD calculated at EGH during 2000-2012.

Month/Year	2000	2001	2002	2003	2004	2005	2006
Jan	2042.2 ± 158.0	2164.6 ± 297.3	2078.8 ± 252.3	1940.7 ± 65.8	1950.1 ± 82.7	1980.5 ± 117.8	2056.6 ± 182.7
Feb	1978.6 ± 164.7	2096.7 ± 175.2	1907.6 ± 73.8	2123.3 ± 248.0	2071.5 ± 111.1	1999.1 ± 119.8	2005.8 ± 119.6
Mar	2016.7 ± 191.3	2027.6 ± 111.7	1979.4 ± 110.2	2122.0 ± 186.2	1988.0 ± 130.3	2052.0 ± 193.6	1931.9 ± 59.2
Apr	1996.4 ± 112.1	1974.1 ± 138.7	2031.1 ± 150.4	2033.3 ± 158.1	1998.9 ± 133.3	1976.1 ± 93.1	1979.4 ± 74.4
May	1965.9 ± 81.1	1994.6 ± 94.4	1925.8 ± 77.0	1919.1 ± 72.8	1946.3 ± 60.9	1914.0 ± 41.7	1933.2 ± 62.1
Jun	1982.1 ± 121.8	1964.3 ± 94.5	1921.6 ± 74.8	1963.4 ± 68.9	1868.4 ± 43.5	1924.5 ± 60.7	1954.2 ± 100.8
Jul	1968.2 ± 93.6	1966.8 ± 114.4	1916.6 ± 77.0	2007.9 ± 124.5	1910.6 ± 110.7	1919.4 ± 75.0	1920.3 ± 67.1
Aug	1962.4 ± 65.7	1960.3 ± 122.1	1980.9 ± 68.1	2019.7 ± 111.7	1942.2 ± 122.3	1967.8 ± 100.7	1921.0 ± 87.3
Sep	1979.5 ± 98.8	1985.4 ± 147.3	2075.9 ± 265.8	2052.9 ± 161.2	1922.9 ± 93.4	1961.5 ± 75.8	1946.2 ± 59.4
Oct	1979.4 ± 122.2	1994.2 ± 122.4	2010.5 ± 125.9	2066.3 ± 126.4	1985.5 ± 84.6	2001.6 ± 158.7	2041.5 ± 129.6
Nov	1981.2 ± 142.4	2023.1 ± 121.1	2034.6 ± 166.2	2055.7 ± 136.2	2059.9 ± 187.8	2056.9 ± 205.9	1915.0 ± 38.8
Dec	2040.9 ± 191.0	2102.2 ± 252.9	2095.7 ± 196.8	2095.0 ± 237.3	2043.9 ± 215.5	2105.7 ± 213.3	1993.0 ± 162.5
Annual average	1991.1 27.6	2021.2 65.9	1996.5 68.2	2033.3 66.8	1974.0 62.4	1988.3 59.2	1966.5 48.5

**Averages expressed in ppb CH_4*

***Annual standard deviation was calculated from monthly averages*

Table D5. (Continuation) Monthly averages of CH_4 and 1SD calculated at EGH during 2000-2012.

Year	2007	2008	2009	2010	2011	2012
Jan	2013.1 ± 166.6	1932.9 ± 78.8	2038.2 ± 126.2	2060.4 ± 135.0	2005.1 ± 95.7	2027.3 ± 196.9
Feb	1956.3 ± 80.2	2148.5 ± 331.6	2024.4 ± 79.1	2047.6 ± 94.7	1995.8 ± 91.7	2050.6 ± 150.3
Mar	2026.2 ± 103.0	1951.0 ± 42.4	1990.1 ± 99.8	1954.6 ± 40.9	2075.7 ± 136.6	2061.5 ± 131.8
Apr	1961.9 ± 79.9	1991.7 ± 72.8	1983.8 ± 77.7	2000.8 ± 68.6	2043.5 ± 126.2	1963.2 ± 44.5
May	1946.0 ± 67.7	1993.1 ± 80.4	1953.5 ± 58.3	1987.5 ± 56.8	1931.4 ± 34.3	1983.2 ± 63.2
Jun	1898.2 ± 36.6	1909.6 ± 45.5	2034.1 ± 73.1	1947.8 ± 62.4	1924.1 ± 46.0	1933.0 ± 45.7
Jul	1933.3 ± 66.6	1909.3 ± 74.4	1976.0 ± 41.1	1907.4 ± 31.8	1948.3 ± 47.7	1938.7 ± 52.7
Aug	1961.1 ± 65.5	1900.8 ± 85.4	1954.9 ± 75.7	1947.1 ± 76.4	1948.8 ± 60.1	1947.1 ± 42.6
Sep	2020.7 ± 107.7	2026.5 ± 136.6	1970.4 ± 71.8	1970.4 ± 75.1	1984.3 ± 142.4	1965.8 ± 59.2
Oct	2096.1 ± 157.9	1983.8 ± 73.1	2006.7 ± 97.9	1971.9 ± 74.4	1962.8 ± 74.7	2017.5 ± 88.8
Nov	2000.7 ± 141.5	1980.5 ± 97.7	1955.8 ± 85.2	2064.5 ± 130.8	2096.8 ± 194.3	2033.3 ± 117.7
Dec	2161.7 ± 319.1	2054.0 ± 128.3	2064.7 ± 152.6	2121.5 ± 131.0	1930.3 ± 28.8	2025.1 ± 136.8
Annual average	1997.9 73.4	1981.8 71.1	1996.1 37.2	1998.5 62.4	1987.2 58.3	1995.5 45.5

**Averages expressed in ppb CH_4*

***Annual standard deviation was calculated from monthly averages*

Table D6. Annual averages of CH_4 by wind sector and 1SD calculated at EGH during 2000-2012.

Year/Sector	N	NE	E	SE	S	SW	W	NW
2000	2002.0 ± 235.5	1995.8 ± 200.7	2067.9 ± 261.4	1991.9 ± 186.9	1923.1 ± 99.9	1919.5 ± 97.3	1959.8 ± 122.5	1983.8 ± 157.2
2001	2041.7 ± 217.8	2037.9 ± 184.7	2105.8 ± 335.2	2041.8 ± 362.5	1916.3 ± 81.9	1911.0 ± 72.0	1962.5 ± 130.9	2024.0 ± 210.5
2002	1987.8 ± 171.7	2017.0 ± 186.8	2079.0 ± 230.4	2073.9 ± 495.8	1913.4 ± 89.0	1890.9 ± 66.2	1922.1 ± 84.3	1976.5 ± 131.0
2003	2081.0 ± 281.1	2104.2 ± 265.9	2104.3 ± 271.9	2050.3 ± 261.1	1942.5 ± 127.0	1917.3 ± 85.3	1953.9 ± 103.9	2022.6 ± 195.7
2004	1998.5 ± 194.4	1997.7 ± 194.1	2029.3 ± 196.5	2005.8 ± 175.3	1914.8 ± 157.3	1906.5 ± 86.4	1951.5 ± 147.6	1980.9 ± 173.7
2005	1953.4 ± 106.0	1976.7 ± 142.9	2044.4 ± 187.5	1967.9 ± 95.5	1918.6 ± 86.3	1900.1 ± 65.9	1938.5 ± 98.2	1979.6 ± 146.3
2006	2012.3 ± 178.5	1991.2 ± 131.2	2025.1 ± 141.5	1966.6 ± 102.6	1911.0 ± 68.8	1902.7 ± 67.9	1968.2 ± 127.2	2003.2 ± 172.0
2007	2032.2 ± 230.1	2043.2 ± 255.8	2048.7 ± 188.4	2074.8 ± 296.3	1920.2 ± 81.0	1933.6 ± 137.4	1998.5 ± 195.5	2020.5 ± 176.9
2008	2159.5 ± 356.8	2070.4 ± 236.8	2056.3 ± 226.7	1996.0 ± 184.4	1925.2 ± 103.2	1926.5 ± 110.6	1965.7 ± 124.4	2021.8 ± 202.1
2009	2066.1 ± 184.6	2017.4 ± 157.0	2040.6 ± 146.7	2013.5 ± 127.0	1964.4 ± 103.7	1956.7 ± 114.2	2012.4 ± 141.6	2039.6 ± 157.2
2010	2061.5 ± 219.4	2018.5 ± 151.4	2051.6 ± 181.7	2023.9 ± 162.2	1970.5 ± 129.3	1949.1 ± 98.9	1998.5 ± 139.3	2004.4 ± 120.3
2011	2109.8 ± 279.1	2051.9 ± 200.6	2092.5 ± 216.2	2022.6 ± 160.3	1960.3 ± 146.9	1936.1 ± 78.4	1962.1 ± 115.4	2009.2 ± 147.1
2012	2076.4 ± 228.5	2053.9 ± 183.2	2073.7 ± 168.6	2040.4 ± 186.9	1949.8 ± 99.0	1942.8 ± 81.5	1991.9 ± 128.0	2026.5 ± 190.1

**Averages are expressed in ppb CH_4*

***Annual standard deviation was calculated from monthly averages*

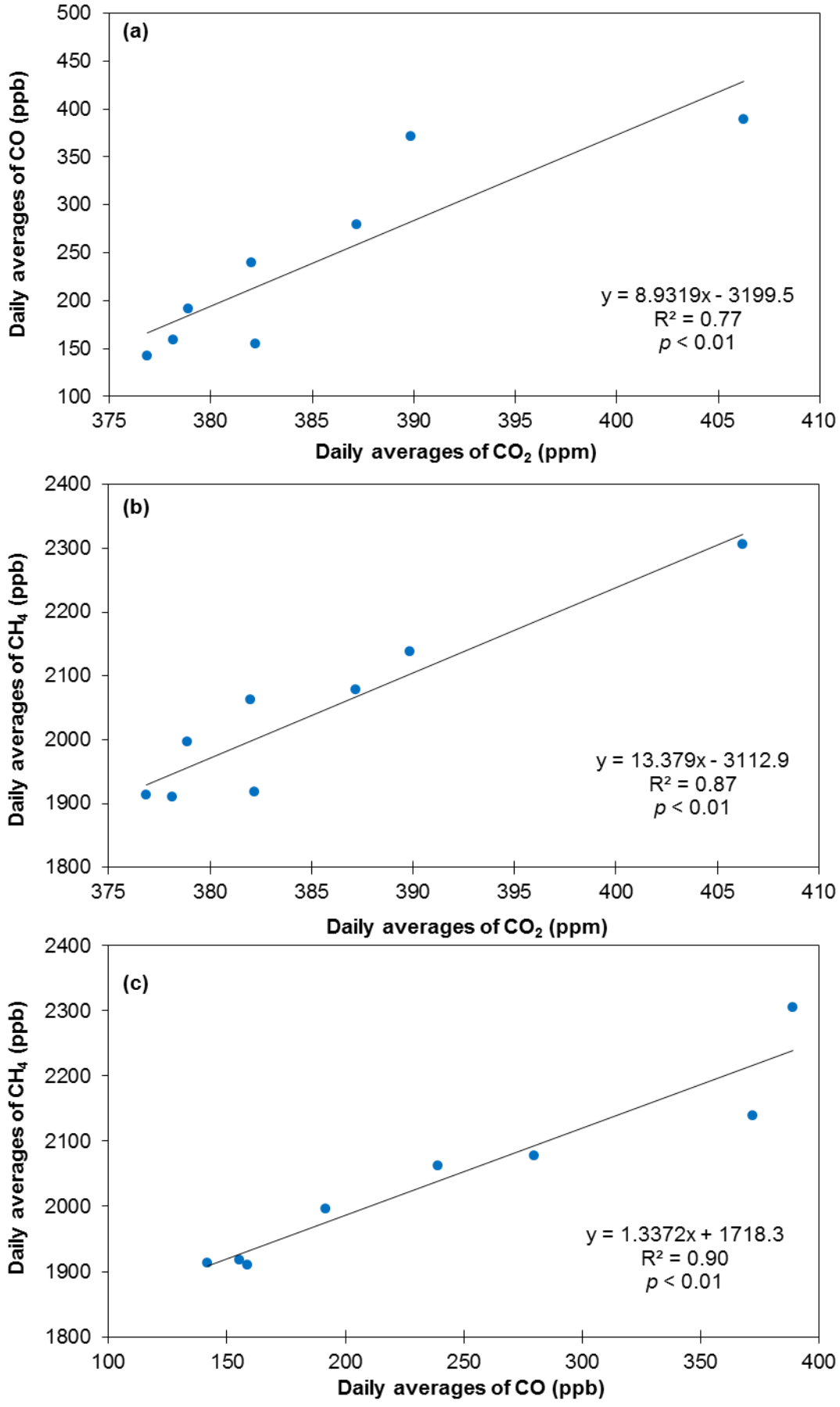

Figure E1(a). Linear correlation of daily averages of CO_2 and CO; **(b).** CO_2 and CH_4; **(c).** CO and CH_4 recorded at EGH during the summer smog episode in July 2003.

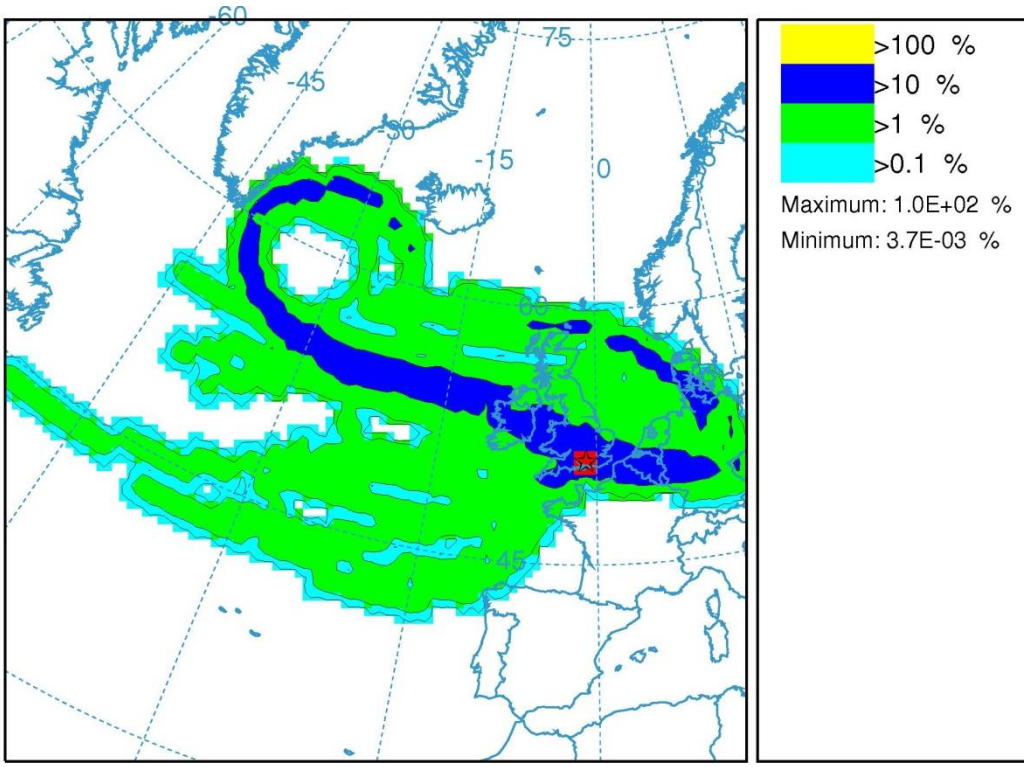

Figure E2. Air mass back trajectories analysis of air masses arriving at EGH at 00:00, 06:00, 12:00 and 18:00 GMT at 500 m above ground level during the summer smog in July 2003. Frequencies are represented in the colour scale.

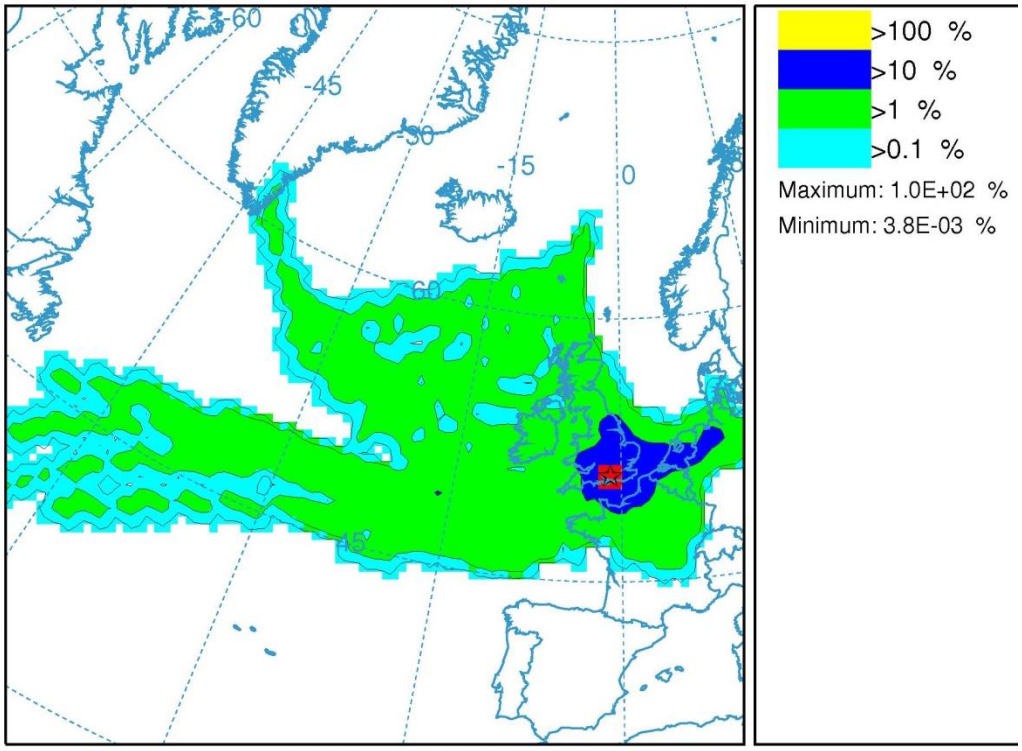

Figure E3. Air mass back trajectories analysis of air masses arriving at EGH at 00:00, 06:00, 12:00 and 18:00 GMT at 500 m above ground level during the summer smog in August 2003. Frequencies are represented in the colour scale.

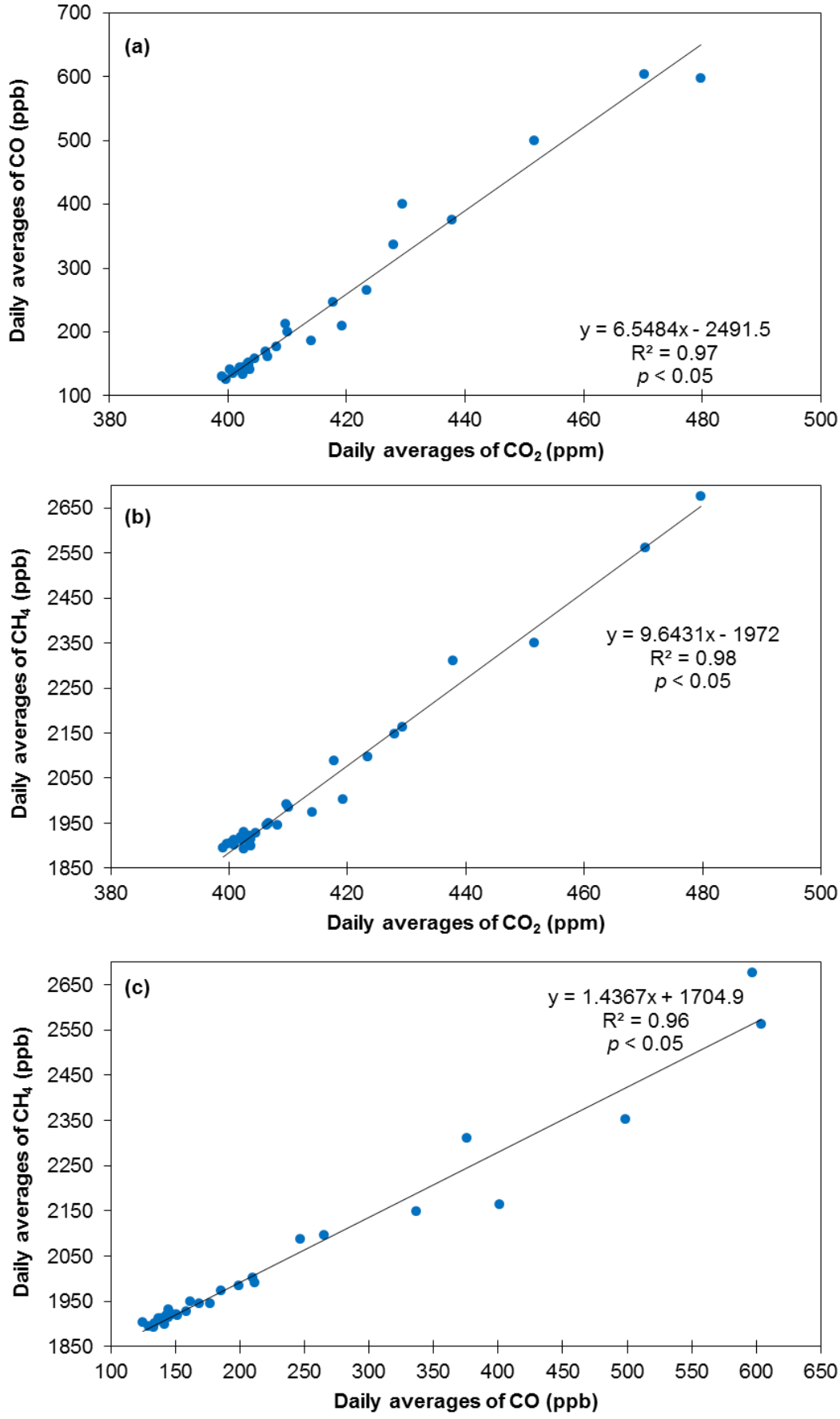

Figure E4(a). Linear correlation of daily averages of CO_2 and CO; **(b).** CO_2 and CH_4; **(c).** CO and CH_4 recorded at EGH during the winter pollution episode in January 2012.

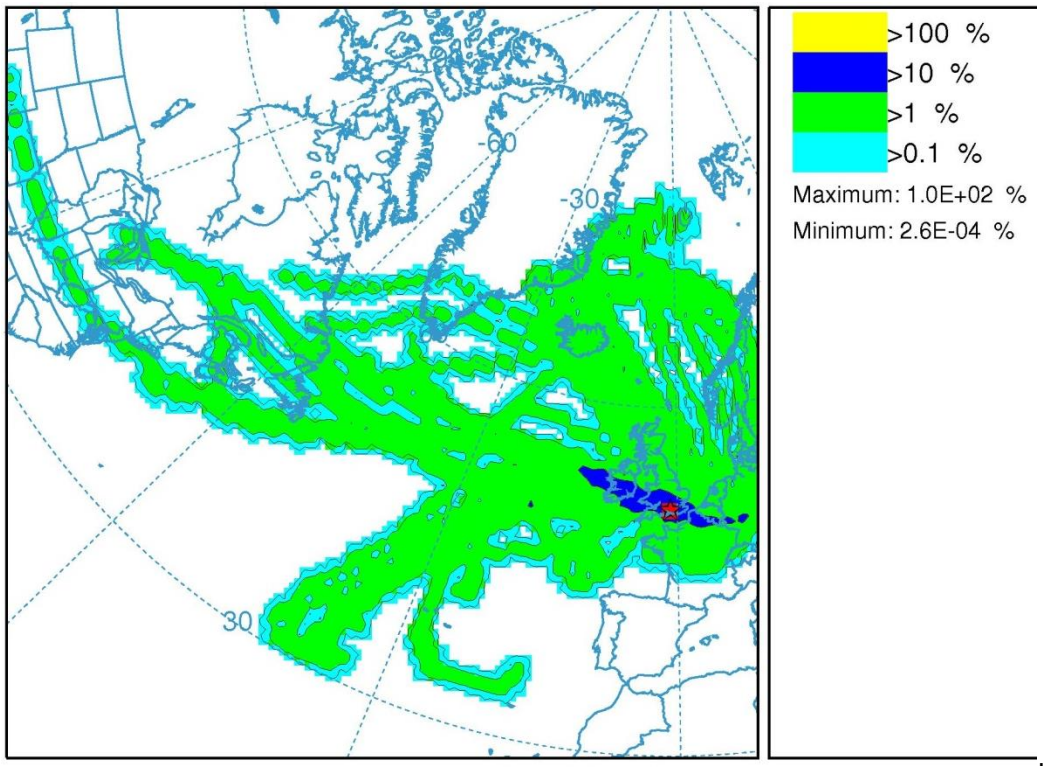

Figure E5. Air mass back trajectories analysis of air masses arriving at EGH at 00:00, 06:00, 12:00 and 18:00 GMT at 500 m above ground level during the winter pollution episode in January 2012. Frequencies are represented in the colour scale.

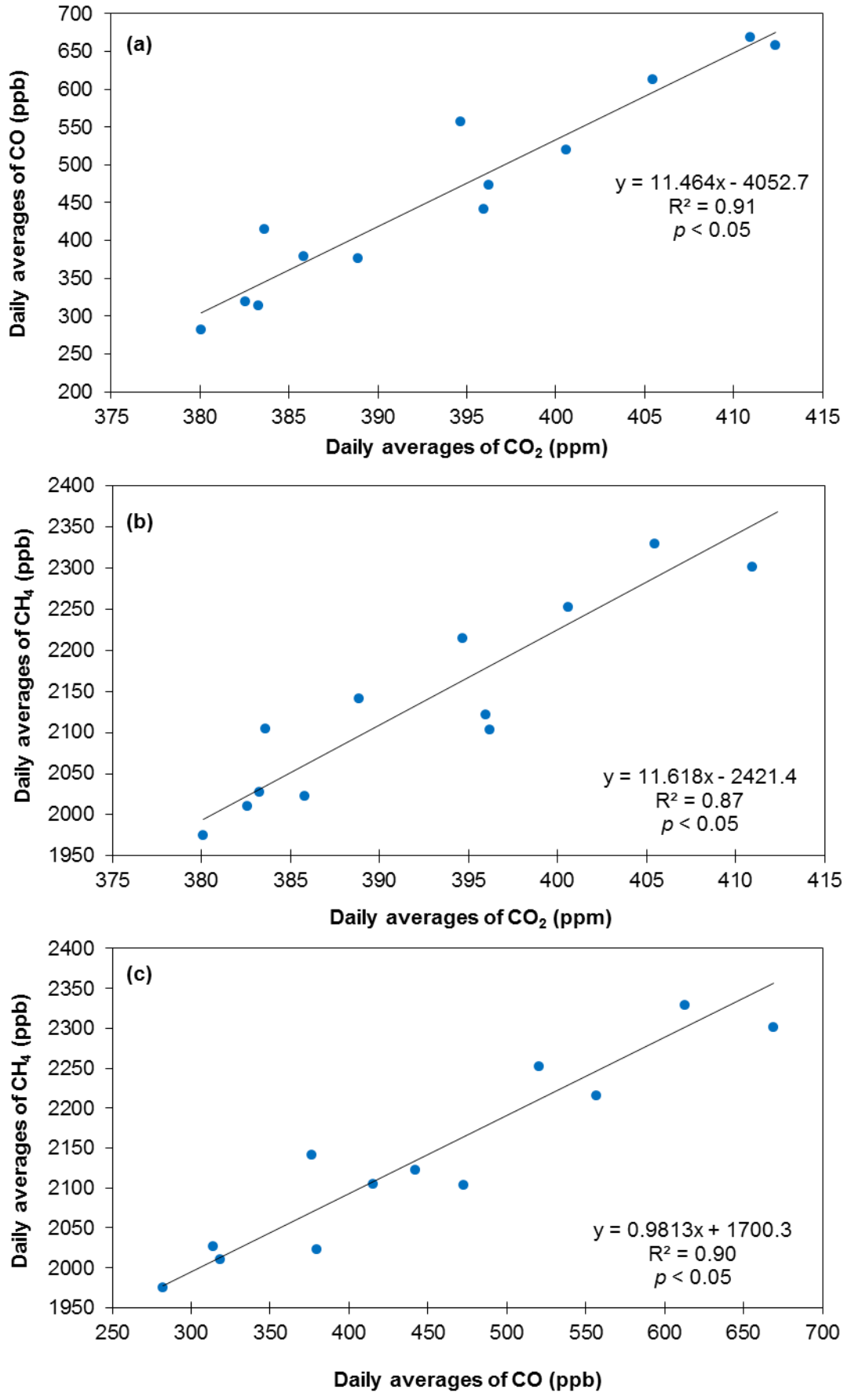

Figure E6(a). Linear correlation of daily averages of CO_2 and CO; **(b).** CO_2 and CH_4; **(c).** CO and CH_4 recorded at EGH during the Easter pollution episode in April 2012.

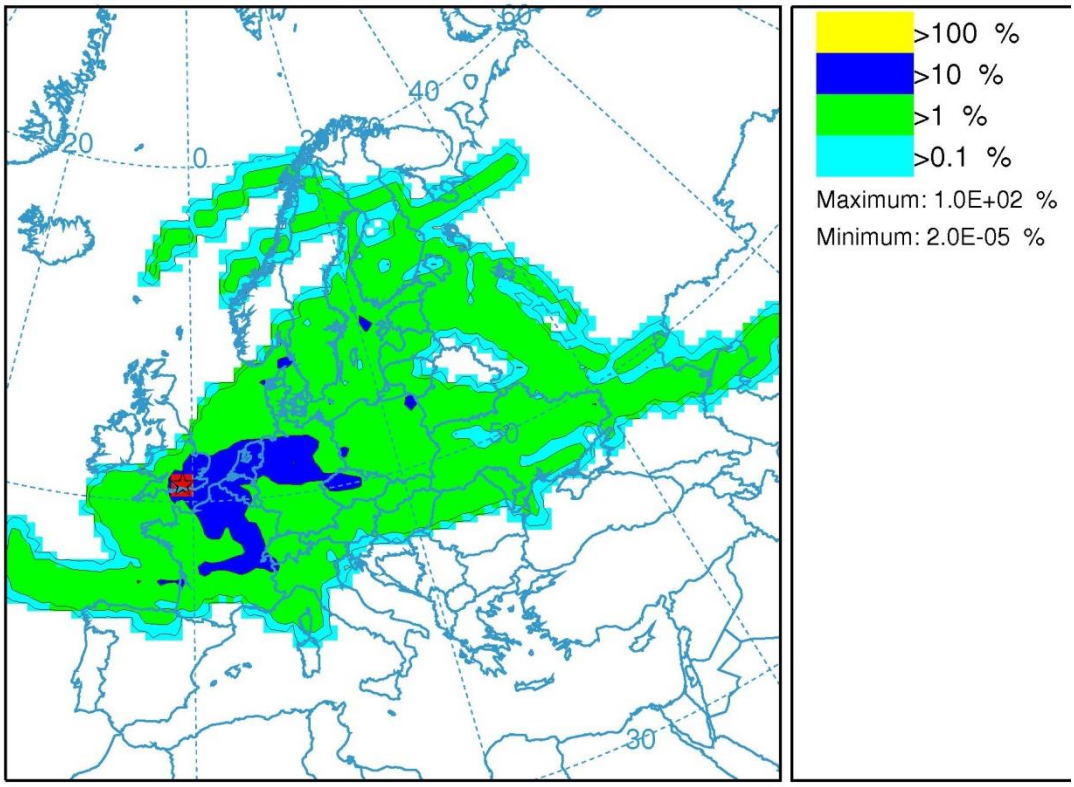

Figure E7. Air mass back trajectories analysis of air masses arriving at EGH at 00:00, 06:00, 12:00 and 18:00 GMT at 500 m above ground level during the Easter pollution episode in April 2003. Frequencies are represented in the colour scale.

E1. Air mass back trajectories

The long-range transport episode recorded from 11-23 April 2003 is used as example to perform the air mass back trajectory analysis.

Air Resources Laboratory's HYbrid Single-Particle Lagrangian Integrated Trajectory (HYSPLIT) model computes simple air parcel trajectories and complex dispersion and deposition simulations. The model calculation method is a combination of the Lagrangian approach, which uses a moving frame of reference as the air parcels move from their initial location, and the Eulerian approach, which uses a fixed three-dimensional grid as a frame of reference. Advection and diffusion calculations are made in a Lagrangian framework following the transport of the air parcel, while pollutant concentrations are calculated on a fixed grid (NOAA, 2014).

1. Access to the "HYSPLIT-WEB site" (http://ready.arl.noaa.gov/HYSPLIT_traj.php)

2. Select "Compute archive trajectories".

3. Choose the Number (1, 2 or 3) and Type of Trajectory (Normal, Matrix or Ensemble).

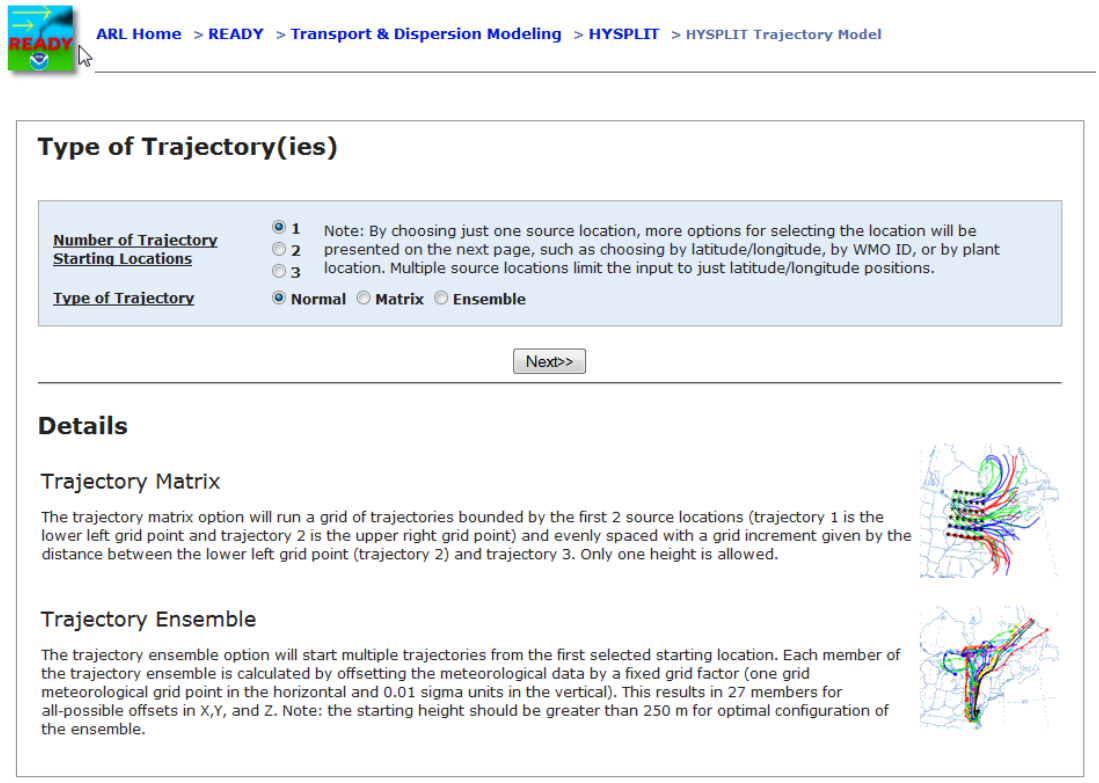

4. Select the Meteorological Data and Starting Location screen. Select meteorological data: GDAS (global, 2006-present). Provide latitude and longitude for EGH (51.4257, -0.5568).

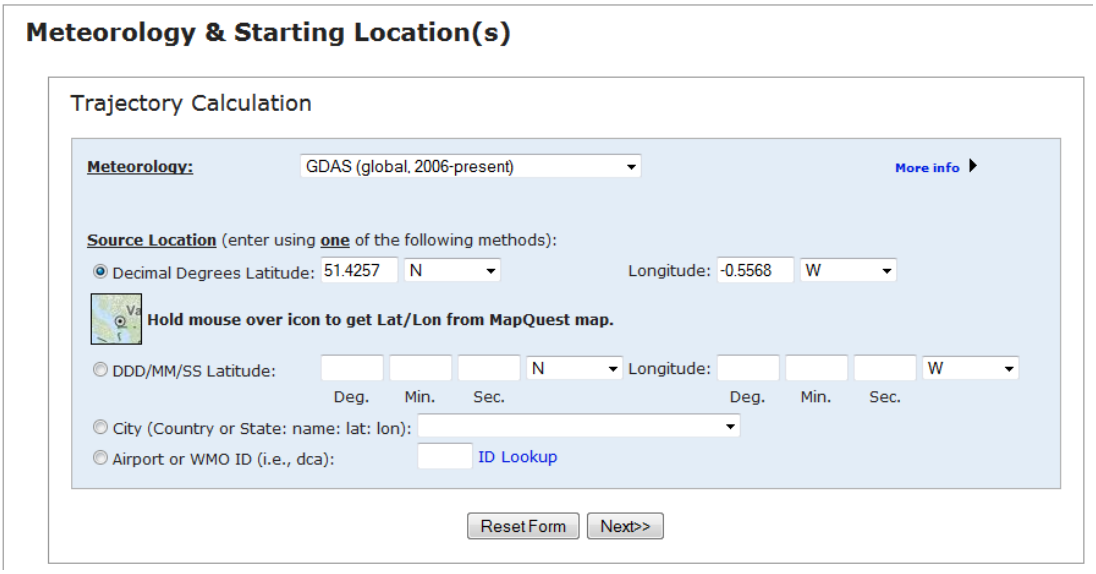

5. Details of GDAS1 (global, 2006-present) dataset. Select GDAS1 file = gdas1.jan12.w2

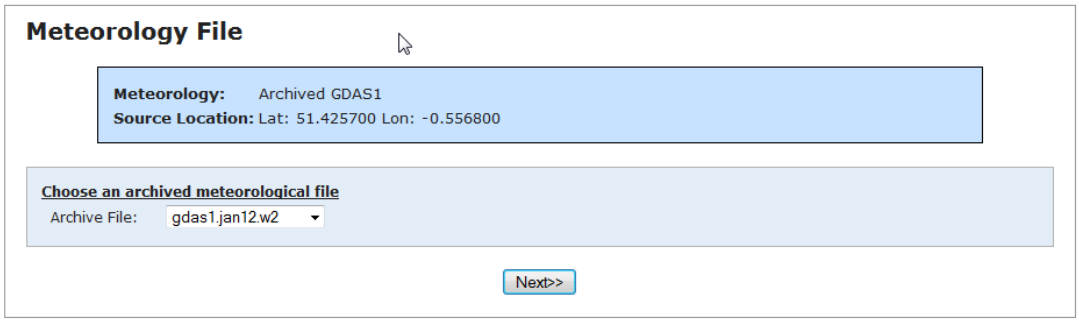

6. Edit Default Model Parameters and Display Options

Trajectory Direction: Backwards

Vertical Motion: Model vertical velocity

This field asks for the vertical motion calculation method. Model Vertical Velocity uses the meteorological model's vertical velocity fields; other options include Isentropic (constant potential temperature) and Isobaric (constant pressure; useful for balloon flight calculations). Most applications should use Model Vertical Velocity.

Start Time: The default time is the time of the first record in the meteorological data set.

Total Run Time: 96 hours = 4 days (std time used because of chemistry)

Specify the duration of the calculation in hours. The default number in the case of forecast trajectories corresponds to the maximum length of the forecast dataset. The maximum run time is limited by trajectory type due to computational requirements:

- Forecast and Archived trajectories: 315 hours
- Ensemble trajectories
  - ✓ Forecast: 84 hours
  - ✓ Archived: 120 hours
- Forecast and archived matrix trajectories: 84 hours
- Balloon splitting trajectories: 84 hours

If the model runs out of meteorological data it will terminate automatically.

Lat/Long: Check they match previously entered values for EGH.

Start height: 500 meters AGL (meters above ground level)

Start Height 1, 2, or 3

Up to 3 simultaneous trajectories can be calculated at multiple levels. Enter the heights with the lowest height in input box 1. Then check the box for either metres above model ground level or metres above mean sea-level. If entered as metres above mean sea-level, the model will convert them to metres above model ground level during the trajectory

calculation. If they are below the model ground level, they will be assigned a height of zero metres above model ground level.

- Plot resolution (dip):
- Plot Resolution

Choose the size of the final graphic image in dots-per-inch (dpi). The larger the dpi, the clearer the lines/text.

- Vertical plot height units: meters AGL
- Plot Meteorological data along trajectory YES

Dump meteorological data along trajectory: tick terrain height box for terrain height. If not ticked air mass height provided.

Diagnostic meteorological variables can be output in the trajectory endpoint file (tdump). These variables are the values used or computed by HYSPLIT at each trajectory endpoint location. The choices are: terrain height (m), potential temperature (K), ambient temperature (K), rainfall (mm per hour), mixed layer depth (m), relative humidity and downward solar radiation flux (W/m**2). These variables can be useful in diagnosing the weather and mixing potential along the trajectory.

7. Select ”Request trajectory”

Hysplit run results = output your trajectory plot and traj end point file (text file of output). You have to wait for the results to appear.

Note: on the plot the terrain height is in black and the meters above sea level of the air mass is in red.

Click “Your Trajectory Plot” to download gif file.

Click “Trajectory endpoints file” to download text file.

Model Run Details

Request trajectory

The archived data file (GDAS1) has data beginning at 01/ 8/12 0000 UTC.

Model Parameters

Trajectory direction: ○ Forward ◉ Backward (Change the default start time!) More info

Vertical Motion: ◉ Model vertical velocity ○ Isobaric ○ Isentropic More info

Start time (UTC): Current time: 11:02 — year 12 | month 01 | day 11 | hour 12 More info

Total run time (hours): 24 More info

Start a new trajectory every: 0 hrs Maximum number of trajectories: 24 More info

Start 1 latitude (degrees): 51.425700 More info

Start 1 longitude (degrees): -0.556800 More info

Start 2 latitude (degrees):

Start 2 longitude (degrees):

Start 3 latitude (degrees):

Start 3 longitude (degrees):

Level 1 height: 500 ◉ meters AGL ○ meters AMSL More info

Level 2 height: 0

Level 3 height: 0

Display Options

GIS output of contours? ◉ None ○ Google Earth (kmz) ○ GIS Shapefile More info

The following options apply only to the GIF, PDF, and PS results (not Google Earth or Google Maps)

Plot resolution (dpi): 96 More info

Zoom factor: 70 More info

Plot projection: ◉ Default ○ Polar ○ Lambert ○ Mercator More info

Vertical plot height units: ○ Pressure ◉ Meters AGL ○ Theta More info

Label Interval: ○ No labels ◉ 6 hours ○ 12 hours ○ 24 hours More info

Plot color trajectories? ◉ Yes ○ No

Use same colors for each source location? ◉ Yes ○ No More info

Plot source location symbol? ◉ Yes ○ No

Distance circle overlay: ◉ None ○ Auto More info

U.S. county borders? ○ Yes ◉ No More info

Postscript file? ○ Yes ◉ No More info

PDF file? ◉ Yes ○ No

Plot meteorological field along trajectory? ○ Yes ◉ No Note: Only choose one meteorological variable from below to plot More info

Dump meteorological data along trajectory: More info

- ☐ Terrain Height (m)
- ☐ Potential Temperature (K)
- ☐ Ambient Temperature (K)
- ☐ Rainfall (mm per hr)
- ☐ Mixed Layer Depth (m)
- ☐ Relative Humidity (%)
- ☐ Downward Solar Radiation Flux (W/m**2)

Request trajectory